Using novel portable air quality monitors to improve personal exposure and dose estimations for health studies

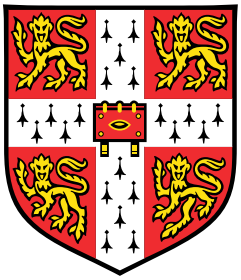

Anika Krause

Supervisor: Prof. R. L. Jones

Department of Chemistry
University of Cambridge

This dissertation is submitted for the degree of
Doctor of Philosophy

Jesus College

September 2020

Abstract

Poor air quality is a severe issue for society, affecting the health and well-being of huge parts of the population worldwide. To efficiently reduce the risk of premature death associated with air pollution, a deeper understanding of the causal links between air pollution exposure and human health is needed. However, conventional health studies are restricted by methodological limitations such as miss-estimations of personal exposure and the interdependence between different pollutant species when using traditional outdoor exposure metrics.

Taking advantage of recent advancements in sensor technologies and computational techniques, this dissertation presents a novel methodological approach to improve air pollution exposure and dose estimates for epidemiological research.

The novel methodology combines personal air quality monitors (PAMs) measuring nitrogen oxides (NOx), carbon monoxide (CO), ozone (O_3), and particulate matter (PM), with a time-location-activity model to generate accurate personal air pollution exposure estimations under field conditions. The monitors were comprehensively characterised and deployed in different exposure studies in the UK, China, Germany, and Kenya, supporting wider studies of air pollution and human health.

The PAM measurements showed excellent agreement with standard instrumentation in indoor, outdoor, and commuting environments. Field deployments involving hundreds of participants revealed the substantial exposure misclassification introduced when using ambient measurements as metrics of exposure. The correlation between individual pollutants usually observed at air quality monitoring stations was found to substantially decrease using the high spatial resolution of the portable sensors, allowing more refined estimates of the health effects of different pollutants.

The deployments showed that local emission sources had often a far more important impact on personal exposure than regional sources, and the air pollution composition changed distinctively between local microenvironments. The home environment was identified as an important exposure site, particularly in areas where populations rely on biomass burning for domestic energy and cooking. In industrialised countries, peak exposure events were recorded during commuting, although they frequently represented a minor component of the overall dose. By separating regional from local air pollution and classifying exposure by microenvironment, this work has made first steps towards assigning personal exposure to individual emission sources. The findings of this dissertation should lead to a paradigm shift in quantifying air pollution exposure in epidemiological studies and drive evidence-based policy to reduce the global burden of disease.

Declaration

This dissertation is the result of my own work and includes nothing which is the outcome of work done in collaboration, except where specifically indicated in the text.
The contents of this dissertation are original and have not been submitted in whole, or in part, for consideration for any other degree or qualification in this, or any other university. In accordance with the Faculty of Physics and Chemistry guidelines, this dissertation contains fewer than 60,000 words.

Auf alles, was schön ist in der Welt. Und auf uns.

Acknowledgements

Firstly, I would like to acknowledge my supervisor Prof Rod Jones for providing me with the opportunity to work in his group. I have greatly appreciated his invaluable insight and advice, as well as his continuous encouragement throughout the course of my PhD.
I am incredibly lucky to have Dr Lia Chatzidiakou as my research partner and dear friend. Her scientific guidance was essential for the progress of my PhD. Moreover, I could always count on her, may it be for last minute weekend-shifts to hit a deadline, medical care in field campaigns, or overcoming a writing-up crisis. For this, I am extremely grateful.
Also, I would like to thank Dr Alex Archibald, Dr Anja Schmidt and Prof Stuart Clarke for their kind support and advice.
I have had the pleasure to work with a group of very knowledgeable, kind, and welcoming colleagues. Particularly, I want to thank Dr Lekan Popoola for his patient and rich advice concerning data analysis, his help during field campaigns and the provision of air quality reference data from the Chemistry department; Andrea Di Antonio for answering many PM-related questions and providing a load of information about the Vajont dam disaster; Ray Freshwater for his technical support and keeping us safe at all times; Lizzy Martin for developing an algorithm for the indoor decay analysis as well as for some great basketball games; and Conor Bolas for keeping my time in Cambridge at a constant level of fun, may it be during departmental lunch breaks or May Balls. Extended thanks also go to the other members of the 4th floor team including Steven, Battist, Sarah, Le, Shiwei, Bin, Geoff and Francis. You made this PhD a very pleasant experience!

The largest part of this dissertation is based on data from field campaigns which would not be available without the help of a great number of people. I would like to acknowledge Peking University for providing ambient air quality data for the AIRLESS project, and the University of York (Freya Squires and James Lee) for supplying indoor reference measurements of NO_2 . Furthermore, thanks goes to the entire AIRLESS team for helping with collecting the personal exposure data during the field campaigns. Additionally, I want to thank Yiqun Han, Teng Wang, Hanbin Zhang, Li Yan and Samuel Cai in particular for their cultural support and life-saving

translations in countless situations.
Thanks goes to Natasha Grist, Alexandra Winkles and John Pharoah for their support in the organisation and conduction of the fieldwork in Kenya. Furthermore, I want to acknowledge Hans-Guido Mücke and Wolfram Birmili for providing me with the opportunity of a research exchange at the Umweltbundesamt. Thank you for this very inspiring experience!
Over 300 volunteers agreed to participate in our studies in the UK, China and Kenya. Thank you all for your contribution to this piece of research.

I am very thankful to John Sheldrick and Jesus College for making this PhD possible with their generous financial support.

Last but not least, I am incredibly grateful for the continuous and loving support of my family and friends. Your understanding, patience and uplifting humour have been truly invaluable to me and kept me sane and cheerful throughout this time.

Table of contents

List of figures

List of tables

Academic output

This work has led to a number of research articles which have either already been published or are still under review / in preparation (see below). Some parts of the wording, all of which I am primary author on, may have been transferred directly from one document to the other. Rather than acknowledging individual components of the articles in the text, an overview of all publications related to this PhD, including the contributions of individual authors, is given below.

First author publications

Characterising low-cost sensors in highly portable platforms to quantify personal exposure in diverse environments

Lia Chatzidiakou, Anika Krause, Olalekan A. M. Popoola, Andrea Di Antonio, Mike Kellaway, Yiqun Han, Freya A. Squires, Teng Wang, Hanbin Zhang, Qi Wang, Yunfei Fan, Shiyi Chen, Min Hu, Jennifer K. Quint, Benjamin Barratt, Frank J. Kelly, Tong Zhu, and Roderic L. Jones. *Atmospheric Measurement Techniques*, 12, 4643–4657. 2019.

Author contributions: LC and AK have contributed equally to this paper. It was conceptualised by LC, AK, BB and RLJ. The sensor platform was developed by LC and MK and deployed by LC, AK, YH, TW, HZ, QW and SF. The data curation was performed by LC, AK, OAMP, ADA, YH, FAS and SC. LC, AK, OAMP, ADA and RLJ contributed to the formal data analysis. Resources were provided by MH, JKQ, BB, FJK, TZ and RLJ. The software was developed by LC, AK and MK. Data were visualised by LC and AK. The original draft was written by LC and AK and reviewed and edited by OAMP, YH and RLJ.

Relevance: This publication was used to form the major part of Chapter 3 and parts of Section 2.1.

Low-cost sensors and indoor air quality: A test study in three residential homes in Berlin, Germany.

Anika Krause, Jiangyue Zhao, Wolfram Birmili
Gefahrstoffe Reinhaltung Luft (Air Quality Control), 79(3), 87-92. 2019

Author contributions: This project was part of a bigger study conducted by JZ, WB and other colleagues [157]. The idea was conceptualised by AK and WB. Research data were collected by AK and JZ, analysed by AK and WB and visualised by AK. The original draft was written by WB and AK and reviewed by JZ.

Relevance: This article was published as part of a collaboration with the German Environment Agency (UBA). Parts of this publication are included in Section 2.1. Although not yet published, Section 6.3.2 is based on data that has been collected during the same collaboration.

Using low-cost sensor technologies and advanced computational methods to improve dose estimations in health panel studies: Results of the AIRLESS project

Lia Chatzidiakou, Anika Krause, Yiqun Han, Wu Chen, Li Yan, Olalekan A.M. Popoola, Mike Kellaway, Yangfeng Wu, Jing Liu, Min Hu, AIRLESS team, Ben Barratt, Frank J. Kelly, Tong Zhu, and Roderic L.Jones
Journal Of Exposure Science And Environmental Epidemiology. 2020

Author contributions: LC and AK have contributed equally to this paper. It was conceptualised by LC, AK and RLJ. The sensor platform was developed by MK and LC. The field deployment was performed by LC, AK, YH, LY, WC and the AIRLESS team. The PIs of the two cohorts were YW and JL. MH was in charge of the Peking University monitoring station. The data curation was performed by LC and AK. LC, AK, OAMP and RLJ contributed to the formal data analysis. Data were visualised by AK and LC. Resources were provided by BB, FJK, TZ and RLJ. The original draft was written by LC and AK and reviewed and edited by YH, BB and RLJ

Relevance: Parts of Chapters 4 and 6 are based on this publication.

Classification of time-activity location patterns for improved estimations of personal exposure to air pollution using state-of-the-art sensor technologies and advanced computational techniques

Lia Chatzidiakou, Anika Krause, Benjamin Barratt, and Roderic L. Jones.
in preparation

Author contributions: LC, BB and RLJ conceived the experiment, LC and AK conducted the experiments and analysed the results. LC and AK drafted the manuscript.

Relevance: Parts of Section 6.2 are based on this publication.

Co-authored publications

Effects of AIR pollution on cardiopuLmonary disEaSe in urban and peri-urban reSidents in Beijing: protocol for the AIRLESS study

Yiqun Han, Wu Chen, Lia Chatzidiakou, Anika Krause, Li Yan, Hanbin Zhang, Queenie Chan, Ben Barratt, Rod Jones, Jing Liu, Yangfeng Wu, Meiping Zhao, Junfeng Zhang, Frank J. Kelly, Tong Zhu, and the AIRLESS team.
Atmospheric Chemistry and Physics. Currently under review

Author contributions: TZ and FK are co-principle investigators of AIRLESS, designed the study, and revised the manuscript. YH participated in the study design, coordinated air pollution monitoring and clinical measurements in Pinggu site, and drafted the manuscript; WC coordinated the clinical measurement in PKU site; LC, AK and RJ designed the personal monitor PAM and were involved in the monitor deployment and data ratification; YH, LY, HZ, XC, YC, WX, AJ, YZ and YL are key staff participated in the clinical measurements in Pinggu site; WC, YW, TX, YF XH and TW are key staff participated in the clinical measurements in PKU site; HZ and BB participated in the residential air pollution measurement; XQ, MZ and JZ involved in the design of laboratory biomarkers. JL coordinated the CMCS cohort; YL, XG and QC coordinated the INTERMAP cohort, ME, PE, RJ, JL, MZ, JZ, and YW are

co-investigators of AIRLESS study and revised the manuscript. All authors read and approved the final version of the manuscript and ensure this is the case.

Relevance: Parts of Section 2.3.2 are based on this publication.

Difference in ambient-personal exposure to $PM_{2.5}$ and its inflammatory effect in local residents in urban and peri-urban Beijing, China: Results of the AIRLESS project

Han, Y.; Chatzidiakou, L.; Yan, L.; Chen, W.; Zhang, H; Krause, A.; Xue, T.; Chan, Q; Liu, J; Wu, Y; Barratt, B.; Jones, R. L.; Zhu, T.; and Kelly, F. J.
FARADAY Discussions. Currently under review.

Author contributions:
YH participated in the study design, coordinated air pollution monitoring and clinical measurements in peri-urban site and prepared original draft; LC designed the personal monitor and involved in the monitor deployment and exposure analysis and prepared original draft; LY HZ and WC are key investigator involved in the clinical measurement in peri-urban and urban site; HZ and BB involved in the exposure analysis; TX participated in the statistical analysis for the health effect; YW and QC coordinated the INTERMAP cohort; JL coordinated the CMCS cohort; AK and RJ involved in the personal monitor design and validation; TZ and FK are co-principle investigators of AIRLESS, designed and supervised the study, and revised the manuscript.

Relevance: Section 4.5 is based on parts of this publication.

Glossary

Air pollution Contamination of air by any chemical, physical or biological agent (here: gaseous and particulate pollutants).

Ambient pollution The air pollution levels measured at static air quality monitoring stations are referred to as ambient or outdoor concentrations. As the monitoring stations are usually designed to measure the regional pollution concentrations away from any direct sources, the ambient concentration can also be regarded as regional background or baseline concentrations.

C-reactive protein Blood component, rises rapidly in response to tissue injury, infection and inflammation [135] (see Table A.4).

Coefficient of correlation Pearson's correlation coefficient R contains information about the strength and direction of the linear relationship between two *different* variables [51]. In this work, it was used to compare the concentration measurements of two different pollutant species (e.g. CO and NO).

Coefficient of determination The coefficient of determination R^2 is the squared coefficient of correlation R and provides a measure of how well a predicted variable agrees with the observed value [130]. It is therefore used to compare two measures of the *same* variable (here: the concentration of a pollutant such as NO_2). R^2 only describes the shared variability of two variables [51] and does not contain information about the absolute difference between predicted and observed value. Therefore, it was complemented with the root mean square error (RMSE, see Equation 3.1).

Confidence interval (CI) The 95% confidence interval (CI) is used to estimate the precision of the odds ration (OR). A large CI indicates a low level of precision of the OR, whereas a small CI indicates a higher precision of the OR. It is important to note, however, that unlike the p value, the 95% CI does not report a measure's statistical significance. In

practice, the 95% CI is often used as a proxy for the presence of statistical significance which is assumed when the CI does not overlap the null value (e.g. OR = 1). [51].

Dose The air pollution dose is the "amount of contaminant that is absorbed in the body of an exposed individual over a specified time" [101]. The physiological dose is influenced by weight, health condition and other characteristics of the individual; environmental factors and the contaminant itself [101], and is consequently very complex to quantify. The inhaled dose can, however, be approximated as the *potential dose* or *intake* which assumes the total absorption of the contaminant by the body [101, 96]. In this dissertation, the term *dose* refers to the *potential dose* .

Exposure metric An exposure measurement of a pollutant used to estimate the pollutant mass delivered into the respiratory system.

Exposure misclassification Difference between a chosen measurement method of a pollutant, usually measurements of the ambient air at postcode level or coarser, and the true exposure of a person [33].

Fraction of exhaled NO (FeNO) Marker for respiratory inflammations [120] (see Table A.4).

Inhalation rate Volume of air breathed in by a person per unit of time.

LOD Limit of Detection. Conventionally, the LOD of air pollution sensors is determined by measuring the sensor noise in zero air. In this work, the LOD was established from field calibration data.

Measurement accuracy Closeness of the agreement between the measurement of a quantity (here: the pollution concentration measured by a portable sensor) and the true value of that quantity (here: the pollution concentration measured by a reference instrument) [64]. Both, systematic errors (or bias) and random errors (precision) impact the accuracy. The systematic component of the measurement accuracy can be improved by instrument calibration.

Measurement error Difference between a measured quantity and the true value of a quantity [68]. It can therefore be used to describe the accuracy of a measurement method.

Measurement precision Measure of the agreement between measurements of the same quantity obtained under stipulated conditions [64]. It is only influenced by the distribution of random errors and can be improved by averaging observations over time.

Measurement reproducibility Precision of measurements of the same quantity obtained by different instruments but with the same measurement method (= reproducibility conditions) [64]. In this work it describes the agreement of different personal monitors that are exposed to the same air pollution concentration (i.e. when being colocated).

Measurement uncertainty Statistical dispersion of the values attributed to a measured quantity [68]. It can be interpreted as the "expected" measurement error.

Microenvironment A volume of air space with [an approximately] homogeneous pollutant concentration [48].

Monocyte count Type of white blood cells, their count can be predictive of cardiovascular events [117] (see Table A.4).

Odds ratio (OR) Measure of association between an exposure and a health outcome. The OR represents the odds that an outcome will occur given a particular exposure, compared to the odds of the outcome occurring in the absence of that exposure.
OR = 1 Exposure does not affect odds of outcome
OR > 1 Exposure associated with higher odds of outcome
OR < 1 Exposure associated with lower odds of outcome.

Personal exposure Air pollution concentration in the direct surrounding of a person, see Section 1.2.2. To take the exposure duration into account, the *integrated* or *cumulative exposure* can be calculated by integrating exposure over time (unit: µg m^{-3} min). More commonly used is, however, the *average exposure* which is defined as the integrated exposure divided by the exposure duration (unit: µg m^{-3}) [96].

$PM_{2.5}$ $PM_{2.5}$ is defined as the mass of dry particles that pass through a size selective inlet with a 50% cut-off efficiency at 2.5 µm aerodynamic diameter [133, 50]. The aerodynamic diameter of an irregular particle is defined as the "*diameter of the spherical particle with a density of 1000 kg/m^3 and the same settling velocity as the irregular particle*" [60].

Pollutant concentration The terms "air pollution concentration" and "air pollution level" refer to the amount of air pollution in the air. It is typically measured in micro grams per cubic meter or in parts per billion. The latter unit strictly refers to a mixing ratio not a concentration. In this work, however, the term "concentration" is used for all units. In the case of particulate matter, the term concentration always refers to the mass concentration (µg m^{-3}).

Pollutant ratio Ratio between the concentrations of two pollutants. May give indication of the emission source and toxicity of the air pollution mixture.

Rural In the context of the AIRLESS project, rural refers to the monitoring site and study cohort from Pinggu village which is actually located in the peri-urban periphery of Beijing. Therefore, it is often also referred to as the peri-urban site.

Time budget Amount of time an individual spent on different activities within a specified period (e.g. one week).

Chapter 1

Introduction

1.1 Health effects of air pollution

For centuries, air pollution has been a concern for societies all over the world. Records of the nuisance of smoke and concerns about possible health effects have already been documented more than two thousand years ago. For instance, ancient Greek policy documents regulated the location of pollution sources well beyond the city walls to protect the population [21].
But only in the 20th century did researchers begin to conduct more systematic investigations of the links between air pollution and human health. One famous example is Wilkins' study on the London Smog in December 1952 [148], when air stagnation and other meteorological conditions led to an accumulation of air pollution in the city. Figure 1.1 shows the sulfur dioxide (SO_2) and particulate matter concentrations (in graph referred to as smoke) as well as the number of deaths that were recorded during that event. The death rate increased with a small time lag after the smog began, and it continued to be high for a few days after the pollution had already cleared up, indicating the lagged effects of air pollution exposure on health.

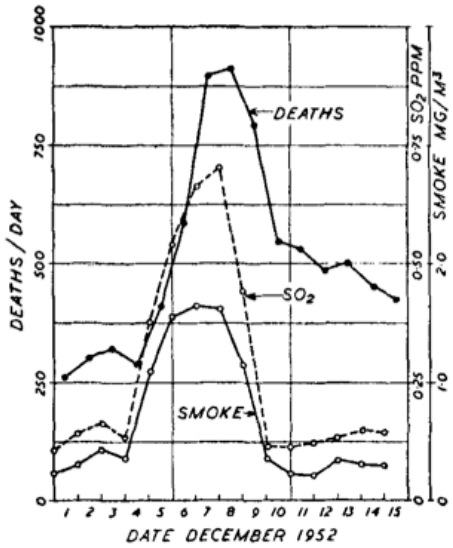

Fig. 1.1 Daily air pollution and death rates during the London Smog of December 1952. From Wilkins et al. [148].

The Harvard Six City Study [46], a long-term longitudinal cohort study of the health effects of air pollution commenced in 1975, was the most significant scientific effort to quantify the detrimental effects of air pollution on mortality and morbidity of the population. The project monitored over 8,000 participants in six U.S. cities for 14-16 years to examine the linkage between exposure to air pollution and mortality. The results in Figure 1.2 show the city specific mortality rates[1] plotted against the mean air pollution levels of each of the six cities. A significant association between air pollution and mortality was found, which is clearly demonstrated in Figure 1.2. Laden et al. carried out a follow up study for 8 years in a period of reduced air pollution concentrations (1990-1998), finding that a reduction of air pollution was associated with lower mortality risks [80].

[1] adjusted for personal factors, such as smoking habits, level of education, body-mass index, day of the week and temperature

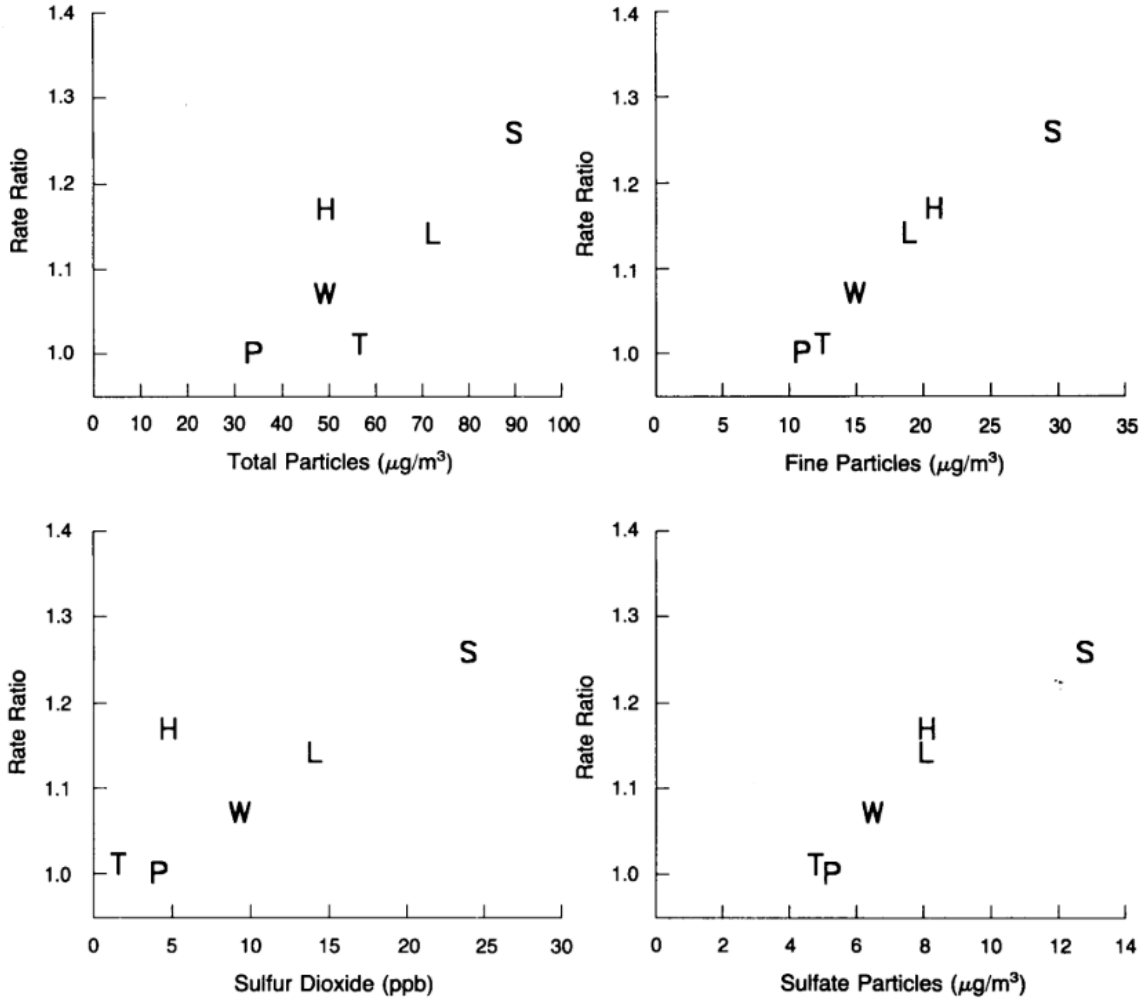

Fig. 1.2 Estimated adjusted mortality-rate ratios and air pollution levels in six cities in the USA. Mean values are shown for the measures of air pollution. P denotes Portage, Wisconsin, T Topeka, Kansas; W Watertown, Massachusetts; L St. Louis; H Harriman, Tennessee; and S Steubenville, Ohio. From Dockery et al. [46].

In the past 30 years, air pollution has received an increasing amount of attention within the research community. Figure 1.3 from Zell et al. presents the number of publications related to air pollution in the years 1955-2006, showing a large increase of publication numbers since 1990. The intense research in recent decades has produced robust scientific evidence that exposure to poor air quality increases morbidity and mortality rates of the global population [34, 149, 23, 137, 31].

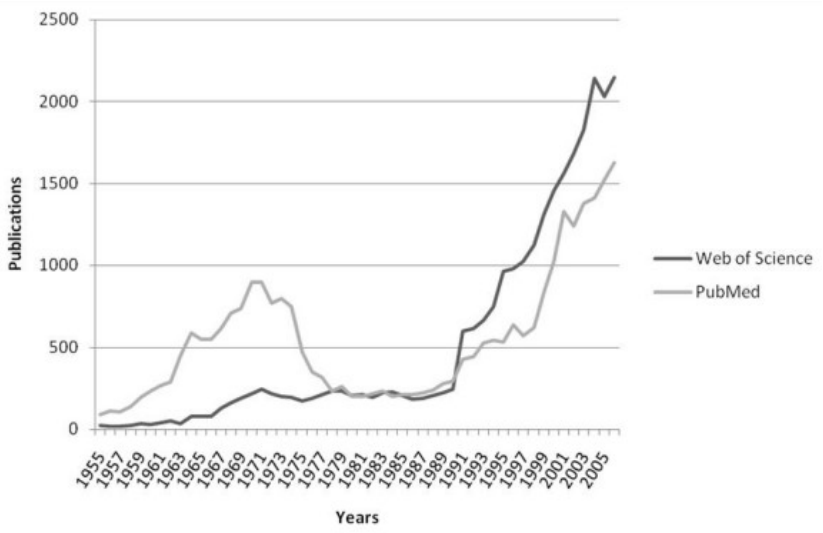

Fig. 1.3 Publications related to the topic air pollution 1955- 2006. Comparison of results in "Web of Science" and "PubMed". From Zell et al. [155].

In 2015, the Global Burden of Disease report found that non-communicable diseases (NCDs) are the major cause of premature deaths worldwide, and identified exposure to ambient and household air pollution among the leading environmental risk factors [52]. While the number of global deaths caused by communicable diseases and perinatal, maternal and nutritional conditions is decreasing, the mortality due to NCDs is rising [100]. Mathers and Loncar projected that this trend will further continue in the future as shown in Figure 1.4. It is therefore essential to understand the causes and risk factors leading to NCDs in as much detail as possible.

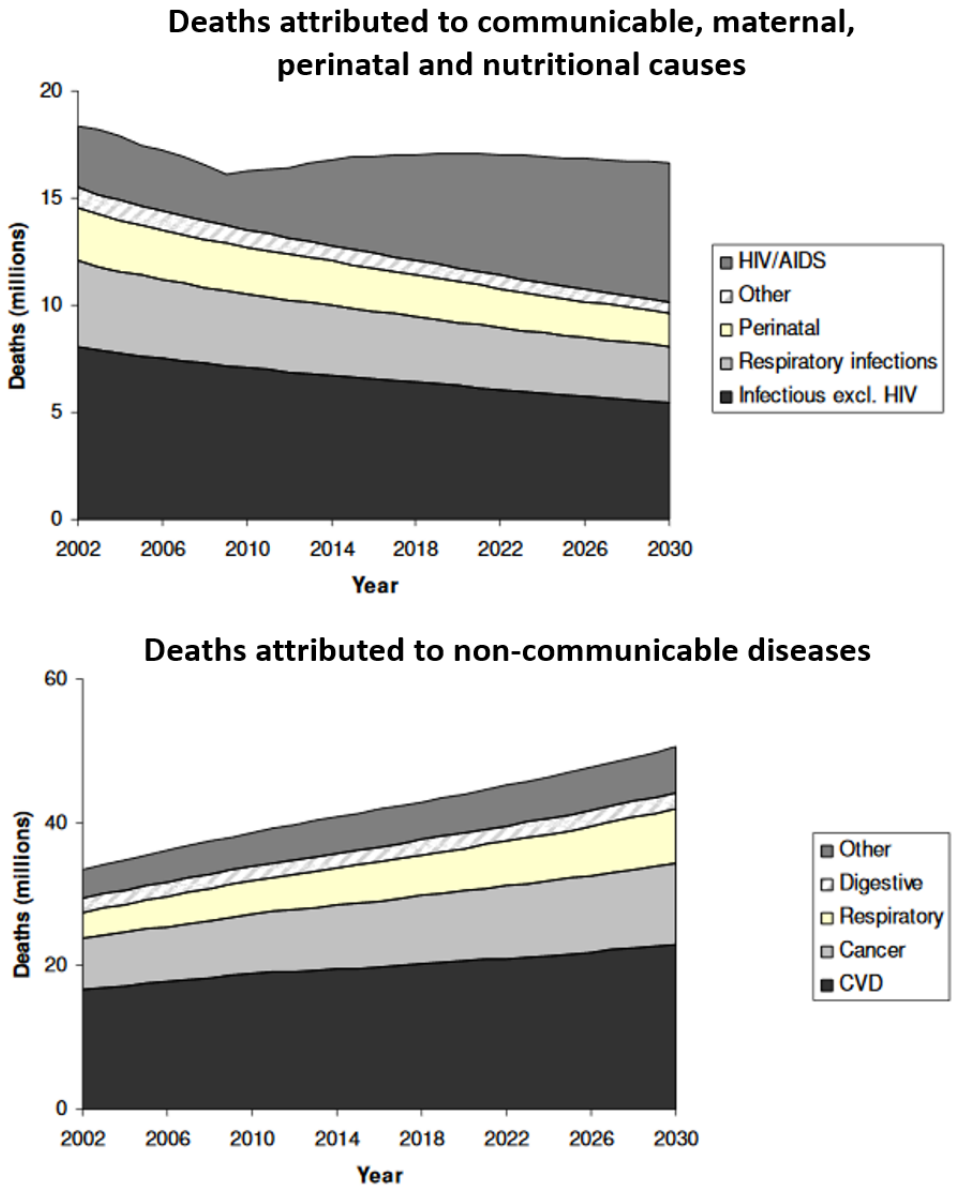

Fig. 1.4 Baseline projections of global deaths from communicable, maternal, perinatal and nutritional causes (top) and non-communicable disease (NCD), 2002-2030. From Mathers and Loncar [92]. CVD - cardiovascular disease. Note the different y-axis scales: The number of deaths attributed to NCD is approximately twice as high as the number attributed to communicable diseases.

Poor air quality has been mainly associated with cardiovascular conditions including increased blood pressure, heart attack and stroke; and respiratory diseases, such as chronic obstructive pulmonary disease (COPD), lung cancer and pneumonia. But studies suggest that air pollution may also affect other organs, such as the brain or the reproductive system. For instance, air pollution has been associated with metabolic diseases, premature births and decreased birth weight, as well as with neurological and psychiatric conditions such as Alzheimer's disease, Parkinson's disease and depression[137]. Figure 1.5 provides a full overview of the detrimental health effects associated with air pollution. Despite this improved understanding over the last decades, uncertainties remain as it is unclear which components of the air pollution mixture cause the specific health outcomes [53]. The limitations that hinder epidemiological studies in drawing more specific associations will be discussed in the following section.

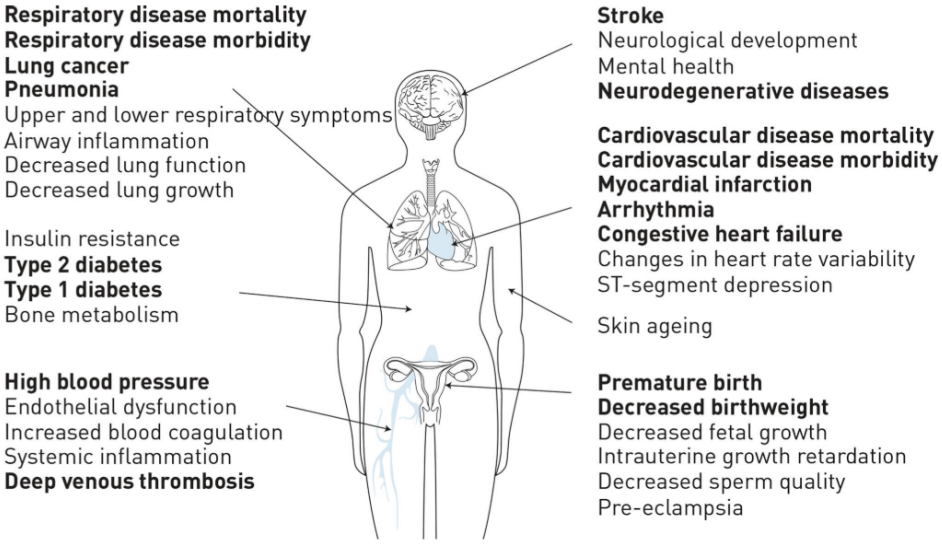

Fig. 1.5 Overview of diseases, conditions and biomarkers affected by outdoor air pollution. Bold type indicates conditions currently included in the Global Burden of Disease categories. From Thurston et al. [137]

1.2 Limitations of conventional epidemiological studies

Studies like Dockery's analysis of the London Smog event or the Six city study (Section 1.1) established clear links between air pollution and mortality, but they have also left some questions unanswered. Decades after these compelling historical studies, the research community struggles to draw specific associations between health outcomes and individual pollutants due to the inherent limitations of epidemiological studies [53].

Conventionally, epidemiological studies have relied on indirect approaches such as stationary air quality measurements or air quality models to estimate the exposure risk of a population (see Section A.1.1 in the Appendix). These methods are capable of generating exposure data for very large cohorts, increasing the confidence of the health effect estimates in epidemiological studies [96]. Relying on these indirect approaches entails, however, two major limitations of conventional epidemiological studies outlined below.

1.2.1 Correlation between individual pollution species

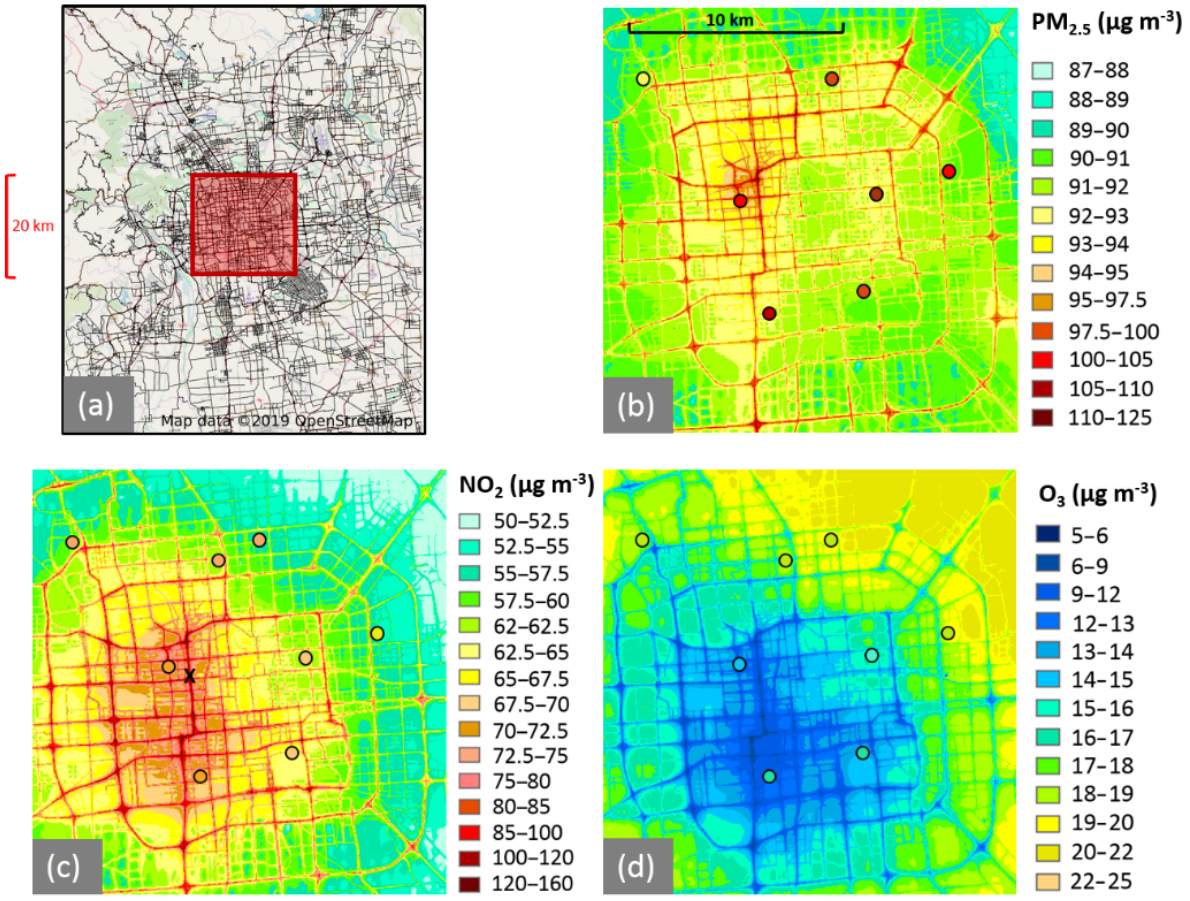

Fig. 1.6 Modelled mean outdoor $PM_{2.5}$ (b), NO_2 (c), and O_3 (d) concentrations in Beijing (winter 2016) based on an emission inventory from 2013. From Biggart et al. [15]. $PM_{2.5}$ and NO_2 are positively correlated, NO_2 and O_3 are negatively correlated.

Different pollutant species are often highly correlated in ambient air quality measurements due to common sources [23]. As an illustrative example, Figure 1.6 shows the mean concentrations

of particulate matter ($PM_{2.5}$), nitrogen dioxide (NO_2) and ozone (O_3) in Beijing modelled based on observations from China National Environmental Monitoring Center [15]. In regions of elevated $PM_{2.5}$ levels, the NO_2 concentrations were also elevated. The two pollutants were closely correlated while the NO_2 and O_3 levels were clearly anticorrelated.
Goldberg's study on the interpretation of epidemiological studies of ambient air pollution concluded that *"it is impossible using standard epidemiological designs to uniquely identify any individual component of air pollution as a causal agent of a health effect because of simultaneous exposure to all or a subset of ambient pollutants"* [53].
Historical evidence presented in the previous section from the London Smog Study and the Six City Study (Figures 1.1 1.2) found a clear association between the exposure to air pollution and mortality but not which specific component of the air pollution was responsible for the increase in mortality because the different pollutant species (SO_2 and PM) were closely correlated. A reanalysis of the Six City Study concluded that increases in mortality *"may be attributed to more than one component of the complex mixture of ambient air pollutants"* [77].
Similarly, a recent report of the Committee on the Medical Effects of Air Pollutants (COMEAP) [33] on the associations of long-term NO_2 exposure and mortality reviewed studies that used multi-pollutant models to determine the combined health effects of two or more pollution species, finding that the combined health effects of two pollutant species were *"similar to, or slightly larger than, the single-pollutant association reported with either pollutant alone"* (i.e. effect(a + b) = effect(a) = effect(b)). This suggests that summing up the health effects of the individual components of a pollutant mixture would substantially overestimate the health effect of the mixture. This discrepancy illustrates the limitation of epidemiological research that relies on spatially and temporally aggregated data to reliably determine the harmful potential of one individual pollutant species.

1.2.2 Exposure, dose and exposure misclassification

To standardise the concepts around human exposure to air pollution, in 1982 Wayne Ott defined the term *exposure* as an event that occurs when a person comes in contact with an air pollutant of a concentration c at a specific time [107]. Based on this definition, this dissertation uses the term *personal exposure*, or simply *exposure*, to refer to the pollutant concentration in the direct environment of a person. Consequently, the exposure is given in units of concentration[2]
In contrast to personal exposure, the term *outdoor* or *ambient exposure* refers to pollutant concentrations measured by air quality monitoring stations which are located outdoors. Epi-

[2]For instance, if a person was located in an environment containing 15 µg m^{-3} of $PM_{2.5}$, their personal exposure to $PM_{2.5}$ would be 15 µg m^{-3}.

demiological studies often use these ambient exposures as proxies for personal exposure [121]. In this work, ambient exposures will be always explicitly referred to using the terms *outdoor*, *static* or *ambient*.

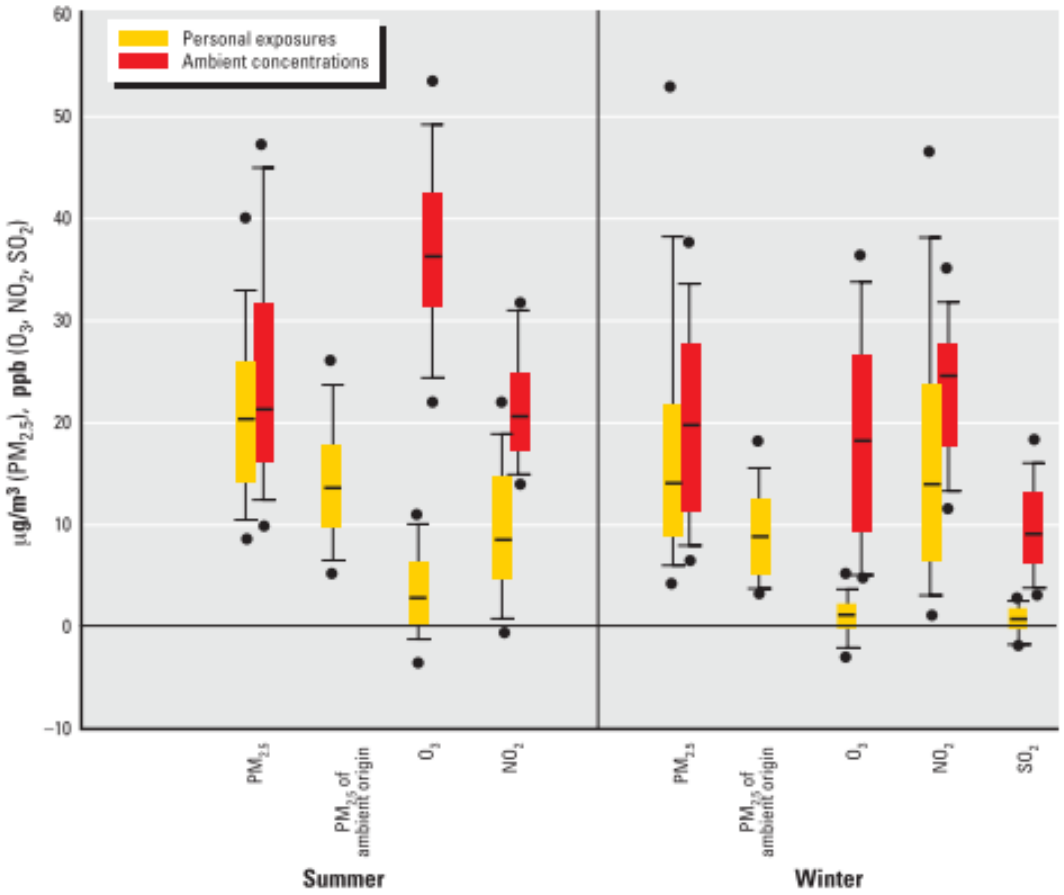

Fig. 1.7 Boxplots showing the distribution of ambient concentrations and personal exposures of 56 subjects in Baltimore by season and pollutant. $PM_{2.5}$ of ambient origin was determined by comparing the sulphate ($[SO_4]^{2-}$) content of personal and ambient $PM_{2.5}$ filter samples. From Sarnat et al. [121].

Exposure misclassification *"refers to differences between the exposure metrics used in [an] epidemiological study and the 'true' exposure of the population at risk"* [33]. Conventional epidemiological studies rely on exposure estimates from static outdoor monitoring stations which are often only sparsely distributed over large areas and averaged over 1, 8, or 24 hours [108]. Air pollution concentrations may, however, vary significantly in space and time because they are affected by various factors such as local emission sources, surface losses or filtering effects of buildings [74, 79]. For instance in the UK, two- to three-fold differences of NO_2

concentrations were found within distances of 50 meters or less [65] whereas air quality monitoring stations typically cover areas of several square kilometres[3].
Studies that investigated the relationship between personal and ambient air pollution measurements found poor correlations (often approaching 0) between the two parameters [11, 144]. Figure 1.7 from Sarnat et al. demonstrates this by comparing personal exposure measurements from 56 subjects (yellow) with ambient concentrations recorded over the same time period (12 days; red) [121]. The concentration ranges of the two exposure metrics differ significantly, in some cases by a factor of almost 10.
Although exposure misclassification is a well known issue in the scientific literature, it has rarely been accounted for in health studies [124]. Refining the exposure metrics in epidemiological studies may, however, lead to different or previously uncovered associations between air pollution and health [18, 122]. For instance, Goldman et al. found that *"health risks per unit increase in pollutant concentration associated with primary air pollutants are predicted to be attenuated by up to 80% when central monitor data are used [instead of spatially refined exposure metrics]"* [54].

The air pollution *dose* is the "amount of contaminant that is absorbed in the body of an exposed individual over a specified time" [101].
The physiological dose is influenced by weight, health condition and other characteristics of the individual; as well as by environmental factors and the contaminant itself [101], and is consequently very complex to quantify. The inhaled dose can, however, be approximated as the *potential dose* or *intake* which assumes the total absorption of the contaminant by the body [101, 96]. In this dissertation, the term *dose* refers to the *potential dose*.
The air pollution dose, i.e. the amount of air pollution that is inhaled by the body, does not only depend on the pollutant concentrations the person is exposed to, but also on their individual characteristics and the person's inhalation rate, and hence on their level of physical activity [141] (see Section 6.1). Neglecting the inhalation rates of the population sample may introduce further uncertainties in health studies. For instance, Int Panis et al. (2010) found that cyclists received a $PM_{2.5}$ dose 4.3 times higher than (physically less active) car drivers; even though both groups were exposed to similar pollution levels [63].
The combination of exposure misclassification and the neglect of activity levels may lead to large errors in the air pollution dose estimations of study populations, and consequently to large uncertainties in the resulting associations between air pollution exposure and health effects.

[3]For instance, the London Air Quality Network (LAQN) operates ca. 100 monitoring stations [London Assembly] across an area of ca. 1500 km^2 (Greater London) representing a population of almost nine million people.

1.3 Importance of personal monitoring

The previous section stressed that epidemiological research on air pollution is still fraught with large uncertainties due to inaccurate exposure measures and static populations. These methods suffer from inter-pollutant correlations and exposure misclassification. To overcome these challenges, air pollution exposure measurements need to be tied to individuals; which requires changing exposure estimation techniques to more portable and flexible approaches. Personal monitors reduce the exposure misclassification and are considered the gold standard for accurate exposure measurements [96]. Moreover, the low costs and simple use make personal sensors attractive for citizen science and awareness-raising projects. However, the miniaturisation and flexible operating conditions will inevitably compromise the the performance of personal monitors compared to established standard instrumentation that can be operated under controlled environmental conditions. Scientists have expressed their concerns regarding the performance of the sensors, and remarked that mass applications by non-experts, who are unaware of the limitations of the monitors, may lead to large volumes of erroneous air quality data which may mislead policy decisions on air pollution mitigation strategies [84]. Many scientists have stressed the importance of a thorough, ideally standardised validation process to ensure sufficient data quality of newly developed personal sensors [84, 27, 69, 136, 98, 116, 12]. The following section provides an analysis of recent studies that deployed personal air quality monitors with regard to the performance assessment of the deployed sensors. The overview combines the work of two literature reviews on personal sensors from Rai et al. (2017) [116] and Morawska et al. (2018) [98].

Rai et al. reviewed various performance characteristics[4] of a large range of low-cost air pollution monitors, finding that *"while many scientific studies have utilised low-cost PM and gaseous sensors in a variety of air pollution monitoring activities, only a few have reported sensor performance characteristics and the associated data quality"*.

Morawska et al. systematically reviewed low-cost sensors and monitoring platforms that have been applied in research and/or citizen science projects up to 2017. Morawska concluded that, although recent developments in the field of miniaturised sensors *"enable a revolutionary shift in air pollution monitoring and assessment"*; insufficient performance assessment might lead to unsuitable applications of the low-cost sensors.

Most sensors assessed by Rai et al. and Morawska et al. focused on measuring only one or

[4] accuracy (agreement between sensor and reference instrument), reproducibility (agreement between colocated sensors, R^2_{xx}), limit of detection (LOD), interference with environmental factors such as wind, temperature, pressure and relative humidity (ΔX_{met}), response times (t_r), cross-interference with other pollutant species (ΔX_{X-Y}), sensor stability is the change in sensitivity over long time intervals (ΔX_t), and the impact of particle characteristics such as size distribution and composition on particulate matter measurements (ΔX_{part})

two pollutant species whereas multiple pollutant approaches might be required to overcome the current challenges in epidemiological research ([39], see Section 4.4.1). Hence, the following analysis will focus on multi-pollutant[5] monitoring platforms.

Table 1.1 combines the large database of sensor evaluation studies created by Morawska et al. (Supplement) with the rigorous performance criteria of Rai et al. . The table summarises which of Rai's performance criteria were addressed in each study and whether they were acknowledged only (+), corrected for in a generic way (e.g. using correction factors provided by the manufacturer, ++), or experimentally quantified and individually corrected for each sensor (+++).

Due to different environmental conditions, the sensor performance found in controlled laboratory experiments might differ from the performance found in static daily life environments (indoor, outdoor) or mobile sensor applications. Therefore, Table 1.1 specified the experimental environments in which the sensor performance was tested.

Out of the 21 examined studies, 16 colocated the personal sensors with static outdoor monitoring stations, but only 12 of these were in close proximity with the reference. Laboratory tests to evaluate the sensor performance were performed in 7 studies, usually in addition to outdoor colocations (6 of 7). Out of the 4 studies that performed additional tests (other), one study assessed the indoor sensor performance by placing it into an experimental room of a known volume and injecting pollutants of a defined concentration into the room[25]. Three studies assessed the performance of the monitors in movement by comparing the mobile (outdoor) measurements to nearby static reference stations [49, 58] or by qualitatively comparing the pollution levels between different microenvironments [66].

Of the 21 validation studies, only one study [94] assessed all 7 selected performance criteria quantitatively while the majority of studies evaluated only one or two criteria. Most studies focused on the accuracy (i.e. agreement between sensor and reference), the limit of detection (LOD) and sensor interference with the environment. Just six studies were concerned with the sensor response time (3 x quantified, 3 x mentioned) and only one study [132] considered the PM composition by separating the particles into size bins via a cyclone inlet. Note, however, that their low-cost instrument ("Mini Air Station") was designed for static use only. Another study discussed the impact of PM characteristics on PM measurements theoretically [26]; the rest did not consider these limitations at all. Six studies did not address any of the performance criteria [20, 55, 62] or only mentioned some of the criteria in their discussion[49, 75, 123].

Table 1.1 demonstrates that many studies that deployed personal multi-pollutant monitors did not sufficiently characterise their instruments. Most studies determined the accuracy of

[5] measuring more than two pollutants

the sensors by comparing them to reference instruments. However, these experiments were mostly conducted outdoors and under static conditions, whereas the monitors need to be deployed indoors and in a mobile configuration to collect personal exposures. Other performance characteristics, such as the LOD and the cross interference with other pollutants, were rarely considered, making sensor performance comparisons between studies difficult. The impact of particle characteristics on particulate mass measurements still poses a big challenge in the field of miniaturised sensors that has not been properly addressed by any of the reviewed studies. This overview stresses the need for more thorough validation procedures for novel sensors that should ideally follow standardised protocols.

Table 1.1 Overview of studies that evaluate the performance of portable air pollution monitors based on the performance criteria by Rai et al. [116] (legend at bottom of table). All studies reviewed by Morawska et al. [98] that assessed multi-pollutant monitors were compared.

Ref	**Monitor name**	**Dimensions** (cm)	**Pollutants**	**Colocation with ref** lab	outdoor	other	$\mathbf{R^2_{xx}}$	**LOD**	ΔX_{X-Y}	ΔX_t	ΔX_{met}	ΔX_{part}	$\mathbf{t_r}$
[1]	unnamed	35x25x15*	CO, NO_2, PM				+++	+	-	-	-	-	-
[17]	6 different monitors	various	various		x		-	-	++	-	++	-	-
[20]	uSense	35x25x15*	CO, O_3, NO_2	x	x**		-	-	-	-	-	NA	-
[25]	unnamed	NA	CO, VOC, NO_2, CO_2, O_3			x	+++	+	-	-	+	NA	+++
[26]	AQMesh	25x22x17	NO, NO_2, O_3, CO, PM	x	x		+++	+++	+++	+++	+++	+	-
[30]	APOLLO	NA	CO, CO_2, NO_2, PM, VOC	x			-	+	-	-	++	-	+++
[49]	EveryAware	20x15x8*	VOC, CO, O_3, NO_2, CO, H_2		x**	x	-	-	+	-	+	NA	-
[55]	ILM	43×33×20	PM, UFP, NO_2, O_3		x		+++	-	+	+	+	-	-
[58]	unnamed	30x20x15*	CO, O_3, NO_2, UFP			x**	-	-	-	-	-	NA	-
[59]	unnamed	NA	CO, NO, NO_2, CO		x**		-	+	-	+	++	NA	+
[62]	VIEW	NA	SO_2, O_3, CO		x		-	-	-	-	-	NA	-
[66]	CamPerS	19x9x3	NO, NO_2, CO	x	x	x	+++	+	+	-	++	NA	-
[67]	AQMesh	25x22x17	NO, NO_2, O_3, CO, SO_2		x		+++	+	+	+++	+++	-	-
[75]	AirSensEUR	40x30x20*	O_3, NO_2, NO, CO				-	+	+	+	+	NA	-
[85]	Makerbot	NA	CO, O_3, NO, NO_2, SO_2	x	x		++	+++	+++	+	+++	NA	-
[94]	unnamed	19x9x3	CO, NO, NO_2	x	x		+++	+++	+++, ++	+++	++	NA	+++
[95]	CanarIT	18x16x6.5	O_3, NO_2, VOC, PM		x**		+++	+	-	-	+	-	-
[110]	M-Pods	15x10x5*	CO, VOC, NO_2, O_3, CO_2	x	x		+++	+	+	+++	++	NA	+
[123]	AQMesh	25x22x17	NO, NO_2, O_3, CO, PM		x		+	-	+	+	+	-	-
[132]	MAS	29x25x16.5	NO_2, PM, CO	x	x		-	+++	+	+	+++, ++	++	+
[152]	MSS	18x12x4	CO, SO_2, O_3, NO_2, CO_2		x		+++	+	-	-	-	NA	+

Performance criteria after Rai et al. [116]: R^2_{xx} - Reproducibility; LOD - limit of detection; ΔX_{X-Y} - cross-interference with other gases; ΔX_t - drift / stability over time; Δ X_{met} - interference of meteorological changes (temperature, humidity, pressure, wind); ΔX_{part} - impact of particle characteristics; response time - t_r

+ criterion was acknowledged (e.g. mentioned in the description of the monitor or discussed in the limitations) but not quantified or corrected for

++ criterion was corrected for in calibration process (e.g. correction of temperature effects in NO sensors with auxiliary electrode)

+++ criterion was experimentally quantified and corrected for (if applicable)

- criterion was neglected in performance assessment; NA criterion is not applicable for selected pollutants

* dimensions estimated from picture

** reference instrument not colocated

CO - carbon monoxide, CO_2 - carbon dioxide, $NO_{(2)}$ - nitrogen (di)oxide, O_3 - ozone, PM - particulate matter, VOC - volatile organic compounds, UFP - ultrafine particles, SO_2 - sulfur dioxide, H_2 - hydrogen

1.4 Aim and objectives of this dissertation

Although there is clear evidence that air pollution has a negative impact on human health; inadequate exposure metrics led to exposure misclassification and interdependence between pollutant species which impede the creation of reliable and specific epidemiological evidence. Recent advancements in portable sensing technologies enable a paradigm shift in air quality data collection [79, 93, 83], but concerns about the performance and validity of such data remain [84].

The overall aim of this study is to develop a novel methodological framework that estimates personal air pollution exposure and dose reliably at high spatial and temporal resolution. The specific objectives of this study are:

1. To assess the performance of a personal air quality monitor (PAM) across distinct geographical settings and meteorological conditions, and to deploy it to diverse cohorts;
2. To improve air pollution dose estimations by combining activity information with exposure measurements at the individual level;
3. To compare the novel approach with conventional epidemiological methods;
4. To demonstrate the value of the novel analysis methods to disaggregate personal exposure by the type of emission source; and
5. To present a number of case studies which provide insight into air pollution risks of different environments and activities.

Chapter 2

Design, operation and deployment of the personal air quality monitor (PAM)

The previous chapter emphasised the urgent need to tackle the growing problem of air pollution in order to protect the global population from non-communicable diseases and premature death. Current limitations in epidemiology prevent scientists to uncover causal relationships between individual pollutant species and specific health effects. Novel sensing technologies allow a paradigm shift from static outdoor to personal exposure monitoring in large-scale studies, and have the potential to address current epidemiological limitations such as exposure misclassification and multicollinearity in health models introduced by the correlation between individual pollutant species.

The following chapter introduces the Personal Air Quality Monitor (PAM), a novel sensing device which is the central subject of this dissertation. Section 2.1 describes the setup of the monitor; calibration and data processing protocol of the collected measurements are explained in Section 2.2. Section 2.3 describes the datasets collected during four main PAM deployments in the UK, China, Germany and Kenya, which build the backbone of this work.

2.1 The Personal air quality monitor

The PAM [1] (Figure 2.1) is a portable platform to measure several air pollutants and additional physical parameters including temperature, relative humidity, acceleration, ambient noise levels, and location (the monitored quantities are presented in Table 2.1). Owing to the compact and

[1] Atmospheric Sensors Limited, Bedfordshire, UK. Developed at the Centre for Atmospheric Sciences, University of Cambridge.

lightweight design (13 cm × 9 cm × 10 cm, ca. 500 g), as well as the long battery life[2], the PAM can be used for personal air pollution exposure assessment without interfering into daily life activities. The PAM can be worn with a shoulder strap or attached to a belt. No other input is required by the user other than to place it daily in a base station for charging and data upload. The device works unattended and under almost silent conditions, which makes it suitable for deployments in home and working environments. The combined cost of the sensors alone is less than £600 and the total cost of the PAM is less than £2,000 making it a "lower-cost" system [38]. Combined with the low maintenance costs, this allows deployments in large scales as well as in areas with little research infrastructure.

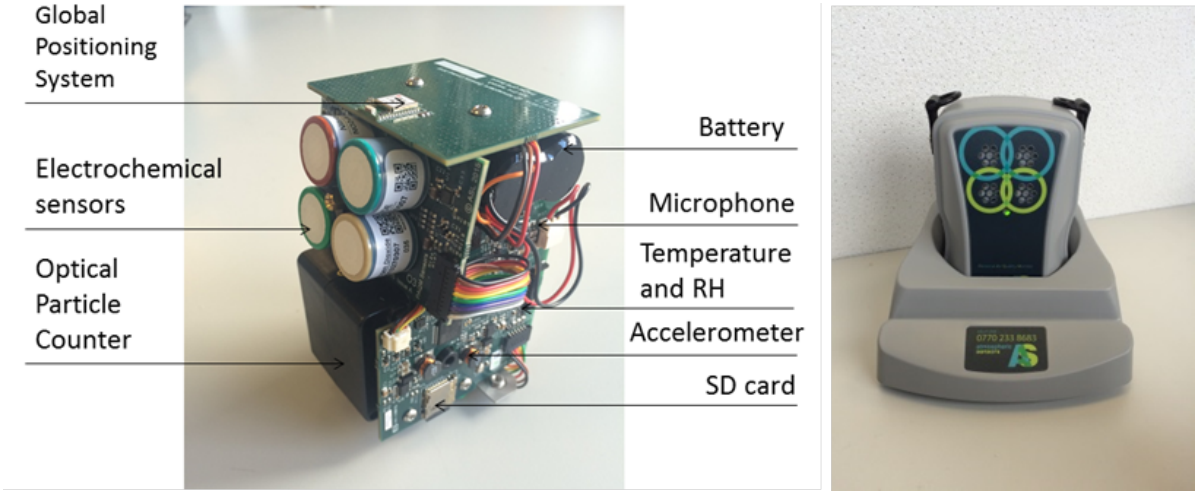

Fig. 2.1 Setup of the PAM (left) and PAM in charging station (right).

Table 2.1 Summary of parameters monitored by the PAM and their corresponding sensor types. A more comprehensive overview of the raw PAM outputs including sampling rates and units is given in Table 2.2.

Parameter	**Method**
CO, NO, NO_2, O_3	Electrochemical sensors
PM_1, $PM_{2.5}$, PM_{10}	Optical particle counter (OPC)
Relative Humidity (RH)	Electrical resistive sensor
Temperature	Thermocouple
Physical activity	Tri-axial accelerometer
Background noise	Microphone
Spatial coordinates	Global Positioning System (GPS)

[2] 29 hours between charges, optical particle counter turns off after approximately 15 hours.

The sensor types integrated into the PAM were chosen based on sensor sensitivity, selectivity, environmental interference, size and cost. A brief overview of different miniaturised air pollution sensors is given in Section A.1.1.2 in the Appendix. The advantages and disadvantages of the sensors integrated in the PAM are discussed in the following paragraphs.

2.1.1 Electrochemical sensors for gaseous pollutants

For the measurements of CO, NO, NO_2 and O_3, electrochemical (EC) sensors were selected. Although metal oxide sensors are less costly and slightly smaller than EC sensors, they have higher power requirements and are less reliable as they suffer from measurement instability and drift, poor selectivity, and temperature and RH effects [116]. EC sensors may also be affected by temperature and RH fluctuations, however, the interference is less severe and can be corrected with appropriate post-processing [27, 29]. The selectivity of EC sensors can be improved with appropriate electrode materials and filters, although cross-interference between some gases (e.g. O_3 and NO_2) still remains [27, 136]. By selecting both O_3 and NO_2 sensors for the PAM, the cross interference between these two pollutants can be adjusted through post-processing (Section 2.2). Spectroscopic sensors would be more sensitive to the target gas and less affected by RH or temperature [93]. However, these sensors were not chosen due to selectivity issues and much higher costs [136].
The PAM integrates Alphasense A4 sensors (CO-A4 [7], NO-A4 [9], NO_2-A43F [6], Ox-A431 [8]) of 20 mm diameter that are based on an amperometric principle of operation [150] for the quantification of carbon monoxide (CO), nitric oxide (NO), nitrogen dioxide (NO_2) and ozone (O_3). The devices operate on a four electrode system, where the conventional setup of working, counter and reference electrode is supplemented with an additional auxiliary (or non-sensing) electrode, to compensate for the temperature dependence of the cell potential [114]. A more detailed description of the operation principle is given in Section A.2.1.1 in the Appendix.
Earlier variants of these EC sensors have been extensively characterised in laboratory conditions and in static outdoor sensor networks (for example [94]). Those studies provided evidence that, after appropriate post-processing, the sensors had a linear response to the targeted pollutants and achieved excellent performance with limits of detection (LOD) < 4 ppb, demonstrating their suitability for atmospheric air quality measurements.

2.1.2 Optical particle counter ($PM_{2.5}$)

To measure particulate matter, an optical particle counter (OPC) was selected. These type of devices are able to classify particles into different size ranges which allows a size-specific correction of RH interference [44]. However, all optical PM sensing devices suffer from the limitation that they cannot detect particles below a certain diameter (300 - 500 nm, depending on sensor setup [69]). Acoustic resonators or microbalances present substantially smaller alternatives to OPCs which do not suffer from a limited detectable size range. However, temperature interference and signal saturation due to mass loading might impede deployments over longer time periods or in highly polluted environments [146].
The PAM integrates a commercially available miniaturised particle counter (Alphasense OPC-N2 [5]) which uses Mie scattering for real-time aerosol characterisation. Particles pass through a sampling volume illuminated by a light source (in this case a laser) and scatter light into a photo detector. The amplitudes of the detected scattering pulses are related to the particle size. The OPC counts these pulses and typically sorts them into different particle size bins [145]. The OPC-N2 classifies particles in 16 sizes (bins) in the range 0.38 - 17 µm. The procedure to convert the particle counts into mass concentrations is described in Section 2.2.3. The laboratory comparison of this OPC model with reference instrumentation showed a high degree of linearity [127]. Similarly, studies evaluating the OPC performance in outdoor static deployments [44, 37] showed that, once site- and season-specific calibrations were applied, the miniaturised sensor could be used to quantify number and mass concentrations of particles with an accuracy and precision similar to other standard commercial PM instruments. Although the OPC-N2 is capable of measuring PM_1, $PM_{2.5}$ and PM_{10}, this work will focus on $PM_{2.5}$ measurements only. This fraction was chosen because the PM_1 measurements are regarded as less reliable since a major part of the fraction (<0.38 µm) cannot be detected by the OPC [127], and PM_{10} may be less relevant for health outcomes, as $PM_{2.5}$ penetrates deeper into the body [149].

2.2 From the raw measurements to the final exposure data

This section describes the procedure to clean, calibrate and ratify the PAM data to generate reliable exposure and dose estimations from the raw PAM recordings. Figure 2.2 gives an overview of the individual steps from the raw outputs of the PAM to a final dataset. User-friendly, bespoke scripts have been developed to automate the management and post-processing of the large volume of raw data collected with the PAM networks. All post-processing and

data analysis was performed in R software [115]. The concentration of each pollutant was determined from the very raw output of the sensors (given in voltages and counts, see Table 2.2). This way, full control over the data and the physical significance of each processing step was maintained. After each post-processing step, the data were stored in a separate SQL table[3] to allow immediate access at each stage (Level 0 to Level 3).

The following sections describe the data processing steps to generate a fully calibrated and ratified exposure dataset (Level 2 in Figure 2.2). The estimation of the air pollution dose (Level 3) is described in Chapter 6. The "evolution" of the PAM data through each step is visualised using measurements of a participant (U123) from the AIRLESS project as illustrative example. The participant lived in urban Beijing and volunteered to carry the PAM for one week of their daily life. Further details of the AIRLESS project are given in Section 2.3.2.

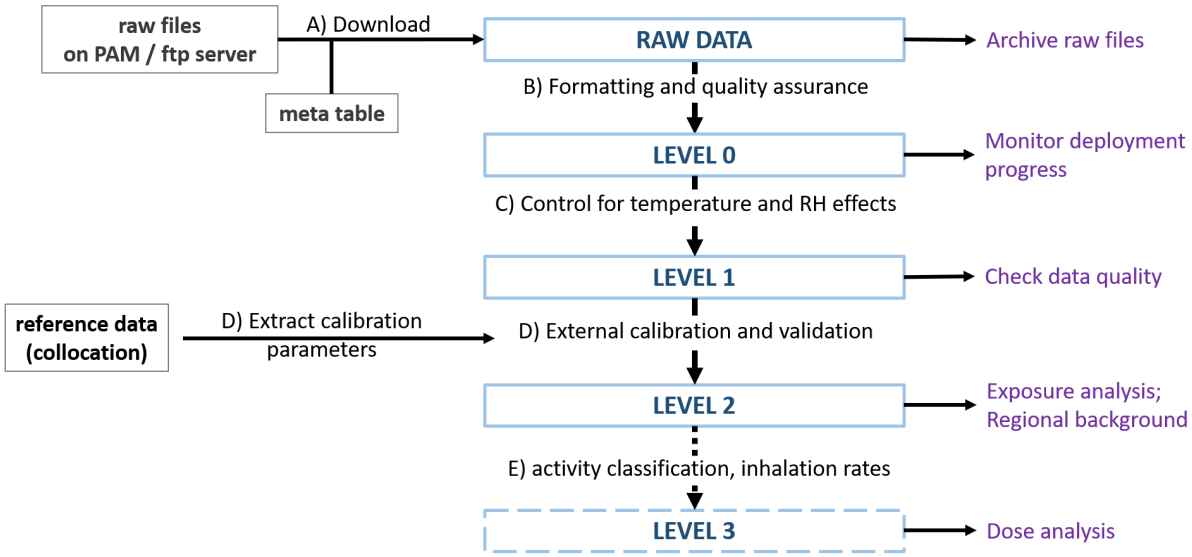

Fig. 2.2 Flow chart of the individual processing steps to convert raw PAM data into a final dataset that can be used for personal exposure and dose assessments. Required input data on the left (in grey boxes), processing steps in the middle (blue boxes) and function/application of the output of each data processing step on the right (purple). The estimation of the air pollution dose (Level 3) is described in Section 6.2.

[3]The PostgreSQL relational database management system is used because it is open source, has an unlimited row-storage capacity and allows the querying of large quantities of data in a flexible manner while maintaining performance as the volume of data grows.

2.2.1 Level 0: Data download, formatting and quality control

Raw PAM measurements

The measurements were recorded as comma separated values (".csv") which were segmented into individual 15-minutes files and saved on an SD card inside the monitor. From there they were uploaded through GPRS to a secure access FTP server using a phone SIM card placed inside the charging station of the PAM. Alternatively, the data could be manually downloaded from the SD card inside the PAM (e.g. when no network connection was available).
Table 2.2 gives an overview of the raw output parameters of the PAM. The time resolution of the collected measurements varied between the sensors (see "Sampling time" column). In this work, the data were averaged on-board over 1-minute intervals[4] before they were written into the .csv file.
Each measurement was assigned to a time stamp taken from the GPS sensor. When no GPS was available, the time stamp of the internal PAM clock, which was daily synchronised with the GPS time, was used.
Due to heat generated by the internal battery, the PAM's internal temperature was higher than the ambient temperature. The external temperature outside the PAM case was modelled based on experimental data and output by the PAM as "adjusted temperature".
The gas measurements (NO_2, O_3, CO, NO) were collected with electrochemical sensors as described in Section 2.1.1. Particulate matter was measured via an OPC (Section 2.1.2) with a sampling time of 20 sec per minute to save battery power. Estimations of the PM_1, $PM_{2.5}$, PM_{10} mass concentrations from the bin counts were already provided by the manufacturer. However, these were discarded as they were not corrected for humidity effects.
The noise and acceleration recordings were intended for relative comparison only (not calibrated). Four threshold values for each of the two parameters were experimentally set, and the PAM recorded how often and for how long these thresholds were crossed each minute (100 Hz sampling rate).
The quality of the GPS connection was assessed via the number of satellites the PAM was connected to and the horizontal dilution of precision. The GPS connection can be obstructed by building walls, therefore these parameters could be used to distinguish between indoor and outdoor locations.
Besides the raw PAM outputs, external parameters were required for the creation of the final exposure dataset. These included measurements from reference instruments for the PAM

[4] The time resolution of the PAM can be customised.

calibration and a meta table that contained the deployment information of the PAM networks (deployment times, assigned PAM of each participant, etc).

Table 2.2 Raw output parameters of the PAM as they were uploaded to the server.

Parameter	**Output unit**	**Sampling time**	**Comments**
General			
node ID		1 min	individual PAM ID number
date, time		1 min	from internal PAM clock and GPS
internal and adjusted temp	°C	4 sec	adjusted = external temperature
internal and adjusted RH	%	4 sec	adjusted = external RH
remaining voltage in battery	V	1 min	
input voltage from base station	V	1 min	charging variable
Air Pollution: Gases			
working electrode signal of each electrochemical sensor	mV	0.01 sec	
auxiliary electrode signal of each electrochemical sensor	mV	0.01 sec	
Air Pollution: Particulate Matter			
sample flow rate	mL/sec	1 min	20 sec sampling, 40 sec off
sampling period	s	1 min	set to 5 sec
bin counts	counts	1 min	16 size bins (OPC model N2)
PM_1, $PM_{2.5}$, PM_{10}	µg m^{-3}	1 min	provided by manufacturer
Background noise			
microphone RMS level	mV	0.01 sec	Root mean square level; 1 min cycle = 6000 samples/min; output parameters below
mean RMS level	mV	1 min	mean over 1 min cycle
min RMS level	mV	1 min	minimum over 1 min cycle
max RMS level	mV	1 min	maximum over 1 min cycle
standard deviation of the RMS	mV	1 min	SD over 1 min cycle
counts when the RMS value crosses threshold	counts	1 min	thresholds: 5, 10, 20, 40 mV
counts when the RMS value is greater than or equal to threshold	counts	1 min	thresholds: 5, 10, 20, 40 mV
Acceleration			

SVM	mg	0.01 sec	Signal Vector Magnitude; average acceleration over x, y and z axis
mean SVM	mg	1 min	mean over 1 min cycle
min SVM	mg	1 min	minimum over 1 min cycle
max SVM	mg	1 min	maximum over 1 min cycle
SD of the SVM	mg	1 min	standard deviation over 1 min cycle
counts when the SVM crosses threshold	counts	1 min	thresholds: 0.8, 0.9, 1.2, 1.3g
counts when the SVM is greater than or equal to threshold	counts	1 min	thresholds:0.8, 0.9, 1.2, 1.3g
Location (GPS)			
longitude, latitude	degrees	1 min	
altitude	m	1 min	
number of satellites	counts	1 min	Quality of GPS connection
Horizontal dilution of precision	m	1 min	Quality of GPS connection

The data processing script automatically downloaded all 15-min file segments that were recorded during a specified period of time (determined via the meta table) from the ftp server and archived the files in local directories. The raw segments were bound to a time-continuous data frame. Figure 2.3 shows a time series of the raw output signals from the NO_2 sensor and the OPC. Both graphs are dominated by large outlier values that were caused by corrupt data entries.

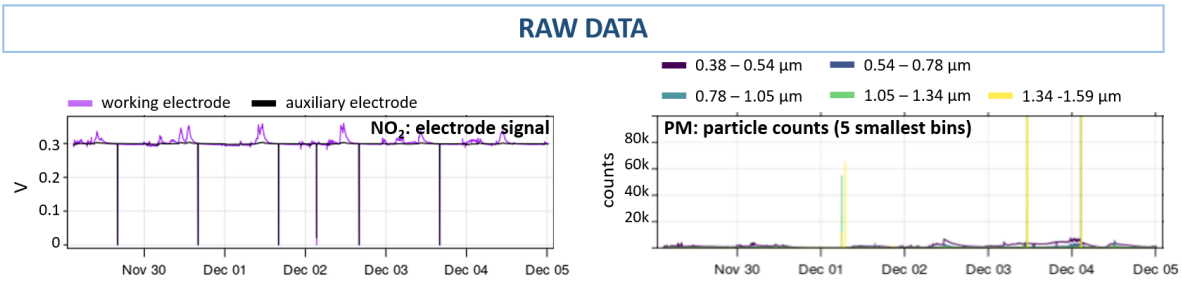

Fig. 2.3 Illustrative example of the raw output from the air pollution sensors. Left: Electrode signals of the NO_2 sensor. Right: Particle counts of the 5 smallest size bins of the OPC. Time in UTC.

Level 0: Basic data quality control

Corruption of data rows when writing onto the SD card might lead to erroneous data entries in the raw measurements (e.g. large signal spikes as seen in Figure 2.3). Entries that contain values outside a physically meaningful range (e.g. RH > 100% or Longitude > 180°) were discarded. An overview of the defined data ranges for each variable is given in Table A.2 in the Appendix.

The Level 0 data were stored in an SQL data base and could be visualised instantaneously as a time series or a spatial plot to monitor the deployment progress daily (e.g. to identify malfunctioning sensors or participants who forgot to charge the PAMs over night). An example of the resulting Level 0 data is given in Figure 2.4, with the outputs of the NO_2 sensor on the left. The working electrode signal (magenta) represents the sum of the signals caused by electrochemical reactions with the target gas (NO_2) and by environmental interference (e.g. temperature fluctuations). The auxiliary electrode, which was not exposed to the gas, recorded only the effect of the environmental changes. More details of the principle of operation are given in Section A.2.1.1.

The right graph of Figure 2.4 shows a time series of the particle counts in the 5 smallest size bins of the OPC (0.38-1.59µm). The highest particle counts were observed at diameters between 380 and 540 nm.

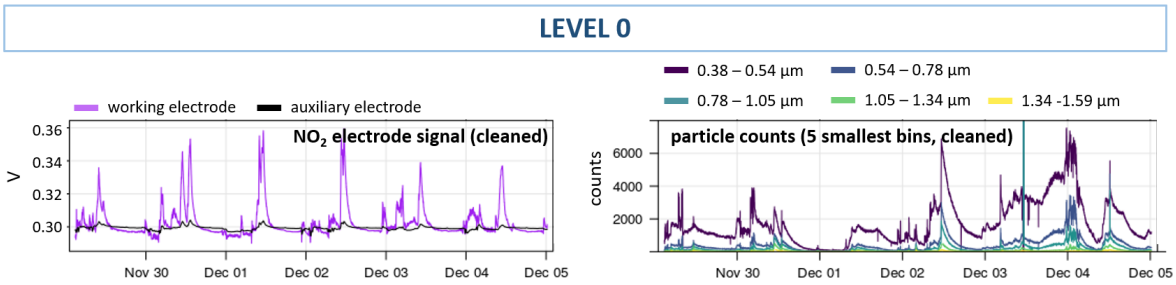

Fig. 2.4 Illustrative example of the Level 0 output from the air pollution sensors (raw data cleaned from corrupt data entries). Left: Electrode signals of the NO_2 sensor. Right: Particle counts of the 5 smallest size bins of the OPC. Time in UTC.

2.2.2 Level 1: Artefacts caused by temperature and humidity

False responses of the EC sensors to rapid temperature changes

Moving rapidly between microenvironments that differ in temperature (e.g. from outdoors to a warmer indoor environment) causes false peaks in the EC sensor measurements [3]. The

response and recovery time following rapid temperature transitions was experimentally determined by moving the sensors between a heated indoor environment (>20°C) and a cooler outdoor environment (10-15°C; see Section A.2.1.3 in the Appendix). The recovery times varied between the different gas sensors, with the CO sensor being affected by the temperature change for longer (< 15 min) than the NO, NO_2 and O_3 sensors (< 5 min).
To account for the false sensor responses, the temperature transitions were automatically detected based on the RH changing rate[5]. A 15-min window for CO and a 5-min window for NO, NO_2 and O_3 measurements was removed from the data. Note that in the first cleaning step (Section 2.2.1), the entire data entry was deleted when a physically unrealistic value was identified, whereas only the readings of the EC sensors were removed at rapid temperature transitions. The left of Figure 2.5 compares NO_2 measurements before (cyan) and after (black) the removal of the false temperature transition signals.
Though it potentially excludes peak exposure events, as rapid temperature changes often occur when people leave heated buildings and enter (colder) traffic environments to commute, this correction method removes typically less than 0.1% of the exposure data. The PM measurements were not affected by these temperature transitions.

Hygroscopic growth of airborne particles

Due to their hygroscopic features, atmospheric particles grow in diameter when exposed to ambient humidity. To maintain the comparability of PM levels between environments of different humidities, the PM mass concentration is defined as the *dry* particulate mass per volume of air. Standard PM measurement instruments dry the particles before the PM mass concentration is measured. This feature was, however, not available for the PM sensor used in this work. Instead, the hygroscopic growth of the particles was corrected for using the method of Di Antonio et al. [44].
This method assumes that the particle diameter increases by a specific growth factor g when exposed to a certain level of humidity. The growth factor g depends on the particle hygroscopicity κ (i.e. the ability to uptake water) , as well as on the RH value the particle is exposed to (Equation 2.1). In this work, the value of $\kappa = 0.61$ was adopted from Di Antonio et al. who had optimised it for urban aerosols in Europe. The growth factor was set to one (i.e. no change of the particle diameter) at RH values below 35% due to efflorescence effects of the particle material [44].
The growth factor was used to retrieve the dry diameter of a particle D_{dry} from the wet particle

[5]The RH sensor of the PAM reacted quicker to environmental changes than the temperature sensor

diameter measured by the OPC at a certain RH $D_{wet}(RH)$. As a result, a new particle number distribution over the 16 size bins was obtained which was then used to calculate the RH adjusted PM mass concentrations (see Section 2.2.3).

The right of Figure 2.5 compares the raw $PM_{2.5}$ measurements (cyan) with the RH corrected measurements (black). It shows that the RH correction has a particularly significant effect at RH values above 65%.

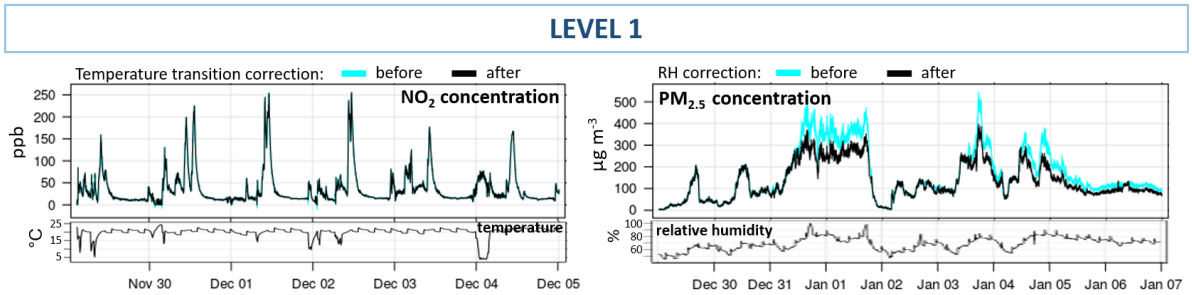

Fig. 2.5 Comparison of PAM output before (cyan, Level 0) and after (black, Level 1) temperature and RH effects were corrected.
Left: Correction of the effect of fast temperature transitions on the NO_2 measurements. Right: Correction of the RH interference with optical PM measurements.
The "saw tooth" patterns in the temperature and RH measurements below the pollutant graphs were caused by the charging cycle of the PAM battery. Time in UTC.

$$g(RH) = \frac{D_{wet}(RH)}{D_{dry}} = \left(1 + \kappa \frac{RH}{100 - RH}\right)^{\frac{1}{3}} \tag{2.1}$$

g	growth factor
D_{dry}	particle diameter in dry state
$D_{wet}(RH)$	particle diameter at a given RH
κ	degree of hygroscopicity
RH	relative humidity

2.2.3 Level 2: Calibration and validation with external reference

Level 0 and Level 1 dealt with data formatting, storage and QA/QC procedures. Level 2 uses measurements from colocation deployments of the PAMs next to certified reference instruments to calibrate the monitors, correct for potential sensor-sensor variability, and to validate the sensor performance.

The colocations were performed under similar environmental conditions and in the same geographical area in which the monitors had been or were to be deployed. The advantage of this

approach over laboratory calibration was that the sensors were exposed to the actual air pollution levels and meteorological conditions under which they were expected to operate. Furthermore, it provided the opportunity to evaluate any potential site-specific cross-interference. In the following section, colocations from the AIRLESS winter campaign are presented as illustrative examples. During the AIRLESS project, 60 PAMs were colocated with reference instruments on the roof of Peking university in Beijing for each 19 days in winter and in summer. Further details of the AIRLESS project are given in Section 2.3.2.

Conversion of raw EC sensor signals into gas concentrations

A linear regression model (Equation 2.2) was applied to the colocation data (reference and PAM data) to determine the calibration parameters a - d needed to convert the raw sensor signals (mV) into mixing ratios (ppb). The temperature dependence of the working electrode can be corrected through the auxiliary electrode AE which may, however, have a different sensitivity than the working electrode WE ($a \neq b$). The cross-sensitivities between the NO_2 and O_3 measurements were corrected via parameter c (the cross sensitive gas Y is NO_2 for O_3 measurements and vice versa). As the CO and NO sensors were found to be sufficiently selective, c was set to zero for the calibration of those sensors.

$$[X]_{ref} = aWE_X + bAE_X + cWE_Y + d \tag{2.2}$$

$[X]_{ref}$	Reference measurement of pollutant X [ppb]
a	sensitivity of the working electrode [ppb / mV]
WE_X, AE_X	raw signal of the working and auxiliary electrode [mV]
b	sensitivity of the auxiliary electrode [ppb / mV] (accounts for temperature)
c	cross sensitivity with gas Y [ppb / mV], c = 0 for CO and NO
WE_Y	raw signal of the working electrode of the cross sensitive gas Y [mV]
d	intercept [ppb]

The calibration model was evaluated by splitting a colocation dataset into two parts: a training period to determine the model parameters, and a testing period to subsequently validate these. The performance test found an excellent performance of the calibration model (see Section 3.1). It should be noted, however, that relationships in regression models should not be extrapolated beyond the range of observations (including meteorological conditions). The calibration periods should therefore be made sufficiently long to cover the temperature and concentration ranges in which the sensors are deployed [38].

As a last data cleaning step, any negative gas measurements that might be caused by sensor

noise at low pollutant concentrations or incomplete removal of the temperature transitions were discarded.

From particle counts to PM mass concentrations

The $PM_{2.5}$ mass concentrations were generated from the particle counts of the RH-corrected size bins of the OPC. The mass of the particles in each size bin was estimated via Equations 2.3 and 2.4 (inserting the dry particle diameter D_{dry} for D_i), assuming a spherical particle shape and a fixed particle density of ρ = 1.65 g cm^{-3} [111]. The particle number concentration n_conc_i was calculated by dividing the particle counts of each bin i by the sampling volume (Equation 2.5). The particulate mass concentration was then calculated as the product of particle mass and number concentration (Equation 2.6 [44]), summed over all size bins.
$PM_{2.5}$ is defined as the mass of dry particles that pass through a size selective inlet with a 50% cut-off efficiency at 2.5 µm aerodynamic diameter[6] [133, 50]. This means that 50% of the 2.5 µm particles contribute to the $PM_{2.5}$ mass, while a larger proportion of the smaller particles and a smaller amount of bigger particles also contribute to the $PM_{2.5}$ fraction. Hence, the different size bins do not equally contribute to the $PM_{2.5}$ mass. A size-specific penetration factor p_i was applied to the mass concentration of each size bin to account for the penetration efficiency [50] (Equation 2.6).

$$V_i = \frac{\pi}{6}(D_i)^3 \tag{2.3}$$

$$M_i = \rho V_i \tag{2.4}$$

$$n\_conc_i = \frac{N_i}{V_{sample}} \tag{2.5}$$

$$PM = \sum_i p_i M_i n\_conc_i = \frac{\sum_i p_i M_i N_i}{V_{sample}} \tag{2.6}$$

[6]The aerodynamic diameter of an irregular particle is defined as the "diameter of the spherical particle with a density of 1000 kg/m^3 and the same settling velocity as the irregular particle." [60]

V_i	volume of a particle in size bin i
D_i	diameter of particles in bin i
M_i	mass of a particle in bin i
ρ	density of particle material
n_conc_i	number concentration of particles in bin i
N_i	particle counts in bin i
V_{sample}	sampling volume
PM	particle mass concentration
p_i	penetration factor

In the final step, a linear fit between the RH-corrected PM measurements and the reference measurements was performed. A scaling factor for each OPC was extracted to account for particle densities differing from the one initially assumed, and for the under-prediction of mass due to undetected smaller particles and sensor-sensor variability (e.g. caused by different reflectivities of the optical sensor components).

Validation of the concentration measurements

The comparison between PAM and reference was used to ratify the pollutant measurements and identify malfunctioning sensors or potential errors in the calibration process. Figure 2.6 compares the calibrated Level 2 data (PAM 165) with reference measurements of NO_2 and $PM_{2.5}$ during the colocation deployment of the AIRLESS campaign. The PAM measurements closely followed the concentrations measured by the reference instrument, as shown in the time series (top). The high agreement between the PAM sensors and reference instruments can also be found in the scatter plots (bottom, coefficient of determination $R^2 \geq 0.90$), suggesting that any interference with other pollutants or meteorological factors has been sufficiently corrected for. A more comprehensive validation of the sensor performance is given in Chapter 3.

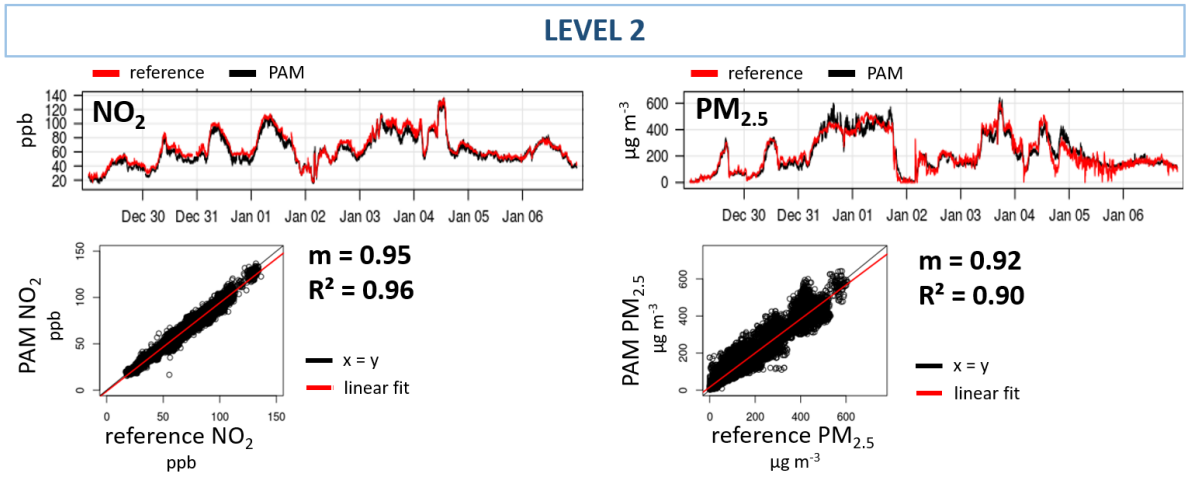

Fig. 2.6 Comparison of the final NO_2 and $PM_{2.5}$ concentrations (Level 2) with colocated reference measurements in form of a time series (top) and scatter plots (bottom). Time in UTC.

The pollutant concentrations resulting from Level 2 were fully calibrated and ratified. They served as personal exposure (i.e. the concentration in the direct environment of a person) measurements of participants and may be used, among others, for the evaluation of exposure risks (Chapter 4) or source attribution analyses (Chapter 5). The measurements may be further refined by estimating the air pollution dose, i.e. the amount of air pollution that is inhaled by the body, which is described in Chapter 6.

2.3 Deployment of the PAM: Measurement campaigns

The previous section introduced the PAM as alternative to conventional exposure measurement methods. In this work, a total of 85 PAMs were deployed in four different countries as indicated in Figure 2.7. The measurement data collected in these settings form the backbone of this dissertation. Table 2.3 gives an overview of the gathered personal exposure data including deployment dates, duration and location; numbers of deployed PAMs and study volunteers; a brief description of the type of experiment; and the percentage of captured observations[7]. In total, 3,771 measurement days were collected from over 300 volunteers. The data capture during the field deployments was generally high with 77-93% of the theoretically possible number of records being obtained (see Equation 2.7).

[7]Data loss can be due to missed charging of the PAM, failed data transmission or data removal in the basic cleaning step, see Section 2.2.

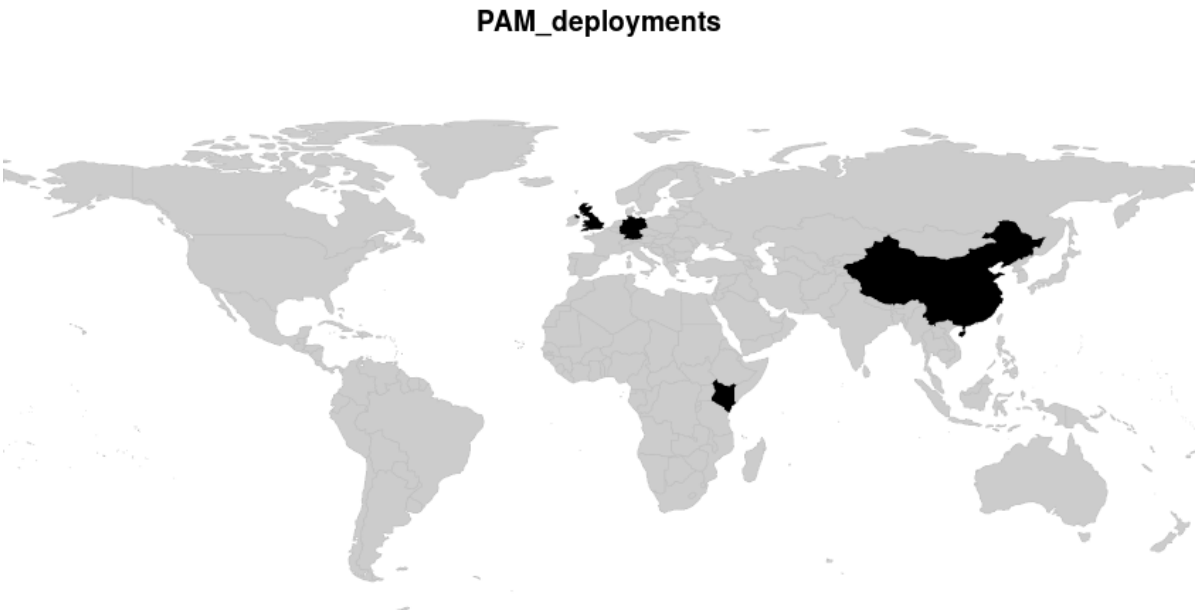

Fig. 2.7 World map with countries in which PAM deployments for this work were conducted marked in black.

For calibration and validation purposes (see Section 2.2.3), the PAMs were colocated with reference instruments in each project. A summary of the colocation datasets is given in Table 2.4. More information about the reference instruments used for each colocation are given in Table 3.1 in Chapter 3.
The following sections will describe the data collection procedure for each of the four field campaigns this work is based on.

Table 2.3 Overview of the collected personal exposure datasets.
Ambient air quality data and baseline participant questionnaire data (not applicable for metro project) are available to complement all datasets.

Project	**Collection period**	**Location**	PAMs	N	**Deployment type**	t (d)	c	**Additional data**
Pilot	July-Dec 2015	Cambridge, London (UK)	18	38	personal exposure in daily life	388	81%	activity diaries
AIRLESS	Nov 2016-July 2017	Beijing, Pinggu (China)	60	251	personal exposure in daily life	3288	79%	medical data
Metro	Sep 2018	Berlin (Germany)	1	NA	exposure in metro systems	1	93%	manual location tracking
Cooking fuels	May 2019	Dunga Beach (Kenya)	6	12	cooking exposure in households	94	77%	Cooking fuel use

PAMs - Number of deployed PAMs; N - number of participants; t (d) - total recorded time in days; c - percentage of captured observations

Table 2.4 Static colocations of PAMs with reference instruments during the four main field deployments for calibration and validation purposes.

Project	**Collection period**	**Location**	**PAMs**	**t(d)**	c	**Reference data**
AIRLESS	Nov 2016-July 2017	regional background, Beijing	60	2x19	winter: 85% summer: 54%	Peking University
AIRLESS	May 2017	indoor (residence), Beijing	2	12	86%	York University
Pilot	Nov 2015	regional background, Cambridge	3	10	99%	Cambridge University
Metro	Sep 2018	highly frequented road, Berlin	1	7	94%	Berlin air quality network (BLUME)
Cooking exposure	July 2019	main square of Dunga village	6	24	63%	AQMesh (Cambridge)

t(d) - colocation time in days; c - data capture (number of recorded observations/theoretical number of observations between deployment start and end)

$$c = \frac{N_{recorded}}{N_{theoretical}} \tag{2.7}$$

$N_{recorded}$ number of recorded observations

$N_{theoretical}$ theoretical number of observations between deployment start and end

2.3.1 Pilot project in Cambridge and London, UK

The pilot deployment of the PAM aimed to test the acceptability of the PAM as novel sensing technology and the feasibility of collecting data with it during daily life activities. The dataset was also used to develop the time-location-activity classification described in Chapter 6. The deployment used a small sample of 38 participants in London and Cambridge in 2015.

Data Collection

Healthy participants from London and Cambridge were recruited via the exhibition of flyers and email distribution lists at the Department of Chemistry (University of Cambridge) and the Department of Analytical Environmental Sciences (King's College London). Participants who were willing to participate in the study were asked to carry the PAM close to their body for one week of their daily lives while keeping an activity diary via a smart phone app (smart phones were supplied by the university on request). The reported activities were defined by the volunteers and later sorted into activity categories with assigned inhalation rates[8] following Table 2.5. Additional information such as age group, sex and socio-economic status were acquired via a questionnaire. The participants did not receive compensation for their contribution; however a

[8]The inhalation rates were used to calculate the air pollution dose, see Chapter 6.

brief evaluation of the activity and location dependent exposure data was created and send to them as feedback.

Table 2.5 Categorisation of reported activities in participants' diary logs during the Pilot project. Assigned inhalation rates were also used for the dose estimations in the AIRLESS project (see Chapter 6).

Category	**Reported Activities**	**Inhalation rate (L/min)**	**Reference** [141]
home	home (excluding sleep), resting, eating, cooking, shower, computer, TV, reading/studying, housework	general: 8.94	Table 6-5
sleep	sleeping	5.50	Table 6-48
other static	work, lab, meeting, lecture, cinema, cafe, pub, restaurant, church, library, hospital, dentist, shopping	predominantly sedentary: 8.51	Table 6-40
transit	walking	22.2	Table 6-40
	cycling	moderate activity: 39.2	Table 6-42
	car, taxi, bus, bus stop	9.87	Table 6-40
	motorcycle	as car: 9.87	Table 6-40
	tube, train, overground, incl stations	mean (car - sitting): 9.19	Table 6-40
NA, no label	left monitor home, monitor covered, *no diary entries*	general: 8.94	Table 6-5

Outdoor air pollution levels were available from a monitoring station on the roof of the Chemistry Department in Cambridge and from North Kensington station[9] of the London Air Quality Network (LAQN [King's College London]). All 24 sensors were deployed in a controlled indoor environment over a period of 25 days (Aug 1st - Aug 26th 2015) to assess their reliability and reproducibility before the field deployment. Due to space restrictions only 3 sensors were colocated with reference instruments on the roof of Cambridge University (Nov 6th - Nov 16th 2015). The calibration parameters from this colocation (extracted as described in Section 2.2.3) were extrapolated to the entire sensor network using the indoor colocation data.

[9] A part of the ambient measurements in London was considered unreliable and discarded as described in Section A.2.2.1 in the Appendix.

Description of the cohort

In total, 38 volunteers agreed to participate in this study of which 85% carried the PAM for the 7 suggested study days or longer. Figure 2.8 gives an overview over the length of the individual participation times.
The characteristics of the cohort retrieved from the questionnaire are shown in Figure 2.9. Most participants were aged between 20 and 50 years. The majority of the cohort performed office based occupations which are mainly associated with sedentary activities. All 38 participants used central or electric heating; 7 participants used a gas stove, 19 an electric stove and one participant used both cooking methods. The heating and cooking type might be relevant for personal exposures as they might generate indoor pollutant emissions.
Figure 2.10 shows the visited locations of all participants in London and Cambridge coloured by different modes of transport (as reported in activity diary). Commuting in Cambridge was mainly dominated by cycling and walking whereas participants in London used a mix of transport modes including tube, train, buses, walking and cycling.
The tracked movements on the maps, as well as the willingness of many volunteers to extend the participation time, indicate that the participants did not feel restricted by the PAM when pursuing their daily activities.

Environmental conditions

During the main data collection period (20^{th} Oct - 15^{th} Dec 2015), the temperature ranged from -2°C to 19°C (mean: 11°C) and the RH from 48% to 98% (mean: 82%). The ambient pollutant concentrations differed little between London and Cambridge. Mean ambient concentrations during the main deployment period were 8 ppb for NO, 14 ppb for NO_2, 282 ppb for CO, 19 ppb for O_3 and 10 µg m^{-3} for $PM_{2.5}$ (for more details see Table A.3 in the Appendix).

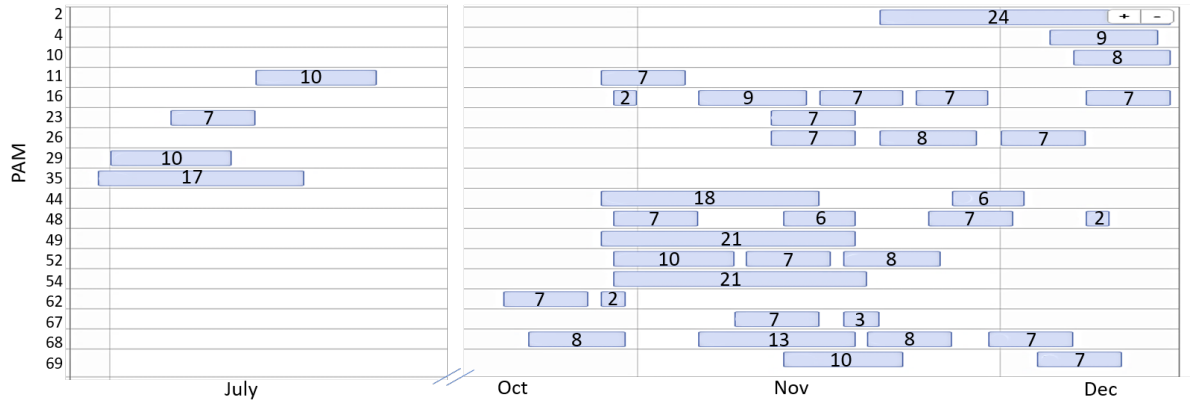

Fig. 2.8 Participation times of individuals in the pilot project cohort. Each bar represents one participant (grouped by PAM number at the y-axis), the number inside the bar gives the days of participation. 15 subjects carried the PAM for 7 days, 6 participants cancelled the deployment earlier (after 2-6 days) and 17 participants offered to keep the PAM for longer (up to 24 days). The average participation time was 8.9 days.

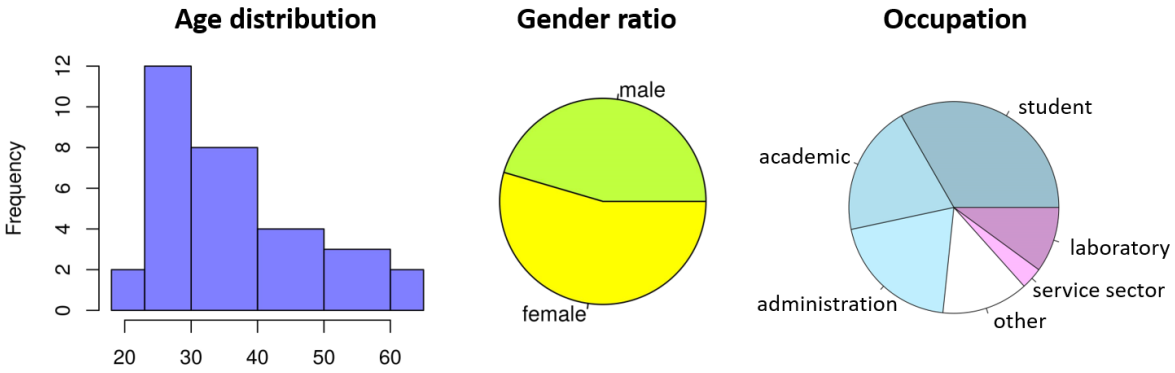

Fig. 2.9 Descriptive statistics of the pilot cohort (London and Cambridge combined). Left: histogram of age distribution; middle: gender ratio; right: occupations of participants - occupations associated with low physical activity in blue shades.

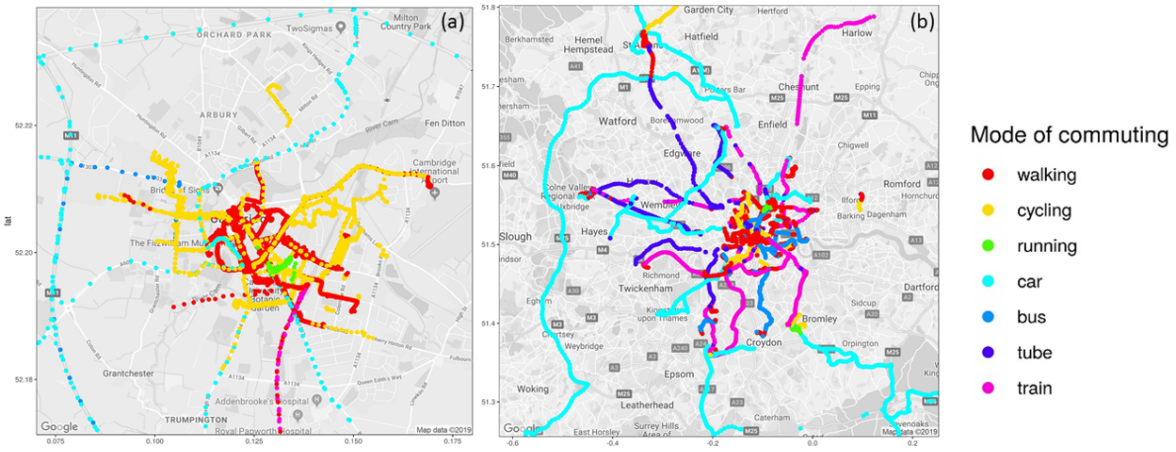

Fig. 2.10 Visited locations of all participants during the pilot project split by different modes of transport (as reported in activity diary). Left: Cambridge, right: London.

2.3.2 AIRLESS project in Beijing, China

A major part of this dissertation is based on data from the AIRLESS[10] study which aimed to find more reliable links between air pollution exposure and acute health effects by introducing novel methods of exposure and health assessment. AIRLESS was part of the cross-disciplinary, international research programme "Air Pollution and Human Health in a Chinese Megacity" (APHH) which was joint-funded by the UK Natural Environment Research Council (NERC), the Medical Research Council (MRC) and the National Natural Science Foundation of China (NSFC). The AIRLESS project was the first epidemiological study that linked personal exposure data with biological markers on an individual level. The study protocol of the AIRLESS project was comprehensively described by Han et al. [57]. A brief summary of the project, with focus on the collection of personal exposure data, is given in the following section.

Data collection

The project was based on two comprehensive field working campaigns: one in winter and one in summer. The data were collected at two monitoring sites: Peking University (PKU) campus and its surroundings in the city of Beijing as urban site; and Pinggu, a village which is about 70 km outside of Beijing, as a rural site (see Figure 2.11). Air quality monitoring stations were recording meteorological data and air pollution levels away from direct emission sources in both sites (details of the available reference instruments are given in Table 3.1 in Chapter 3). Medical data and questionnaires were collected in clinics which were located close to the air quality monitoring stations. Both clinics were equipped with 30 monitors each which were distributed to the study participants by trained nurses. The volunteers were recruited from previous established cohorts; in the urban site from the Chinese Multi-Provincial Cohort Study (CMCS [87]), in the rural site from the International Study of Macro/Micro-nutrients and Blood Pressure (INTERMAP [129]). The subjects were asked to carry the PAM for seven days while continuing to engage in their daily activities. The medical state of the individuals was assessed by members of the AIRLESS team from PKU and King's College London who collected different biomarkers to measure changes in cardiopulmonary functions at Day 0, Day 3 and Day 7. Table A.4 (Appendix) lists all collected biomarkers. The PAM was handed out on Day 0 and collected at Day 7. The data quality of all deployed PAMs was monitored daily and participants were contacted when problems (e.g. with charging) occurred. The participants received compensation for their contribution in form of food and household products, and a brief summary of their exposure and health measurements was sent to them as feedback.

[10] "Effects of AIR pollution on cardiopuLmonary disEaSe in urban and peri-urban reSidents in Beijing"

After the field deployment, all PAMs were located for 18 days next to the reference instruments of PKU (urban site). They were put into air-permeable shelter boxes to protect them from rain and direct solar radiation. The data gained during this colocation were used to calibrate the monitors and evaluate their performance. An overview of the deployment dates is given in Figure 2.12.

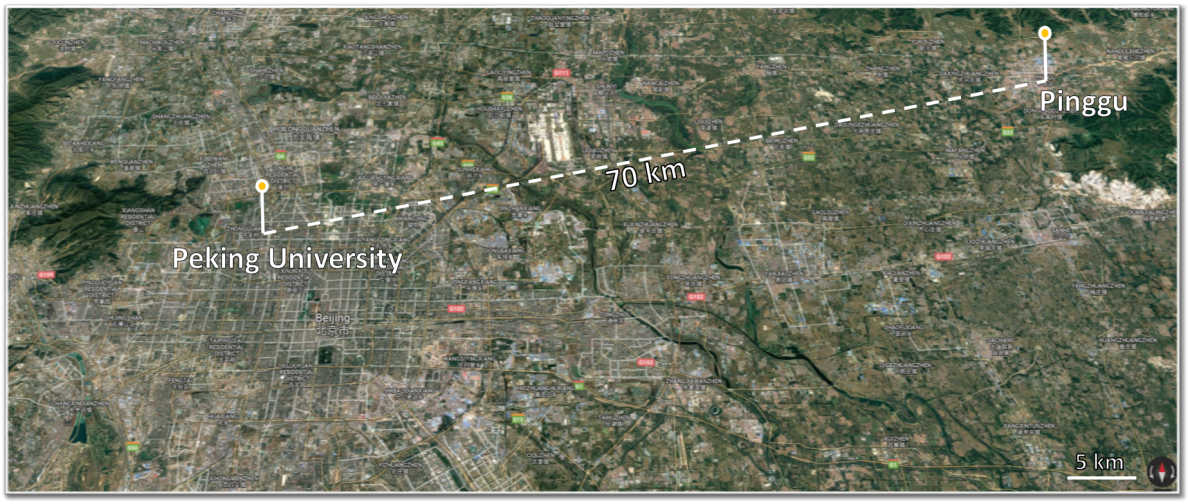

Fig. 2.11 Deployment sites of the AIRLESS project.

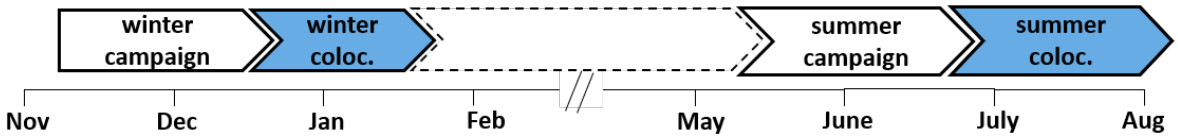

Fig. 2.12 Deployment periods of AIRLESS project in 2016 and 2017. Detailed dates are summarised in Table 2.6.

Table 2.6 Deployment dates of the AIRLESS project

	Winter campaign	**Summer campaign**
Sensor checks and repairs, transport to clinics	03/11/2016 - 12/11/2019	10/05/2017 - 21/05/2017
Indoor validation experiments		11/05/2017 - 22/05/2017
Field deployment	14/11/2016 - 21/12/2016	22/05/2017-26/06/2017
Colocation with reference instruments	28/12/2016 - 15/01/2017	28/06/2017-16/07/2017

Description of the cohort

In total 251 individuals participated in this study. Figure 2.13 shows the visited locations of both cohorts over the winter field campaign (corresponding maps of the summer campaign are shown in Figure A.6 in the Appendix). The large spatial area that the measurements covered indicates that the PAM did not restrict the mobility of the participants and that they readily carried the monitor with them. Figure 2.14 summarises socio-economic and exposure-relevant information of the cohorts. The rural cohort (age range: 45-70 years) was mainly engaged in agricultural activities and housekeeping, whereas the major part of the urban cohort (age range: 55-75 years) was already retired and only a fraction was pursuing a profession (mainly employees of Peking University).

The rural and urban cohort differed distinctively in their heating methods. According to the baseline questionnaires, 86% of the urban cohort depended on central heating (remaining 14% unspecified), whereas peri-urban households used a combination of charcoal- or firewood-fueled stoves with chimney ventilation (91%), charcoal- or firewood-fueled braziers (100%) and electric heaters (83%) to heat their homes in winter. Figure 2.14 shows the different cooking fuels used in the rural and urban cohorts, revealing that the majority of both cohorts used gas stoves. However, a small fraction (10%) of the rural cohort relied on coal or biomass burning as primary cooking stove.

Environmental conditions

During the winter campaign, outdoor temperatures ranged from -9°C to 16°C (mean: 1°C) and the relative humidity (RH) from 7 to 91% (mean: 46%). In contrast, the participants (PAM measurements) were exposed to average temperatures of 20°C in the urban site and 11°C in the

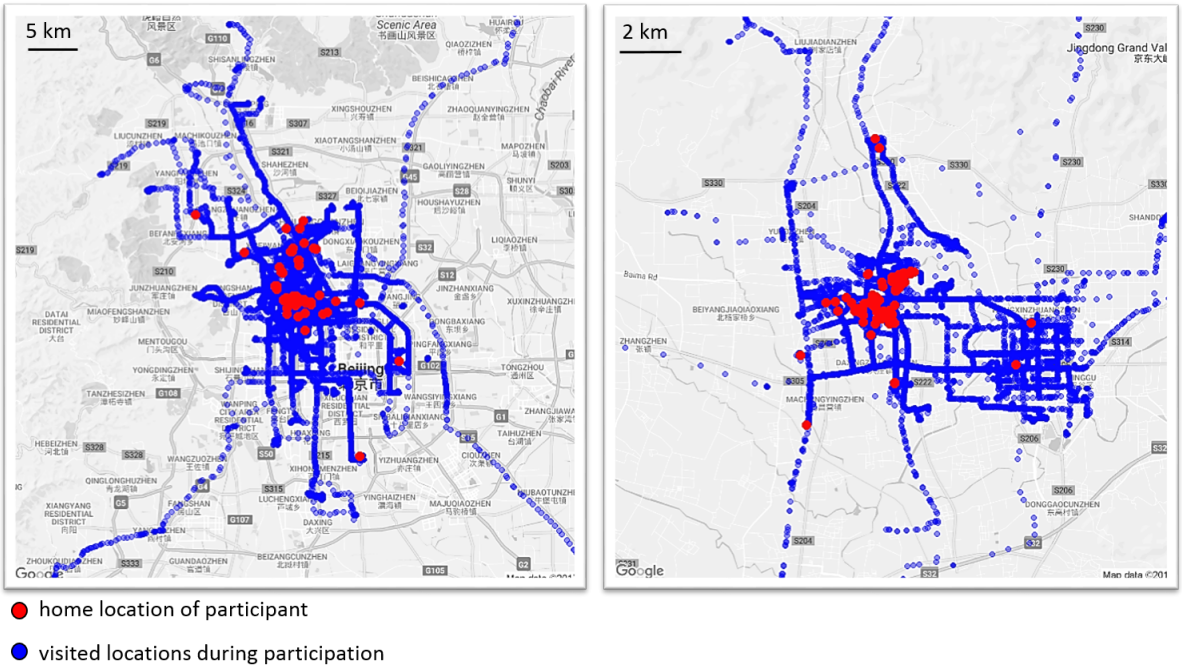

Fig. 2.13 Maps indicating the participant movement (blue) and home locations (red) of the urban (left) and rural (right) cohort during the winter campaign. Corresponding maps for the summer campaign can be found in the Appendix (Figure A.6)

rural site[11] during the winter campaign because they spent a major part of their time in heated buildings. In the summer campaign, outdoor temperatures and RH ranged between 15-41°C (mean: 27°C) and 11-100% (mean: 55%), respectively. Participants were exposed to similar temperatures (mean: 25°C in both cohorts).

[11] Rural cohort was engaged in more outdoor activities and their building insulation might be less efficient than in Beijing city.

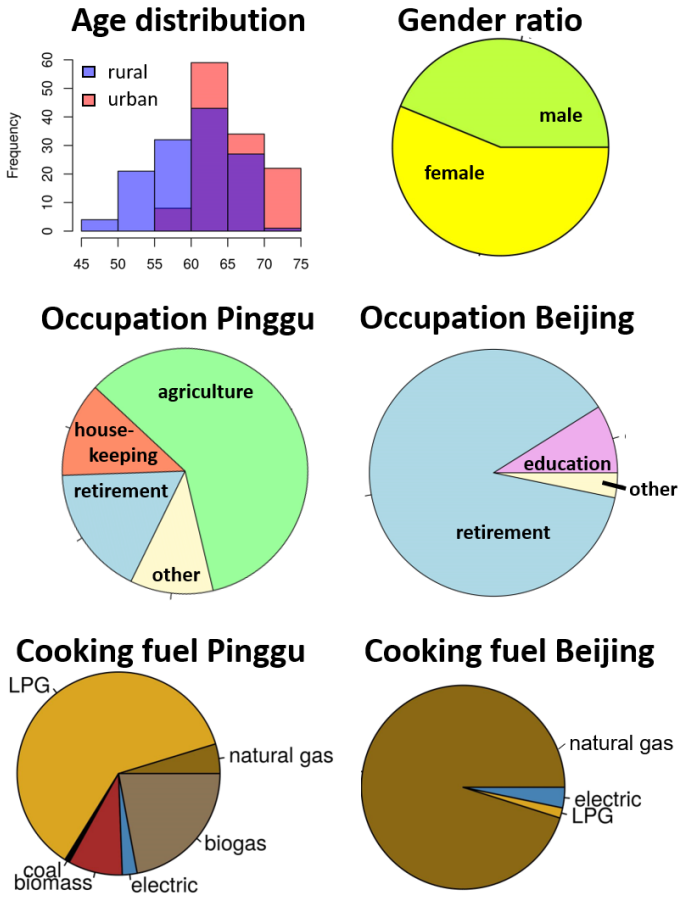

Fig. 2.14 Participant statistics of the AIRLESS cohorts (based on questionnaire answers). Top row: Age distribution and gender ratio (rural and urban combined). Middle row: reported occupations of the rural (left, N = 128) and the urban cohort (right, N = 123). Bottom row: Cooking fuels used in the rural and urban cohort.

2.3.3 Case studies in highly polluted microenvironments

2.3.3.1 Air pollution in metro systems in Berlin, Germany

During a research exchange with the German Environment Agency and the Leibniz Institute for Tropospheric Research, an experiment aiming to characterise air pollution exposures in the Berlin metro system was conducted. Short air pollution exposure snapshots were taken in three metro lines and three metro stations (Figure 2.15) which were selected to ensure maximum variability.

Metro lines: The U1 and U2 pass through the city centre, whereas the U5 moves through suburban regions in the outskirts of Berlin. The U2 line is mainly subterranean, while the major part of the U1 line is overground. U5 contains both, underground and overground passages. For

the air quality assessment inside the metro trains, a PAM was placed in the passengers' seating area. Due to a poor GPS connection in the underground system, a time sheet of the visited metro stations was kept and GPS data manually added to the dataset afterwards.

Metro stations: Alexanderplatz was selected because it is the most frequented metro station in Berlin, the second (Gesundbrunnen) is the deepest metro station, while the third (Tierpark) is located in a suburban area of Berlin. Static deployments of one PAM (20-30 min) were performed in the selected metro stations.

Measurements have been collected in the metro stations and lines described above on Sept 10th 2018, after the monitors had been calibrated with reference instruments from a kerbside monitoring station (Frankfurter Allee) of the Berlin air quality network (BLUME; Sept 4th - Sept 10th morning, see [76]). The average outdoor temperature was 15°C (average RH 52%).

Fig. 2.15 Selected metro stations and metro lines for air quality measurements in Berlin. Frankfurter Allee: static kerbside measurements for calibration.

2.3.3.2 Domestic exposure using different cooking fuels in rural Kenya

This feasibility study was performed in Dunga Beach, a fishing village located on the shores of Lake Victoria, near Kisumu, the third largest city in Kenya (Figure 2.16). The area is characterised by a tropical climate with heavy year-round rainfalls. The data were collected between May 27th and June 13th 2019.

The study was conducted collaboratively by the Cambridge Institute for Sustainability Leadership (CISL), the Cambridge Department of Chemistry, Biogas International Limited (BIL) and AstraZeneca. The overarching aim of this project was to evaluate the impact of introducing innovative energy sources into rural communities in Kenya. The role of the Department of Chemistry in this project was to quantify the changes in household air pollution when switching from traditional indoor biomass burning to domestically generated biogas as household energy source (primarily for cooking).

Before the start of the air quality project, 50 households in Dunga had already been equipped with the new biogas technology. It consisted of a digester unit located outside the house which used microorganisms to convert organic waste such as cow-dung, household food waste and shredded water hyacinth[12] into biogas which was then simply piped into the household where it was connected to a double-ring stove and ready to burn.

Of the 50 biogas households, 8 were randomly selected for the experiment. A control group of 4 additional households using traditional cooking methods was simultaneously monitored. As outdoor air quality monitoring stations were not available, the ambient air quality was monitored by three AQMesh[13] units distributed over the study area. The locations of the selected households and outdoor monitors are shown in Figure 2.17.

A PAM was placed into the kitchen of each selected household. Each deployment lasted for 7-8 days in which the participants were asked to keep a diary of the cooking methods used for each meal. The exact cooking times were determined using the indoor CO concentrations as proxy for cooking activity (further described in Section A.2.2.4 in the Appendix). The costs of the used electricity (for charging the PAMs) and participants' time investment were financially compensated. Only two of the 8 biogas households used solely biogas. The other households continued to use traditional fuels parallel to biogas. The most common traditional cooking fuel was charcoal. Occasionally, the use of wood, papyrus and liquefied petroleum gas (LPG) was reported.

[12] Water hyacinth is an invasive weed having a disastrous ecologic and economic effect on lakes and waterways across Africa.

[13] Environmental Instruments Ltd, UK

For calibration, the PAMs were colocated with the AQMesh instruments as reference after the deployment (13/06/2019 - 05/08/2019). However, the NO_2 and O_3 measurements of the AQMesh instruments were not reliable enough (temperature interference) to serve as reference. Hence, the NO_2 and O_3 measurements of the PAM had to be excluded from this study.

Fig. 2.16 Location of Dunga Beach (deployment area). Image: Googlemaps

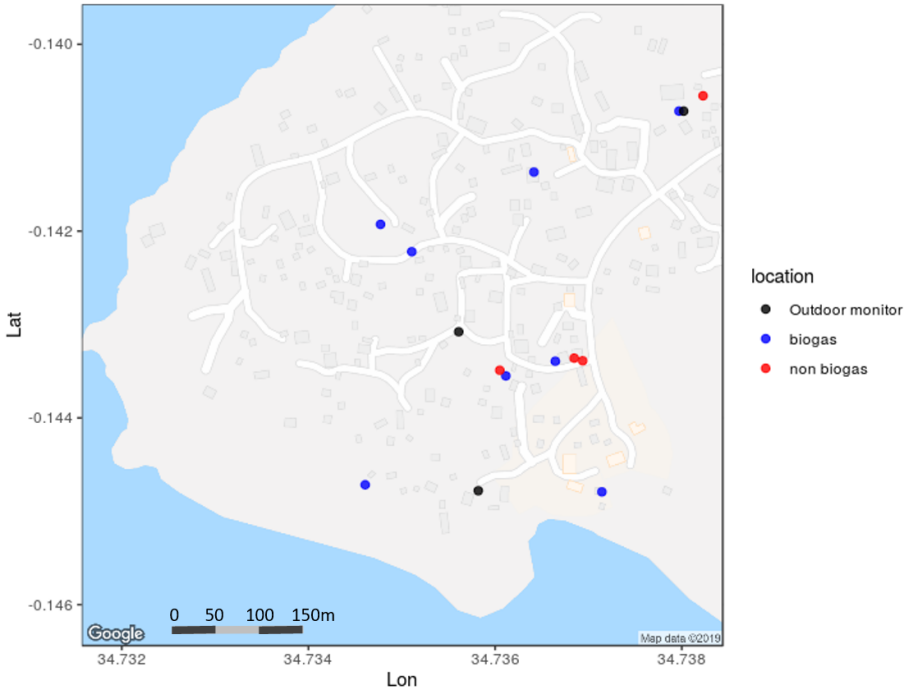

Fig. 2.17 Locations of selected households using biogas (blue) and traditional cooking methods (red), and locations of ambient measurements (black) in Dunga Beach. Map: Googlemaps

2.4 Chapter summary

This chapter described the methodological framework applied to generate the data this work builds upon. The main focus of this dissertation lies on the Personal Air Quality Monitor (PAM), a portable measurement platform which, thanks to its wearability and high spatio-temporal resolution, promises to address current limitations in exposure epidemiology.
The PAM integrates five miniaturised pollutant sensors measuring the concentrations of NO, CO, NO_2, O_3 and particulate matter, as well as additional sensors to measure auxiliary parameters such as temperature and location. A complex data processing scheme was applied to ensure high data quality and convert the raw PAM data into ratified pollutant concentrations.
Overall, 85 PAMs were deployed in four different countries to gather a total of 3771 measurement days. The largest dataset of this work was collected during the AIRLESS project in which 60 PAMs were deployed to a total of 251 volunteers residing in urban and peri-urban Beijing during winter and summer seasons. Previous to the AIRLESS project, a pilot project was conducted to assess the deployment feasibility of the PAM in daily life. Furthermore, this work evaluates two case studies in highly polluted microenvironments: underground train systems and domestic environments that operate biomass burning as energy source for cooking.
The following chapters will draw on these datasets to assess the performance of the PAM, demonstrate its potential to improve personal exposure and dose estimations, and provide insights into air pollution risks of different environments and activities.

Chapter 3

Characterisation of the PAM performance

The previous chapter introduced the PAM as a wearable multi-pollutant sensor with the potential to improve personal exposure and dose estimations, and thus, advance our understanding of the detrimental health effects of air pollution. As described in Section 1.3, a wide range of portable air pollution monitors has already been developed for personal exposure measurements but only few had their performance and reliability thoroughly evaluated. Negligent or incomplete sensor testing remains one of the biggest concerns among exposure scientists. To address these concerns and to advance the application of novel sensor technologies in exposure science, this chapter aims to comprehensively evaluate the performance of the PAM when deployed outdoors, indoors and in motion. To account for environmental variability, the performance was evaluated across seasons, in different geographical areas with distinct air pollution levels (UK and China), and in urban and rural locations.

The sensor performance was generally assessed by evaluating the level of agreement between the measurements of one or multiple PAMs and certified reference instruments that were placed in vicinity to them in the local environment where the PAMs were deployed. Sensor performance may vary significantly with season (e.g. temperature and RH artefacts) while meteorological conditions may affect the variation in outdoor air pollution levels directly (e.g. stability of the atmosphere) and indirectly by socioeconomic patterns (e.g. increased energy demand for heating). Similarly, indoor air may be directly affected by the seasonal variation of outdoor air pollution, and indirectly through the change of the behavioural patterns of occupants between seasons (e.g. window adjustment to achieve thermal comfort). To account for variations in environmental and air pollution levels that might affect sensor performance, five static colocation experiments were conducted in China and the UK: four experiments in different outdoor environments across varying seasons, (Sections 3.1 and 3.2), and one

experiment in an indoor environment (Section 3.3). The performance of the PAM in movement was assessed with two short-term experiments (pedestrian and vehicle) in Section 3.4. Details of the reference instrumentation, including the description of the colocation sites, principle of operation and instrument models, are summarised in Table 3.1.

Table 3.1 Details of the reference instruments used for the performance evaluation of the PAM. Time resolution of all measurements was 1 min.

Deployment	**Site description**	**NO, NO_2**	**CO**	**PM**	**O_3**
Outdoor China	Urban background in Peking University (PKU) campus, Beijing	Chemiluminesence, Thermo Fisher Scientific model 42i	Nondispersive Infrared, Thermo Fisher Scientific model 48i	$PM_{2.5}$*: TEOM (Tapered Element Oscillating Microbalance)	UV absorption, Thermo Fisher Scientific model 49i
Outdoor UK	Urban background at the Department of Chemistry, Cambridge	Chemiluminesence, Thermo Fisher Scientific model 42i	Nondispersive Infrared, Thermo Fisher Scientific model 48i	Aerosol spectrometer, FIDAS PALAS 200S	UV absorption, Thermo Fisher Scientific model 49i
Indoor residential China	Indoor deployment in an urban high-rise Beijing flat	NO_2 cavity attenuated, phase shift spectroscopy (CAPS), Teledyne API T500U	NA	aerosol spectrometer, GRIMM 1.108	NA
Commuting environment UK	Monitoring vehicle equipped with commercial instruments driving in central London	NO_2 CAPS, Teledyne API T500U	NA	Nephelometer (scattering), Met One ES642	UV absorption, Teledyne API T400

*Due to malfunctioning of the TEOM in PKU during the non-heating season, measurements from a TEOM at a nearby governmental site (Haidianwanliu $\sim$ 3 km, time resolution 1 h) were used. NA: not available.

The deployments in China were part of the AIRLESS project (Section 2.3.2) whereby the outdoor colocation was performed for 1 month each during winter and summer after they had been deployed to the AIRLESS cohorts (see Figure 2.12 and Table 2.4 for deployment dates). The colocation in the UK involved PAMs that had been previously deployed to 150 participants of a COPD cohort for 2 years continuously [97]. Taking into account the strong seasonal variation in air pollution levels, the performance of the PAM was evaluated during both the "heating" (when the majority of householders heat their home on a regular basis) and the "non-heating" season (see Section 3.2). The residential central heating season in Beijing is from 15 November to 15 March (Beijing municipal government), while in the UK the equivalent heating season is 5.6 months (October-March/April) [19].

To evaluate the agreement between two concentration measurements the coefficient of determi-

nation R^2 as well as the gradient of the linear fit between two sensors were assessed. Figure 3.1 compares the concentration measurements within a network of PAMs that were colocated during the AIRLESS winter campaign, indicating a high reproducibility (i.e. agreement between different sensors measuring the same quantity) of the sensors. This level of agreement between individual sensors was found across all colocation experiments (UK and China) and seasons, even when the ambient concentrations were close to the LOD (mean $R^2 \geq 0.80$ for EC sensors and $R^2 \geq 0.91$ for the OPC; see Table A.5 in the Appendix). Hence, the results of the performance evaluation of one selected PAM appear representative of the entire sensor network.

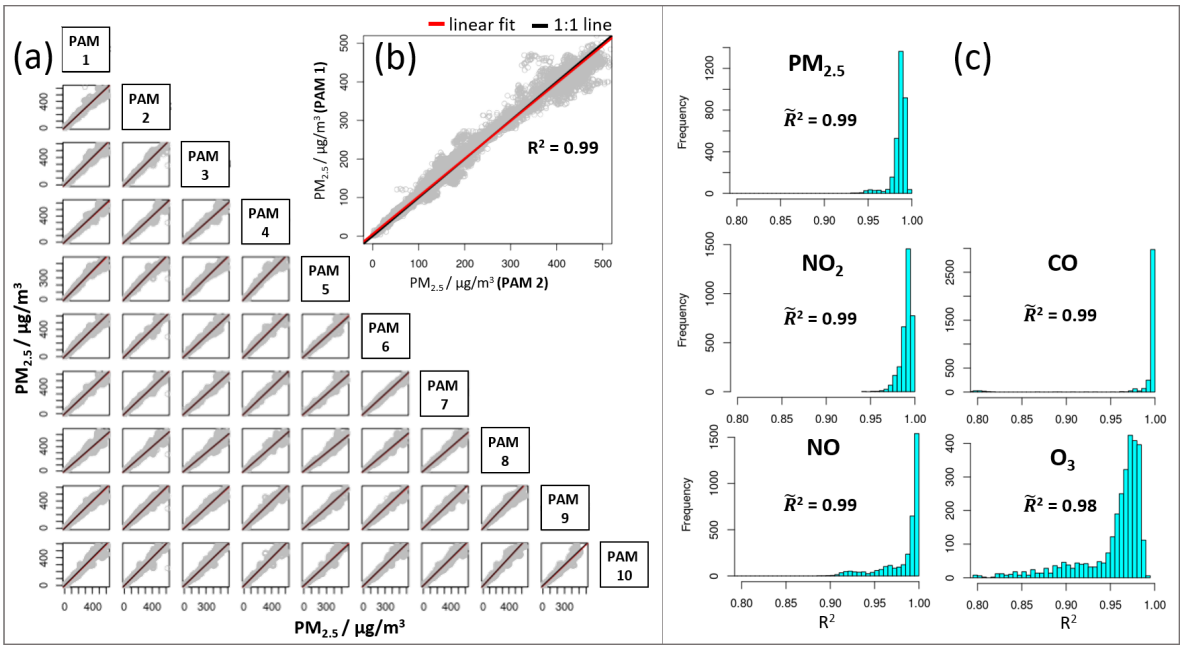

Fig. 3.1 Reproducibility of a PAM network (in that case 59 PAMs) that was colocated outdoors in Beijing during the heating season after one 1 month of field deployment to participants. (a): Scatterplot of the $PM_{2.5}$ measurements between 10 sensor pairs. The 1:1 line in black; and linear fit line in red. (b): "Close-up" of a scatterplot from (a) of one representative sensor pair. (c): Histograms of the coefficient of determination (R^2) between all sensor pairs with median values $\tilde{R}^2$ given for each species. R^2 values during this deployment were higher than 0.90 for all pollutants indicating the high reproducibility of the sensors' readings (see Table A.5 for all colocations). O_3 sensors $R^2 > 0.80$ due to very low ambient levels close to the LOD of the sensors.

3.1 Performance of the calibration model and limit of detection

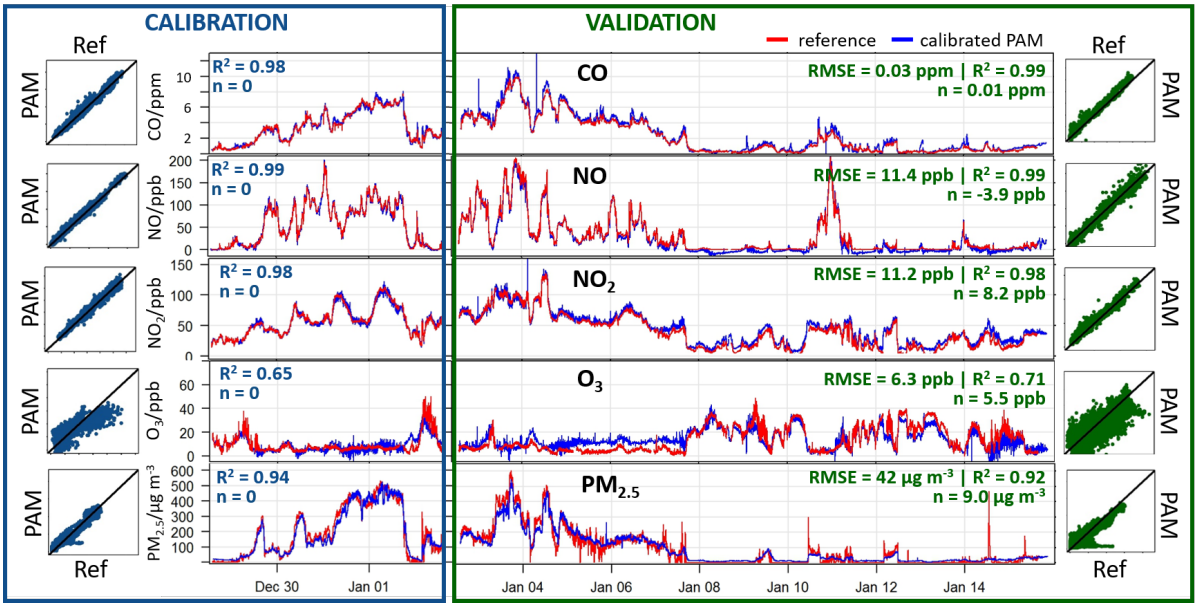

Fig. 3.2 Outdoor colocation of one representative PAM with certified reference instruments in China (winter 2016/17) split into a training and a validation set to evaluate the performance of the PAM calibration method. The first five days were used to calibrate the monitor, the remaining colocation data (14 days) were used to validate the extracted calibration parameters. The scatterplots on each side show the correlations between reference and PAM measurements with the 1:1 line in black. The scale of the X- and Y-axis of the scatterplots is identical to the concentration scale given in the time series of the corresponding pollutant (e.g. 0-12 ppm for CO).

The performance of air quality monitors does not solely depend on the physical functionality of their components but also on the data correction and calibration approaches applied to process the raw measurement data [86]. This section uses the dataset of the AIRLESS winter campaign to evaluate the performance and reliability of the PAM calibration procedure described in Section 2.2.3.

The AIRLESS sensor network (N=59) was colocated with static reference instruments from Peking University (more deployment details in Section 2.3.2). The collected dataset was split into a training (i.e. calibration) and a validation period. The calibration coefficients (e.g. electrode sensitivity) were extracted from the training period as described in Section 2.2.3, and then applied to the raw PAM data of the validation set. The resulting PAM measurements were then compared to those from the reference instruments.

Figure 3.2 demonstrates the procedure at the example of one representative PAM from the sensor network. A time series of the PAM measurements (blue) compared with the reference measurements (red) during both, the calibration period (training set, left) and the validation period (right) is shown in the centre. Scatter plots between the PAM and reference measurements are shown on each side of the split datasets, with the adjusted coefficient of determination R^2 and intercept n of the linear fits given in the corresponding colour.

The PAM measurements were highly correlated with the reference instruments during the calibration period ($R^2 \geq 0.94$, for O_3 $R^2 = 0.65$). This agreement remained high during the validation period ($R^2 \geq 0.92$, for O_3 $R^2 = 0.71$), suggesting that the calibration parameters generated from the training set may be applied to measurements beyond the calibration periods. Table 3.2 presents the mean coefficients of determination $\bar{R}^2$ averaged across the entire sensor network (N=59) during the calibration and the validation period. The agreement between PAM and reference does not significantly differ between the training and the validation period (difference of $\bar{R}^2$ within one SD) which indicates an overall reliable calibration process across the entire PAM network.

Approximately a quarter of the dataset (5 days) was selected as a training set in Figure 3.2. The test was repeated for different training periods between 1 and 16 days, finding that the agreement between PAM and reference (R^2) in the validation period remained stable for training periods longer than 3 days. The training period must be of sufficient length to cover the environmental conditions under which the sensors will be deployed (here in the validation period) [38], which was achieved after 3 days. Due to the small difference observed in sensor performance between the training and the validation period, the following section will use the entire colocation periods for the calibration and the evaluation of the sensor performance.

The calibration parameters obtained from the training period did not vary significantly between the two AIRLESS deployments in winter and in summer which were 6 months apart, indicating that the sensors exhibited stability over these timescales. Calibration parameters were also very similar across the sensor network. Although sensors produced under the same specifications tend to have similar parameters, it is still important that a local calibration of the sensors is performed under similar environmental conditions as those found during the deployment.

Greater variability of the calibration parameters was observed between different geographical locations (e.g. UK and China). However, as novel sensor technologies advance rapidly, different sensor variants were used in the different projects that were performed years apart. Therefore, the variability of the calibration parameters between different locations can be most likely attributed to sensor variation rather than potential effects of the local environment.

Table 3.2 Mean coefficients of determination (R^2) between PAM and the reference instruments, averaged over the entire PAM network (N=59, AIRLESS winter colocation), for the training and the validation period.

	CALIBRATION SET $\bar{R}^2 \pm$ **SD**	**VALIDATION SET** $\bar{R}^2 \pm$ **SD**
CO	0.98 ± 0.01	0.99 ± 0.01
NO	0.98 ± 0.03	0.97 ± 0.06
NO_2	0.99 ± 0.00	0.97 ± 0.02
O_3	0.81 ± 0.09	0.83 ± 0.15
$PM_{2.5}$	0.97 ± 0.01	0.92 ± 0.03

The calibration-validation approach described above may also be used to estimate the limit of detection (LOD) of the sensors. Conventionally, the LOD of air pollution sensors is determined in the laboratory, by placing them into a test chamber filled with zero air (i.e. air that does not contain the target pollutant), and determining the sensor noise under these conditions [128]. However, this approach is time- and labour-intense, especially for large numbers of sensors. More importantly, the sensor performance under controlled laboratory conditions might differ significantly from the sensor performance in the field [116]. Therefore, in this work the LOD was established from field calibration data.

The intercept of the linear fit between PAM and reference data was set to zero by default in the training period through the calibration process. Ideally, this intercept would remain zero in the validation period. However, small intercepts were found in the linear fit between PAM and reference during the validation period. This is illustrated in Figure 3.2 where the intercept of n = 0 during the training period diverged, for instance, to n = 0.01 ppm for CO or n = -3.9 ppb for NO. In this work, these deviations were established as the LOD.

The mean LOD for each pollutant was determined by averaging the intercepts across the whole PAM network. The mean intercepts $\bar{n}$ and their standard deviation are given in Table 3.3. The LOD values determined from the field calibration agree with the results from laboratory calibrations in previous publications (e.g. Mead et al. [94] found the LODs of the electrochemical sensors below 4 ppb). The LOD of the CO sensor was found to be higher (13 ppb) which is, however, due to the known high intrinsic noise and LOD of the reference instrumentation [134].

Table 3.3 Limits of detection of the PAM determined from field calibration. $\bar{n}$ - mean intercepts (validation period); SD - standard deviation of n (validation period). All data from colocation of 59 PAMs (AIRLESS winter).

	$\bar{n}$	SD (n)
CO / ppm	0.013	0.008
NO / ppb	-3.0	4.3
NO_2 / ppb	1.7	2.1
O_3 / ppb	1.8	2.3
$PM_{2.5}$ / µg m^{-3}	8.8	4.1

3.2 Outdoor performance of the PAM

In the following section, the sensing performance of multiple PAMs was tested against static outdoor reference instruments under varying meteorological conditions (ambient temperature range: -3.6°C to 36.3°C, RH range: 15% to 96%) and levels of air pollution (e.g. range of mean CO concentrations: 192 ppb to 2561 ppb).
In total, four outdoor colocation deployments have been performed: each one in the UK and China, during the heating and non-heating season. In each experiment, PAMs were placed in protective shelters close to the inlets of the certified air pollution monitoring stations.
Figures 3.2, 3.3, Figure 3.4 and 3.5 illustrate the four colocation experiments, comparing the measurements of each two[1] randomly selected PAMs (blue, black) with the reference measurements (red). The left side of each Figure (a) shows a time series of the measurements, the right side presents scatter plots between the two PAMs (reproducibility, b) and between a PAM and the reference instrument (accuracy, c).

While the figures assess the accuracy of individual PAMs, the performance parameters across all N PAMs of each colocation experiment were averaged and presented in Table 3.4[2]. Besides the coefficient of determination (R^2), the root-mean-square error (RMSE, Equation 3.1) between PAM and reference has been included as performance criterion. R^2 can be a misleading indicator of sensor performance when measurements are taken close to the LOD of the instruments. The RMSE can be a complementary parameter of R^2 for the evaluation of performance, as it summarises the mean difference between measurements from the sensor and certified

[1] Figure 3.2 compares only one PAM to the reference. The reproducibility of the PAMs during the AIRLESS winter colocation is shown in Figure 3.1

[2] This table includes is a very comprehensive and detailed performance evaluation. For an overview of the broader conclusions see Section 3.2.3.

instruments.

Additionally, the ambient temperature and RH (median, range: 5% - 95%) as well as the mean and maximum pollutant concentration measured by the reference are presented in Table 3.4 to describe the ambient conditions of each colocation. Because the air pollution sensors were exposed to the internal conditions of the PAM (see Section 2.2.1), the internal temperatures of the PAM are also presented in Table 3.4.

$$\text{RMSE} = \sqrt{\frac{1}{n}\sum(c_{estimator} - c_{true})^2} \tag{3.1}$$

Table 3.4 Overview of sensors' performance during outdoor colocations in China and the UK. Median values (range: 5th - 95th percentiles) of the ambient and internal temperature and relative humidity (RH) are presented. The 95th percentile of the reference concentration measurements over the entire colocation period is given as maximum concentration. The mean adjusted coefficients ($\bar{R}^2$) and root-mean-square errors (RMSE) indicate the agreement between the measurements of the sensors and reference instruments. Average values across each network of N sensors are given. The colocation in China in June is shown in italics as sensors were regularly exposed to temperatures higher than 40°C where they did not show linear temperature responses. Summary given in Table 3.5. Equivalent table for sensor reproducibility in Table A.5.

		Heating season		**Non-heating season**	
Location Start date - end date (total hours)		China 28/12/2016 - 15/01/2017 (447h)	UK 27/10/2017 - 13/11/2017 (408h)	*China* *28/06/2017 - 16/07/2017 (432h)*	UK 26/03/2018 - 10/04/2018 (342h)
Illustrative graphical example		Figure 3.2	Figure 3.3	*Figure 3.4*	Figure 3.5
Ambient conditions	Ambient Temp (°C)	1.1 (-3.6 - 6.1)	9.3 (4.3-14.4)	*29.9 (22.8-36.3)*	8.3 (4.7-18.1)
	Ambient RH (%)	40 (15-79)	81 (61-93)	*68 (43-96)*	83 (48-93)
Internal conditions of the PAM	Internal Temp (°C)	10.5 (5.3-18.0)	15.9 (11.0-20.8)	*40.2 (32.7-45.8)*	17.7 (12.2-26.8)
	Internal RH (%)	27 (14-44)	52 (39 -59)	*38 (23 - 55)*	52 (34 - 60)
Number of sensors (N)	[-]	N = 59	N = 3	*N = 59*	N = 3
CO	Maximum (mean) mixing ratio (ppb)	6845 (2561)	357 (237)	*916 (575)*	276 (192)
	$\bar{R}^2$	0.98	0.74	*0.71*	0.67
	mean RMSE in ppb (percentage of max)	31 (0.5%)	31.6 (8.9%)	*212 (23%)*	33.3 (12.1%)
NO	Maximum (mean) mixing ratio (ppb)	132 (38)	19 (5)	*5 (1)*	6 (2)
	$\bar{R}^2$	0.94	0.89	*0.2*	0.58
	mean RMSE in ppb (percentage of max)	11.7 (8.9%)	3.0 (15.8%)	*13.0 (260%)*	2.2 (36.6%)
NO_2	Maximum (mean) mixing ratio (ppb)	98 (42)	35 (15)	*42 (22)*	19 (10)
	$\bar{R}^2$	0.84	0.9	*0.2*	0.84
	mean RMSE in ppb (percentage of max)	11.8 (12.0%)	3.0 (8.6%)	*13.3 (31.7%)*	2.6 (13.7%)
O_3	Maximum (mean) mixing ratio (ppb)	33 (13)	30 (16)	*109 (49)*	44 (28)
	$\bar{R}^2$	0.87	0.92	*0.8*	0.89
	mean RMSE in ppb (percentage of max)	3.6 (10.9%)	2.7 (9%)	*14.9 (13.7%)*	4.2 (9.5%)
$PM_{2.5}$	Maximum (mean) conc. (µg m^{-3})	432 (114)	32 (12)	*110 (55)*	37 (3)
	$\bar{R}^2$	0.93	0.57[a]	*0.65*[b]	0.8
	RMSE in µg m^{-3} (percentage of max)	37 (8.6%)	9 (28%)[a]	25 *(22.7%)*[b]	2 (5.4%)

[a] Due to unavailable data, PM mass measurements are not corrected for RH effects. [b] Comparison with governmental station ca 3 km away.

3.2.1 Sensor performance during the heating season

During the outdoor colocations in the heating season, ambient temperatures ranged from -4 to 6°C in China and between 4 and 14°C in the UK. Air pollution in China was characterised by elevated levels of CO and $PM_{2.5}$ for extended time periods (haze events). Compared with pollutant levels in the UK, the concentrations of CO and $PM_{2.5}$ were approximately 10 times higher while the contrast in ambient NO_2 levels was less pronounced with levels in China only approximately 3-fold higher.

Illustrative examples for the outdoor colocations in China and the UK are given in Figures 3.2 and 3.3, respectively. The performance of all N PAMs during the heating season is summarised in the first two result columns of Table 3.4.

The O_3, NO and NO_2 sensors exhibited excellent performance ($\bar{R}^2 \geq 0.84$) in both geographical settings. The median RMSE values were close to the LOD of the sensors (< 3 ppb) in the UK and slightly higher in China (< 12 ppb). In both deployments, the RMSE values of these gaseous sensors were negligible compared to the ambient concentration ranges of the targeted pollutants (less than 16% of the maximum mixing ratio recorded by the reference instruments). While the median $\bar{R}^2$ between the CO sensor and the corresponding reference was reasonably high in both outdoor deployments (≥ 0.74), the median RMSE values were also quite large (< 32 ppb). In fact, this is due to the previously mentioned high intrinsic noise and LOD of the reference instrumentation (> 40 ppb, [134]), which is much higher compared to that of the electrochemical sensors.

Following the RH correction of the size-segregated particle measurements (Section 2.2), the PM mass quantification with the miniaturised OPC agrees with the TEOM reference instrument with an adjusted $\bar{R}^2$ of 0.93. The low RMSE values (8.6% of the maximum concentration) demonstrate that the scaling factor adequately addresses the under-prediction of mass due to undetected smaller particles when derived from field calibration in the local environment. Due to unavailable measurements, the PM measurements in the UK could not be corrected for RH effects, which resulted in only a moderate correlation with the reference instrument ($\bar{R}^2 = 0.57$, Figure 3.3).

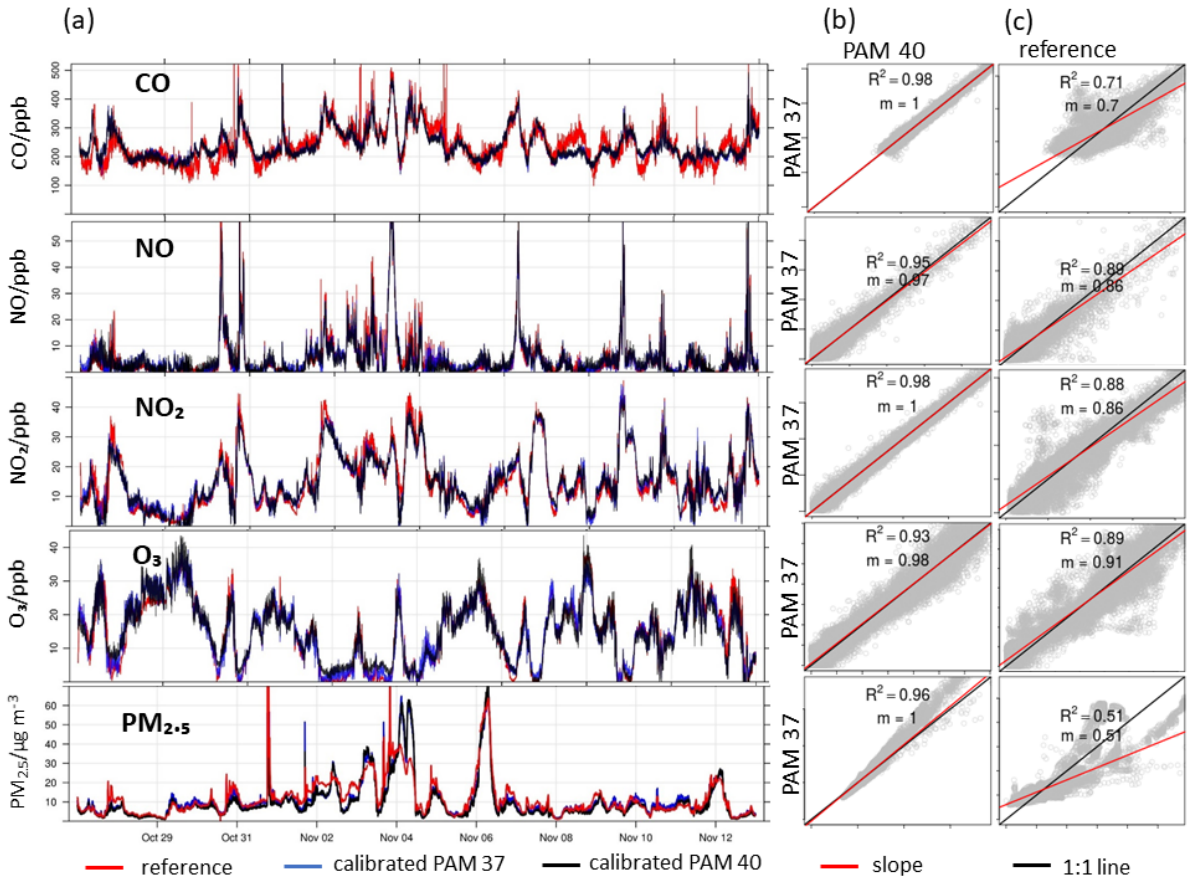

Fig. 3.3 Outdoor colocation of two PAMs with reference instruments in Cambridge for three weeks during the heating season. The PAMs had been previously deployed for two years to participants of a London cohort with chronic pulmonary disease. (a): Time series of two PAMs (blue, black) and the reference instruments (red). Due to unavailable data, the PM measurements of the PAM are presented without the RH correction resulting in an over-prediction of PM mass during certain periods. (b): correlation between PAMs and (c) correlation between PAM and reference. The 1:1 line in black; and gradients m in red. The scale of the X- and Y-axis of the scatterplots is identical to the concentration scale given in the time series of the corresponding pollutant.

3.2.2 Sensor performance during the non-heating season

One outdoor colocation in China (Figure 3.4) and one in the UK (Fig 3.5) were performed during the non-heating season, both over periods of 2 weeks. The performance of all N PAMs during the warmer season is summarised in the two columns on the right of Table 3.4.
In the UK, the seasonal variation in ambient temperatures, RH and pollution levels was relatively small. In contrast, in China, the seasonal variation was large with ambient temperatures reaching up to 36.3°C (median: 29.9°C) and generally lower pollution levels compared to the heating season. However, in both geographical settings, O_3 was significantly elevated.
The performance of the O_3 sensor remained reliable across all colocation experiments with median $\bar{R}^2 \geq 0.80$ and RMSE values < 15 ppb, which might provide valuable insights into the health effects of this pollutant because (a) ozone is a strong oxidant with a high potential to affect the body ([105]) and (b) has the highest concentrations during the non-heating season compared to other pollutants which usually peak during the heating season.
Due to a malfunction of the PM reference instrument (TEOM) during the non-heating season at PKU, the PAM PM measurements had to be compared with a TEOM installed at a nearby governmental site (Haidianwanliu). Although not closely colocated (∼3 km), the gradient between the PAMs and reference measurements was close to one (average m = 0.96, see example Figure 3.4) and there was still a notable correlation ($\bar{R}^2$ = 0.65) with a median RMSE of 25 µg m^{-3} indicating that, away from direct sources, PM concentrations are essentially homogeneous over relatively large urban areas. Compared with the heating season, PM concentrations in China were significantly lower, whereas PM levels in the UK varied little with season. After correcting for the effects of RH on PM, the PAM performance in the UK during the non-heating season significantly improved compared with the heating season (RMSE = 2µg m^{-3} within the particle size range 0.38-17 µm).
While the performance of the O_3 and OPC sensors remained reliable across seasons and geographical settings, the performance of the CO, NO and NO_2 sensors decreased significantly ($\bar{R}^2$ $\geq$ 0.20) during the hottest parts of the non-heating season in China due to extreme temperatures (internal median temperatures of the PAM: 40.2°C, 5%-95%: 32.7-45.8°C, Table 3.4). It should be noted that NO levels were close to the LOD of the sensor, which also affects the $\bar{R}^2$ values. We conclude that the measurements of the CO, NO and NO_2 sensors should be interpreted with caution when the sensors are exposed to temperatures above 40°C. However, during the field deployment to participants, the sensors were exposed to lower temperatures due to occupants adjusting their thermal environment for comfort (see Fig. A.9) which did not impact the sensor performance.

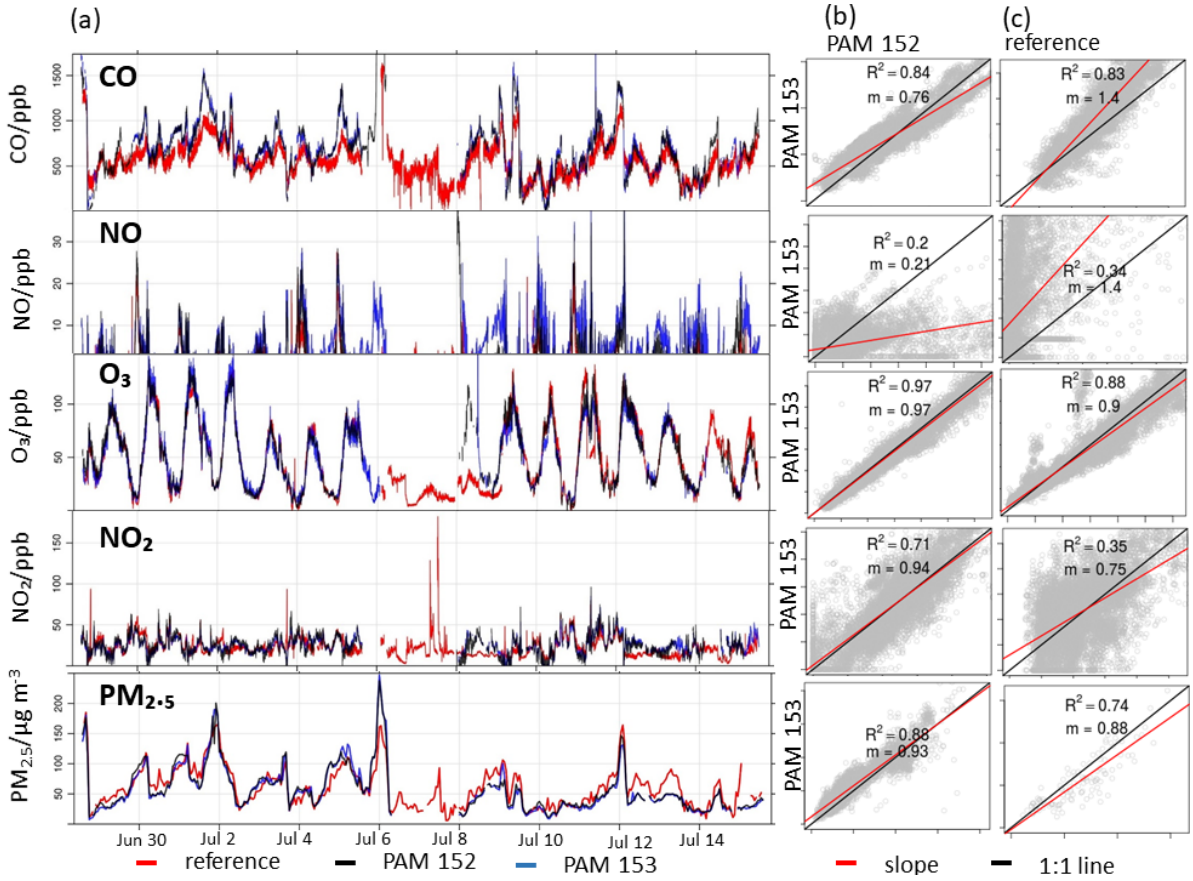

Fig. 3.4 Outdoor colocation of two PAMs with reference instruments in China during the non-heating season (June). The PAMs have been previously deployed in China for two months to participants of a cardio-pulmonary cohort. Due to malfunctioning of the TEOM in PKU during the non-heating season, measurements from a TEOM in a nearby governmental site (Haidianwanliu $\sim$ 3 km, time resolution 1 hour) were used for comparison with the PAM. (a): Time series of two PAMs (blue, black) and the reference instruments (red). (b): correlation between PAMs and (c): correlation between PAM and reference. The 1:1 line (x=y) in black; and gradients m in red.The scale of the X- and Y-axis of the scatterplots is identical to the concentration scale given in the time series of the corresponding pollutant.

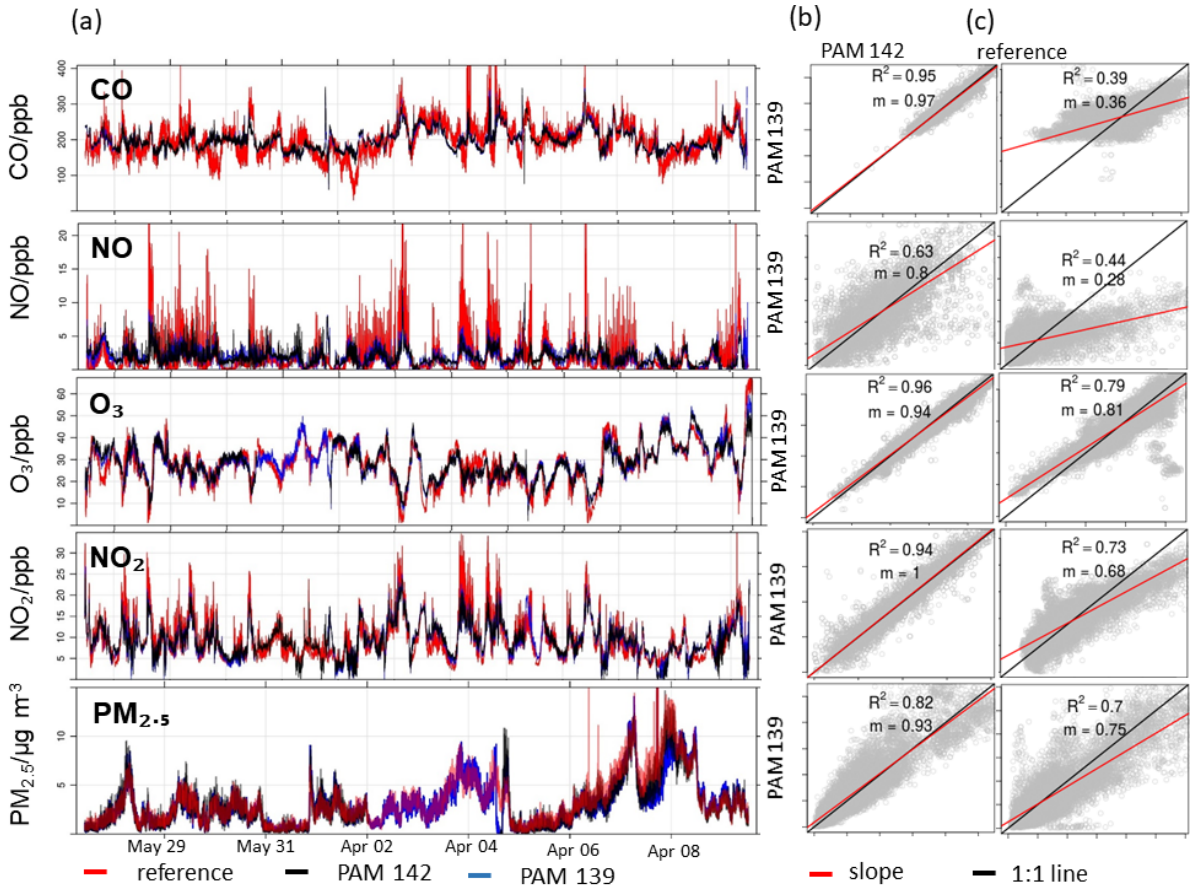

Fig. 3.5 Outdoor colocation of two PAMs with reference instruments in the UK during the non-heating season (April- May). (a): Time series of two PAMs (blue, black) and the reference instruments (red). (b): correlation between PAMs and (c): correlation between PAM and reference. The 1:1 line (x=y) in black and gradients m in red. The scale of the X- and Y-axis of the scatterplots is identical to the concentration scale given in the time series of the corresponding pollutant.

3.2.3 Summary of the outdoor performance

Sections 3.2.1 and 3.2.2 comprehensively described the performance of each pollutant sensor of the PAM under diverse conditions. This section provides an overview of the main conclusions from the static outdoor colocation experiments. Table 3.5 summarises the sensor performance characteristics from Table 3.4 and the factors that may have impacted the agreement between reference and PAM.

The performance of the CO sensor was comparable with the reference instruments during the heating season in China. In the other three colocation experiments it was impaired by external factors, such as sensor overheating and intrinsic noise of the reference instrument. Further validation experiments in Section 5.1.3 indicate that the CO sensors generally agree with the reference when not impacted by external factors.

In three of the four outdoor colocation experiments, ambient NO concentrations were close to or below the LOD of the NO sensors, resulting in low correlations between the NO sensors and the reference. At higher NO concentrations, however, they showed a strong agreement with the reference. Because emission sources in the direct environment of an individual caused the personal NO exposures to frequently exceed the ambient concentrations (Chapter 4), deployment measurements were performed within the concentration range in which the NO sensor performed sufficiently.

The NO_2 sensor performance was good or very good across all experiments apart from the non-heating season in China where extreme ambient temperatures (internal PAM temperature > 40°C) deteriorated the sensor performance. The O_3 sensors also showed good or very good performance across all seasons and locations, despite the extreme temperatures during the summer colocation in China.

The RH corrected $PM_{2.5}$ measurements agreed well with the reference instruments. The agreement was impacted when the RH correction could not be applied, or when the PAM data had to be compared to a non-colocated reference instrument (ca. 3 km distance).

In summary, the outdoor performance of the PAM in a static configuration was sufficient for personal monitoring purposes, provided appropriate data processing (including RH correction of $PM_{2.5}$) and suitable environmental conditions (T < 40°C; pollution concentrations > LOD).

Table 3.5 Summary of the sensor performance of the PAM during the four outdoor colocation experiments (UK and China, during the heating and non-heating season). The performance was classified based on a combination of RMSE and R^2 between PAM sensors and reference. The exact correlation parameters are given in Table 3.4. Factors that may have impacted the agreement between PAM and reference are given in brackets (1-5, legend below).

Location	**Season**	**CO**	**NO**	**NO_2**	**O_3**	**$PM_{2.5}$**
China	heating	very good (1)	very good	good	good	very good
China	non-heating	medium (1, 2)	low (2, 3)	low (2)	good (2)	medium (5)
UK	heating	medium (1)	medium (3)	very good	very good	low (4)
UK	non-heating	medium (1)	low (3)	good	good	good

Performance classification

very good	$R^2 > 0.9$	AND	RMSE < 10% of max. concentration
good	$R^2 > 0.8$	AND	RMSE < 15% of max. concentration
medium	$0.6 < R^2 < 0.8$	AND	RMSE < 25% of max. concentration
low	$R^2 < 0.6$	OR	RMSE > 25% of max. concentration

Impact on PAM-reference agreement

1	High intrinsic noise of reference instrument
2	Internal PAM temperature > 40°C
3	Pollutant concentration close to LOD (mean $\geq$ 5 ppb)
4	RH correction not applicable
5	Reference instrument not colocated

3.3 Indoor performance of the NO_2 and PM sensors

Low-cost air pollution sensors have widely been characterised in outdoor colocation experiments as they were described in the previous sections. However, little is known about the performance of these sensors in indoor environments, where people spend most of their time ([73]), and environmental conditions (e.g. temperature, RH) as well as emission sources may be significantly different compared with nearby outdoor environments.

When comparing indoor pollution concentrations measured by PAMs with outdoor pollution levels obtained at reference stations, it was found that, in the absence of local emission sources, the indoor CO and NO levels were similar to the outdoor concentrations whereas the NO_2, $PM_{2.5}$ and O_3 levels were much lower than outdoors (see Section 4.3). It is widely recognised that, due to its high reactivity, O_3 concentrations inside buildings are usually much lower than outdoors [96, 149, 153]. Previous studies on the indoor to outdoor (I/O) ratio of air pollutants in residential buildings found I/O ratios ranging from 0.4 to 1.6 [61] for NO_2 and I/O ratios in a broad range from 0.2 to 2.5 for $PM_{2.5}$; however, average values of the ratios were close to one (1.01-1.08). The low I/O ratios for NO_2 and $PM_{2.5}$ found during the AIRLESS deployment were surprising, especially considering the strong indoor sources.

To ensure that the low indoor concentrations were not caused by sensor artefacts, the OPC and NO_2 sensor were tested against reference instruments in an urban flat in central Beijing during the non-heating season (May 2017).

One PAM was deployed in the living area next to two commercial instruments that were used to provide reference measurements: (1) a cavity attenuated phase shift spectroscopy instrument (CAPS Teledyne T500U) for NO_2 and (2) a portable commercial spectrometer (GRIMM 1.108) for particulate matter measurements (Table 3.1). The results are shown in Figure 3.6. During the experiment the occupants relied on natural ventilation, adjusting the windows freely to achieve thermal comfort. Median indoor temperatures were 26.0°C (5%-95% range: 17.1-28.8°C), and the median internal PAM temperature was 33.0°C (5%-95% range:24.3-36.2°C), which is comparable with the temperature range during the non-heating season field deployment to participants (median internal temperature: 35.0°C, 5%-95% range: 28.5-39.9°C, Figure A.9). The sensors were calibrated as described in Section 2.2 using the the sensitivities extracted from the outdoor colocations of the heating and non-heating seasons combined. The performance of the low-cost sensors in the indoor environment (Figure 3.6) was comparable to the outdoor performance demonstrated in the previous section ($R^2 \geq 0.93$; gradient m = 0.97 and m = 1.1; RMSE = 3 ppb and 7µg m^{-3} for NO_2 and $PM_{2.5}$, respectively), proving their suitability to quantify indoor air pollution levels for these species when adequately calibrated under similar

environmental conditions. The low NO_2 and $PM_{2.5}$ concentrations observed in Figure 4.1 were therefore not an artefact of corrupt sensor responses but represented concentrations close to the real ones. The pollutant losses in the indoor environment of a representative participant (U123) were further analysed by quantifying the concentration decays of each pollutant (Section 5.2.1), finding that $PM_{2.5}$ and NO_2 were in fact affected by pollutant sinks lowering the indoor concentrations compared to the outdoor levels.

Similar to Section 3.1, this indoor experiment extracted the calibration parameters from a training dataset (here: the combined outdoor colocation periods in winter and summer) and applied them to a validation dataset (here: the indoor colocation period). The excellent agreement of the PAM measurements with the indoor reference reinforces the conclusion from Section 3.1 that the developed linear model is robust and can reliably be applied beyond the calibration periods to a mainly indoor dataset collected during the deployment to the participants
This section validated the indoor performance of the NO_2 and $PM_{2.5}$ sensors of one PAM. The performance of two large PAM networks measuring personal (i.e. mainly indoor) exposures will be further evaluated in Section 5.1.3.

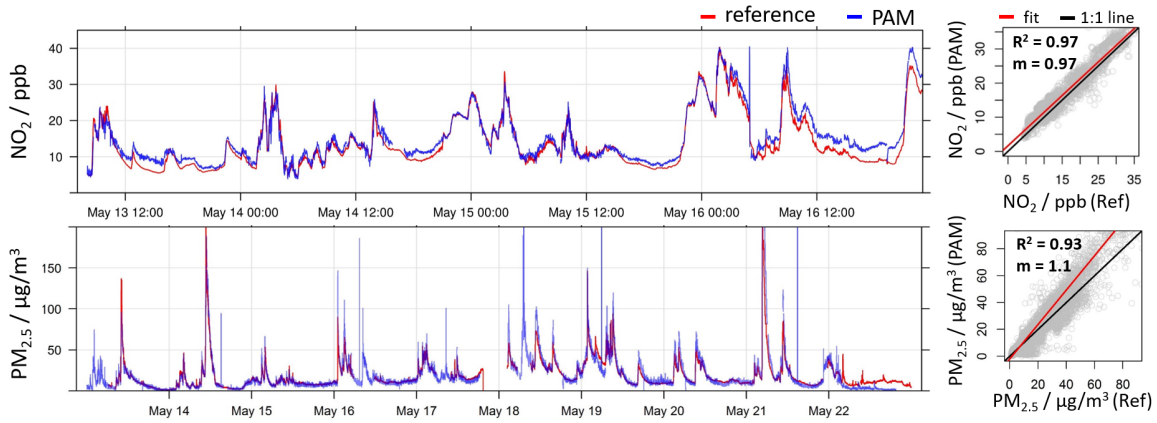

Fig. 3.6 Indoor colocation of a PAM (blue) with portable commercial instrumentation as reference (red; Table 3.1) in an urban flat in China during the non-heating season. Left: Time series of the measurements. Right: Scatter plots between commercial instruments and miniaturised sensors. The 1:1 line is in black and linear fit in red. Mass concentrations were calculated from particle counts within the size range 0.38 -17 µm and same aerosol density for both instruments

3.4 Mobile applications of the PAM

The aim of this section is to evaluate the PAM reproducibility and accuracy while in motion, with pedestrian and on-vehicle deployments.

3.4.1 Reproducibility of the PAM during a pedestrian deployment

Multiple (in this case nine) PAMs were carried by a pedestrian while keeping an activity diary and walking between two indoor environments via a busy road in Cambridge, UK (weekday in January). Using NO measurements (the main traceable component from combustion engines) as an illustrative example, Figure 3.7 shows the simultaneous measurements of all PAMs as a time series (a) and the scatterplots between the measurements of two of those PAMs separated into indoor (b) and outdoor data (c).
Significant changes of the pollution levels were observed when moving between the different environments, illustrating the high heterogeneity of personal exposure in daily life. Compared with the indoor environments, walking in traffic resulted in elevated pollution exposure events. As illustrated in the time series of Figure 3.7, the difference in pollution levels between the three micro-environments was significantly higher than the variability between PAM measurements. Table 3.6 gives an overview of the median correlations between the sensors of the colocated moving network. In indoor environments an excellent agreement between all sensors (median $R^2 \geq 0.96$) was found, indicating a high sensor reproducibility. An exception was the O_3 sensor, which showed a poor between-sensor correlation due to very low indoor and outdoor concentrations near the LOD of the sensor (< 5 ppb). There was still a good agreement between the sensors in the road environment, although it was lower than indoors (median $R^2 \geq 0.85$) due to highly heterogeneous air pollution concentrations driven by complex factors (e.g. canyon air mixing, moving vehicle sources, topology). This signifies that in such environments air pollution concentrations might differ on such short spatial and temporal scales that even sensors that are less than 1 m apart from each other capture a slightly different exposure profile.

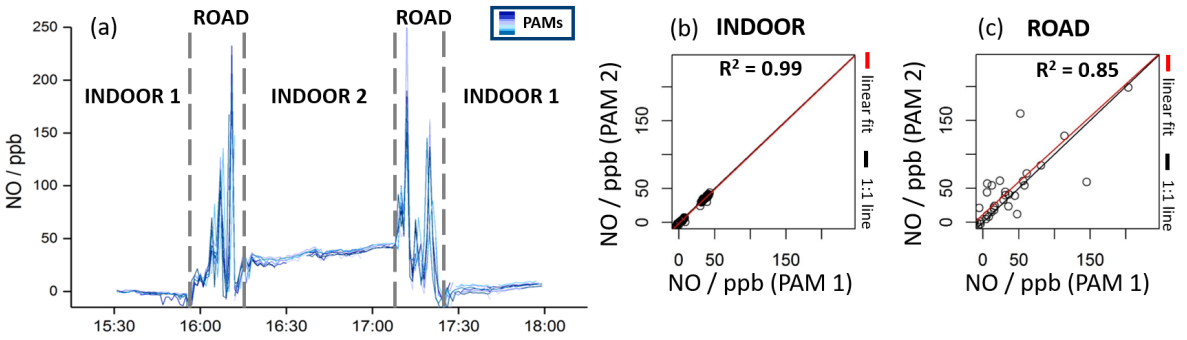

Fig. 3.7 Short-term deployment of nine PAMs carried simultaneously by a pedestrian moving between two indoor environments (laboratory, café) in Cambridge, UK, in January 2018. (a): Time-series of NO measurements from the PAM sensors (blue lines). (b) and (c): Scatterplots between two of those PAMs, where indoor data was separated from outdoor data. The 1:1 line in black; and linear fit line in red.

Table 3.6 Correlations between PAM sensors. Adjusted R^2 values of each sensor pair of the simultaneously carried PAMs were determined. Median values $\bar{R}^2$ of all combinations are presented in the table below. Very low O_3 levels (< 5 ppb) resulted in poor between-sensor correlations and are given in italics.

	Median $\bar{R}^2$	
	Indoor	Outdoor
NO	0.99	0.87
NO_2	0.96	0.94
O_3	*0.16*	*0.46*
CO	0.99	0.95
$PM_{2.5}$	0.99	0.85

3.4.2 Accuracy of the PAM during a vehicle deployment

A PAM was mounted on the roof of a battery-powered vehicle equipped with multiple commercial instruments (Table 3.1) mapping air pollution levels in London at speeds of up to 60 km h^{-1} for 1 day during the non-heating season (Figure 3.8). The PAM was mounted on the roof with the OPC inlet facing forwards and the EC sensors facing to the sides. The reference instrument inlets were located on the car roof as well. No correlation between car speed and RMSE values in the gaseous and particulate measurements was observed as the OPC contains an airflow measurement unit which compensates for any wind or internal flow dependence. Considering the high spatial variability of air pollution in traffic environments (as discussed in the previous section), the accuracy of the PAM in a mobile configuration was high for all targeted pollutants ($\bar{R}^2 \geq 0.54$). To illustrate the large degree of variability of air pollution concentrations over time, the investigated area was mapped throughout the day multiple times with the highest concentrations of $PM_{2.5}$ and NO_2 recorded during the morning rush hour.

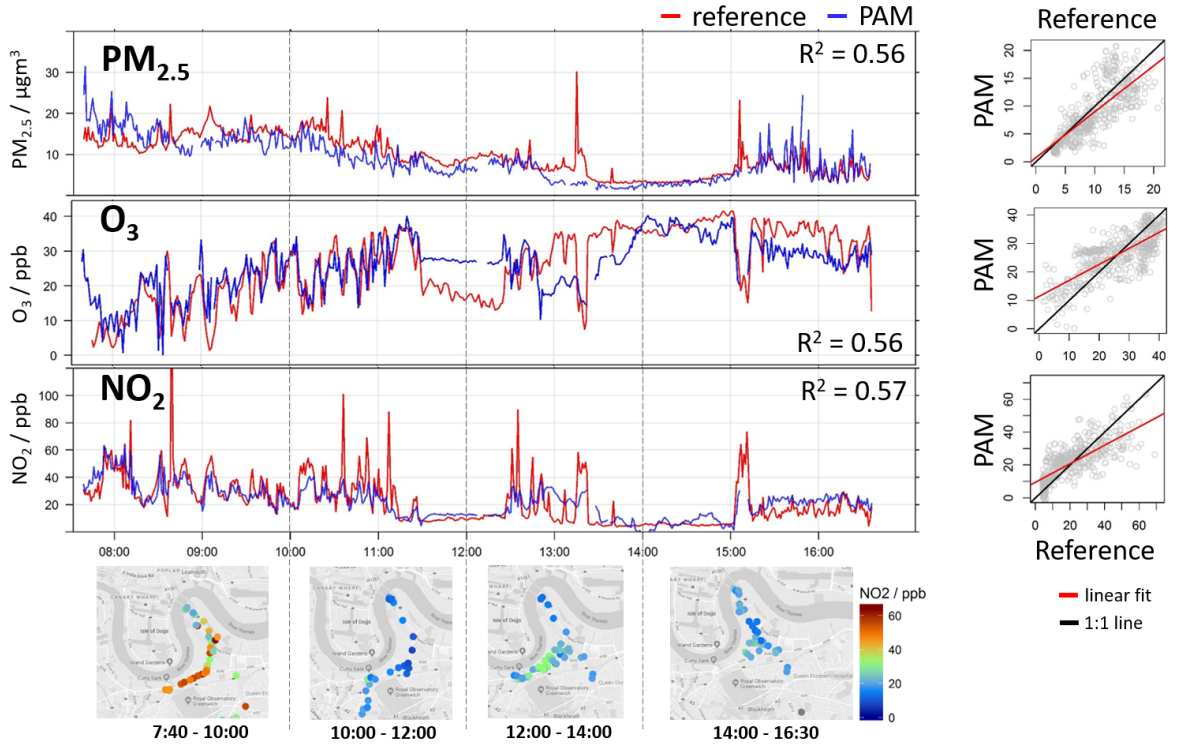

Fig. 3.8 The vehicle deployment in London, UK: a PAM was attached to a car equipped with multiple commercial instruments (Table 3.1) for four days. (a): Time-series of PAM measurements (blue) and commercial instruments (red). (b): Corresponding scatterplots between measurements from commercial instruments and the PAM in motion. The 1:1 line in black; and linear fit line in red. (c): Maps (map data 2019 Google) of the mobile deployment over 2-hour windows illustrating the large temporal variability of NO_2.

3.5 Chapter summary

This chapter demonstrated that, with suitable calibration and post-processing, the performance of currently available low-cost air quality sensors, in this case incorporated into a highly portable personal monitor (the PAM), is comparable with the performance of reference instrumentation across a wide range of conditions:

- in diverse outdoor environments with varying emission sources (urban background and traffic);
- across seasons (over a wide temperature and RH range);
- in two geographical settings with differing air pollution levels and meteorological profiles (UK and China);
- in indoor environments (residential, laboratory, café), and
- in static and in non-static deployments.

There are certain performance caveats with the PAMs which, once identified, are likely to be addressed in future generations of sensors:

- The performances of the CO, NO and NO_2 sensors were found to degrade at temperatures above 40°C. However, such extreme environmental conditions were not encountered when the personal exposure measurements were obtained (Section 2.3), i.e. the performance criteria were met during the field deployment.
- A limitation of all optical PM sensors, low-cost or reference, is that they cannot measure small particles below a critical size threshold (typically 200–400 nm). This chapter shows that by appropriate local calibration, this shortcoming can be largely accounted for.

The key conclusion of this chapter is that, when suitably operated, the personal air pollution monitors can deliver traceable high-quality exposure metrics which can address scientific, health and policy questions for the indoor and outdoor environment in a way that has not been previously possible.
Based on the conclusions of this chapter, it can be assumed that the personal exposure data collected in the UK, China, Germany and Kenya (Section 2.3) are reliable and of appropriate quality for the exposure analysis described in the three following chapters.

Chapter 4

Improving personal exposure estimates: PAM vs monitoring station

Due to limitations in cost, instrument availability and participant burden, air pollution epidemiology has traditionally relied on proxies to represent the exposure of a person. The metrics used to describe personal exposure usually come from monitoring stations that measure the outdoor pollutant concentrations rather than representing the actual pollution exposure of a person. In the scientific literature this is called *exposure misclassification*. It is defined as the difference between a chosen exposure metric, usually derived from measurements of the ambient air at postcode level or coarser, and the true exposure of a person [33].

This chapter uses the exposure measurements from the AIRLESS project to demonstrate the potential of portable air quality monitors to improve the accuracy of personal exposure estimates and therefore to support epidemiological research in drawing more reliable associations between air pollution and health impacts. The chapter additionally addresses considerations on the suitability and reliability of novel sensor technologies to advance our understanding on multi-pollutant exposures on health. Collecting personal exposure measurements of multiple pollutants at unprecedented spatial and temporal resolution could enable researchers, for the first time, to directly and accurately assess the toxicity of a specific pollutant, or indirectly reflect source-related health effects. Section 4.4 introduces the concept of breaking the correlation between individual pollutants (and thus reducing the multi-colinearity between different pollutant species in health models), as well as the concept of looking at their ratios to infer sources.

4.1 An illustrative example of exposure misclassification (AIRLESS panel)

As part of the AIRLESS project, personal exposure measurements were collected with a network of PAMs in rural and urban Beijing (see Section 2.3.2). In the following, these personal exposure measurements are compared with simultaneous observations from static air quality monitoring stations in close proximity to participants' home locations.

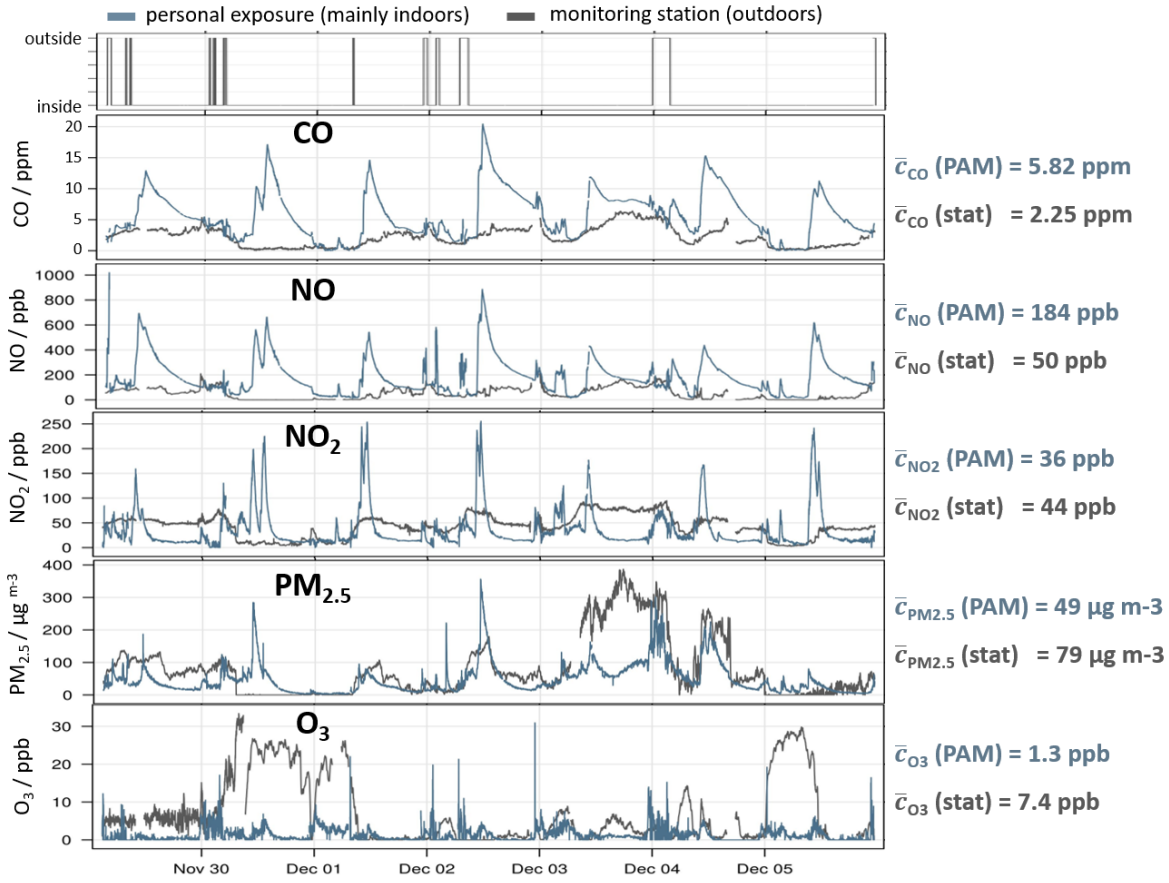

Fig. 4.1 Time series of the air pollution exposure of a representative AIRLESS participant (urban participant U123 carrying PAM 165 during the heating season). Personal exposure measurements (PAM, blue) are compared with data from the closest monitoring station (station, grey) to the participant's home (ca. 5 km, see map in Figure A.10 in the Appendix). Mean exposures are given on the right. The top row indicates whether the participant is outdoors or indoors (based on time-activity model, see Section 6.2). PAM and reference measurements and time-activity classification are in 1 min resolution. Time in UTC.

Using a representative participant as an illustrative example, Figure 4.1 highlights the complex issues of personal exposure to multiple pollutants during daily life. On one hand, personal

CO, NO, NO_2 and $PM_{2.5}$ concentrations regularly exceeded the outdoor levels suggesting the presence of strong indoor emission sources. The fairly regular diurnal pattern of operation indicates that occupant behavioural patterns (i.e. cooking activities in a gas stove) caused personal exposures up to 10 times higher than the ambient pollution levels. On the other hand, when no emission sources were active, the personal NO_2, O_3 and $PM_{2.5}$ levels were much lower than the outdoor concentrations, indicating the presence of indoor pollution sinks. In the case of ozone particularly, the personal indoor exposures were up to 25 times lower than the ambient concentrations, due to the high indoor reactivity of the pollutant. On the contrary, indoor CO and NO approached the outdoor concentrations because they are relatively stable in these timescales in indoor environments. As a result, the mean personal CO and NO exposures (given on the right of Figure 4.1) were higher than the mean ambient concentrations, whereas the personal O_3, NO_2 and $PM_{2.5}$ concentrations were on average lower than the ambient concentrations. These findings were found to be broadly representative across the two AIRLESS cohorts as demonstrated in Section 4.3.

These results emphasise the significant differences between personal and ambient pollution concentrations. The extent of this exposure misclassification depends on the reactivity of the pollutant, as well as on the characteristics of the individual environments a person is located in (e.g. distinct air pollution sources and sinks). The potential of novel sensor technologies to expand the spatial and temporal coverage of personal exposure measurements of multiple pollutants allows to capture the high variability between individuals, microenvironments, seasons and settings. The interrelationships between personal and outdoor levels are quantified in more detail in Chapter 5.

4.2 Exposure misclassification vs. measurement uncertainty

The comparison in the previous section is based on the assumption that the PAMs measure the true personal exposure of a person. However, the observations from portable monitors also contain uncertainties due to measurement error which is a major concern in the research community [84]. To address such concerns, this section compares the exposure estimation error introduced by the poor spatial resolution of monitoring stations (exposure misclassification) with the exposure estimation error due to the instrument uncertainty of the personal monitoring devices.

Figure 4.2 uses again the example of AIRLESS participant U123 to illustrate this comparison. For clarity reasons, the graph here shows only one day of the volunteer's participation week ($3^r d$ Dec 2016), comparing the NO_2 concentrations measured at PKU monitoring station (grey)

with the personal NO_2 exposures measured with a PAM (blue, cf. Figure 4.1). The instrument uncertainty was determined as the RMSE (Equation 3.1) of the PAM compared to a reference station when the two instruments were colocated (see Section 3.2). The RMSE of U123's PAM was 12.2 ppb which was close to the average RMSE found for NO_2 during the AIRLESS winter campaign (11.8 ppb, see Table 3.4). This uncertainty was added as confidence intervals of the personal exposure measurements in Figure 4.2 (blue shades).
The difference between the personal NO_2 concentrations and the observations from the outdoor monitoring station represents the exposure misclassification. For most of the day, this difference was substantially larger than the instrument uncertainty of the PAM, may it be introduced by indoor sinks that caused lower personal NO_2 exposures or by local emission sources that led to higher personal NO_2 exposures than captured at the station. This illustrative example demonstrates that the PAM improves the accuracy of personal exposure estimations despite measurement uncertainties that may be higher than those of established air quality instruments.

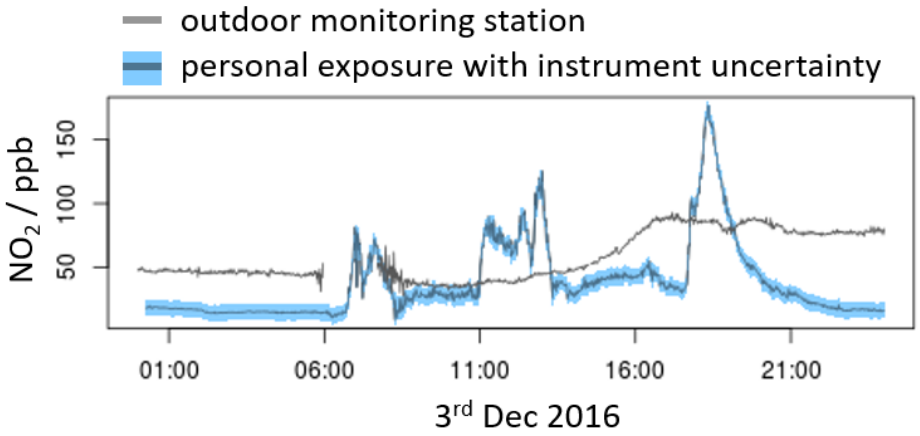

Fig. 4.2 Instrument uncertainty vs. exposure misclassification: One day of personal NO_2 exposure measurements of participant U123 (blue) compared to outdoor NO_2 from PKU monitoring station (grey, cf. Figure 4.1). The instrument uncertainty of the PAM (RMSE) is illustrated as confidence interval around the personal measurements. The difference between personal exposure and stationary measurements due to indoor chemical sinks and local sources is substantially larger than the instrument uncertainty.

Table 4.1 looks at the comparison between instrument uncertainty and exposure misclassification across the entire AIRLESS sensor network. The instrument uncertainty for each pollutant was determined as the RMSE between PAM and reference instrument during the AIRLESS winter colocation as described in Section 3.2. Similarly, the RMSE between monitoring station

Table 4.1 Comparison between exposure misclassification of static monitoring stations and measurement uncertainty of the PAM. Normalised RMSE values between PAM and station (see footnote), averaged over entire sensor network. Data from AIRLESS winter campaign.

	instrument uncertainty	exposure misclassification
CO	0.12	1.00
NO	0.25	1.04
NO_2	0.28	3.68
O_3	0.33	5.89
$PM_{2.5}$	0.31	2.80

and personal measurements was calculated as a measure for the exposure misclassification[1]. For better comparison across the pollutants, the RMSEs were normalised by dividing their values by the mean concentration of each pollutant measured with the corresponding method. The resulting normalised RMSE (nRMSE) values, averaged over the entire AIRLESS sensor network, are summarised in Table 4.1.

The instrument uncertainty was in a comparable range for all five pollutant sensors (nRMSE between 0.12 and 0.33). The CO sensor showed the lowest uncertainty (nRMSE = 0.12), due to the outstanding performance of this sensor already demonstrated in Chapter 3. The O_3 sensor had the highest uncertainty (nRMSE = 0.33) which might be attributed to the relatively low O_3 concentrations during winter. The exposure misclassification of the stations was substantially (up to over 17 times) larger than the measurement uncertainty of the PAM for all pollutants. This crucial finding emphasises that the personal monitoring devices are, despite their lower accuracy compared to static monitoring stations, a more reliable alternative for the quantification of personal exposures of individuals.

The misclassification of the CO and NO exposure estimations was comparable, whereas the NO_2, $PM_{2.5}$ and O_3 misclassification was distinctly higher. This agrees with the findings from Section 4.3 and can be attributed to the interactions of pollutant-specific sinks and sources which will be further discussed in Chapter 5.

[1]Note that the reference instruments at the monitoring station were used as true values and the PAM as estimator of the measured pollutant concentrations to calculate the instrument uncertainty. For the exposure misclassification, the PAM measurements served as true values and the station measurements as estimator for personal exposures.

4.3 Seasonal and spatial variability of daily life exposures in China

This chapter has so far highlighted the necessity of collecting personal exposure measurements at high spatial and temporal resolution to capture the strong variability of sources and chemical sinks in the environment of an individual. This section examines how these relationships vary across the AIRLESS cohorts and between seasons.

The average air pollution exposure of each participant was calculated with two methods: (1) by averaging their PAM measurements over the entire participation time (one week) $\bar{c}$(PAM) and (2) by averaging the measurements of the closest monitoring station over the same time period $\bar{c}$(station) to generate the exposure estimates from ambient air as they are conventionally used by epidemiological studies (see Section 1.2). These two exposures were plotted against each other (Figure 4.3). In an ideal scenario, the exposure metric ($\bar{c}$(station)) would accurately predict the true exposure of a participant ($\bar{c}$(PAM)), and all points should fall on the identity line (x=y). Deviations from this line may be attributed to exposure misclassification. Points above the identity line indicate that the true personal exposures were higher than the ambient estimates while points below suggest that the personal exposures were lower. A larger vertical distance between a data point and the identity line indicates a larger exposure misclassification for the corresponding participant.

As the people spend on average over 90% of their time indoors [73] (see also Figure 6.17), the exposure misclassification can be mainly attributed to the air quality differences between indoor and outdoor environments. Keeping this in mind, the following points describe the relationships between ambient measurements and personal exposures for each pollutant in winter and summer based on Figure 4.3.

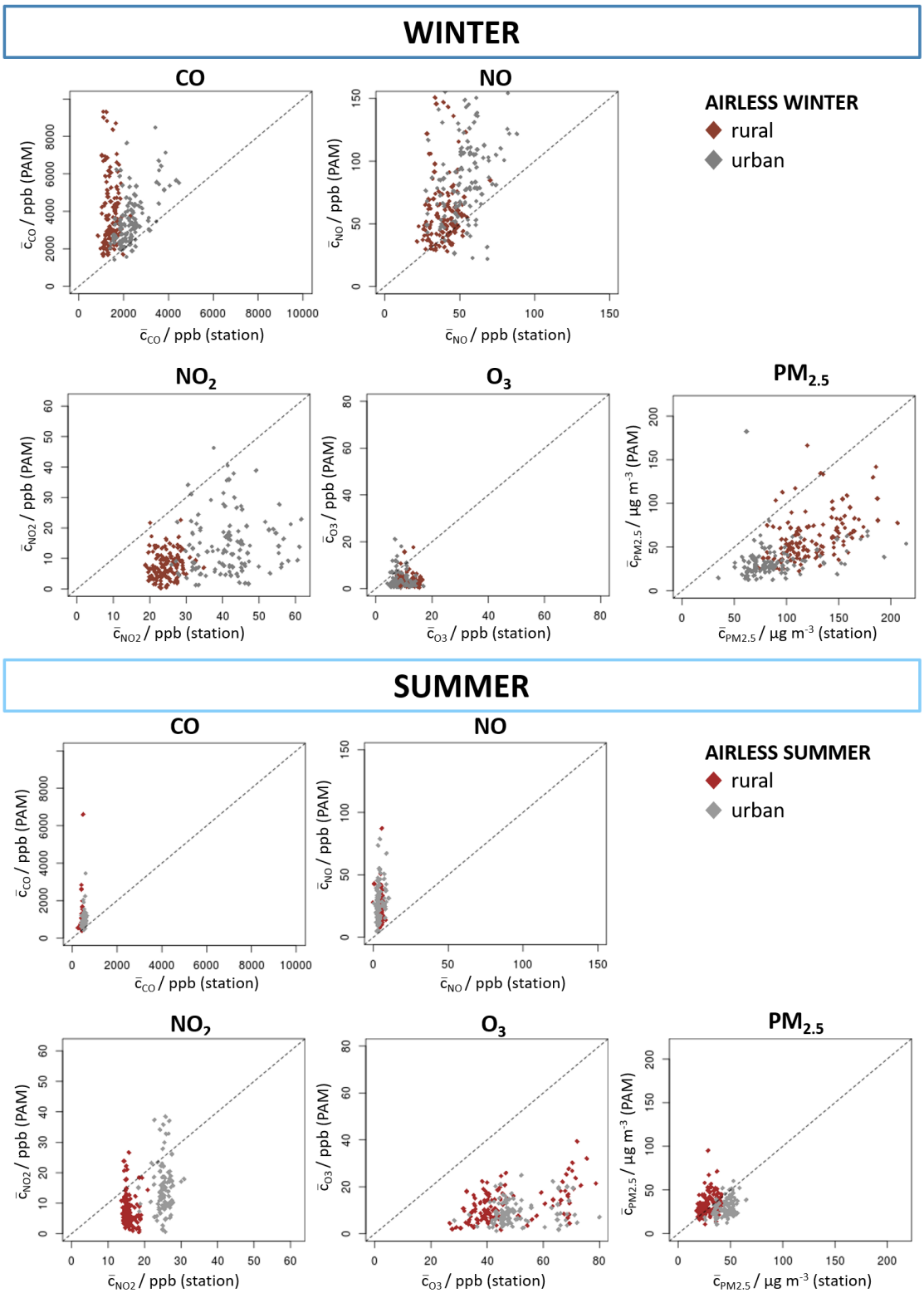

Fig. 4.3 Personal exposure of each participant (measured by PAM, y-axis) plotted against average exposure estimates based on static observations over the same time period (monitoring station, x-axis) in winter (top) and summer (bottom). Every dot represents one participant, marking their average exposures measured over their participation week. Identity line (x=y) dotted in black.

Differences between personal and ambient concentrations in the urban and rural site during the in winter season (top of Figure 4.3)

- The personal CO and NO exposures were generally higher than the exposure estimations based on ambient measurements. The outdoor concentrations of both these gaseous pollutants were higher at the urban site, however personal exposure of urban and peri-urban participants was comparable, stressing the importance of sources close to the individual on overall exposure.
- In contrast to CO and NO, the personal NO_2, O_3 and $PM_{2.5}$ concentrations were generally lower than the ambient estimations. Local pollution sinks significantly reduced personal exposure to these harmful pollutants.
- Following the trend of CO and NO, ambient NO_2 concentrations were substantially higher in the urban environment than at the rural site which can probably be ascribed to the higher traffic volume in Beijing city. This difference was, however, less marked in the personal exposure estimations where the majority of the urban exposures was in the same range as the rural personal exposures. This indicates that the local NO_2 sinks and sources may have a stronger impact on personal exposures than the ambient levels.
- The ambient O_3 levels were slightly lower at the urban site, probably because O_3 reacted with the higher local NO_2 concentrations. However, no difference between the rural and urban cohort was observed in the personal exposure estimates due to the previously mentioned strong indoor sinks.
- Contrary to NO_2 levels, the ambient $PM_{2.5}$ concentrations were higher at the rural site. The personal exposures were also higher in the rural cohort. This indicates stronger local $PM_{2.5}$ sources in the rural area which might be attributed to bio fuel burning for domestic energy use (urban: mainly central heating, rural: mainly charcoal and firewood-based; see Section 2.3.2).

In general, the personal exposures of individuals that are exposed to the same ambient pollution levels vary substantially (shown as the vertical spread of the points). This variability can be ascribed to the complex interactions of local pollution sinks and sources in the individual microenvironments.

Differences between personal and ambient concentrations in the urban and rural site during the summer season (bottom of Figure 4.3)

The ambient pollution levels in summer were lower than in winter for all pollutants except for ozone. Higher O_3 levels in summer were caused by the raised intensity of UV light which increases the O_3 production. Large-scale meteorological analysis performed by Shi et al. suggests that the higher ambient air pollution levels in winter were due to more frequent air stagnation and weak southerly circulation [125]. Winter outdoor air pollution was characterised by several high $PM_{2.5}$ pollution events, whereas, during the summer there were events of high O_3 concentrations.

- As in the winter season, personal levels of CO and NO were higher than the ambient levels. The absolute values of the personal exposure were, however, lower than in winter driven by lower outdoor concentration and weaker local sources. The variability between individuals was larger than the variability between sites showing the relative importance of local sources on personal exposure.
- Similar to the case in winter, the ambient NO_2 levels in the urban site were higher than in the rural site, and the opposite case was observed for the $PM_{2.5}$ concentrations. These local differences were even more distinct in summer.
- Although the ambient O_3 concentrations were significantly higher in the summer, the major part of the personal O_3 exposures was in the same range as the personal O_3 exposures observed in winter. This indicates the presence of strong local O_3 sinks.
- The personal $PM_{2.5}$ concentrations were very similar to the ambient $PM_{2.5}$ levels during the summer time (points close to 1:1 line). This might be due to increased building ventilation in the summer.

A distinct profile of exposure is evident between the urban and rural panels, as the urban participants are exposed to significantly higher levels of NO_2 while the rural panel is exposed to significantly higher concentrations of particulate matter. These marked differences indicate variable sources of exposure in the two panels, which will be discussed in more detail in Section 4.4, and their implications on health in Section 4.5.

Figure 4.4 summarises the personal air pollution exposures of the two AIRLESS cohorts (blue boxplots) and the exposure estimations based on monitoring station observations (white boxplots). Note that here, the 1-min time resolution of the concentration measurements was preserved rather than averaging the exposures over the participation time of each volunteer as done in Figure 4.3. This way, peak exposure events were included.
As already observed in Figure 4.3, the ambient concentrations of all pollutants but O_3 were substantially higher in winter than in summer. The personal CO and NO exposures followed this seasonal trend and were on average higher than the ambient levels. The difference between personal and outdoor concentrations was much higher during winter indicating stronger sources in proximity to the participants compared with the summer.
Contrary to personal CO and NO levels, which broadly followed the outdoor trends, the NO_2, O_3 and $PM_{2.5}$ levels were significantly lower than the ambient levels in both seasons and showed little ($PM_{2.5}$ and O_3) or no (NO_2) seasonal variation. The personal measurements show that there is a substantial exposure misclassification that could be introduced when using outdoor measurements as exposure metrics and the extent of the error depends on season and reactivity of each pollutant.

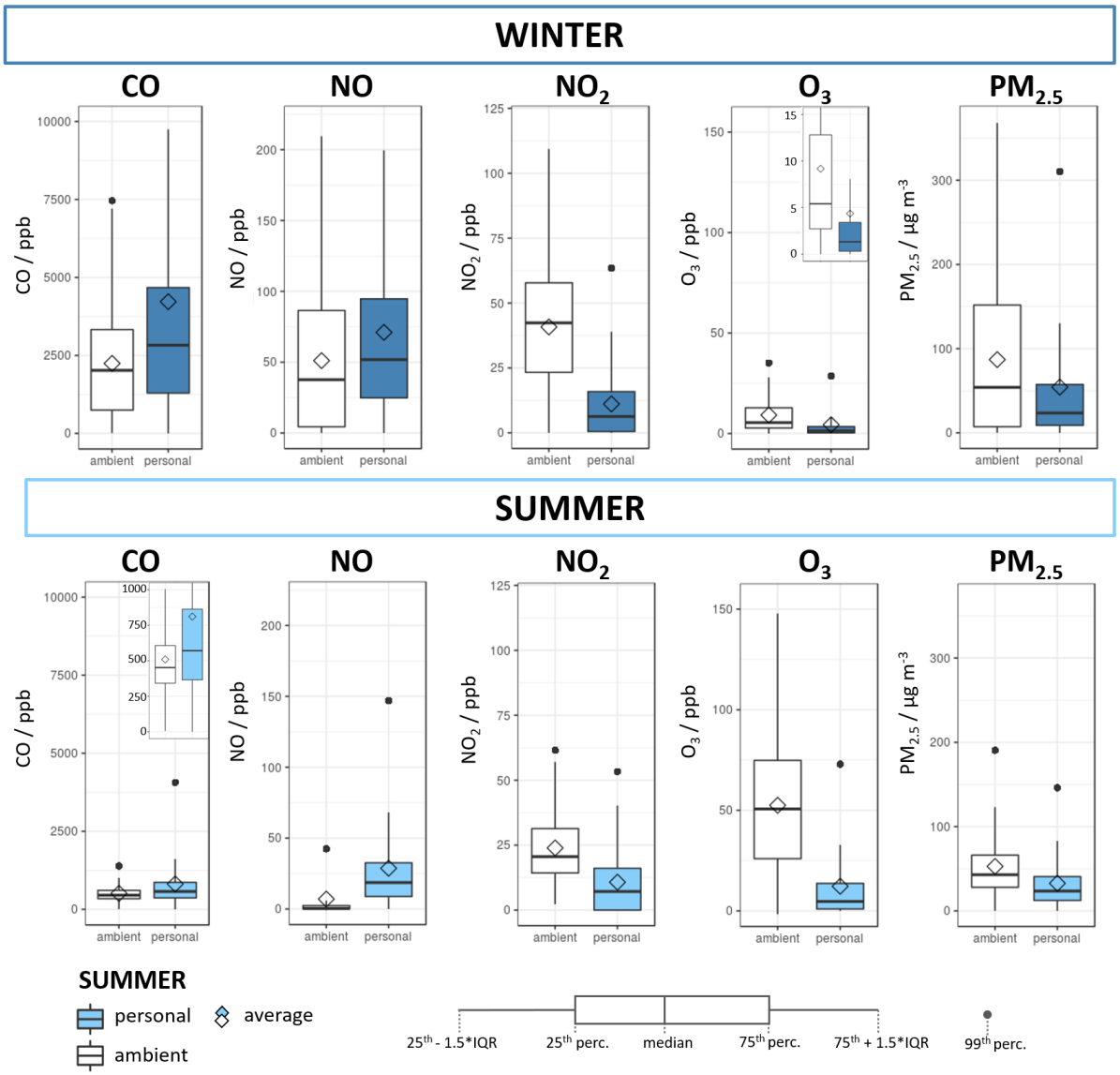

Fig. 4.4 The white boxplots illustrate outdoor air pollution levels measured at the reference monitoring stations at the urban and peri-urban sites during the summer (May-June 2017) and winter (Nov-Dec 2016) campaigns. The blue boxplots show the personal exposure levels measured with 60 PAMs deployed to 251 participants at the urban and peri-urban site during the same periods. Stable pollutants left (CO, NO), reactive pollutants right ($PM_{2.5}$, NO_2, O_3).

4.4 Relationships between different pollutant species

When measured at low spatial and/or temporal resolution, pollutants with common sources often appear correlated, as is the case between traffic related pollutants (e.g. $PM_{2.5}$ and NO_2) in outdoor environments. Section 1.2 highlights that such correlations between individual pollutants inhibit epidemiological studies from identifying single air pollutant species as causal agents for health outcomes.
Section 4.4.1 will examine whether the use of personal monitors has the potential to break this correlation and therefore to ultimately allow epidemiological research to identify individual pollutants as causal agents for adverse health effects. The *ratio* between two pollutant species might substantially vary in different environments and provide information about the air pollution mixture and, therefore, the type of emission sources in the direct environment. Section 4.4.2 assesses the concentration ratios between the measured pollutant species, comparing the observations from a monitoring station with those from a PAM.

4.4.1 Correlation between pollutants

The correlation between CO and NO was investigated by comparing measurements of a representative personal monitor with the observations collected at the nearest static monitoring station. The recorded concentrations over this period were plotted against each other in a scatter plot and linearly fitted for the calculation of the coefficient of correlation R. Figure 4.5 compares the CO-NO correlation found at the monitoring station of Peking University (top figure) against the personal exposure measurements of PAM 174 during the winter field deployment (deployed to five participants over the course of the campaign, bottom figure).
Despite measured in relative vicinity, the two exposure measurements differ both in their profile as well as in average pollution levels. The time series recorded by the monitoring station tracks rather slow changes of the surrounding air pollution levels, whereas the PAM captures short term events from local sources which can be seen as sharp peaks in the time series. The CO concentrations recorded by the PAM were higher than the CO levels seen by the fixed monitoring station: While PKU reference station measured CO levels of maximum 6 ppm, the CO concentrations collected by the PAM often exceeded 10 ppm with high exposure events of up to 30 ppm. Similarly, the NO measurements of the monitoring station rarely exceeded 200 ppb whereas short term NO exposures in the PAM measurements reached much higher concentrations of up to 600 ppb.
The high concentration peaks experienced by the PAM show that the monitor was exposed to air pollution sources in close vicinity. The monitoring station is instead relatively far away

from any direct pollution sources and therefore exposed to a mixture of different emissions from its wider environment blended with ambient air.

The scatter plots on the right of Figure 4.5 where linearly fitted to determine the correlation coefficient R. The linear fit of the observations from the monitoring station is shown as a red line in the top scatter plot. The blue line in the bottom graph indicates the linear fit of the PAM measurements. For comparison, the linear fit of the stationary measurements was added to the bottom graph as a red dashed line.

A relatively high correlation was observed between the CO and NO concentrations measured at the monitoring station (R = 0.85) which is also visible in the strong similarity of the two corresponding time series. The two pollutants are less correlated when measured by the PAM (R = 0.37). Note that a large number of PAM observations fall onto the same gradient as the monitoring station (highest point density around the red dashed line). These observations occurred when the participants were exposed to the regional CO and NO concentrations (away from local emission sources) which were also measured at the monitoring station. The distinction between local and regional air pollution sources is further discussed in Chapter 5.

Figure 4.6 shows the correlations between all possible combinations of air pollutant species when measured at PKU monitoring station (top) and when measured with a portable monitor (bottom). The measurements from the station show high correlations between all pollutant combinations (R = 0.55 - 0.85; ozone is anti-correlated with other pollutants: R = -0.39 and -0.68). The correlation between the different pollutants is substantially reduced in the PAM observations (R = 0.24-0.38, ozone: -0.05 and -0.16). The reduction of the pollutant-pollutant correlation emphasises the value of personal exposure monitoring since it may help epidemiological studies to disaggregate the health effects of different air pollutant species.

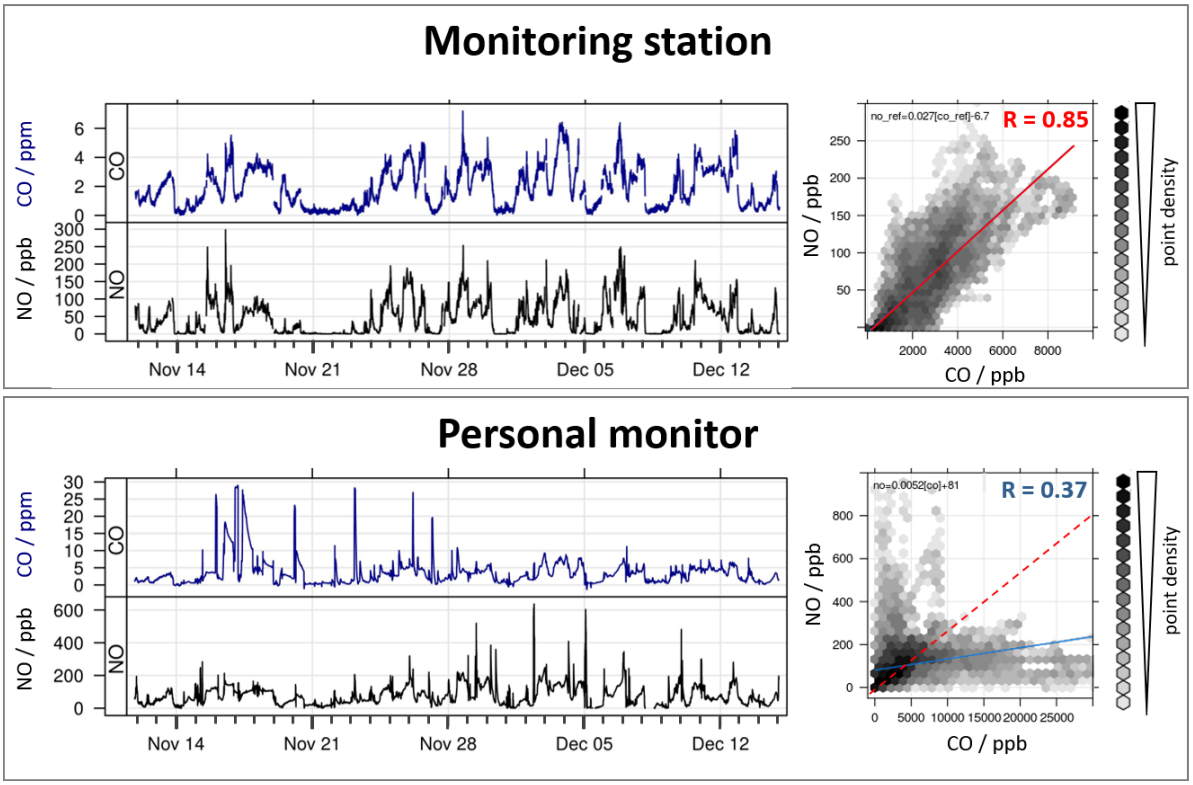

Fig. 4.5 Correlation between the concentration measurements of two different pollution species measured at PKU monitoring station (upper panel) and with a PAM (lower panel) deployed to five participants over the course of the campaign. Both datasets were collected over the same time period and at the urban site (Beijing) during the winter campaign. Left: time series of CO (blue) and NO (black) measurements. Right: hexbin plots of the corresponding measurements with linear fit and correlation coefficient R. The linear fit of the monitoring station data is shown as red dashed line in the bottom plot (PAM data) for comparison.

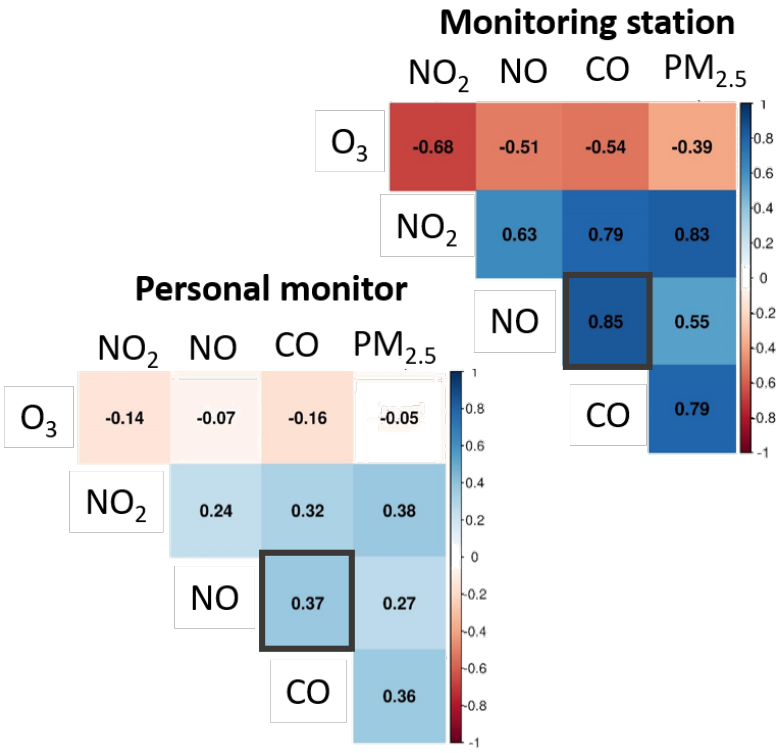

Fig. 4.6 Correlation coefficients between the concentration measurements of different pollution species when measured by a monitoring station (at urban site, upper graph) and with a portable air quality monitor deployed to five participants (PAM 174 - urban cohort, lower graph). All measurements from the winter field deployment (14/11-20/12/2016). The black square frames mark the pollutant pair that is shown in Figure 4.5.

4.4.2 Ratio between pollutants

The previous section showed that the concentrations of different pollutant species were strongly correlated when measured at ambient monitoring stations. Consequently, there was also a relatively constant ratio between the concentrations of those species, caused by a relatively constant mix of emission sources in the wider surroundings of the station.
Figure 4.7 illustrates this at the example of the relationship between NO_2 and $PM_{2.5}$ in urban and rural Beijing. The pollutant exposures of each participant of the AIRLESS cohorts were averaged over their participation period (same as in Figure 4.3). The mean $PM_{2.5}$ exposure of each participant were plotted against their mean NO_2 exposure. The exposure estimations based on stationary outdoor measurements (left) were compared with the exposures measured by the PAMs (right). The bottom graph of Figure 4.7 shows a histogram of the ratios between the mean $PM_{2.5}$ and NO_2 exposures with a solid line indicating the median and a dashed line indicating the mean ratio.

Stationary exposure estimates: At the rural site, the $PM_{2.5}$ levels were usually ca. 5 times higher than the NO_2 levels (red line in histogram), whereas at the urban site $PM_{2.5}$ was only twice as high as NO_2 (blue line). The lower $PM_{2.5}/NO_2$ ratio at the urban site can be attributed to the higher traffic volume in urban Beijing which led to higher NO_2 concentrations in the area. The histogram of the stationary observations (bottom left) shows a very narrow distribution of the $PM_{2.5}/NO_2$ ratios around the value of 2[2] for the urban site and 5 for the rural site, with almost no overlap between the two sites.

Exposure estimates from the PAM: As already shown in Section 4.4.1, the correlation between the two pollutant species was visibly lower in the personal exposure measurements of the PAM. The concentrations of the two pollutants were generally lower when measured with the PAM than at the static monitoring station which agrees with the findings from Figure 4.4. The personal NO_2 exposures were higher in the urban cohort which was, like in the case of the static observations, due to the higher traffic volume in urban Beijing. The personal $PM_{2.5}$ exposures were slightly higher in the rural cohort which might be due to stronger local $PM_{2.5}$ emission sources at this site.
The mean $PM_{2.5}/NO_2$ ratio was around 4 (median: 2.5) in the urban cohort and 17 (median: 8)

[2] Because $PM_{2.5}$ was given as concentrations ($\mu g\ m^{-3}$) and the gas measurements, including NO_2, were given as mixing ratios (ppb), the $PM_{2.5}/NO_2$ ratio is actually not dimensionless. However, this section compares the same ratios measured in two different ways (PAM vs station). Hence, the units are irrelevant for this comparison and were omitted for more clarity.

in the rural cohort. The pollutant ratios based on the PAM measurements differed significantly from the ratios observed at the monitoring station, suggesting that the participants were exposed to a very different air pollution mixture than the one observed in ambient air.
The differences between the mean and median values of the pollutant ratios indicate a wide distribution of the ratios, especially in the rural cohort where the $PM_{2.5}/NO_2$ ratio reached values of up to over 100. The large distribution of the pollutant ratios within one cohort indicates that the air pollution mixtures varied largely between the individuals. This variability was due to the large range of microenvironments and local emission sources individual participants were exposed to. Different microenvironments contain a variety of air pollution sources which emit different amounts of pollution species.The histograms of the rural and urban pollutant ratios overlap which means that the participant-participant variability of the air pollution mixture was higher than the variability between the sites.
Figure 4.7 looked at the ratios between the $PM_{2.5}$ and NO_2 concentrations during the AIRLESS project. Figure 4.8 presents the pollutant ratios for all pollutant combinations measured at a monitoring station (top) and with personal monitors (bottom). The histograms show the distribution of the ratios for the two cohorts, whereby the top pollutant species (columns) is divided by the pollutant species given on the side (rows). For instance, the histogram in the top left corner of each triangle shows the distribution of the observed NO_2/O_3 ratios.
The pollutant ratios observed at the monitoring station were generally very narrowly distributed around the mean ($\approx$ median) value, suggesting a fairly constant air pollution mixture around the monitoring station. The distribution of the ratios measured by the PAMs is much wider compared to the stationary observations, suggesting that the air pollution composition individuals are exposed to varies substantially more than around ambient monitoring stations. This can be explained by the heterogeneity of air pollution sinks and sources in the different microenvironments an individual passes through during daily life. This is further discussed in Chapter 6.
Not only the distribution of the ratios, but also the absolute values of the ratios differed between ambient and PAM measurements. For instance, the mean CO/NO_2 ratio (triangle middle of Figure 4.8) observed at the station was 59 for the rural site and 56 for the urban site, while the same ratio measured by the PAMs was 1327 for the rural site and 402 for the urban site. This stresses the difference in the air pollution mixture observed in personal and ambient exposures, as well as at the two monitoring sites. Different air pollution mixtures are likely to have different toxicities and health impacts. Preliminary results from a health analysis of the AIRLESS data confirmed this hypothesis by showing that some health effects (monocyte

count) of $PM_{2.5}$ were different in the rural than in the urban cohort, suggesting that $PM_{2.5}$ has different toxicities at the two sites (see Section 4.5 in the Appendix).

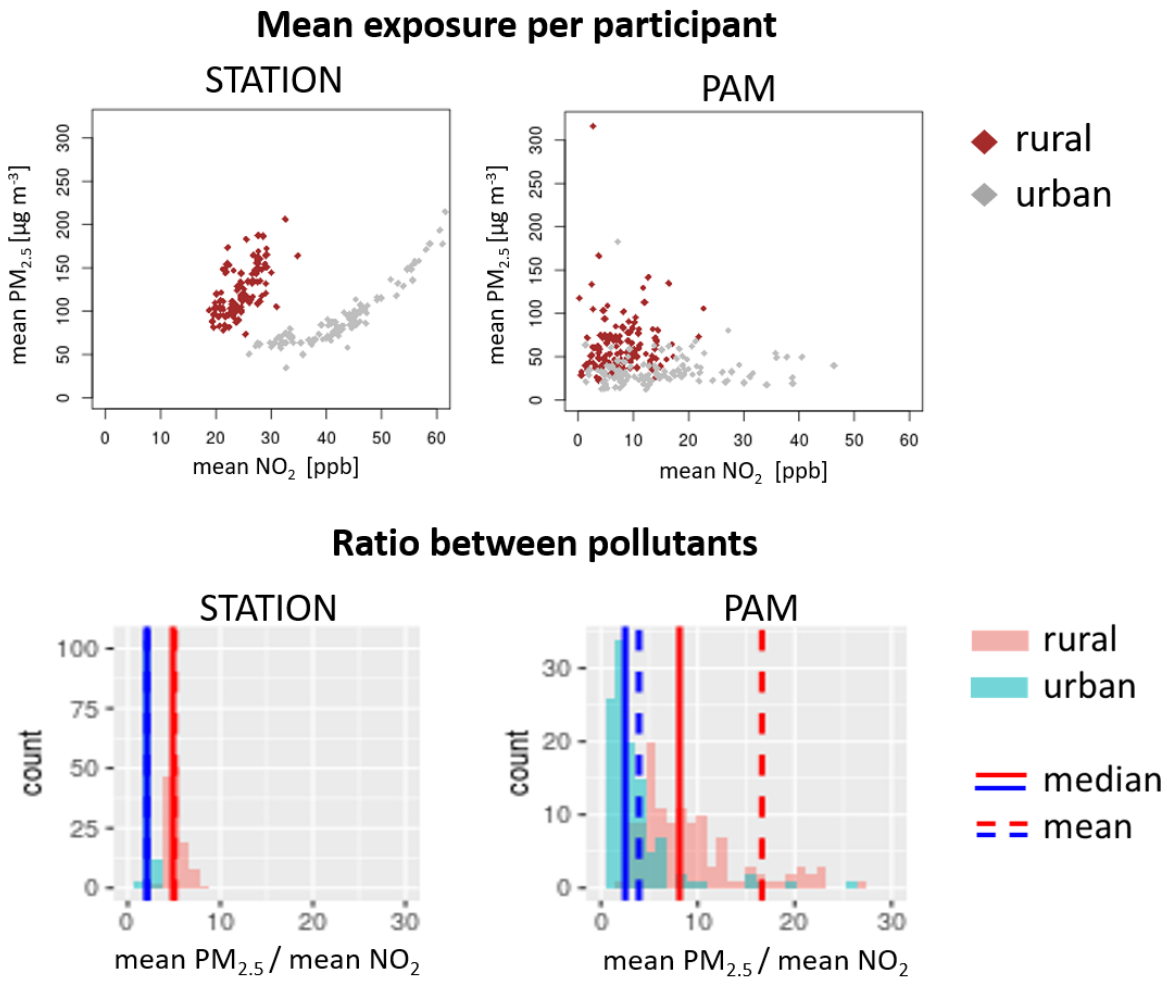

Fig. 4.7 Top: Mean NO_2 exposure of each participant vs mean $PM_{2.5}$ exposure measured by station (left) and by personal monitor (right). Exposure estimates were averaged over the participation week of every participant as in Figure 4.3.
Bottom: Histogram of the $PM_{2.5}/NO_2$ ratios across all participants. The wider distribution of the $PM_{2.5}/NO_2$ ratio is due to different sources and microenvironments which will be discussed in more detail in Chapter 6.

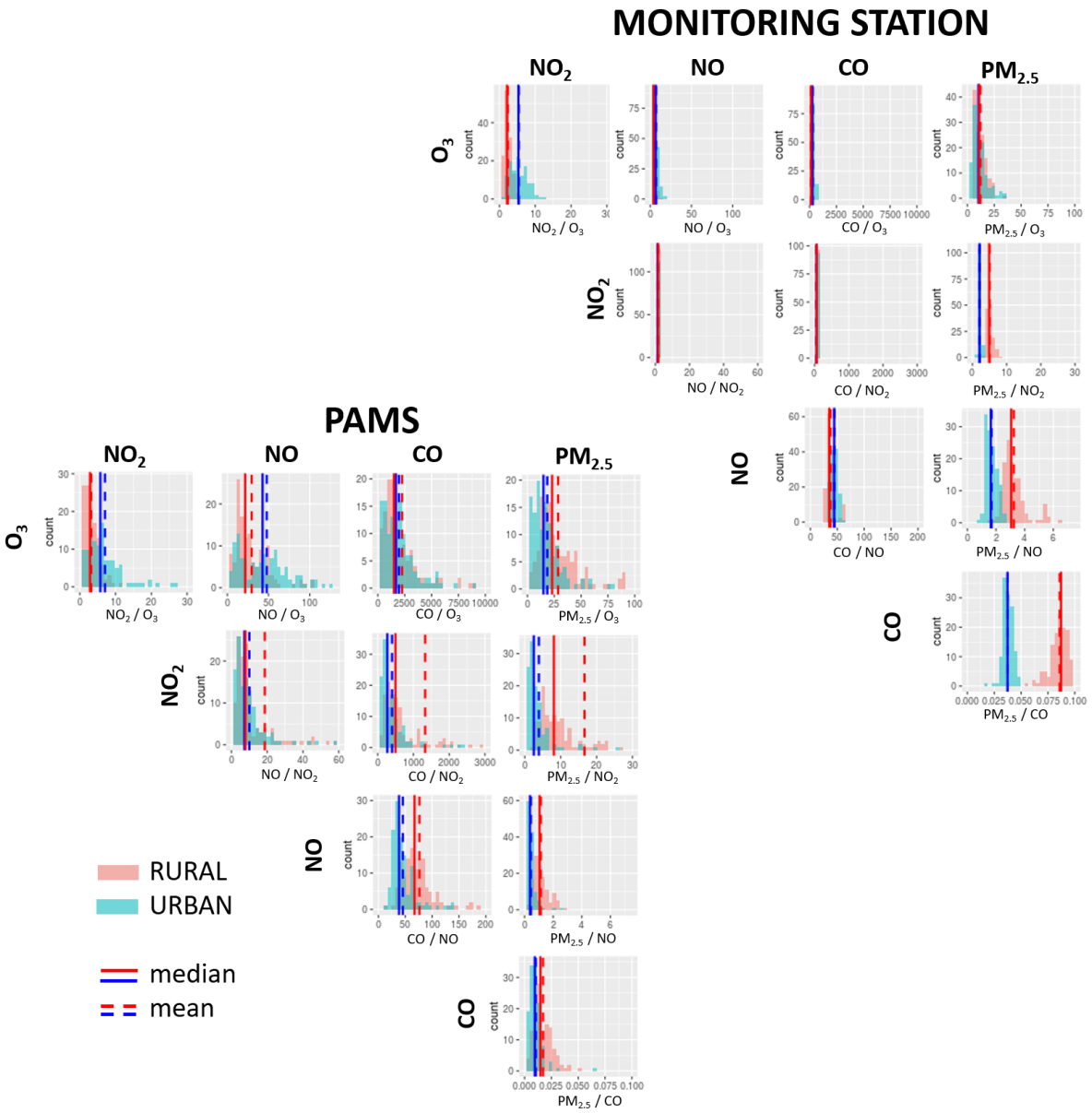

Fig. 4.8 Distribution of the ratios between different pollutants. Ratios calculated as demonstrated in Figure 4.7.

4.5 Preliminary associations between personal exposure to $PM_{2.5}$ and acute health outcomes

The aim of this section is two-fold: firstly to stress the importance of employing accurate personal exposure estimates in health studies; and secondly to highlight the distinct health responses of the two cohorts exposed to different air pollution sources.

The AIRLESS project collected a large number of detailed medical biomarkers (Section 2.3.2). Han et al. [56] conducted a preliminary analysis on the acute inflammatory effects of the exposure to $PM_{2.5}$ using a single-pollutant linear model adjusting for confounding effects (conventional model used in epidemiological studies). In this preliminary analysis, three biomarkers were used: fractional exhaled nitric oxide (FeNO) from exhaled breath to represent respiratory inflammation, and the counts of monocytes and C-reactive protein in the blood serum to represent systemic inflammation (see [56] for details). Inflammation is known to play an important role in the biological mechanisms leading to the adverse health effects of air pollution [22].

Figure 4.9 shows the increase of each medical parameter observed for an interquartile range (IQR) increment of $PM_{2.5}$. The results were compared for an analysis based on ambient exposure metrics, as conventionally used in epidemiological studies (blue), and based on personal exposure metrics measured by PAMs (red) to quantify the impact of exposure misclassification on health models. The assessment of the two cohorts combined (first column of Figure 4.9) showed that significant associations between personal $PM_{2.5}$ exposure and health effect were found for all three biomarkers, while the associations were weaker or insignificant when ambient concentrations were used. This suggests that ambient concentrations may not be adequate to quantify the health effects of $PM_{2.5}$ on individuals.

A striking finding is that the monocyte counts (middle row in Figure 4.9) were significantly associated with increases in personal $PM_{2.5}$ exposures (red) in the urban cohort, but the association was insignificant in the rural cohort. The opposite trend was observed for health predictions based on ambient measurements (blue). The findings from Figures 4.7 and 4.8 suggest that different sets of emission sources in urban and peri-urban Beijing caused a distinct air pollution mixture (and $PM_{2.5}$ composition) at each site. These differences are reflected in the health responses of the two panels as illustrated in Figure 4.9.

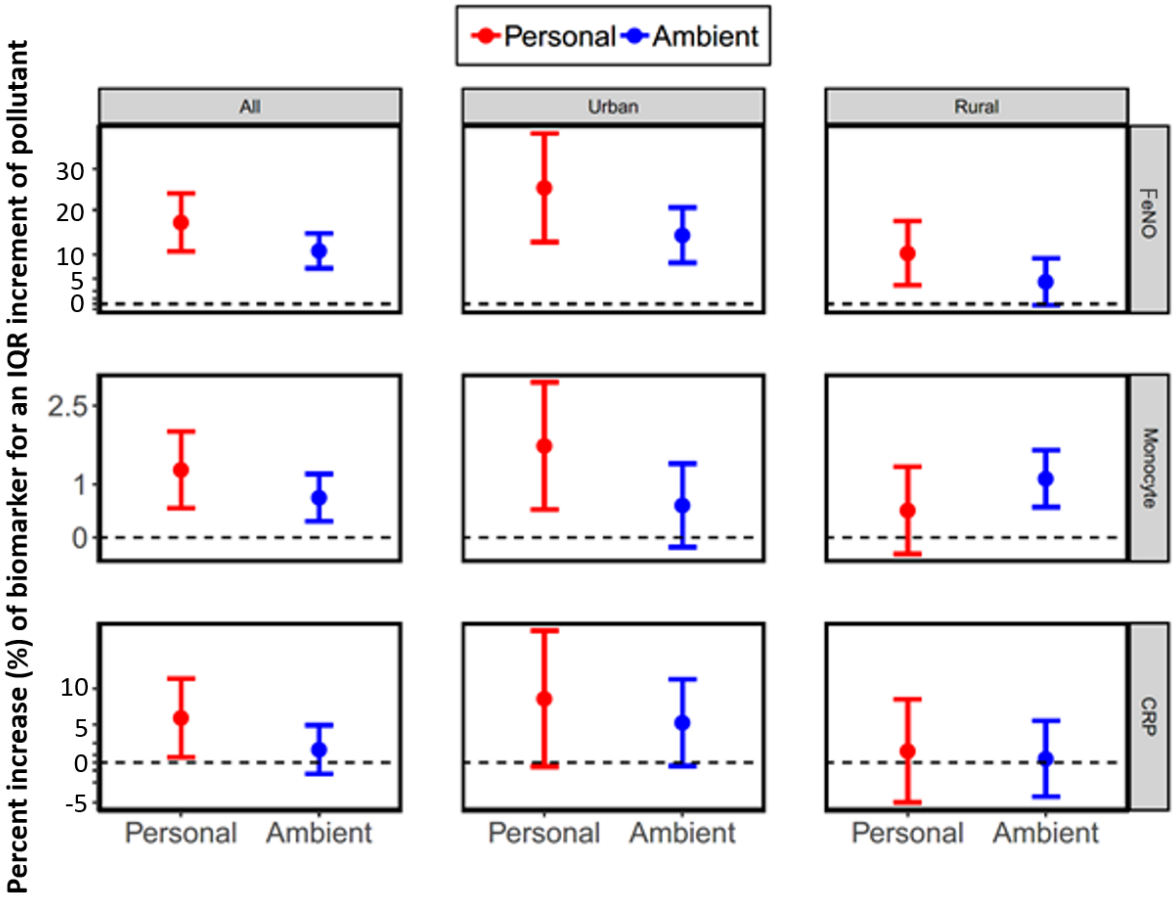

Fig. 4.9 Preliminary analysis of the association between health effects and $PM_{2.5}$ exposure. Odds ratio (OR) with 95% confidence interval (CI) for the occurrence of inflammatory responses associated with an interquartile (IQR) increase of $PM_{2.5}$. The association is assumed significant when OR $\pm$ CI do not cross the zero line. The specific biomarkers selected as indications of systemic inflammation included exhaled NO (FeNO), monocyte count, and C-reactive protein; see Table A.4. The analysis was repeated using ambient $PM_{2.5}$ concentrations (red) and personal exposure data (blue) to assess how the choice of exposure metrics impacts health models. From [56].

4.6 Chapter summary

This chapter explored the potential of portable monitoring devices to improve personal air pollution exposure metrics and corresponding health effect estimations on the example of 251 subjects participating in the AIRLESS project in China.

The measurements of example participant U123 demonstrated that the exposure misclassification (i.e. the difference between static ambient measurements and personal exposures) was large for each pollutant species measured by the PAM. These results were consistent across the two cohorts (rural and urban) and the two seasons. The personal CO and NO concentrations were usually underestimated by the monitoring stations while the personal NO_2, O_3 and $PM_{2.5}$ exposures were overestimated. This is due to different emission sources and indoor reactivities of the pollutant species which will be further discussed in Chapter 5. The exposure misclassification was generally higher in winter than in summer which might be due to different heating and ventilation behaviours of the participants.

A crucial finding of this chapter is that the personal exposure estimation error of conventional exposure metrics, such as ambient observations from monitoring stations, is much larger than the error introduced by the instrument uncertainty of adequately calibrated (Section 2.2) personal monitors: In the AIRLESS project, the mean exposure misclassification of the monitoring stations was approximately 4 (NO) to 17 times (O_3) larger than the measurement uncertainty of the PAMs. As a result, the associations of ambient and personal exposure metrics with health outcomes were inconsistent not only in the magnitude but also in the significance. The exposure metrics collected with the PAM showed a stronger effect on health suggesting that air pollution is more harmful than previously thought. This result indicates the large uncertainties of health effects derived from crude exposure metrics, and that the PAM is, despite its lower accuracy compared to more established air quality measurement methods, a more suitable option for quantifying the air pollution concentrations a person is directly exposed to.

Static outdoor monitoring stations are exposed to air pollution mixtures originating from emission sources in their wider surroundings blended with ambient air. Because these emissions do not vary much over time, the concentrations of the different pollutant species in the mix are often highly correlated which inhibits epidemiological research to draw specific associations between air pollutants and health outcomes. Section 4.4 demonstrated that the pollutant-pollutant correlations were significantly reduced in the PAM measurements compared to static observations which was due to the highly heterogeneous air pollution field the participants were moving through. The ratios between two pollutant species, which contain information about air pollution composition and, hence, the emission sources in the environment, differed also

significantly from the ratios observed at the monitoring stations. The source-related difference in the air pollution mixture was also reflected in the distinct health responses with stronger effect of $PM_{2.5}$ on systemic inflammation in the urban panel compared with the suburban.

In summary, this chapter demonstrated that the personal air quality monitors significantly reduce exposure misclassification and the correlation between pollutant species which are both major limitations in current epidemiological research. The larger measurement uncertainties of the novel portable devices compared to more established reference instruments were clearly outweighed by the high spatial and temporal resolution of the devices which led to more precise personal exposure estimations and a preliminary understanding of the source-related health effects.
These advancements may be crucial to gain a deeper understanding of the detailed effects of individual air pollutant species on the human body, and may also help to design more efficient strategies to mitigate the detrimental health effects of air pollution on populations across the globe.

Chapter 5

Source apportionment of personal exposure using networks of mobile sensors

Static air quality monitoring stations are usually located outdoors and away from any direct emission sources in order to capture the regional air pollution concentrations, i.e. the pollutant levels that are relatively homogeneously distributed over larger areas ($\sim$ km^2). The previous chapter demonstrated that these static measurements are not representative for the air quality in the direct environment of individuals as they move through different microenvironments with varying air quality levels.

The heterogeneity of air pollution between different daily microenvironments is caused by local air pollution sinks and sources that modify the regional air pollution levels. For instance, in the measurements of case example U123 (see Figure 4.1), regional NO outdoor concentrations were found to be around 50 ppb, whereas local emission sources, in this case probably caused by cooking activities, raised the personal NO exposure of U123 to levels of over 800 ppb. Moreover, local air pollution sources are likely to emit a different mixture of pollutants than regional sources. Consequently, the toxicity of the air pollution mixture between microenvironments is likely to vary as well.

This chapter demonstrates how mobile networks of wearable air quality monitors may be used for the source attribution of personal exposure into a local and a regional component to gain more detailed insights into exposure risks in large scale health studies.

Section 5.1 introduces a method to determine the regional pollutant concentration from the measurements of a network of portable sensors. While that section focuses on pollutant species that are approximately inert in the atmosphere, Section 5.2 discusses how the method needs to be adapted for the source attribution of reactive pollutant types. Section 5.3 applies the source

attribution method to personal exposure measurements from the AIRLESS cohorts to analyse the impact of regional and local sources on personal exposure in China.

5.1 Developing a method for the disaggregation of total personal exposure into local and regional components

Based on a conceptual model of personal exposure (Section 5.1.1), a method to extract the regional background concentration from a network of personal sensors is described in Section 5.1.2 and validated in Section 5.1.3.

5.1.1 A conceptual model to understand personal exposure

As people spent the majority of their time ($\sim$ 90%) indoors [73], indoor environments have a major impact on their personal exposure. Therefore, it is important to understand the processes that determine indoor air quality. Equation 5.1 (adapted from [32]) describes the factors that may alter the pollutant concentration inside buildings.

Indoor air pollution can either originate from outdoors via building ventilation and infiltration (k_{vent}), or from indoor emission sources such as cooking, heating or smoking (S_{indoor}). The loss of indoor pollutants can occur through the exchange with cleaner outdoor air (k_{vent}) and through additional indoor pollution sinks like surface reactions or deposition mechanisms. Assuming natural building ventilation [1], the change of the indoor pollutant concentration per time can be expressed via Equation 5.1.

$$\frac{dc_{in}}{dt} = (c_{out} - c_{in})\,k_{vent} - c_{in}\,k_{sink} + S_{indoor} \tag{5.1}$$

c_{out}, c_{in}	pollutant concentration outdoors and indoors (ppb)
k_{vent}	rate coefficient of building ventilation (hour^{-1})
k_{sink}	rate coefficient of indoor losses (pollution sinks) (hour^{-1})
S_{indoor}	emissions from indoor air pollution sources (ppb hour^{-1})

In the absence of indoor emission sources (S_{indoor} = 0), the indoor concentration reaches a steady state[2] in equilibrium with the outdoor concentration. This equilibrium is based on the assumption that the time lag between indoors and outdoors (i.e. the time needed by the outdoor

[1] Air exchange from indoors to outdoors is the same as air exchange from outdoors to indoors

[2] Steady state can be assumed because k_{vent} and k_{sink} are much faster than the change of the ambient pollution.

pollution to penetrate into the building) is negligible.

The indoor-to-outdoor (I/O) ratio of the pollutant concentrations can be determined from Equation 5.1, assuming $\frac{dc_{in}}{dt} = 0$ (steady state) and $S_{indoor} = 0$. The resulting expression for the I/O ratio is given in Equation 5.2. The I/O ratio determines the baseline pollutant concentration in an indoor environment. The stronger the indoor sinks are, the smaller is the I/O ratio.

$$\mathrm{I/O}_{s.s.} = \frac{c_{in}}{c_{out}} = \frac{k_{vent}}{k_{vent} + k_{sink}} = \frac{k_{vent}}{\kappa} \tag{5.2}$$

Additional emission sources (S_{indoor}) cause concentration peaks on top of this baseline that decay exponentially until the concentration reaches the indoor baseline again. By solving the differential Equation 5.1, the indoor pollutant concentration can be expressed as a function of time given as Equation 5.3. The first term of this Equation describes the decay of concentration peaks caused by indoor sources. The decay rate κ is the sum of the building ventilation rate and the loss rate through indoor pollutant sinks ($\kappa = k_{vent} + k_{sink}$).

$$c_{in}(t) = C\,e^{-\kappa(t-t_0)} + \underbrace{c_{out}\frac{k_{vent}}{\kappa} + \frac{S_{indoor}}{\kappa}}_{baseline} \tag{5.3}$$

$$with \quad C = c_{in}(t_0) - baseline$$

κ	pollutant decay rate (k_{vent} + k_{sink})
$c_{in}(t_0)$	indoor pollutant concentration at time t_0

In other words, the indoor decay rate κ depends not only on the ventilation rates but also on the type and reactivity of the pollutant species. Some air pollutants are very stable and not notably affected by indoor sinks. For instance, CO has lifetimes in the troposphere in the order of months [104] and can therefore be treated as approximately inert ($k_{sink} \sim 0$).

Figure 5.1 illustrates two model scenarios that were generated from Equation 5.3. Scenario (A) illustrates the case of an inert pollutant ($k_{sink} \approx 0$), scenario (B) the case of a more reactive pollutant that is affected by indoor pollution sinks ($k_{sink} > 0$). The black line represents the indoor concentration, and the dotted blue line marks the outdoor concentrations.

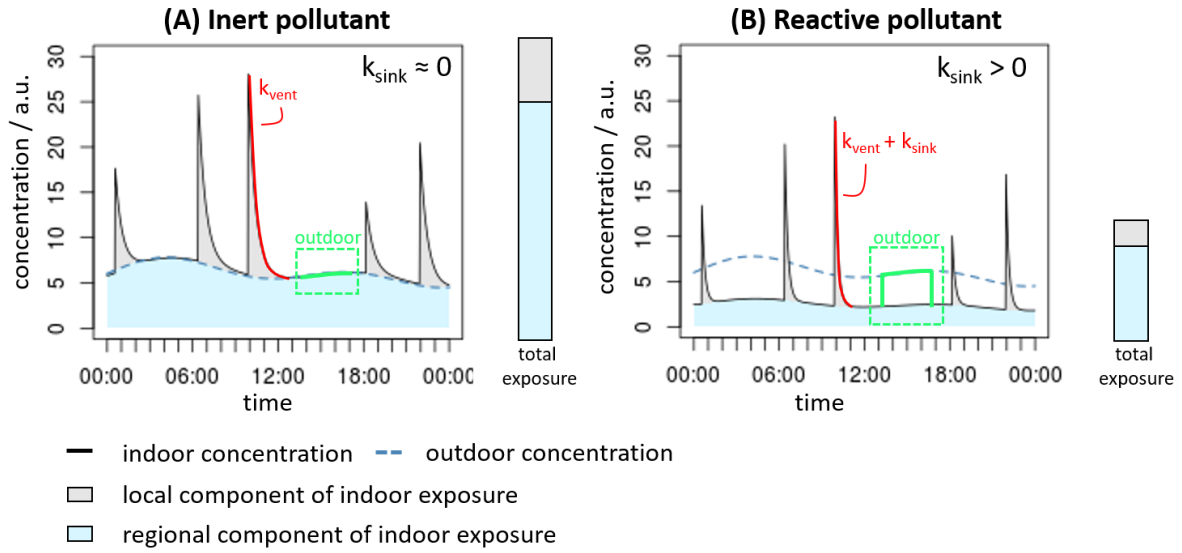

Fig. 5.1 Schematic indoor concentration model based on Equation 5.3. (A) Inert pollutant unaffected by indoor sinks ($k_{sink} = 0$) and (B) reactive pollutant ($k_{sink} = 3\,h^{-1}$). The ventilation rate is constant for both cases ($k_{vent} = 2\,h^{-1}$). Exposure that originates from local sources is shaded in grey and exposure from regional sources is shaded in blue. The bar plot on the right of each graph represents the mean personal exposure for each case and how much the local and regional sources contributed to it.
The green square between 13:00 and 17:00 shows how the personal exposure would change if, instead of being indoors, the individual was being outdoors (assuming no local outdoor sources).

In the absence of indoor emissions ($S_{indoor} = 0$), the indoor concentration of the inert pollutant (case A) is equal to the outdoor concentration (I/O = 1), whereas the indoor concentration of the reactive pollutant (case B) is lower than outdoors (I/O < 1).
Indoor emission sources typically cause a steep increase of the pollutant concentration which then exponentially decreases with a decay rate of $\kappa = k_{vent}$ in case of inert pollutants and $\kappa = k_{vent} + k_{sink}$ for reactive pollutant.

The total personal exposure $c_{personal}(t)$ can be expressed as the sum of a *local* component and a non-local or *regional* component (Equation 5.4) whereby the local signal c_{loc} is attributed to emission sources in the direct environment of a person and the regional component $c_{BG}(t)$ originates from emission sources across the wider region [119].

$$c_{personal}(t) = c_{loc}(t) + c_{BG}(t) \tag{5.4}$$

$c_{personal}$	total personal air pollution exposure
c_{loc}	air pollution attributed to local emission sources
c_{BG}	exposure attributed to regional air pollution (BG = background)

The non-local signal c_{BG} is usually defined as the background concentration of a pollutant which is identical over a large region (e.g. a city) and may originate from sources outside the area of interest [113]. For indoor exposures, the regional component is defined as the regional outdoor pollution that penetrates inside the building via ventilation (k_{vent}). In Figure 5.1, the local component is shaded in grey, and the regional component is shaded in blue. An important observation is that, for inert pollutants (case A), the regional component of indoor exposure (blue shaded) is equal to the regional outdoor exposure (blue dotted line). The regional component of the exposure to reactive pollutants (case B), however, is only a fraction of the regional outdoor concentration.

The bar plots on the right of each graph represent the total personal exposure to the corresponding pollutant, and how much local and regional sources contributed to it. Although the conceptual model assumes the same number and magnitude of indoor emission sources for both cases; the total exposure to reactive pollutants is lower than the total exposure to inert pollutants. Note that the ratio between the local and regional component of the total exposure does not differ between the two pollutant types because air pollution sinks equally affect the regional and local component of personal exposure. The ratio is, however, dependent on the number and intensity of local emission sources as well as by the absolute outdoor air pollution concentrations (see Section A.5.1 in Appendix for details).

The black lines in Figure 5.1 show the modelled pollutant concentrations inside a building. People spend the majority of their time inside buildings, but will also move through outdoor environments. The green square in each graph of Figure 5.1 marks the pollutant concentration a person would be exposed to when moving outside. For inert pollutants there is no difference in exposure because the indoor concentration is equal to the outdoor concentration (assuming no local emissions and a negligible time lag). In case of the reactive pollutants, however, there would be a rapid rise in the personal levels because the person is suddenly exposed to higher pollutant levels outdoors compared to indoors. This distinction is important for determining the regional outdoor concentration from a sensor network which will be discussed in the following sections.

5.1.2 Using networks of sensors to determine the regional concentration of inert pollutants

As demonstrated in the previous section, the total air pollution exposure of a person consists of a regional component that originates from sources in the wider area, and a local component which is caused by emission sources in the direct environment of the person (see Equation 5.4 and Figure 5.1). A similar approach can be adopted for the urban environment, where a relatively homogeneous dispersion of pollutants affected by regional air pollution transport (non-local) and a variety of additional urban (local) emissions sources determine the air pollution levels. Previous studies on urban air quality ([113, 59]) have used dense outdoor monitoring networks of low-cost novel sensor technologies to separate long-range pollution transport (urban background concentration) from local emissions; however, to date no studies have applied this method on personal sensor networks which are moving through (mainly indoor) daily life environments.

This section introduces a method to extract the regional signal of personal exposure from a mobile network of PAMs using the AIRLESS dataset as example (Section 2.3.2). Some pollutant species are stable in indoor environments (Case A) while other pollutants are affected by indoor sinks (Case B) (Section 5.1.1). Because the sensor networks of the AIRLESS project were mainly located indoors (Section 2.3.2), these two cases were considered separately. Using the CO measurements of the mobile sensor networks as an example of an inert pollutant, the regional CO concentrations in Beijing and Pinggu were extracted. The method for the source attribution of personal exposure to inert pollutants is based on the following assumptions:

(1) Inert pollutants are not affected by local air pollution sinks ($k_{sink} = 0$)

(2) Thus, the personal exposure can only be equal to or higher than the regional concentration

(3) Local emissions (c_{loc}) are zero for a large fraction of time [119]

(4) At any given point in time, at least one sensor of the network is away from direct emission sources and only exposed to regional air pollution

In the absence of local air pollution sinks (assumption 1), the indoor to outdoor ratio is approximately one, i.e. the air pollution concentrations that originate from regional sources are equal outdoors and indoors (see Figure 5.1 left graph). Consequently, the minimum personal exposure (both inside and outside) will be the regional pollutant concentrations (assumption 2). Due to the sporadic nature of local emissions (assumption 3), and assuming the sensor network is large enough, at least one sensor will be away from local sources and exposed only to the

regional background levels at any point of time (assumption 4).

Based on similar assumptions, Popoola et al. [113] defined the background concentration as the minimum concentration measured across a sensor network over a defined time period. To account for instrument artefacts, they used the 10th percentile rather than the minimum. Assuming that local pollution sources in indoor environments occur equally frequently as in outdoor environments, this method is applicable to stable pollutants in indoor environments. However, while Popoola et al. extracted the background concentrations over one-hour measurement windows, in this work the background extraction was performed by extracting the 10th percentile value of the 1-min data of the PAM network to retain the high temporal resolution.

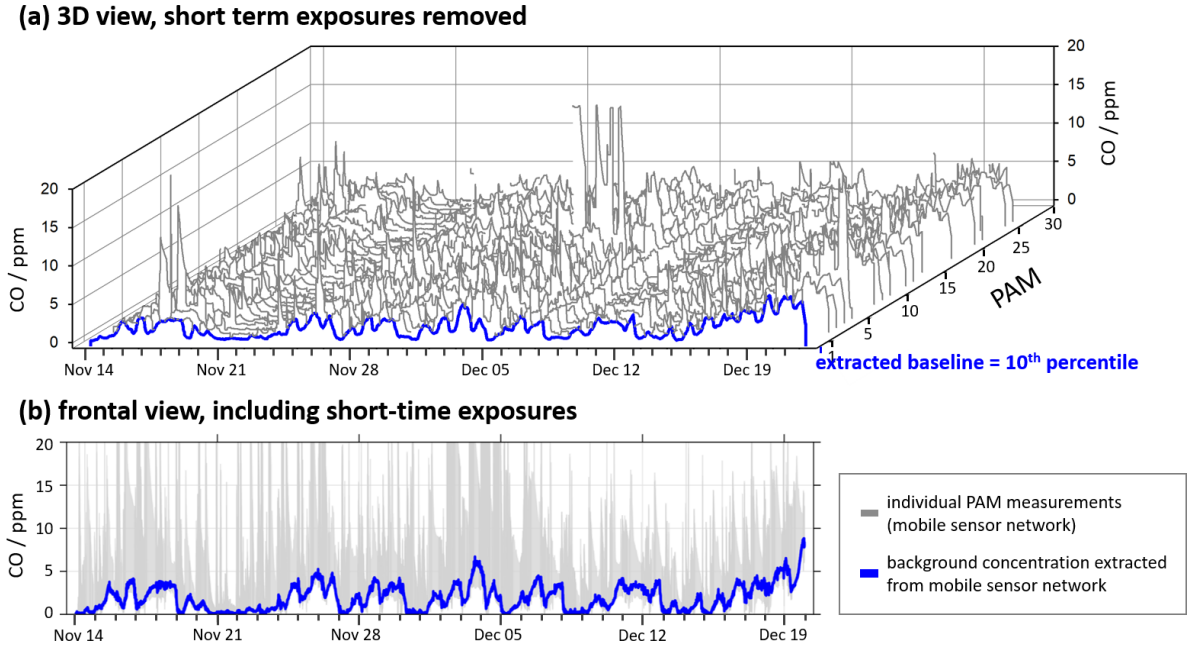

Fig. 5.2 (a) 3D presentation of CO concentration time series measured by 30 PAMs deployed during the AIRLESS winter campaign in urban Beijing (grey). Short term exposure events ("spikes") were removed by applying a rolling 10th percentile over a 3 hour window. The blue line represents the background concentrations extracted from the mobile sensor network. (b) CO measurements of all Beijing PAMs (grey), and CO background signal extracted from mobile network (blue). This graph represents a frontal view of the 3D graph on top but additionally includes short term exposure events.

Figure 5.2 provides a graphical illustration of the extraction method based on the CO concentrations measured during the AIRLESS winter campaign. The top graph shows a 3D presentation of the recorded CO levels of the 30 PAMs carried by the urban cohort of the AIRLESS project. For clarity, short term exposure events were removed by applying a rolling 10th percentile over

a 3 hour window on each PAM measurement. The graph shows that all PAMs follow roughly the same concentration trends.
The bottom graph in Figure 5.2 represents a frontal view of the 3D graph above but including short term exposure events. While each individual monitor captures various short term exposure events caused by local emissions (sharp spikes, grey), a mutual baseline of all PAM measurements is clearly visible. This confirms that all participants are exposed to the same background CO levels when no local emission sources are present. This regional background concentration was extracted by selecting the 10^{th} percentile of all measurements across the sensor network for each point of time (blue), retaining the high temporal resolution. The extraction method was repeated with varying percentiles (from the minimum measurement across the network to the 30^{th} percentile, see Section A.5.2 in the Appendix), finding that the optimum percentile was the 10^{th} percentile (as in Popoola et al).

5.1.3 Comparison of the extracted regional concentration with reference measurements

The outdoor background concentrations that were extracted from the sensor network were compared to the measurements of a nearby monitoring station. Each station was located away from any local emission sources (see Table 3.1) and, therefore, measured the regional background pollution. Figure 5.3 compares the CO measurements from a monitoring station with the regional background concentration that was extracted from a sensor network as described in Section 5.1.2, for both deployment sites of the AIRLESS winter campaign.
The extracted backgrounds (blue) closely follow the measurements taken at the reference station (red). High coefficients of determination ($R^2 \geq 0.87$) and gradients close to one between reference instruments and extracted backgrounds indicate a high agreement between the two regional concentration measurements.
This agreement suggests that the method introduced in Section 5.1.2 is suitable to determine the regional background concentration of inert pollutants. Moreover, the regional concentrations extracted from the sensor network may only agree with the reference when all sensors of the network are well calibrated and functioning correctly. Therefore, the background extraction is an excellent method to validate the performance-in-use of an entire sensor network. The advantage of this validation method is that it can be applied with little effort while the data collection is still ongoing. This way, faulty monitors can be identified and replaced early on.

Furthermore, this method may be used to estimate the outdoor pollution levels in areas where no air quality monitoring stations are available.

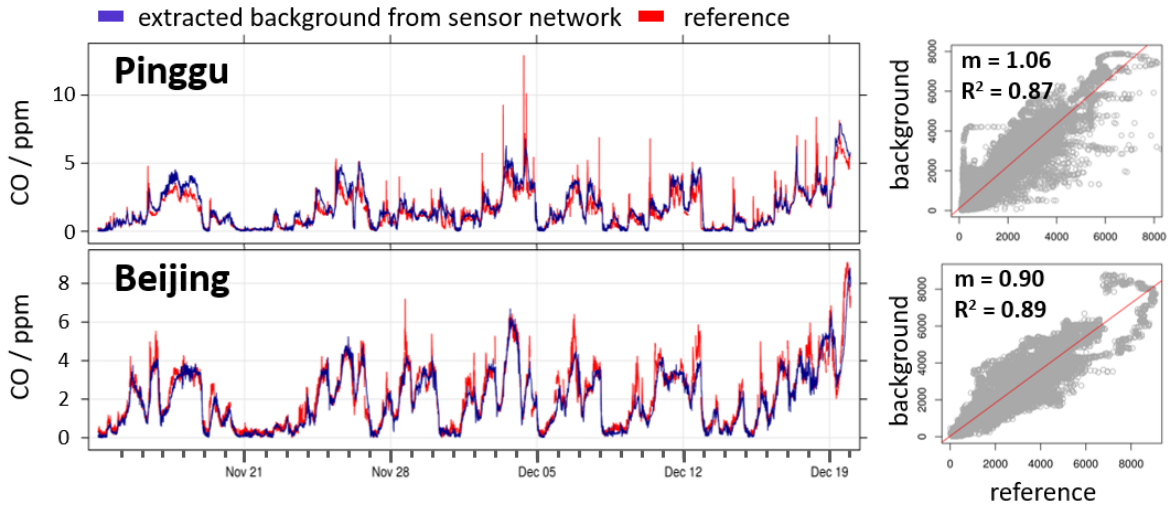

Fig. 5.3 Comparison between the regional background concentrations extracted from mobile sensor networks as described in Section 5.1.2 (blue) with reference measurements from monitoring stations (red). Left: Time series of the two parameters; right: scatter plots of the corresponding measurements on the left. AIRLESS winter campaign. Equivalent graph for summer deployment shown in Figure A.12.

5.2 Source attribution for chemically reactive species

The background extraction method introduced in the previous section is based on the assumption that the personal pollutant concentration does not drop below the regional concentrations. While this requirement is met for inert pollutants, the local concentrations of chemically reactive pollutant species may drop below the regional background due to local pollution sinks which are often found indoors (see case B in Figure 5.1). This section firstly classifies pollutant species by their chemical indoor reactivity. Section 5.2.2 then discusses alternative approaches to determine the regional background concentration of reactive pollutants from the measurements of a mobile sensor network.

5.2.1 Characterising the indoor reactivity of pollutants

Section 5.1.1 conceptualised how concentration peaks of indoor pollutants which are caused by short term emissions, such as cooking, decay exponentially with a rate of κ (see Equation

5.3). This decay rate depends on the ventilation of the building k_{vent} which affects all pollutant species in the same way, and on additional indoor losses k_{sink} that depend on the reactivity of each pollutant species. The stronger a pollutant species is affected by indoor sinks, the faster its decay rate κ.

Figure 5.4 illustrates this principle using the data of example participant U123 (Nov 29th - Dec 1st 2016). The upper time series shows the personal CO exposure of the participant. The CO loss through chemical reactions is assumed to be negligible. Therefore, its indoor lifetime depends on building ventilation only ($\kappa = k_{vent}$). The lower panel shows a time series of the participant's NO_2 exposure over the same period of time. The NO_2 concentrations decayed visibly faster than in the case of CO because they were additionally affected by indoor pollution sinks.

The exponential decays in the exposure time series were automatically detected and fitted[3]. Each detected decay is marked in red in Figure 5.4, with the text quantifying the decay rate determined from the exponential fit. The decay rates of CO vary over time which might be attributed to changes in the building ventilation (e.g. opening of windows or doors), or additional changes in the indoor reactivity (e.g. caused by temperature changes) in case of NO_2. However, all CO decay rates were notably lower than those of NO_2, indicating the presence of a constant removal mechanism for NO_2.

[3]R script developed by Elizabeth Martin and Lia Chatzidiakou

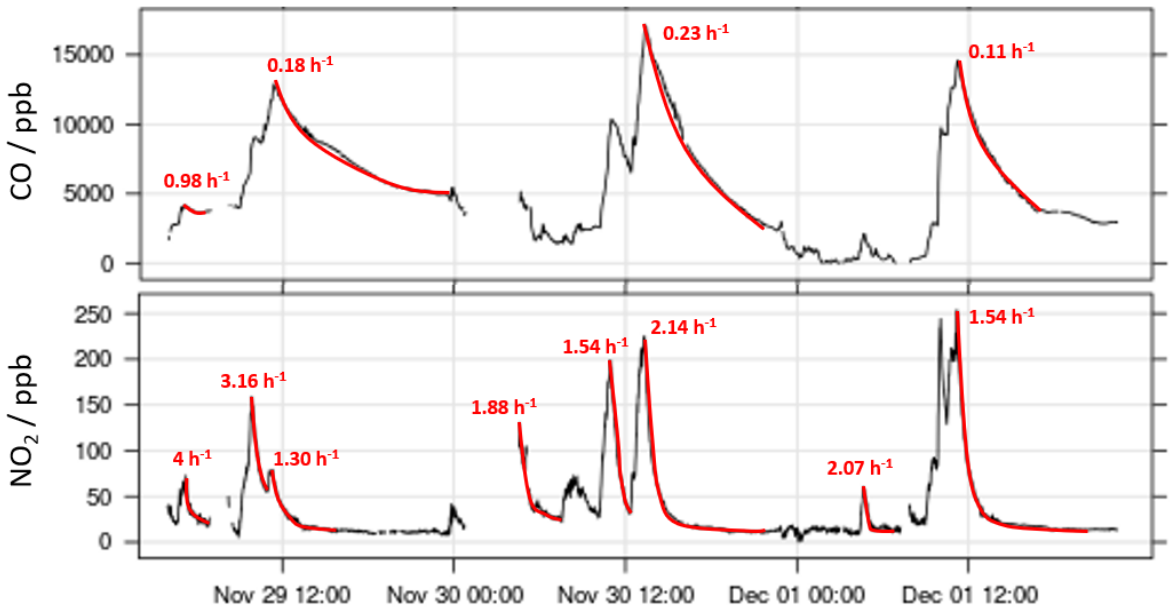

Fig. 5.4 Indoor decay analysis of the CO (top) and NO_2 (bottom) exposures of participant U123 (Nov 29th - Dec 1st 2016, only data at home, time in UTC). The decays of exposure peaks (marked in red) were exponentially fitted to determine the pollutant decay rates (red text). The NO_2 decays were substantially faster than the CO decays because CO was affected by building ventilation only while NO_2 was additionally affected by indoor pollution sinks.

Observations collected in the home microenvironment (classified using the method described in Section 6.2) were selected for further analysis. In total, 7762 exponential decays were detected in the entire exposure dataset of the urban AIRLESS cohort (for all five pollutant species). The decay rates resulting from the exponential fits are summarised as boxplots in Figure 5.5.

Since CO is assumed to be inert, the CO decay rates in the Figure represent the range of the ventilation rates of the urban AIRLESS building stock. The NO decays were found in approximately the same range (CO median decay rate: 0.58 h^{-1}, NO: 0.60 h^{-1}), indicating that the effect of indoor sinks on NO concentrations was negligible, and indoor NO losses were dominated by building ventilation. The NO_2, O_3 and $PM_{2.5}$ decays were generally much faster than the building ventilation rate (median decay rates: NO_2 1.24 h^{-1}, O_3 1.21 h^{-1}, $PM_{2.5}$ 0.85 h^{-1}), indicating additional losses through indoor removal mechanisms. Therefore, these species were classified as chemically reactive pollutant types.

This classification agrees with the results from Section 4.3 which compared the personal (i.e. mainly indoor) exposures measured with PAMs to observations from monitoring stations (i.e. regional background levels) in the AIRLESS project. The findings showed that the personal exposures to NO and CO were generally higher than the regional outdoor concentrations

whereas the personal NO_2, O_3 and $PM_{2.5}$ exposures were substantially lower than outdoors, owing to the reductions from indoor sinks (see e.g. Figure 4.4). As the concentrations of reactive pollutants may drop below the ambient levels, the background extraction method described in Section 5.1.2 is not applicable for these pollutants (assumption 2 is not met).

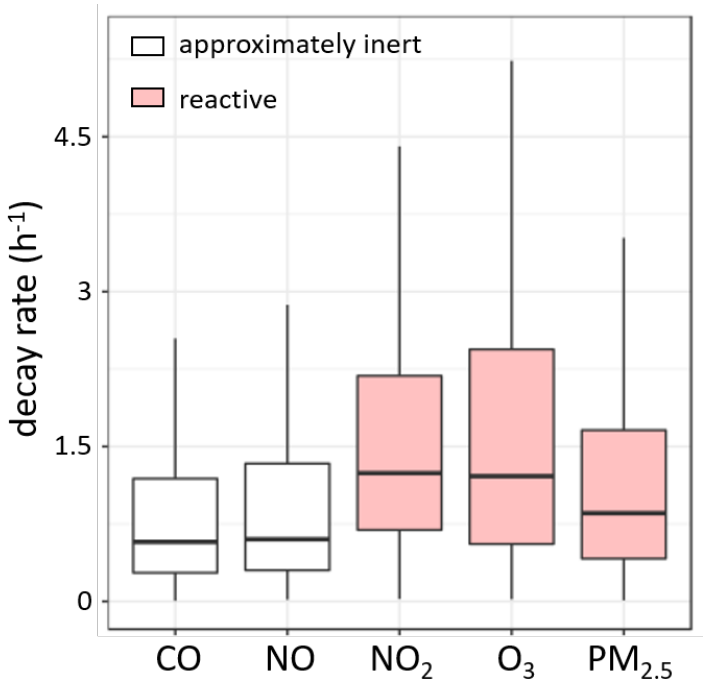

Fig. 5.5 Summary of the indoor decay rates extracted from exponential fits of the exposure data from the urban cohort during the AIRLESS winter campaign. In total, 7762 peaks were fitted in this dataset (5 pollutants, 123 participants, home exposures only). CO and NO were identified as approximately inert. NO_2, $PM_{2.5}$ and O_3 were classified as reactive pollutants because of their faster decay rates compared to CO and NO. Outliers not shown in the boxplots.

5.2.2 Determining the regional outdoor concentration of reactive pollutants

Section 5.1.2 described how the regional background concentration of inert pollutants may be determined as the lowest measurements across a sensor network. This method is based on the assumption that the regional background concentration is homogeneously distributed across all indoor and outdoor environments, and therefore the regional background is the minimum pollutant level a sensor might be exposed to. While this is the case for inert pollutants (case A in Figure 5.1), the concentrations of chemically reactive species (case B) are affected by local air pollution sinks which means that the local pollutant concentrations may drop below the regional

background concentration. The exact fraction to which the outdoor concentration is reduced when entering a building (I/O ratio) differs from household to household. Consequently, the nodes of an indoor sensor network are not exposed to a common baseline. Extracting the lowest concentration of reactive pollutants from a sensor network would only extract the concentration in the household with the strongest local sinks and not the regional background concentration.

To extract the regional outdoor concentrations of reactive pollutants, a different set of assumptions was applied:

(1) The regional outdoor concentration is reduced by indoor air pollution sinks when entering a building ($k_{sink} > 0$)

(2) In the absence of local emissions, the personal exposure is either equal to or lower than the outdoor levels

(3) At least one individual of the cohort has very weak indoor sinks or is exposed to outdoor air at any point of time

(4) Local emissions are sparse events and no more than 10% of the cohort are simultaneously exposed to them

Reactive pollutants reduce the indoor air pollution levels compared to outdoors (assumption 1). Therefore, the personal exposure to reactive pollutants *increases* when the individual moves from indoors to outdoors (see Figure 5.1 green square). Hence, the regional outdoor background would be the maximum concentration measured across the network, if no local emission sources were present (assumption 2). Assuming that local emissions occur only sporadically (assumption 4), they can be accounted for by taking the 90^{th} percentile instead of the maximum. Based on these assumptions, the regional outdoor concentrations may be extracted as the 90^{th} percentile of the measurements across the entire sensor network.
Figure 5.6 illustrates this method at the example of the NO_2 measurements of the urban AIRLESS cohort in the summer (top) and winter (bottom) campaign. The measurements of all individual sensors of the network are shown in grey, and the 90^{th} percentile extracted across these measurements is shown in blue. The outdoor concentrations that were observed at PKU reference station are added in red.
The extracted NO_2 background agrees strikingly well with the reference measurements during the summer campaign. In the winter time, the 90^{th} of the network generally underestimates the outdoor concentrations of the reference, yet it broadly captures the features (e.g. spikes) of

the outdoor levels. This seasonal difference may be attributed to a change of the ventilation behaviour of the cohort. The outdoor concentration may only be captured by the network when at least one sensor is exposed to outdoor air at any time (assumption 3). Keeping in mind that people spend around 90% of their time indoors, it is unlikely that a member of the cohort is located outdoors at all times. In winter, the building ventilation is reduced to a minimum to preserve heat. Consequently, the indoor pollution differs strongly from the outdoor levels. In the summer, however, building ventilation is substantially increased which allows the outdoor air to penetrate into the building and reach the sensors less affected by indoor sinks. As a result, the extracted outdoor concentration agrees better with the reference in summer.

A limitation of this method is the assumption that local emissions occur so rarely that they may not happen to more than 10% of the cohort at the same time (assumption 4). Some common emission sources are bound to specific times of the day. For instance, it is likely that more than 10% of the cohort are exposed to cooking emissions during lunch or dinner time. In this case the 90^{th} percentile may capture these local emissions rather than the regional outdoor levels. These cases can be observed when the extracted outdoor concentration (blue) exceeds the reference measurements (red) in Figure 5.6 (e.g. May 23^{rd} and 24^{th} in summer, Dec 4^{th} and 5^{th} in winter).

The regional background extraction of the $PM_{2.5}$ and O_3 concentrations, as well as of NO_2 for the peri-urban cohort in Pinggu, resulted in similar findings (see Figure A.12 in the Appendix).

In summary, the method of extracting the regional outdoor concentration of reactive pollutants is less accurate than the method for inert pollutants because the assumptions are not met at all times. However, the method may still be used for reliability checks of the sensor network performance, keeping in mind that better agreements between extracted background and outdoor reference are expected in the summer season.

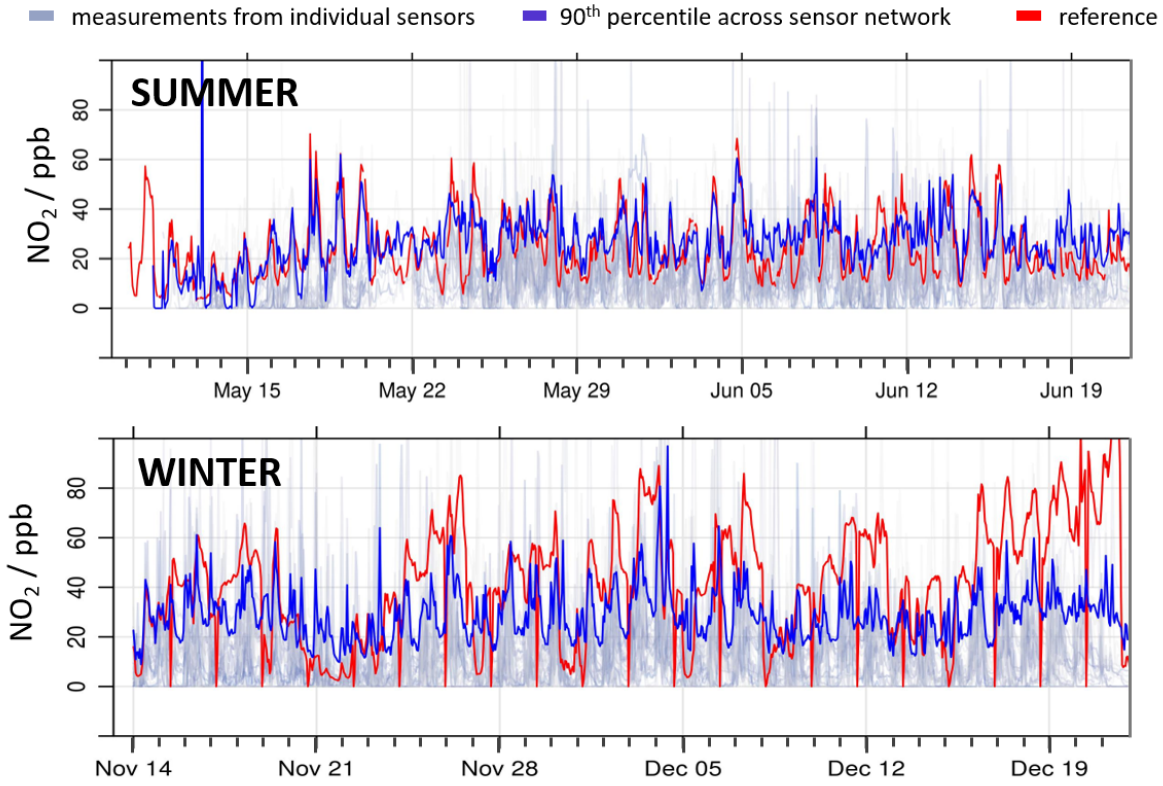

Fig. 5.6 NO_2 measurements of all PAMs from the urban sensor network of the AIRLESS project (grey), and 90th percentile extracted from these measurements (blue; c.f. Figure 5.2 bottom). Observations from outdoor monitoring station in red. The 90th percentile replicates the outdoor NO_2 levels strikingly well in summer. Equivalent graphs for peri-urban sensor network and other pollutant species in Figure A.12.

A crucial difference of reactive pollutants compared to inert species is, however, that the regional outdoor concentration is not equal to the regional component of the total personal exposure (see Section 5.1.1). Therefore, the extracted background of reactive species may not be used to separate the contributions from local and regional sources to the total personal exposure. Alternative methods to determine the regional component of the total exposure are currently under development but exceed the scope of this dissertation. Therefore, the source apportionment of personal exposure in the next section focuses on inert pollutants.

5.3 Separating the contribution of local and regional sources to personal exposure in large scale health studies

This section uses the background extraction method introduced in Section 5.1.2 to disaggregate the local and regional components of individual CO exposures measured in the AIRLESS winter campaign. The Section aims to demonstrate how this source attribution method may introduce new opportunities for epidemiological research to gain a deeper understanding of the health effects of air pollution.

5.3.1 Case example U123

The conceptual model in Section 5.1.1 showed that a person is fully exposed to the regional levels of an inert air pollutant (without reductions through local air pollution sinks), and to additional emissions from local sources. This Section illustrates how the background extraction introduced in Section 5.1.2 can be applied to disaggregate the contributions from regional and local sources to the mean personal exposure using again participant U123 as a representative example.

Figure 5.7 (left) shows a time series of the personal CO exposure of case participant U123 (grey), and the regional outdoor concentration extracted from the sensor network (blue).

The personal exposure of U123 followed a distinct daily pattern of sharp increases occurring every evening around 6-7 pm. These exposure events were driven by local emissions. Their time of occurrence indicates that they might have been caused by cooking activities for dinner preparation. The elevated CO concentrations inside the participant's home slowly decayed over the course of the night and approached the regional background levels at some point of the following day. On some days, the exponential decay was interrupted early and the personal exposure "jumped" down to match the regional outdoor concentration (e.g. mornings of Dec 1st and Dec 5th). These rapid decreases of personal exposure can be explained by the participant moving from inside the house, which still contained elevated CO levels, to an outdoor environment which was affected by regional CO concentrations only.

While the regional concentration changed by maximally 4 ppm over time periods of more than 10 hours, local sources caused the personal exposure to rise by over 15 ppm in less than two hours (e.g. Dec 2nd, 6 pm). This indicates that the variability of the local component was much higher than the variability of the regional component. Capturing this variability might be crucial for a better understanding of the health effects of air pollution since such highly concentrated peak exposures might trigger acute health responses.

The right side of Figure 5.7 shows a bar plot that represents the mean exposure $\bar{c}_{personal}$ of participant U123 over their participation week. The blue component of the bar represents the contribution of regional air pollution to their personal exposure (proportional to the area under the blue line). The remaining part of their personal exposure (grey) was attributed to air pollution from local emission sources (proportional to the area between the grey and the blue line; based on Equation 5.4).
The major part of the participant's CO exposure (61%) originated from local sources whereas the regional air pollution contributed to only 39%. Outdoor air quality monitoring stations may only capture the regional component of personal exposure. Neglecting the local component of personal exposures would introduce large uncertainties (in that case 61%) in the quantification of the health effects of air pollution exposure. More importantly, indoor-generated CO is likely to be co-emitted with other pollutants than outdoor CO, and is therefore potentially a useful proxy of exposure.

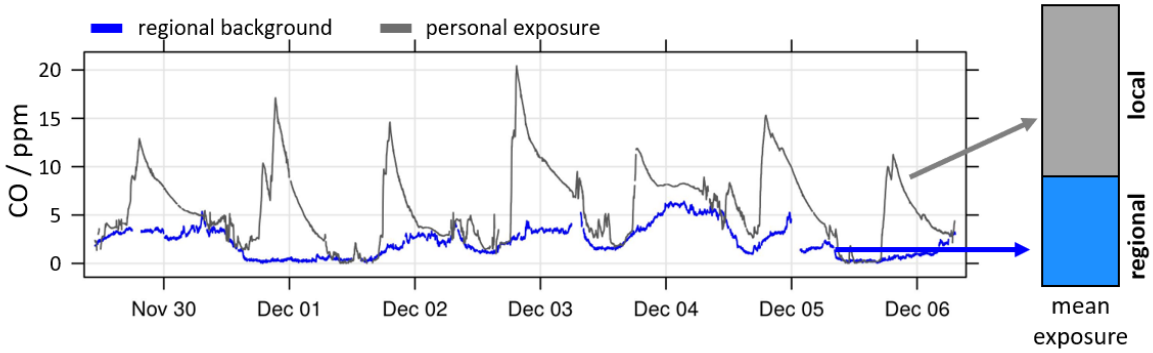

Fig. 5.7 Left: Time series of participant U123's personal CO exposure measurements (grey) compared to the regional CO background levels (blue, extracted from urban sensor network). Right: Mean contributions of local emission sources (grey) and regional air pollution (blue) to the average exposure of the participant. Graph in local time.

5.3.2 Source attribution of exposures from the AIRLESS project

The separation between the local and the regional component of personal exposure described in the previous section was applied to all participants of the AIRLESS cohorts. Each bar in Figure 5.8 represents the mean personal exposure of one participant with the contributions from local sources marked in grey and from regional background pollution in blue. Conventional exposure estimations based on static observations can assign only one exposure value for all participants in a cohort. In Graph 5.8 this value is shown as a dotted line. Note that it is based on measurements from monitoring stations, whereas the contributions of the regional pollution

to the mean exposure (blue bars) are based on the background concentrations extracted from the mobile sensor networks. The two parameters were, however, almost identical for CO as inert pollutant (see Section 5.1.3).

The contribution from regional emission sources was strikingly constant across the two cohorts (with slightly higher levels in the urban site, see Section 4.3). As expected from the personal exposure model in Section 5.1.1, the regional exposure components were very close to the exposure estimations from monitoring stations (dotted lines) as these usually capture the regional pollution levels only. The local components varied considerably more and constituted up to 95% (participant R159 in peri-urban cohort) of the total exposure. Although not shown here, the analysis of the personal CO exposures collected in the AIRLESS summer campaign resulted in very similar findings to those from the winter campaign.

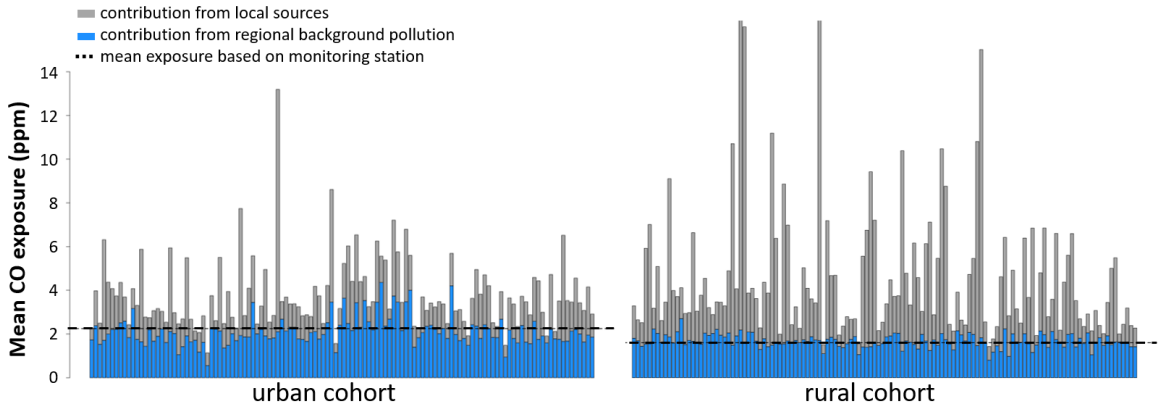

Fig. 5.8 Mean CO exposures (averaged over 7 days) in the urban and peri-urban (rural) cohorts. Each bar represents the exposure of one participant with the contributions from local and regional sources marked in grey and blue, as demonstrated in Figure 5.7. The dashed lines mark the mean exposure based on monitoring station measurements. The mean and standard deviations of the contributions are shown in Figure 5.9.

The results from Figure 5.8 are summarised in Figure 5.9 which shows the mean regional and local contributions to personal exposure, averaged over the two AIRLESS cohorts in winter and summer. The standard deviations of the contributions were added as whiskers to illustrate the variability of each component. A quantitative summary is given in Table A.6 in the Appendix. The lower personal exposure in summer compared to the winter season, which was already found in Section 4.3, can be attributed to a reduction in both the regional and the local emissions. Lower regional levels were observed at the monitoring stations (see Section 4.3). The reduction in local emissions may be attributed to less use of indoor biomass burning for heating, and a

faster removal of local air pollution from indoor environments thorough increased building ventilation.
The contribution from regional air pollution was relatively constant across all participants, especially in the rural cohort: The regional components varied by $\pm$ 0.31 ppm in Pinggu and by $\pm$ 0.68 ppm in Beijing (standard deviation). The local contributions, which in this case amount to exposure misclassification, varied substantially more (SD = 1.56 ppm (rural) - 3.69 ppm (urban)) and contributed on average to 45% (urban winter) - 65% (rural winter) of the total personal exposure.
The exposure differences between participants within a cohort were much larger than the differences between the different sites (urban vs rural). This stresses that epidemiological studies that rely only on regional exposure metrics (static monitoring stations) may suffer from large uncertainties in individual exposure estimations.

Furthermore, the air pollution mixture, and therefore also its effects on the human body, can vary significantly between different emission sources. CO could be a proxy for other potentially harmful pollutants that were co-emitted from the same source. Analysing the health effects of local and regional air pollution separately might help to gain a better understanding of the health effects of air pollution, and how to mitigate these most efficiently.

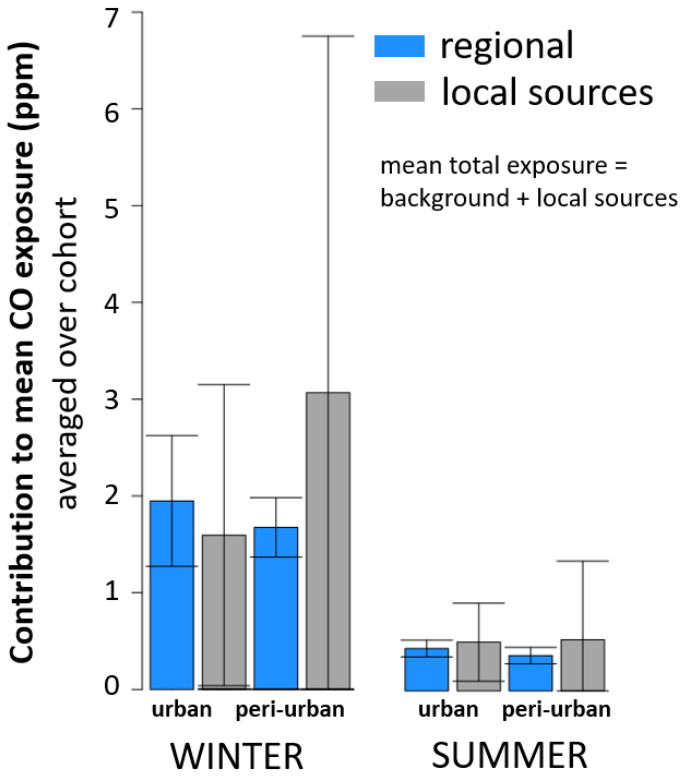

Fig. 5.9 Mean contributions from background air pollution (blue) and local sources (grey) to the total CO exposure (= sum of the two components). Standard deviations were added as whiskers to illustrate the variability between participants. The left part of the graph (winter) is an average over the two cohorts of the data shown in Figure 5.8, the right part represents the equivalent for summer. Quantitative summary in Table A.6.

5.4 Chapter summary

This chapter demonstrated, using the AIRLESS dataset, how mobile sensor networks contribute to a better understanding of the different origins of the air pollution that people are exposed to in daily life.

The methodology described in this chapter builds upon a conceptual model of personal exposure, and a statistical approach using a large sensor network.

Similarly to urban air pollution studies, the total personal exposure to inert pollutants can be expressed as the sum of the regional background concentration and additional local emissions. Hence, the background concentration extracted from the network could be used to separate the regional and local components of personal exposure. The results of this source attribution showed that a large fraction (up to 95%, mean: 55%) of personal CO exposures originated

from local sources. This finding confirms the results from Section 4.3 that outdoor monitoring stations which measure only the regional pollution concentrations massively underestimate the personal exposures to inert pollutants.
The extent to which the local emissions contributed to the total personal exposure varied largely between individual participants. The regional component of personal exposure was, in contrast, relatively stable within each cohort. The exposure variability between participants within one cohort was much larger than the differences in the regional pollution between the two deployment sites (Beijing and Pinggu), suggesting that one monitoring station in each deployment site cannot represent the individual exposures of the surrounding cohorts.
More reactive pollutants such as NO_2 required an adapted extraction method (90^{th} percentile) which in many cases did not capture the fine structure of the regional background pollution or underestimated the outdoor levels, particularly when there was reduced building ventilation (winter). However, general trends (e.g. haze events) and the magnitude of the regional outdoor pollution were still successfully extracted which renders this method useful for sanity checks of the sensor network performance.
As the impact of regional outdoor pollution on personal exposure varies from household to household, the 90^{th} percentile method could not be used to separate the regional and the local components of personal exposure. However, the total personal exposure to reactive pollutants, i.e. local and regional component combined, was still lower than the regional outdoor concentration measured at monitoring stations (see e.g. Figure 4.3). This shows that exposure metrics based on monitoring stations generally overestimate the personal exposures to reactive pollutants.

Generally, the air pollution mixture that originates from local sources is likely to differ from the mixture caused by regional sources. Ongoing work focuses on the disaggregation of personal exposure to reactive pollutants to better understand the air pollution origins. This may also include the investigation of co-emitted pollutants which are not currently detected with low-cost sensors. The composition of particulate matter, and therefore its toxicity, may vary substantially between different source types.
A separate epidemiological analysis of the health impacts of regional and of local air pollution may offer new insights into the medical effects of air pollution. Furthermore, it may help to estimate the scale of intervention policies to mitigate harmful air pollution exposures.

Chapter 6

Activity-specific personal exposure and dose estimations

Analysis of measurements collected with portable air pollution monitors increases the spatial and temporal coverage of personal exposure, providing more accurate exposure estimates (Section 4.2), breaking the correlation between individual pollutants (Section 4.4.1) and disaggregating total exposure into indoor- and outdoor- generated components (Section 5.3). The aim of this chapter is to show how novel sensor technologies coupled with advanced computational techniques can evaluate the exposure risks of different activities and derive air pollution dose estimations in daily life.
Four studies in China, Kenya, Germany and the UK illustrate different aspects of exposure and dose analyses for health studies. The first part of this chapter explains the concept of personal exposure and air pollution dose using a modelled agent (Section 6.1). Section 6.2 introduces a time-location-activity model that automatically classifies the activity pattern of a person using input parameters from a PAM. Section 6.3 examines the variability of personal exposure between different activities, and Section 6.4 looks at additional factors that may influence the air pollution dose. Finally, Section 6.5 compares the results of two cohort studies (AIRLESS and Pilot project) regarding the activity-dependent personal exposure and dose.

6.1 Concepts of personal exposure and air pollution dose

While personal exposure to a pollutant will be similar for individuals in a given microenvironment, the amount of the pollutant actually received by the body, i.e. the air pollution dose, will depend on personal characteristics and also on the volume of air a person breathes in.

The air pollution dose is estimated [1] as the product of the pollutant concentration a person is exposed to c and the breathing rate f of that person during the exposure (Equation 6.1).

$$D(t) = f(t)\,c(t) \tag{6.1}$$

It can be estimated using any of the following three methods:

- **Method A**, often employed in large scale epidemiology, uses air pollution measurements from the static monitoring station closest to the participant's residential address c_{stat}. The method uses one generic inhalation rate (f_{gen} = 8.94 L min^{-1}) (Table 2.5) as the level of physical activity may not be available
- **Method B** assumes the same generic inhalation rate f_{gen}, but utilises highly resolved air pollution measurements in the immediate proximity of the participant (c_{PAM})
- **Method C** estimates the air pollution dose in an optimal way by using air pollution concentrations measured in the immediate environment of each participant at high temporal resolution (c_{PAM}), and inhalation rates derived from the physical activity intensity (f_{act}) for an individual.

Figure 6.1 shows the dependence of the inhalation rate (amount of inhaled air per unit time) on the level of physical activity of diverse people. The graph is based on values from the Exposure Factors Handbook of the EPA [141] which distinguishes five levels of activity: *Sleep* describes sleeping or napping; *sedentary* contains activities such as watching television, reading or simple desk work; *light* activities comprise cooking, ironing, and office tasks; *moderate* activities include house cleaning, walking, light yoga, and leisure cycling (< 15 km/h); and the *high* intensity category contains activities such as cycling, dancing, and running, but also carrying groceries.
The graph demonstrates that the inhalation rate may change by a factor of more than ten depending on the type of activity a person pursues. Consequently, the amount of inhaled air pollution may change drastically with the level of physical activity. For the dose analysis in this chapter, mean inhalation rates for adults (male and female combined) were used (see Table 2.5).

[1] assumes the total absorption of the contaminant into the body, whereas a fraction of the inhaled pollution is exhaled again [96].

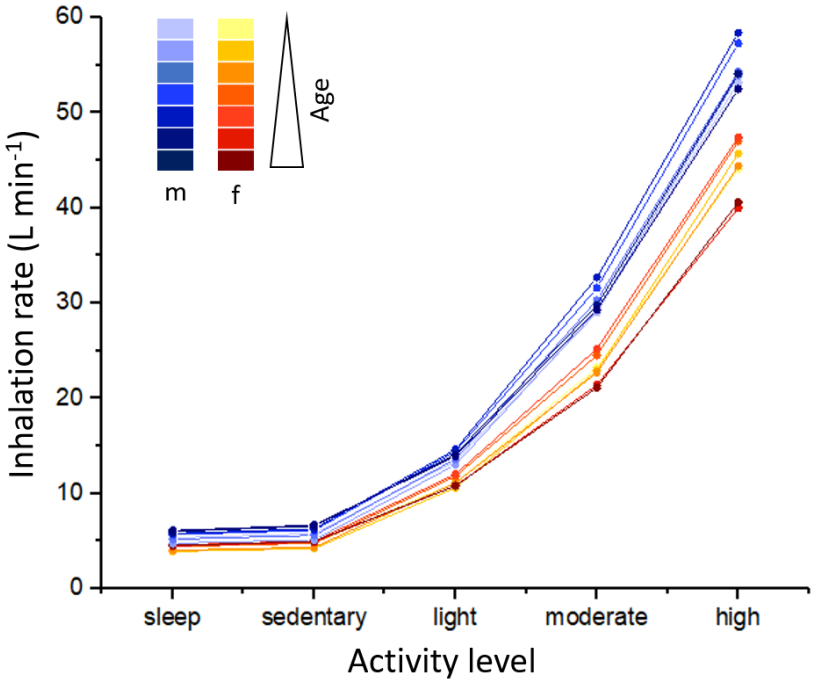

Fig. 6.1 Average inhalation rates for different levels of physical activity. The values are given for males (blue) and females (red) of different age groups between 16 and 81 years. With increasing age the inhalation rate approaches a maximum (varies with activity level and gender) and then decreases again. Values from Tables 6-17 and 6-19 of [141].

The total dose D, i.e. the amount of pollution inhaled over a determined period of time, which may cover various activities, is the integral of the time-dependent dose $d(t)$ over the selected period (Equation 6.2).

$$D = \int d(t)dt = \int f(t)\,c(t)dt \tag{6.2}$$

$d(t)$	dose at time t
D	total dose over defined time period
f	inhalation rate
c	personal exposure (pollutant concentration in direct environment)

The relationship between personal exposure c, breathing rate f, the dose per unit time d and the total dose D is illustrated in a simplified model of a person whose activity pattern is shown in Figure 6.2 and incorporated in Figure 6.3. The model represents an idealised day of an office worker who commutes to work (= sedentary activity) via walking and cycling, and spends the rest of his day at home pursuing other sedentary activities.

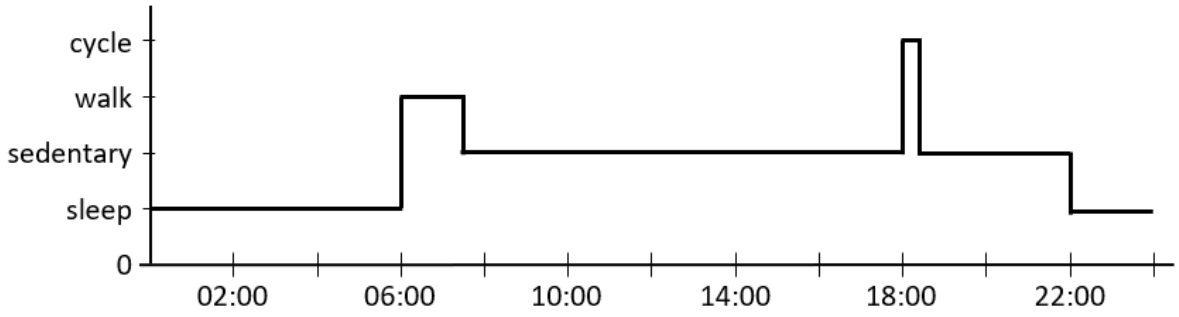

Fig. 6.2 Idealised activity pattern of an office worker who commutes to work (= sedentary) via walking and cycling, and spends his leisure time pursuing other sedentary activities (e.g. eating, reading, television). A simplified exposure and dose analysis of this case example is shown in Figure 6.3.

Part A of Figure 6.3 shows the pollutant concentrations the person was exposed to during the four activities: cycling and walking took place outdoors while sleeping and sedentary activities were performed indoors. For this example, a reactive pollutant such as NO_2 or $PM_{2.5}$ was selected. In the absence of local sources, its concentration is lower in indoor environments compared to ambient levels (Section 5.2.1). For simplicity, the indoor pollutant levels were assumed to be constant across the two indoor microenvironments (work, home); and the pollutant concentration in the street environment was assumed to be equal to the ambient concentration (blue). Note that this is a gross simplification of reality as air pollution concentrations are likely to vary between different indoor environments (e.g. work and home), as well as within highly polluted environments, such as busy streets, which are often more polluted than the background locations.

Part B of Figure 6.3 assigns inhalation rates to the four activities of the case example (c.f. Table 2.5) with lowest inhalation rates during sleeping (5.5 litres per minute) and highest during cycling (39.2 litres per minute). If the activity pattern of a person is unknown, a generic inhalation rate may be applied. In Part B of Figure 6.3 it is shown as the blue bar. Note that the generic inhalation rate[2] (8.94 L min^{-1}) is very similar to the inhalation rate during sedentary activities (8.51 L min^{-1}).

Following Equation 6.1, the product of the exposure levels (A) and the inhalation rates (B) can be defined as the air pollution dose per unit time (here: per minute). **Part D** of Figure 6.3 shows these values for the four different activities. The modelled person inhales substantially

[2]derived from average daily inhalation rate of free-living normal-weight adults; Table 6-5 in [141]

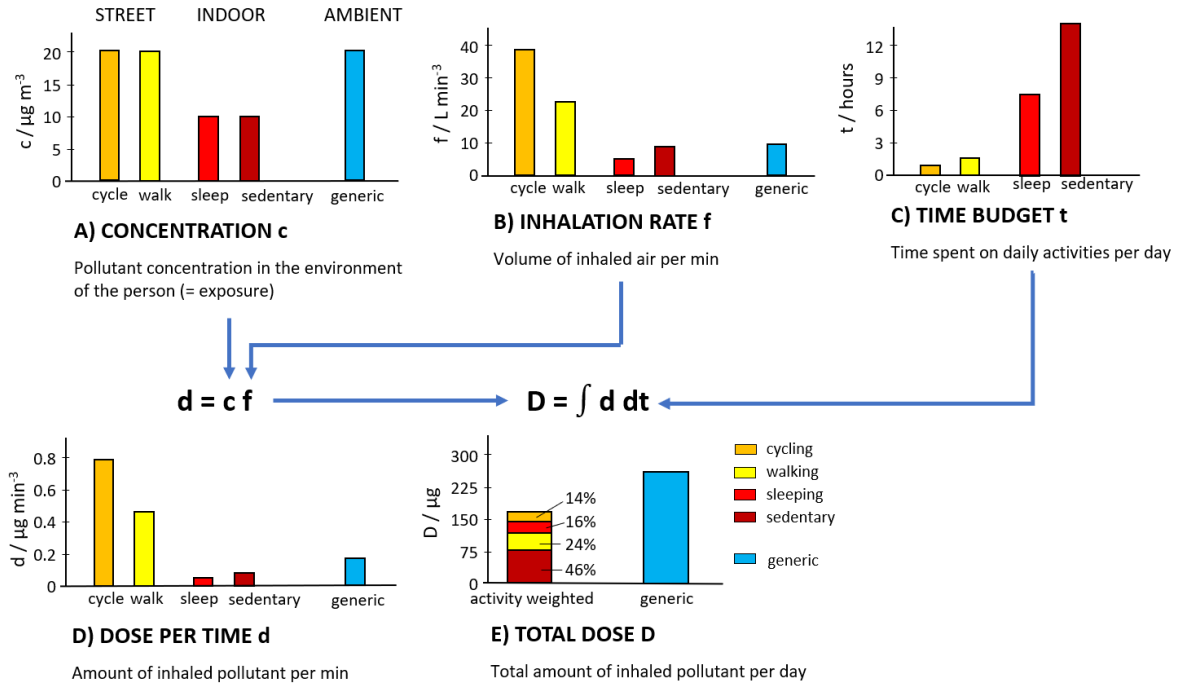

Fig. 6.3 Schematic example illustrating how the combination of personal exposure c (A), activity-specific inhalation rates f (B) and the time t spent on different activities (C) may be used to estimate the pollutant dose per unit time d (D) and the total dose D (E). Based on the activity pattern of the case example shown in Figure 6.2.

more pollution during cycling and walking because both the air pollution exposure and the inhalation rates were highest during these activities.

The blue bar in Part D represents the generic dose per minute which would be assumed if no personal exposure measurements and no information about the activity pattern of the person were available. In this case, the dose per minute is calculated as the product of the ambient concentrations measured at static monitoring stations and the generic inhalation rate of adults (blue bars in Parts A and B, respectively).

Even though the street exposure is assumed to be the same as the ambient levels, the generic dose would massively underestimate the amount of pollution inhaled during cycling and walking by neglecting the activity-specific inhalation rates; and overestimate the inhaled dose during sleeping and sedentary activities.

Part C of Figure 6.3 indicates the total amount of time spent on the four activities. The person was physically active (cycle and walk) for a small fraction of the day (in total 2 hours) and

spent most of his time sedentary (14 hours) or asleep (8 hours).

The time budgets (Part C) may be used to determine the total air pollution dose per day and how much each activity contributes to this daily dose (**Part E** of Figure 6.3). The total dose that was inhaled over the course of each activity is determined by integrating the activity-specific dose per time (Part D) over the time budget of the corresponding activity (Part C, see Equation 6.2). The sum of the individual doses from each activity (coloured fractions of bar) thus gives the total daily dose (left bar in Part E). If no activity information is available, the generic dose per time (blue bar in Part D) is simply integrated over 24 hours. The resulting generic total dose is shown as a blue bar on the right of Part E.
Although the highest amount of inhaled air pollution per time was found during cycling, it contributed to only 14% of the total daily dose. On the other hand, indoor activities that were associated with low amounts of pollution inhaled per time (sleeping and sedentary) were responsible for the major part (62%) of the total dose due to the large fraction of time budget they occupy.
In this case example, the generic approach would overestimate the total daily dose of the participant. Note that the outcome in Part E of Figure 6.3 is totally dependent on the set of assumptions going into the dose calculation (Parts A to C). But as Section 6.4 will demonstrate, these are not unrealistic for pollutants like NO_2 or $PM_{2.5}$, indicating that indoor exposures are driving a significant fraction of the total dose.
Finally, the pollution mixture inhaled during different activities likely originates from different emission sources and, therefore, may contain different chemicals with varying potential toxicity. Therefore, neglecting the activity component in air pollution dose-health relationships might lead to erroneous conclusions regarding the toxicity of air pollution.

6.2 Development and validation of a time-location-activity classification algorithm

The previous section highlighted the importance of time-activity patterns regarding personal exposure/dose and potential health implications. Because it is labour intensive to collect detailed personal exposure profiles at the individual level in large scale studies, it is necessary to develop an automated algorithm for activity detection using readily available parameters.
The time-location-activity model presented in this section automatically classifies behavioural patterns of individuals using auxiliary parameters collected with the PAM (geo-coordinates,

background noise and acceleration levels) as input. As these parameters can be collected with ubiquitous smartphone technologies, this model has wider applicability than the specific sensor platforms. The classifications are extracted by employing machine learning techniques of spatio-temporal clustering, movement analysis methods, geographical information systems (GIS) [106] and rule-based algorithms.

6.2.1 Description of the automated time-location-activity model

The flow chart in Figure 6.4 gives an overview of the data processing steps integrated in the model which are elaborated in this subsection.

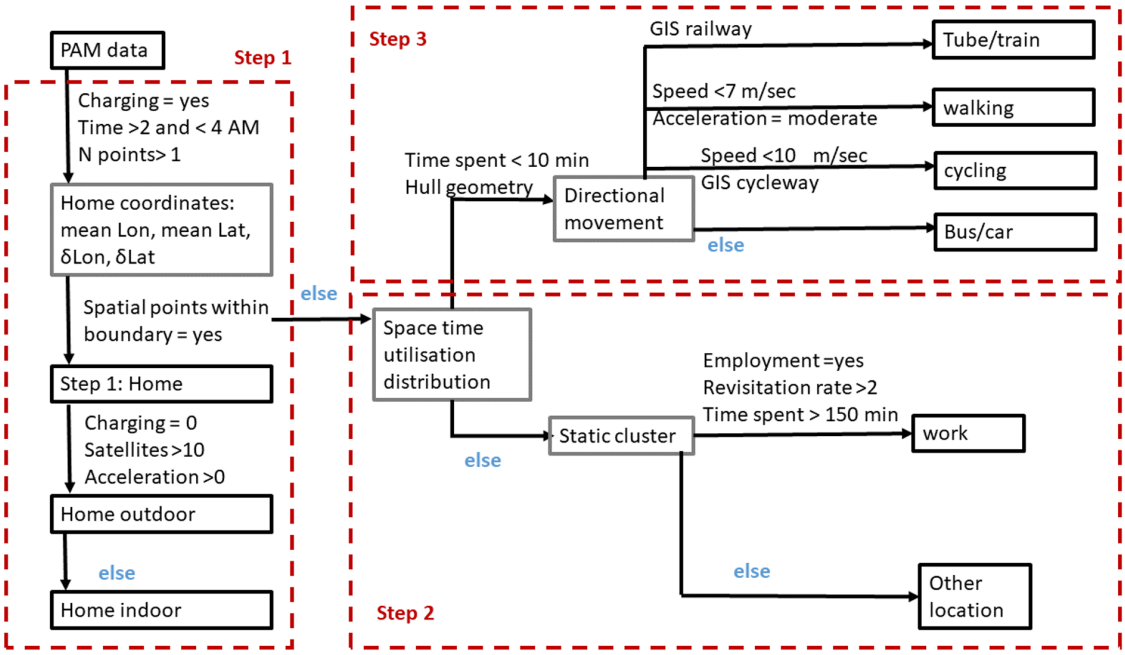

Fig. 6.4 Flow chart of the classification model. In the first step the *home* location was identified with a rule-based model. In step 2, observations outside of the home are separated broadly into directional movement and static clusters using a space-time utilisation distribution [90], i.e. information on the frequency and duration of visits. In the final step 3, segments of directional movement were classified to transportation modes based on acceleration, speed and GIS.

Step 1: Home location

As people may spend as much as 90% of their time at home, the first step aimed to reduce the computational burden in the subsequent analysis using a simple rule-based modelling approach. It was assumed that the monitors were located at home when they were placed in a charging station between 02:00 AM and 04:00 AM (local time).

Using a representative participant from the pilot project, Figure 6.5 illustrates the spatial cluster formed around the home location due to the GPS scattering indoors. The scattering distances δLon and δLat were used to create a spatial zone where all included points were classified as home, and were further subclassified as indoor and outdoor based on a rule-based algorithm of number of visible satellites (with higher numbers typically seen outdoors), acceleration and charging status of the PAM. Missing GPS coordinates were also classified as home if the previous and last observations were in that same category.

If the algorithm was not able to identify home location for a participant in this step (for example, sleeping in multiple locations or a lack of satellite reception during the selected time period), then it was classified in the next step as the location where the participant spent most of their time.

Sleeping was classified based on time of day, relatively lower background noise levels and lower concentrations of the larger particulate matter fraction (PM_{10}) which re-suspend during periods of physical activity of the occupants.

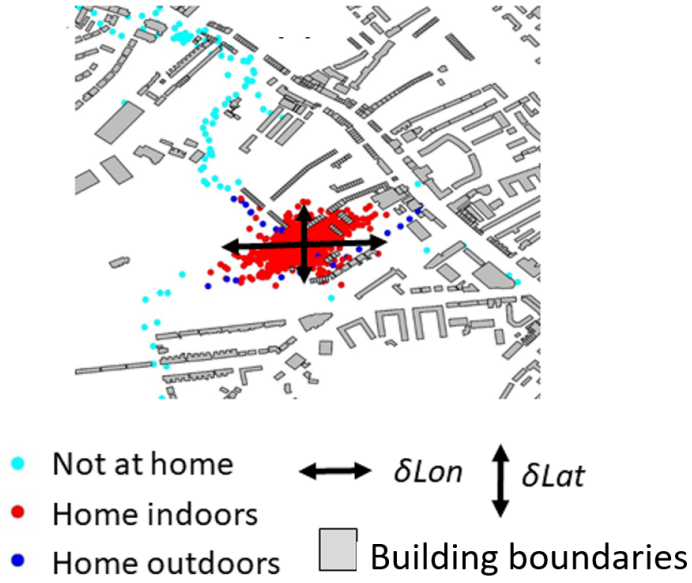

Fig. 6.5 Classification of home location of a representative participant from the pilot project at 1 min resolution. The cyan spatial points indicate observations that do not belong in the home cluster. The red and blue spatial points denote indoor and outdoor locations at home. An excellent agreement was generally found between reported and modelled home location. Map data from OpenStreetMap

Step 2: Separation between static clusters and directional movement

The timestamped GPS data that remained unclassified (i.e. were not within the home boundaries) were analysed using a technique[3] that models space-use and time-use simultaneously to identify spatio-temporal patterns in the data.

Parts (a) and (b) of Figure 6.6 illustrate how the method distinguishes between a participant moving between two locations (directional movement), and a participant remaining at one static location (e.g. at home or at work).

Part (a) shows all locations visited by a representative participant from the AIRLESS cohort, coloured by the amount of time they spent in each place. The space-time analysis also includes the number of times a person re-visits each location (re-visitation rate), and metrics of directional movement. The model automatically computes these parameters from the GPS coordinates of each participant.

The results from the space-time analysis were combined with the home classification from Step 1 to classify each data point in one of three core location categories: home, other static locations and in transit (Figure 6.6 (b)).

[3] implemented using the R package "Time Local Convex Hull" (T-LoCoH) [90]

Work was defined as the static location that has both high re-visitation rates (i.e. ≥ 3 per week) and extended duration of visits. Similarly with the home location, work was further sub-classified to indoor and outdoor locations.

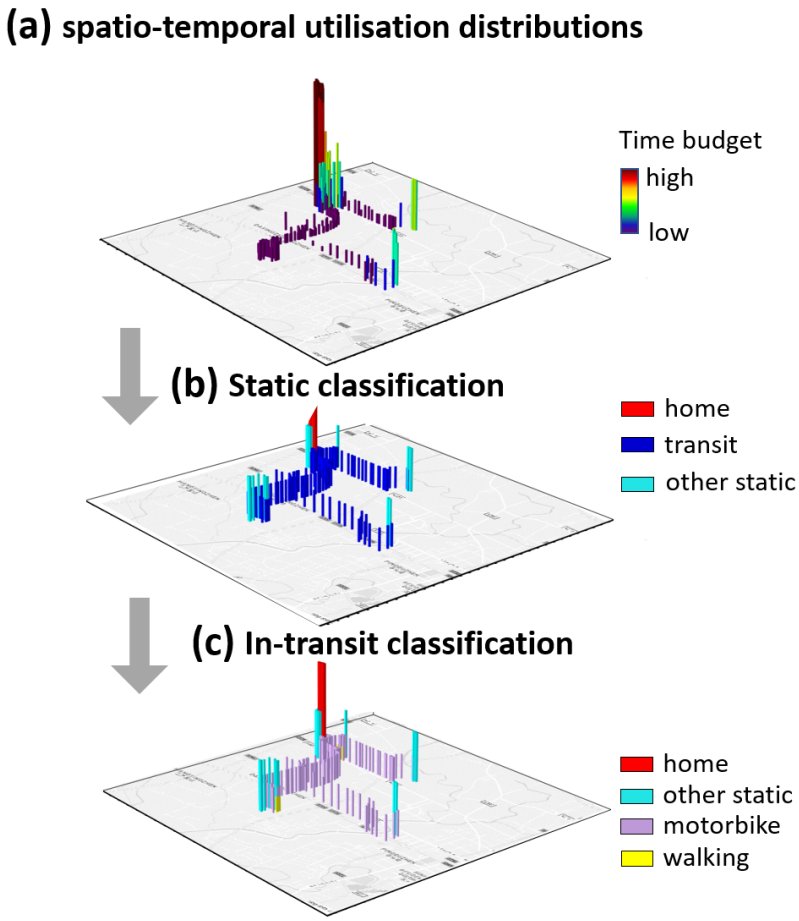

Fig. 6.6 Spatial classification of the PAM data of a representative participant from the AIRLESS winter campaign (rural cohort). (a) 3D map illustrating the relative amount of time spent in visited locations. (b) Separation between static clusters and clusters with directional movement. (c) Classification of mode of transport. Map data Google 2019.

Step 3: Mode of transport classification

Observations belonging to non-static clusters were further analysed with the adehabitatLT package [24] in R. The trajectories between two static locations were partitioned into smaller segments because people may change the mode of transport during a single journey (e.g. walk-

ing then travelling by metro train). Each segment was classified using speed and acceleration, as well as GIS data (obtained from OpenstreetMap [106]) which contains information such as train routes and bicycle paths. The classification included walking, cycling, in-vehicle, motorbike and train/tube. The in-vehicle travel refers to car, taxi or bus.
Figure 6.6 (c) shows the commuting mode classification of the example participant from the AIRLESS project. Their main mode of transport was by motorbike which is relatively common in the area of Beijing.

The time-location-activity algorithm was validated by comparing model classifications with diary entries of 38 volunteers residing in London and Cambridge (Pilot project, see Section 2.3.1). All in all, there was a good agreement between the results of the time-location-activity model and the activity diaries (see Section A.6.1).

6.2.2 Illustrative example of activity classification and dose estimation

Using the time-location-activity model introduced in the previous section, Figures 6.7 and 6.8 illustrate the activity classification and dose calculation using a one-day snapshot of the data from AIRLESS case participant U123 (Dec 2nd 2016).
Figure 6.7 shows how the different activity patterns of the participant affect auxiliary parameters of the PAM (top rows, black). Commuting events can be identified by the rapidly changing GPS coordinates. The rate of change in longitude and latitude is proportional to the participant's speed. For example, motorised travel (B) has a faster rate of change than walking (C). In static locations, longitude and latitude values remained constant.
Background noise and accelerometry readings were highest during commuting (in vehicle B and walking C), and lowest during sleep (A). Drastic temperature and humidity changes happened when the participant moved from indoors to outdoors and vice versa (e.g. when leaving home at 07.00 am) because the outdoor temperature ($\sim$ 0°C) was much lower than indoors.

The inhalation rates varied by a factor of four over the course of the day, with the highest volume of air breathed in during walking (22.2 L/min) and the lowest volume breathed in during sleeping (5.5 L/min).

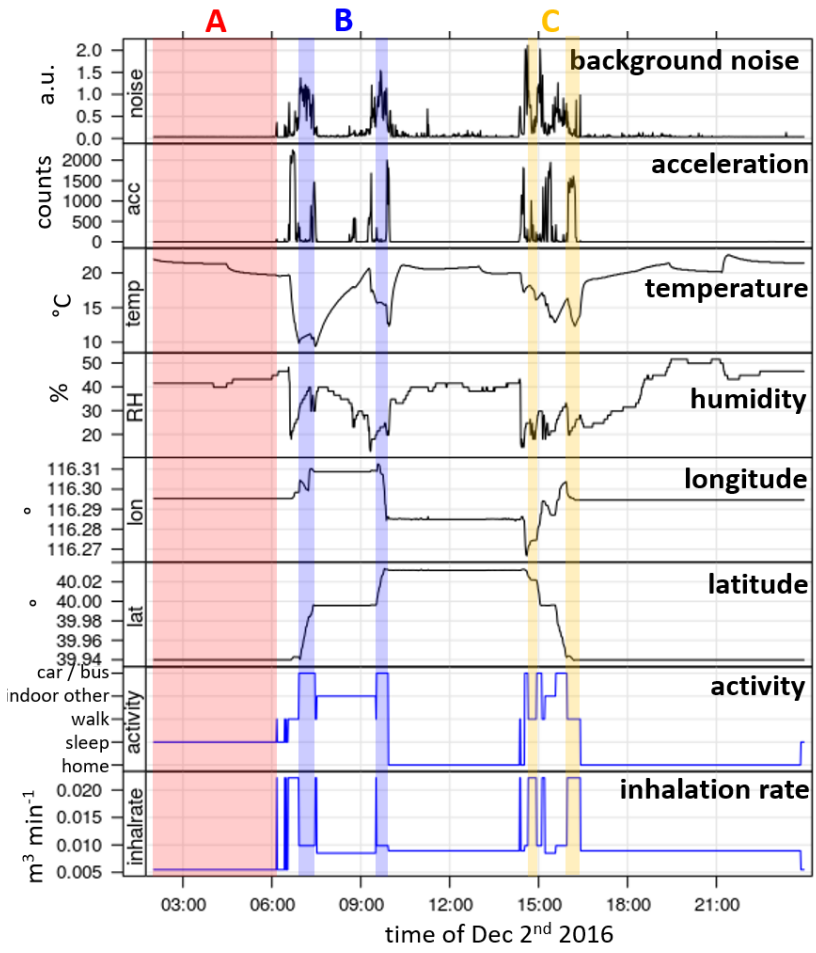

Fig. 6.7 Relationship between auxiliary parameters and participant's activities predicted by the time-location-activity model (see Section 6.2). One-day snapshot of U123 data (Dec 2nd 2016). A - sleeping; B - inside a motorised vehicle (bus /car); C - walking in traffic.
Given in local time (UTC + 8). Temperature and RH outside the monitor maximum noise recordings and acceleration counts above threshold 1 are shown (see Table 2.2).

Figure 6.8 demonstrates how the modelled activities of participant U123 and the inhalation rates derived from these were used to estimate the air pollution dose. The graph shows the same one-day snapshot as Figure 6.7 with the activity classification at the top (blue). The second and third row show the calibrated and ratified NO_2 and $PM_{2.5}$ exposure (Level 2) of the participant. These concentrations were multiplied by the inhalation rate (blue) to estimate the dose, i.e. the amount of pollutant inhaled per minute (bottom row, Equation 6.1).
Reflecting occupancy patterns, indoor exposures showed large variability with lowest $PM_{2.5}$ and NO_2 concentrations during sleeping hours (e.g. 2 am to 6 am), and highest concentrations when indoor emission sources operated indoors (cyan shaded areas "D"). The pollutant levels were similarly elevated in commuting environments (car/bus B or walk C); however, the air pollution dose was much higher during walking due to the higher inhalation rates.
The effect of inhalation rates on dose may be further highlighted by comparing walking in traffic (C, gold) with peak indoor exposures (D, cyan). The air pollution doses were comparable during these two events although indoor peak levels were much higher. A detailed analysis of the air pollution dose risks of different activities is given in the subsequent sections.

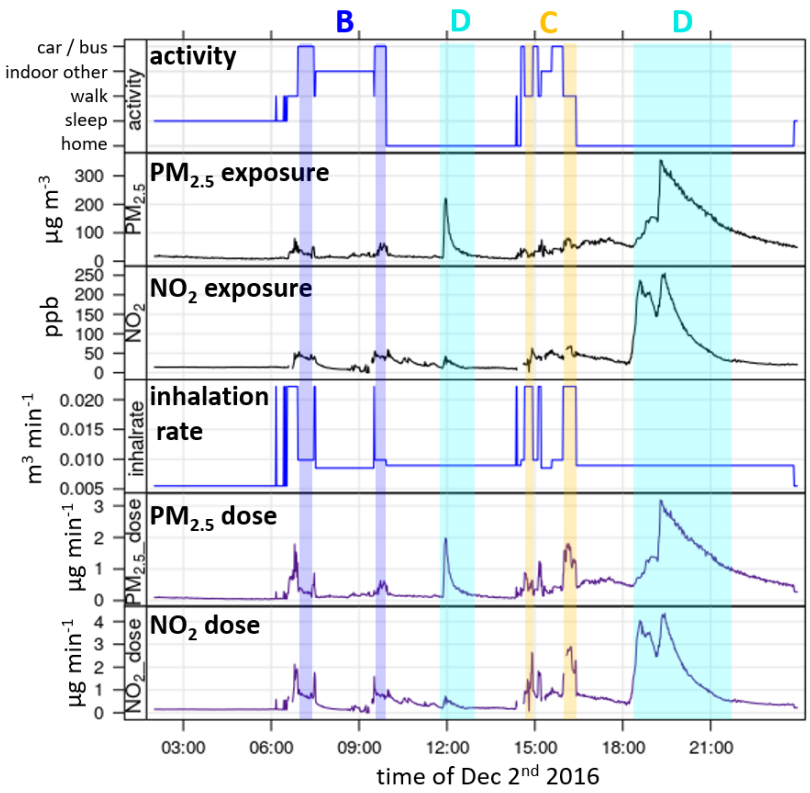

Fig. 6.8 The air pollution dose of a pollutant (purple) is calculated by multiplying the personal exposure to this pollutant (black) with the activity-dependent inhalation rate (blue).
B - inside motorised vehicle (bus /car); C - walking in traffic; D - indoor emission source.
One-day snapshot of U123 dataset (Dec 2nd 2016), given in local time (UTC + 8). For the dose calculation, the NO_2 mixing ratio (ppb) was first converted into a concentration (µg m^{-3}) using a fixed conversion factor of 1.91 µg m^{-3} /ppb.

6.3 Case studies: assessing personal exposure in different microenvironments

In epidemiological studies, data from ambient monitoring stations typically cover the exposure estimates of large study areas, and short-term exposures are assumed to be the same for the entire population in those areas [18]. The following section examines exposure differences between microenvironments in three case studies in the UK, Germany, and Kenya. While these studies only represent snapshots of different exposure scenarios, they illustrate the complexity of air pollution exposures that may be found even within small study areas.

6.3.1 Daily life exposures in the UK

During the pilot project, 38 participants carried a PAM with them while keeping a record of their daily activities. The participation time was on average 8.9 days (see Section 2.3.1, time budgets shown in Figure A.13).

The exposure data of the participants were classified into the activity categories introduced in Section 6.2. The NO_2 and $PM_{2.5}$ exposures measured across the 38 participants during these seven activities are summarised as boxplots in Figure 6.9. NO_2 and $PM_{2.5}$ were selected as example pollutants as these species are regarded as particularly harmful to human health.

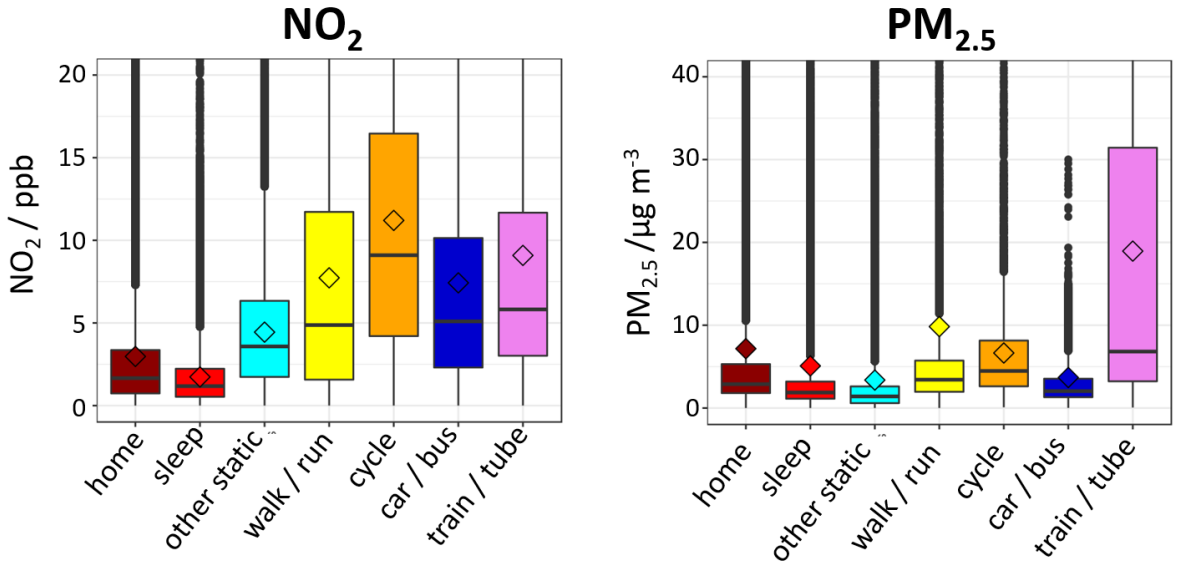

Fig. 6.9 Concentration ranges of NO_2 (left) and $PM_{2.5}$ (right) measured in different microenvironments during the pilot project (Section 2.3.1, London and Cambridge combined). Diamond shapes mark the mean exposure. Activity-location classification derived from diary data. Work is included in the category "other static".

The NO_2 and $PM_{2.5}$ concentrations varied widely between the different activities, with lowest levels during sleep. As the two pollutants are strongly associated with traffic emissions, it is not surprising that their highest concentrations were generally observed during commuting activities. $PM_{2.5}$ exposures in the rail environments were particularly high. A further disaggregation of the rail category (based on the participants' diary entries) showed that this was mainly due to increased $PM_{2.5}$ exposures in the tube (mean train exposure: 6µg m^{-3} , mean tube exposure: 23µg m^{-3}).

NO_2 and $PM_{2.5}$ concentrations were generally lower in indoor environments due to indoor

sinks (Section 5.2.1). Interestingly, even the space inside vehicles seemed to be affected by indoor sinks as the concentrations inside cars or busses were lower than the pollutant levels in the outdoor street environment (walking and cycling).

Table 6.1 Ranking of daily activities by average exposure measured during the pilot project (London and Cambridge combined).

	Highest exposure						**Lowest exposure**
	1	2	3	4	5	6	7
CO	walk / run	home	car / bus	cycle	other static	sleep	train / tube
NO	car / bus	cycle	train / tube	walk / run	home	sleep	other static
NO_2	cycle	train / tube	walk / run	car / bus	other static	home	sleep
O_3	cycle	walk / run	train / tube	car / bus	other static	home	sleep
$PM_{2.5}$	train / tube	walk / run	home	cycle	sleep	car / bus	other static

Table 6.1 gives an overview of all pollutants measured by the PAM, ranking the activities from highest to lowest mean exposure for each pollutant. In general, commuting activities caused higher air pollution exposures than indoor activities (home, sleep, other static). The exposure risk associated with an activity was different for each pollutant. On one hand, the highest $PM_{2.5}$ concentrations were found during commuting in rail systems (train / tube), whereas the same commuting mode was associated with relatively low CO concentrations. On the other hand, CO levels were relatively high at home possibly due to additional indoor cooking emission sources. This highlights the fact that, to comprehensively evaluate the health risk of an activity or microenvironment, multi-pollutant monitoring is essential.

6.3.2 Air pollution in the Berlin metro system

The Pilot UK project found the highest $PM_{2.5}$ exposures in metro systems. In fact, previous studies consistently found substantially higher aerosol levels in various underground transport systems than above ground [91, 151]. The following case study presents a one-day snapshot of the $PM_{2.5}$ concentrations in the metro system of Berlin, Germany. A personal monitor was deployed for short-term experiments in three metro stations and three metro lines in the underground rail system of Berlin (Figure 6.10, for details of the deployment see Section 2.3.3.1).

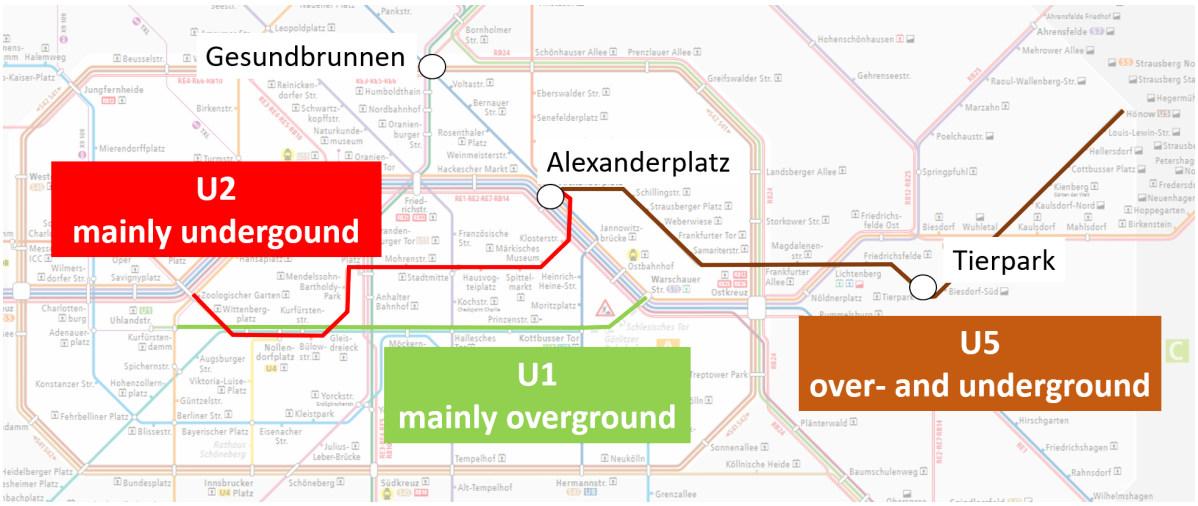

Fig. 6.10 Investigated metro lines and stations in Berlin, Germany.

Figure 6.11 shows the $PM_{2.5}$ concentrations observed at a selected metro station (Gesundbrunnen) and line (U2). The aerosol concentrations measured at the kerbside of a busy 4-lane road were added for comparison (red line). The underground $PM_{2.5}$ levels were so high that the temporal variability of the kerbside $PM_{2.5}$ levels ($< 15\,\mu g\,m^{-3}$) was almost not noticeable.
The time series at the metro station shows a distinct pattern of regularly occurring exposure peaks which coincided precisely with the scheduled departure times of the trains [14]. This pattern was caused by the piston effect, i.e. the approaching train pushing polluted air from the tunnel into the station and the leaving train drawing cleaner air from overground environments into the station. This process caused the $PM_{2.5}$ levels inside the station to change by up to $80\,\mu g\,m^{-3}$ in less than 5 minutes.
When the train emerged from the underground system the elevated $PM_{2.5}$ concentrations inside the metro train decreased and approached the (lower) outdoor concentrations (Figure 6.11 right). Note however, that the measurements were taken in the summer season when the metro cars were strongly ventilated by open windows. It is likely that such quick changes would not be observed in the winter season when less ventilation is present. In that case the air quality inside trains might be even poorer, as air exchange with cleaner outside air is reduced.

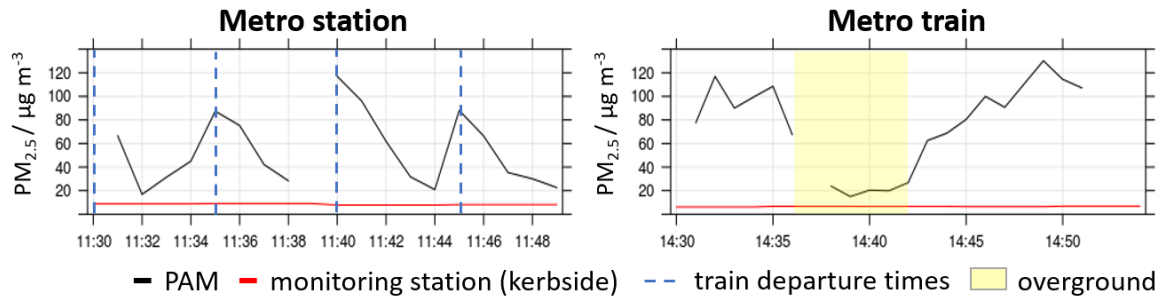

Fig. 6.11 Illustrative examples of the personal $PM_{2.5}$ exposures (black) inside a metro station (Gesundbrunnen, left) and during a metro train ride (U2 line, right), compared with measurements from an air quality monitoring station located at a highly trafficked street (Frankfurter Allee, red). The $PM_{2.5}$ concentrations in the station were strongly correlated to the departure times of the trains (blue line). Overground sections of the line (yellow shaded) were less polluted than underground sections.

The left of Figure 6.12 summarises the $PM_{2.5}$ concentrations measured at the investigated metro stations and metro lines. In line with previous literature, the air quality differed significantly between subsurface and overground sections of the lines. The right part of Figure 6.12 shows $PM_{2.5}$ concentrations measured in different lines of the London Underground for comparison [126]. The aerosol concentrations in the underground parts of the rail system (station and underground sections of the lines; mean: 84 µg m^{-3}) were on average almost 8 times higher than the outdoor levels at the kerbside (mean: 11 µg m^{-3}), and almost twice as high as the exposures in overground sections of the metro lines (mean: 48 µg m^{-3}). These results agree with previous studies on other metro systems finding underground aerosol concentrations being 1.3 to 15 times higher than in the corresponding outdoor environments, and clearly depending on the tunnel depth [91, 126, 151].

Table 6.2 compares the average concentrations measured at the metro system with kerbside and ambient observations for all five pollutants measured by the PAM. While the $PM_{2.5}$ concentrations were higher in the metro environment than on the street, the concentrations of the gaseous pollutants were lower in the subway and in the case of O_3 and NO_2 also lower than the ambient background concentrations, suggesting the presence of indoor sinks in underground systems. The $PM_{2.5}$ concentrations in the Berlin underground were comparable to the $PM_{2.5}$ levels found at the Piccadilly line of the London Underground (study by Smith et al.; right of Figure 6.12). It is remarkable that the metro systems in the two cities contained comparable $PM_{2.5}$ levels although they have very different characteristics (age, depth, ventilation system).
Smith's study was also able to point to differences in the chemical composition of the aerosol

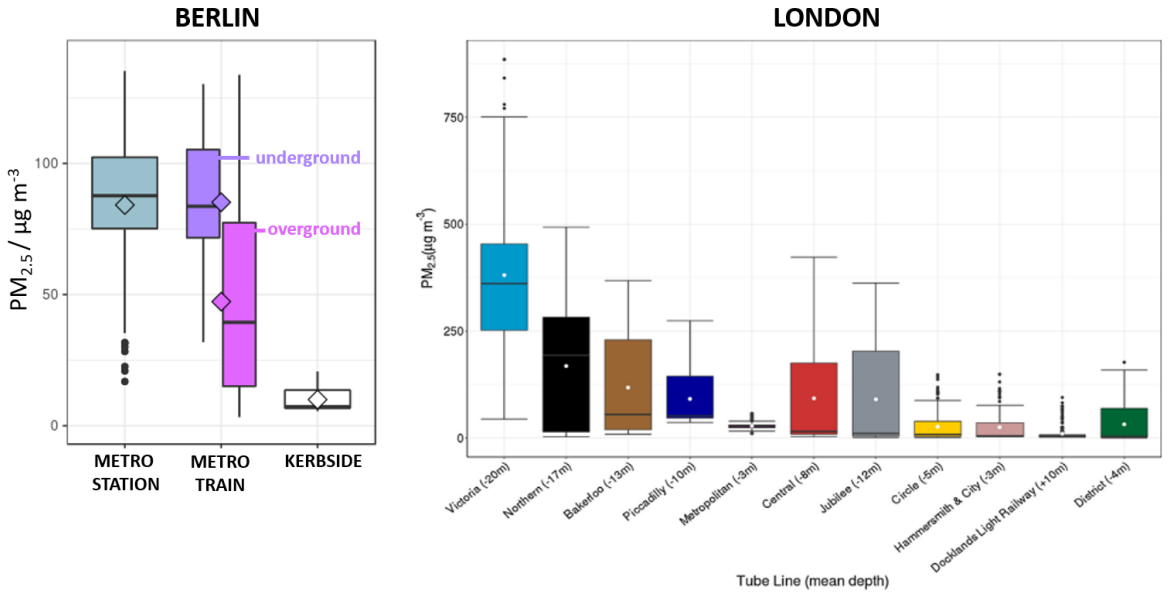

Fig. 6.12 Left: Boxplots comparing the personal $PM_{2.5}$ exposures inside metro stations and trains with the $PM_{2.5}$ concentrations measured at a kerbside monitoring station in Berlin, Germany. Graph includes the measurements from all examined metro stations (Gesundbrunnen, Alexanderplatz, Tiergarten) and metro lines (U1, U2, U5; split into underground and overground sections). Right: $PM_{2.5}$ concentrations measured in different lines of the London Underground [126]. Mean line depth shown in brackets beneath. Note the different scaling of the y-axis.

between sub-surface and above-ground sections of the London tube which may have an important impact on potential health effects. Particulate matter in subway systems is usually characterised by larger fractions of metallic compounds which originate from the wear of steel components of the trains and rails [126]. As these compounds are often regarded as the most toxic compounds in particulate matter [126], special care must be taken when evaluating the health effects of underground air pollution. The measurement technology used in this work (PAM) was not able to capture the different PM compositions, however, the relationship between two pollutant species such as NO_2 and $PM_{2.5}$ might give an initial indication of the emission sources in the surroundings (Figure 6.13).

Overall, confirming and extending previous findings in metro systems, this deployment indicated that different commuting modes result in exposure to a unique chemical mixture with street level commuting dominated by gases and underground systems dominated by particulate matter.

Table 6.2 Mean pollutant concentrations measured during metro commute (stations and trains) and in road traffic, compared with urban background concentrations in Berlin.

	Metro	**Road traffic kerbside**	**Urban BG**
CO / ppb	330	402	NA
NO / ppb	11	13	4
NO_2 / ppb	10	28	17
O_3 / ppb	2	32	35
$PM_{2.5}$ / µg m^{-3}	67	11	NA

Kerbside concentrations from air quality station Frankfurter Allee. Urban BG from air quality stations Neukölln in Berlin (BLUME network [13]). Concentrations averaged over the metro data collection time (10/09/2018 09:00-20:00)

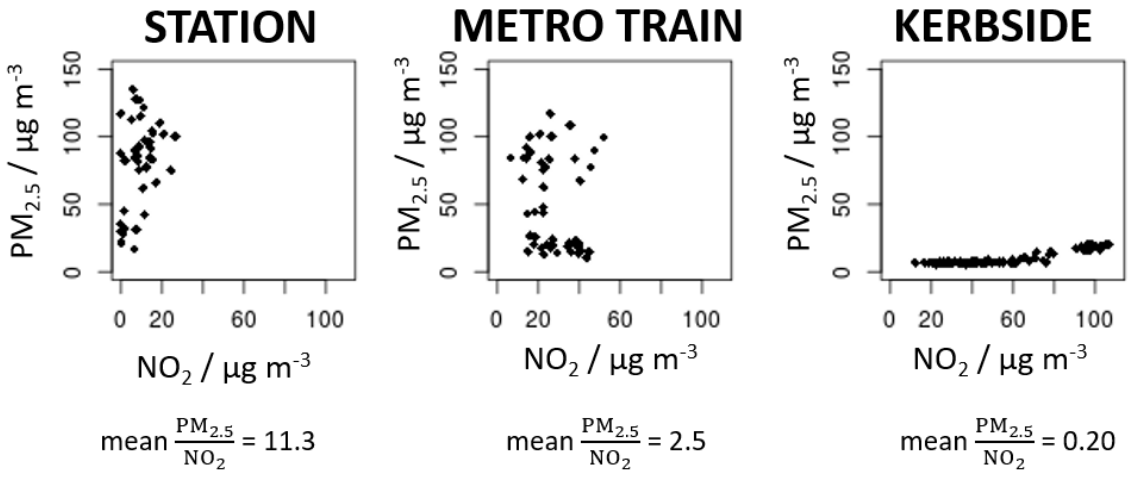

Fig. 6.13 $PM_{2.5}/NO_2$ ratio measured at metro stations (left), inside metro trains (middle) and at the kerbside of a busy street (right). The underground was dominated by $PM_{2.5}$ while the street environment was dominated by NO_2.

6.3.3 Domestic exposures using different cooking fuels

People spend the majority of their time inside their homes [73]. Hence, household air pollution is an important contributor to their overall exposure. According to the WHO, over 4 million people died prematurely in 2012 as a result of this household air pollution [147]. Cooking and heating practices contribute substantially to domestic air pollution, particularly in low- and middle-income countries where people often rely on biomass burning [147]. Even in the UK (no indoor biomass burning), high $PM_{2.5}$ and CO concentrations were measured in the home environments of the pilot participants which likely originated from cooking emissions.
The following case study investigates how cooking practices may affect the air pollution levels in rural Kenyan households. During the study, portable air quality monitors were deployed in the kitchen areas of eight households with newly introduced biogas plants and four households that used traditional cooking fuels (mainly charcoal).
The outdoor air quality was monitored with three AQMesh instruments distributed in strategic locations around the settlement to extract the background air pollution concentrations. Further details of the Kenyan deployment are given in Section 2.3.3.2.

The participants spent on average 77 min per biogas cooking session whereas charcoal cooking events lasted for 127 min. Because of the convenience of the biogas cooker, however, people used it on average 1.7 times more often than the charcoal stove. As a result, the residents spent the same amount of time per day (on average ca. 2 hours) on cooking with both types of fuels. Figure 6.14 presents the CO, NO and $PM_{2.5}$ concentrations measured when the participants were cooking with biogas (green) and with charcoal (grey), compared to the outdoor background concentrations (white). Both biogas and charcoal fuels raised the indoor pollution concentrations to levels approximately 10-15 times higher than the regional outdoor concentrations. Charcoal fuels caused on average higher gaseous pollution levels (CO and NO). Higher CO levels indicate a lower combustion efficiency of the charcoal stove which raises the question whether other pollutant species were co-emitted during the charcoal burning which were not detected by the PAM but nevertheless could have serious toxic effects on the human body.
Biogas generated higher $PM_{2.5}$ levels than traditional cooking fuels. A possible explanation for the higher PM levels might be related to the instrumentation i.e. the light scattering OPC. While convenient due to high portability, low power consumption and low-noise levels, the OPC could not detect soot which might be produced in large quantities during charcoal burning. Furthermore, emissions from cooking may not only originate from the heating source but also from the food itself [138].
The introduction of biogas as cooking fuel reduced the exposure to gaseous air pollutants

during cooking events, but not the exposure to particulate matter. Hence, the use of biogas plants did not result in a clear improvement of domestic air quality. However, it improved the life quality of the residents in other respects such as lower financial costs, reduced time for domestic chores (i.e. firewood collection), convenience and environmental sustainability.

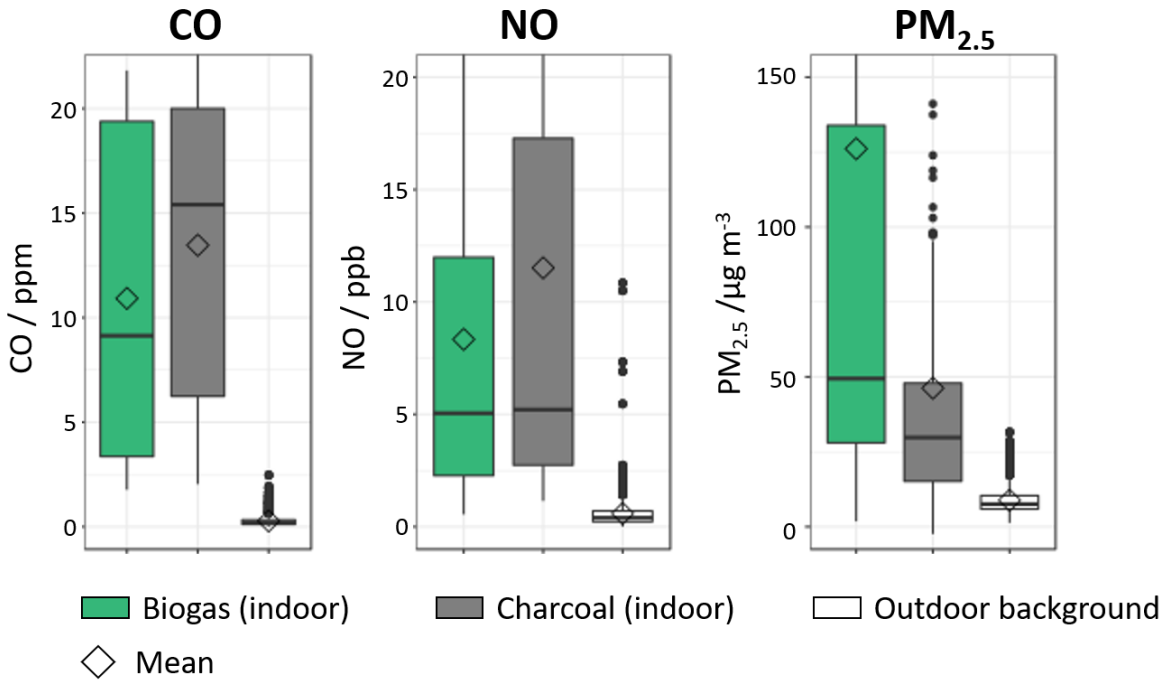

Fig. 6.14 Concentration ranges measured during indoor cooking events using biogas (green) and charcoal (grey), compared to outdoor background pollution levels (white). For technical reasons, NO_2 data were not available (see Section 2.3.3.2). Time periods when the participants were cooking indoors with one cooking fuel only (biogas or charcoal, no other simultaneous fuels in use) were included in the graph.

6.4 Estimations of air pollution dose of the AIRLESS project

The following section combines activity dependent inhalation rates with personal exposure measurements to generate improved air pollution dose estimations for 251 participants.
This novel dose estimation approach will be compared to conventional methods based on generic inhalations rates and static exposure measurements. Section 6.4.1 examines the air pollution dose per unit time that is inhaled during specific activities (c.f. Figure 6.3 D) and Section 6.4.2 looks at their total dose per day (c.f. Figure 6.3 E).

The Section focuses on the data from the winter campaign of the AIRLESS project which has been extensively characterised in Chapters 4 and 5 (data collection described in Section 2.3.2).

6.4.1 Activity specific dose estimates per unit time

Section 6.1 demonstrated how strongly the inhaled amount of pollutant may differ between various activities. For instance, in the example given in Figure 6.3 (Part D), the pollution dose inhaled while cycling was over 10 times higher than the dose inhaled while sleeping, which was due to a combination of different air pollution concentrations and different inhalation rates during the two activities.

This section examines the activity specific dose estimations in the AIRLESS project. Figure 6.15 shows the average pollutant dose per minute inhaled by the AIRLESS participants during different activities, calculated with the three methods A, B and C (Section 6.1).

Method A may not distinguish between different activities; therefore, the same dose estimation is given for all activities (white bar). As method B integrates one generic inhalation rate across all activities, the resulting average dose is proportional to the mean pollutant concentrations the participants were exposed to during the different activities.

The home environment had the biggest impact on the CO dose/min, which was probably caused by indoor emission sources such as cooking and heating (c.f. Section 6.3.3). The average NOx dose/min was highest during street-level transportation, likely due to strong sources in the traffic environment.

When inhalation rates were taken into account (method C), the maximum dose was received during active modes of transport (walking, cycling) owing to the increased physical activity level. In contrast, the dose during sleep was usually the smallest because of the low breathing rate during this activity. The generic inhalation rate (8.94 L/min) was very similar to the inhalation rate during sedentary activities (8.51 L/min). As a consequence, the difference between dose estimation approaches B and C (generic and activity adjusted) was negligible for mainly sedentary activities (home, other static, commuting sitting in vehicles).

The air pollution dose varied by a factor of up to ~ 20 between different activities (e.g. NO_2 dose during sleeping: 0.085 µg/min, during cycling: 1.59 µg/min). Conventional approaches (method A) may not capture this variability and, thus, may be prone to large uncertainties in the dose estimation of individuals.

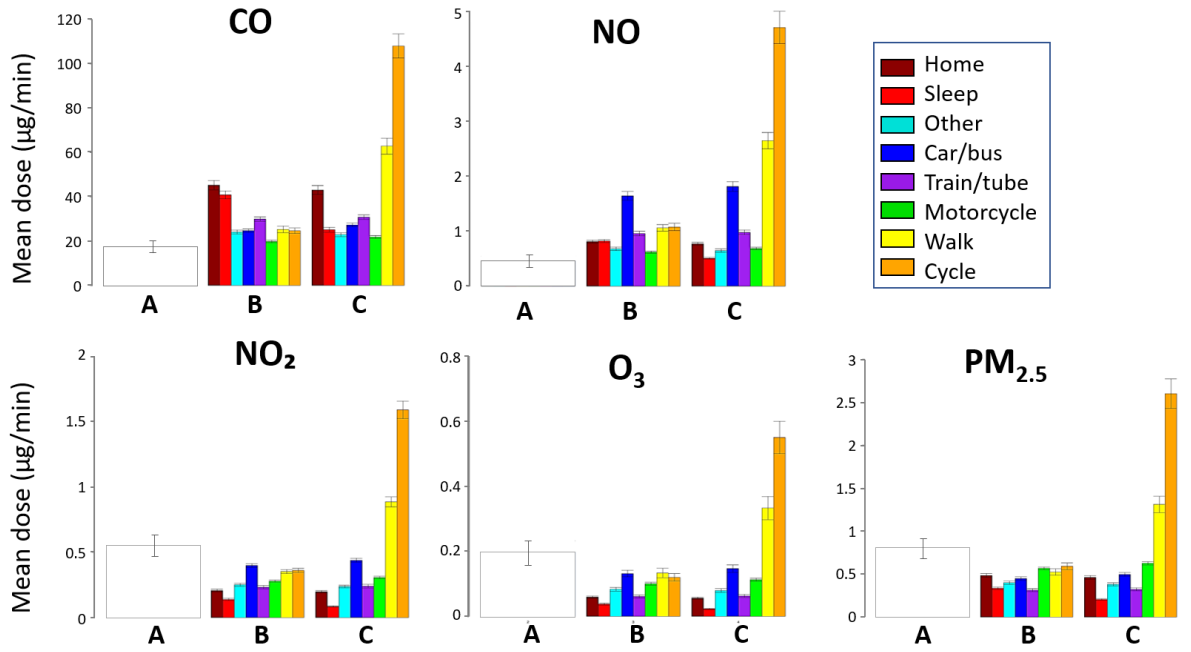

Fig. 6.15 Mean pollutant dose per minute during different activities using the three estimation methods A, B and C (averaged over the urban and peri-urban cohort). Error bars indicate the standard error of dose estimations across the cohort. [28]

6.4.2 Total air pollution estimation across all visited microenvironments

So far, the highest dose per minute was observed during commuting. However, people usually spend only a small fraction (< 10%) of their time in transit [73], so this has only a small impact on their total dose. To date, it is still not clear if exposure peaks or elevated mean exposure levels are significant for health effects. The following section examines the contribution of different activities to the total pollutant dose received over a full day, taking into account the time budgets of each activity (c.f. Figure 6.3 Part E).

The bar plots in Figure 6.16 show the average daily pollution dose of urban and peri-urban participants calculated with the three dose estimation methods described in Section 6.1. As methods A and B are integrating a constant inhalation rate, the average dose depends only on the measured pollutant concentrations in the surrounding microenvironment. Therefore, the difference between methods A and B is a measure of the exposure misclassification between personal and ambient estimates, which was substantial in all cases. For example, the outdoor monitoring stations over-predicted $PM_{2.5}$ exposure by almost four times, while exposure to CO was under-predicted by approximately the same factor.

The difference between method B and method C, both derived from personal measurements,

was marginal despite integrating activity-dependent inhalation rates in method C. This was mostly due to the low physical activity levels of the participants which resulted in an average inhalation rate similar to the generic one used for methods A and B.

On the one hand, the home microenvironment was the most important contributor to the total daily dose, partly because participants spent most of their time there. In addition, strong indoor sources of CO and NO operated there, elevating personal dose. On the other hand, the doses of NO_2, O_3 and $PM_{2.5}$ were lower than the estimates based on ambient exposures due to the indoor reactivity of these pollutants (c.f. Section 5.2.1).

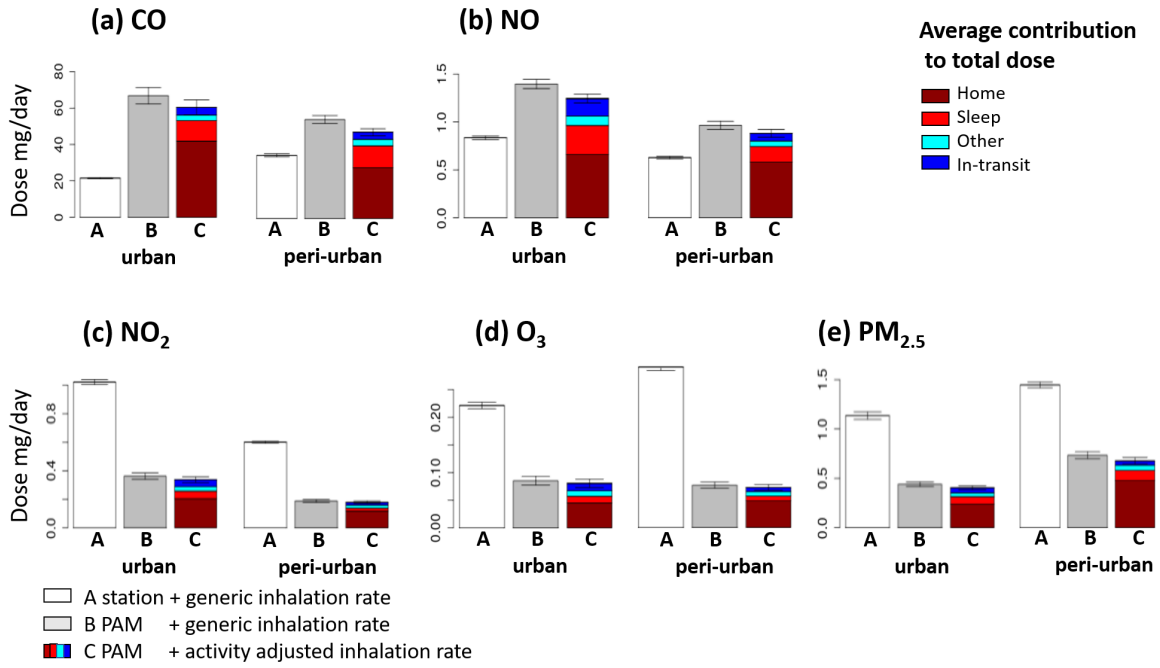

Fig. 6.16 Average daily pollution dose inhaled by the AIRLESS participants during the winter deployment estimated using methods A–C (see Section 6.1). Averaged over the urban (left) and peri-urban cohort (right); error bars indicate the standard error of dose estimations across the cohort [28]

6.5 Comparison between dose estimations from the AIRLESS and the pilot project

Although not representative of the UK or Chinese populations, the comparison of personal doses in this section highlights some differences that may be related to geographical variation

of air pollution or socio-economic factors, and others which may be due to the different characteristics of the specific cohorts.

6.5.1 Differences in time budgets

One factor that determines the total air pollution dose and how much different daily activities contribute to it, is the activity pattern of a participant, i.e. the time a person spent on different activities (Section 6.1). Figure 6.17 shows the time budgets of the project cohorts by hour of the day classified with the time-activity model.

The majority of the participants in both projects stayed at home during the night hours (11pm to 6am). The participants of the pilot project were more mobile than the AIRLESS participants, with larger time fractions spent in transit or at other static locations during daytime hours. This is probably due to differences in the socio-economic and demographic characteristics of the cohorts: the participants of the AIRLESS project were predominantly retired or working from home[4], whereas the participants of the pilot project were younger and mainly working or studying at universities.

The urban participants (both in London and in Beijing) spent generally more time on commuting than the peri-urban participants (Cambridge and Pinggu), probably because commuting distances were greater in the urban cohorts.

[4] A large part of the peri-urban cohort was working in the agricultural sector. However, little outdoor work was performed during the winter months.

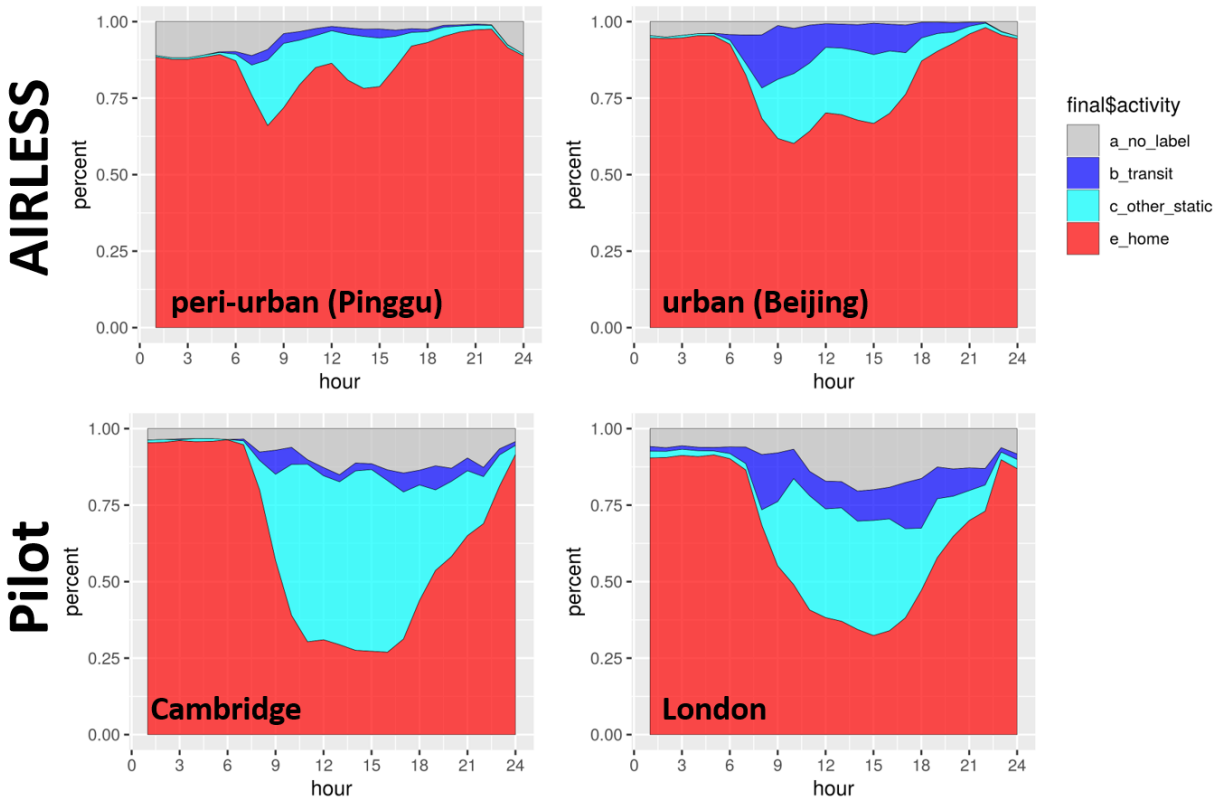

Fig. 6.17 Time budgets of the the AIRLESS (top, winter campaign) and Pilot (bottom) cohorts as predicted by the time-location-activity model (Section 6.2). For each hour of the day the fraction of the cohort spending time at home (red), another static location (cyan) or in transit (blue) is given. The time that could not be classified by the model is shown in grey.

6.5.2 Exposure differences

Figure 6.18 compares personal exposures measured during different activities in the AIRLESS and Pilot project using NO_2 and $PM_{2.5}$ as example pollutants.

The observations from the AIRLESS project were substantially higher than those from the pilot project, with the difference between the two locations being more distinct for the $PM_{2.5}$ exposures than for the NO_2 exposures. This difference was probably due to the higher ambient pollution concentrations in China compared to the UK (mean ambient NO_2 concentrations: 13 ppb (Pilot UK), 33 ppb (AIRLESS China); $PM_{2.5}$: 10 µg m^{-3} (UK), 92 µg m^{-3} (China)). Despite that, the air pollution exposures in rail systems were comparable between the two projects. This is probably due to the London underground being one of the most polluted metro systems in the world [151].

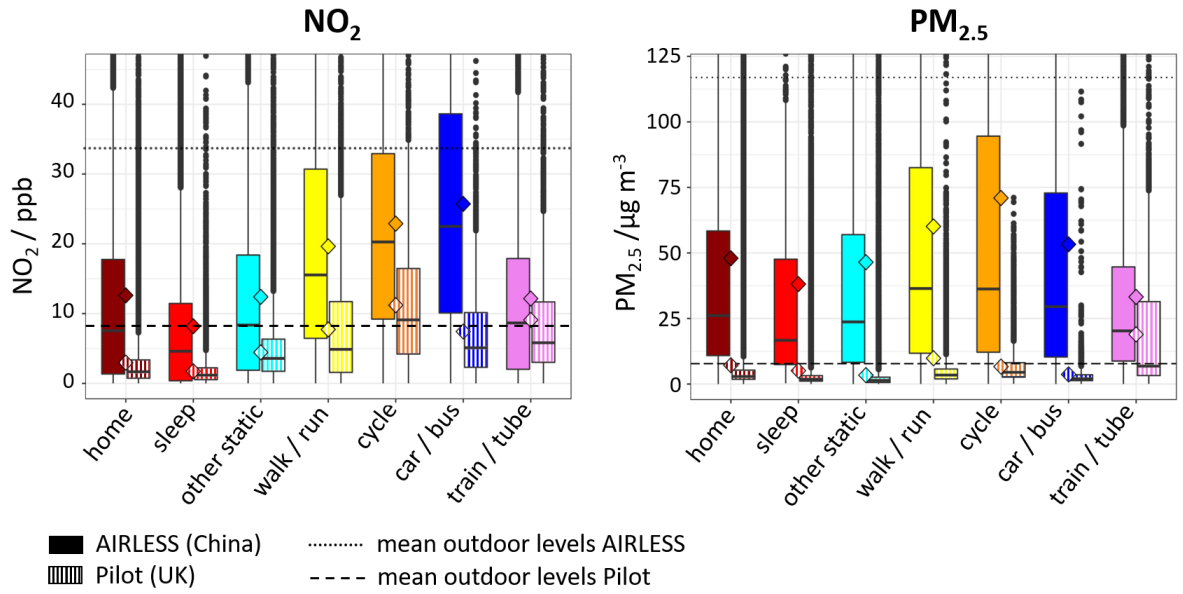

Fig. 6.18 Comparison of the NO_2 (left) and $PM_{2.5}$ (right) concentrations in different microenvironments measured during the AIRLESS (left box for each activity) and the pilot project (right box). The average ambient pollutant concentrations are added as dashed lines. Diamond shapes mark the mean exposure. The exposures from the pilot project can be seen in larger scale in Figure 6.9.

6.5.3 Differences in the air pollution mixture

Besides the absolute exposure differences, the air pollution mixture differed between the two locations. As already demonstrated in Figure 6.13, the ratio between two pollutants such as NO_2 and $PM_{2.5}$ changes between different microenvironments, suggesting different air pollution compositions and potential toxicities.

Figure 6.19 illustrates this using the ratio between $PM_{2.5}$ and NO_2 measured during the pilot project and the AIRLESS project (winter campaign) as an example. In ambient air (measured by monitoring station, left of Figure 6.19) the $PM_{2.5}/NO_2$ ratio was higher in China than in the UK owing to different regional emission sources (UK has more NO_2 emissions from diesel vehicles, China has more $PM_{2.5}$ emissions from coal plants). As personal exposures are driven primarily by local sources, this difference in the ratios was substantially larger with $PM_{2.5}$ dominating personal exposure in China.

Figure 6.20 investigates the relationship between the mean $PM_{2.5}$ and NO_2 exposures of each participant (c.f. Figure 4.7) based on measurements from a static reference station (left) and

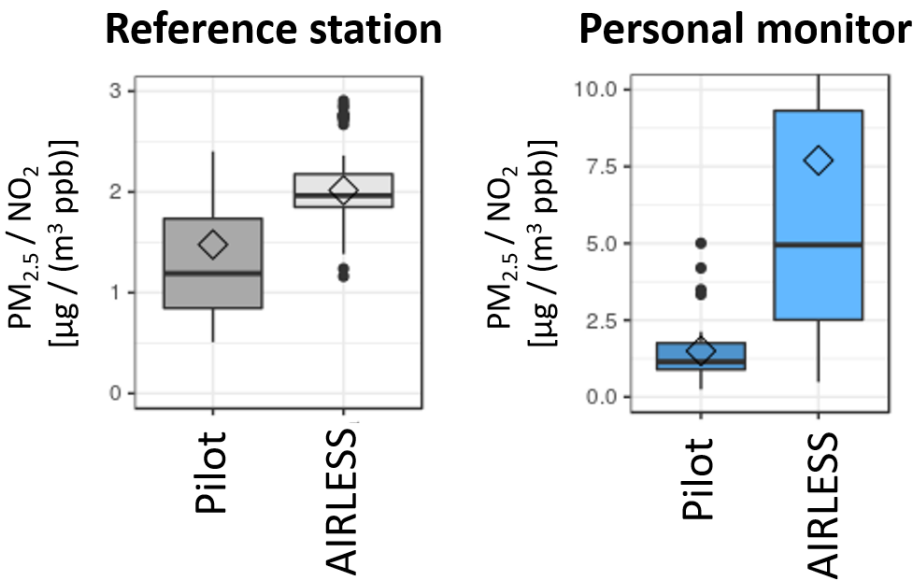

Fig. 6.19 Boxplots of the $PM_{2.5}/NO_2$ ratios observed in ambient air (left) and personal exposures (right) during the AIRLESS and the Pilot project. Note the different y-axis scaling.

based on PAM measurements split by activity (right). As discussed in Section 4.4.1, different pollutant species were highly correlated in the static observations. In other words, the ambient air pollution mixture was relatively constant.The right graphs of Figure 6.20 show the air pollution mixtures split by microenvironment. In line with the findings from Section 4.4.1, the correlation between the two pollutants was substantially reduced in the PAM measurements.

The air pollution mixture changed distinctly between the different microenvironments, which is visible at the different slopes of the linear fits in Figure 6.20. In the Pilot project, the street environment was dominated by relatively high NO_2 levels (low $PM_{2.5}/NO_2$ ratio), probably due to NO_2 emissions from diesel vehicles. The rail systems contained higher $PM_{2.5}/NO_2$ ratios which were likely due to the high $PM_{2.5}$ levels in the London underground (see Section 6.3.2). In the home microenvironment the Pilot participants were exposed to the highest $PM_{2.5}/NO_2$ ratios, possibly due to highly effective NO_2 removal mechanisms inside the buildings. Different patterns were found in the AIRLESS project indicating different types of emission sources in the Chinese microenvironments.

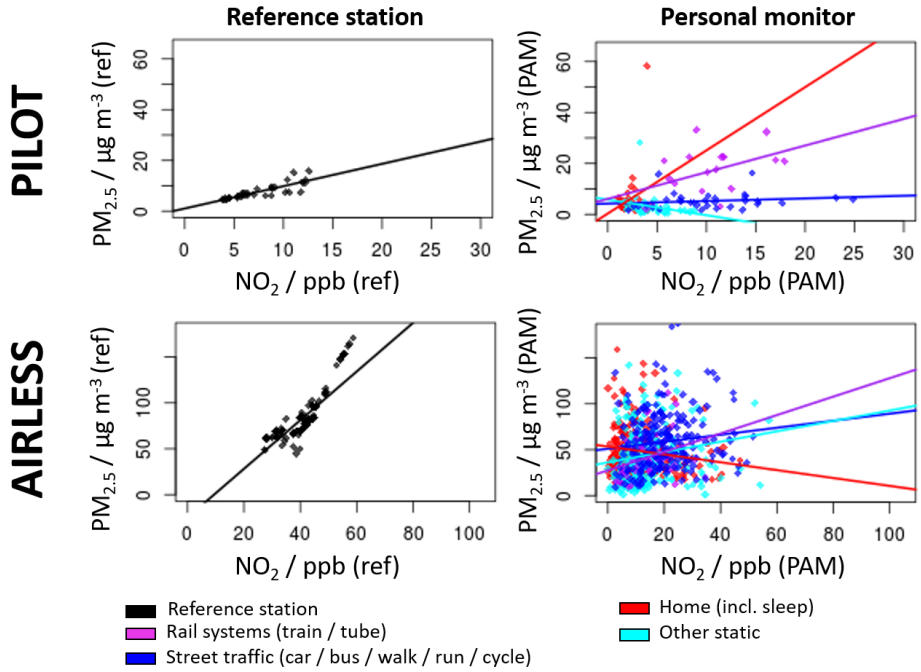

Fig. 6.20 Relationship between $PM_{2.5}$ and NO_2 in static observations (left) and in different microenvironments (right) as indicator for the air pollution mixture. Comparison between Pilot (top) and AIRLESS project (bottom). Exposures averaged by participant.

6.5.4 Contributions of activities to the total air pollution dose

The previously examined time budgets and personal exposures during different activities determine the total daily air pollution dose of the participants (Equation 6.2). The air pollution levels during the AIRLESS project were much higher than the ones observed during the pilot project, resulting in much higher total doses for the AIRLESS participants. To compare the contributions from different activities, each total dose was normalised to 100% (Figure 6.21). The home environment (including sleep) had a much larger impact on the air pollution doses in China (left) than in the UK (right). This can be attributed to the larger amount of time spent at home by the older AIRLESS participants (see Figure 6.17), but also to stronger indoor emission sources in China, particularly in the peri-urban cohort.

Despite the fact that the highest pollution exposures in China were found during commuting (walking, cycling, car; see Figure 6.18), the contribution from transit modes to the overall pollution dose was very small because of the relatively small fraction of time spent in transit. Although indoor environments (home, sleep, other static) contributed less to the pilot doses compared to the AIRLESS doses, they nevertheless constituted a large fraction (> 50%) of the

total dose. This emphasises the urgent need to include indoor exposures in health studies.

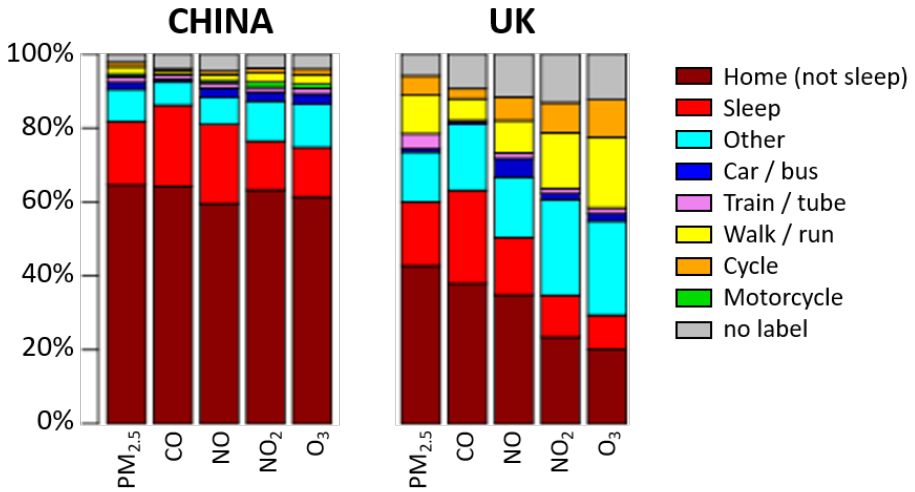

Fig. 6.21 Mean contributions of different activities to the total air pollution dose of the cohorts from the AIRLESS project (left) and the pilot project (right). Doses were normalised to 100%.

Table 6.3 (a) ranks the activities by exposure, i.e. the concentration measured during each activity (c.f. Figure 6.3 A). The highest NO_2 exposures were found in traffic environments (UK: cycling, China: in vehicle), and the lowest levels were found in indoor environments.
Table 6.3 (b) ranks the activities by the average amount of NO_2 that was inhaled by the participants per unit time (c.f. Figure 6.3 D). In this case, the activities which required higher levels of exercise and caused faster breathing rates (cycling, walking) were associated with the highest NO_2 dose per minute, while indoor activities bore the lowest risks.
Table 6.3 (c) shows a completely different picture as the time budget plays a significant role in determining the relative importance of different microenvironments on the total daily dose.

Table 6.3 Ranking of daily activities by NO_2 exposure and dose risk (c.f. Table 6.1). Findings from the AIRLESS project (China) were compared to those from the Pilot project (UK).

	(a) Personal exposure to NO_2						
UK	1 cycle	2 train / tube	3 walk / run	4 car / bus	5 other static	6 home	7 sleep
China	1 car / bus	2 cycle	3 walk / run	4 home	5 other static	6 train / tube	7 sleep
	(b) NO_2 dose per minute						
UK	1 cycle	2 walk	3 train / tube	4 car / bus	5 other static	6 home	7 sleep
China	1 cycle	2 walk	3 car / bus	train/ tube	5 other static	6 home	7 sleep
	(c) Contribution to total NO_2 dose						
UK	1 other static	2 home	3 walk / run	4 sleep	5 cycle	6 car / bus	7 train / tube
China	1 home	2 sleep	3 other static	4 car / bus	5 walk / run	6 cycle	7 train / tube

6.6 Chapter summary

Time-activity patterns are important determinants of personal exposure and dose, but have been largely omitted from health studies due to the difficulty of collecting detailed activity profiles of individuals. This chapter combined a time-location-activity model with data from personal monitors to comprehensively characterise personal exposure and dose during various daily life activities.

As it is not yet clear whether peak exposures or the prolonged exposure to higher pollution levels are more important for health outcomes, a detailed picture of exposure during daily life is necessary. Four case studies were selected to demonstrate driving factors of exposure to air pollution in different microenvironments. The level of physical activity can alter the mean temporary dose by a factor of 10, however, high intensity activities are usually performed over only short periods of time. The impact of inhalation rates is expected to be higher in more active subpopulations such as children.

The disaggregation of air pollution exposures by activity showed that not only the air pollution concentrations, but also the chemical composition differ between microenvironments. A separate epidemiological analysis of the health risks of the exposures in different types of microenvironments may bring new insights into the toxicity of air pollution mixtures originating from various sources. Underground commuting modes in particular were found to significantly elevate PM levels that are potentially more harmful due to the high fraction of metallic compounds.

In summary, this chapter demonstrated how a comprehensive exposure and dose analysis can be achieved by combining a time-location-activity classification model with personal exposure data. Neglecting the air pollution differences between microenvironments and/or the activity patterns of individuals (including their breathing rates) may lead to significant errors in air pollution dose estimations in health studies.

Chapter 7

Conclusions and Outlook

7.1 Main achievements

This work has created and validated a reliable, cost-effective, and convenient method for monitoring personal air pollution exposure with high and well quantified accuracy. It has also highlighted the substantial exposure errors which can be introduced when using conventional exposure measurement methods in large scale epidemiology.
This work represents an important next step for future epidemiological research towards an improved assessment of personal exposure to advance our understanding of the detrimental effects of air pollution.

The novel methodology presented in this work also combined personal air quality monitoring with a time-location-activity model to generate air pollution exposure and dose estimations under field conditions with a level of detail hitherto impossible.

The novel devices were deployed in a range of studies in China, the UK, Germany and Kenya, demonstrating excellent performance in a wide range of environmental conditions and pollution levels. Participants from all these diverse socio-economic backgrounds readily accepted the PAM in their daily lives, making it a practical device for exposure and health studies.

Compared to conventional epidemiological approaches based on air quality monitoring stations, the PAM demonstrated the following advantages:

(a) Potential to establish reliable links between air pollution and health effects by reducing exposure misclassification
Thanks to its wearability and high spatio-temporal resolution, the PAM substantially reduced

the exposure misclassification of static approaches. Its small size, user-friendly application and almost silent operation qualified it as an ideal, unobtrusive tool to measure personal exposures in previously neglected microenvironments such as homes, offices or in public transportation. The PAM was able to capture the high exposure variability between individual members of a cohort caused by their unique behavioural patterns.

(b) Reduction of the multicollinearity between different pollutant species
Ambient air quality observations often suffer from highly correlated concentration measurements of multiple pollutant species which prevent epidemiological studies from identifying specific pollutants as harmful for human health. By capturing the high variability of daily life exposures, this correlation was substantially reduced in the personal measurements.

(c) Capability to assign exposure and health risks to daily life activities
The combination of personal exposure and behavioural information allows on one level to link exposure to health outcomes, and on another level to link exposure to activity. Together, this may generate policy-relevant conclusions in terms of clearly associating specific pollutants either to health impacts or to activities which could be mitigated to reduce exposure.

(d) Ability to characterise personal exposure and dose in under-researched areas
The PAM captured the large heterogeneity of air pollution across urban and rural locations in diverse geographical settings. While rural environments are often characterised by stronger and more diverse air pollution emission sources, their research infrastructure is often not configured to evaluate these exposure risks, perhaps preventing the emergence of policy-relevant evidence. The low production and maintenance costs, and the limited dependence on mains power make the PAM suitable for deployments in countries or areas with less developed research infrastructures to deal with urgent environmental challenges.

Overall, this work has demonstrated not just the feasibility, but also the necessity of understanding personal exposure when undertaking epidemiological studies and is an important step, when combined with other statistical and AI methods, to create population scale estimates of both causal linkages between exposure and health outcomes, and the impacts of politically based interventions.

7.2 Policy relevant findings

This work adopted a multidisciplinary approach to comprehensively characterise personal exposure and dose during daily life scenarios. The following conclusions were drawn from this study.

- indoor environments are the main contributor to the daily air pollution dose;
- local emission sources had often a far more important impact on personal exposure than regional sources;
- the ratios between different pollutant species, and therefore their relative importance in terms of health effects, differed between ambient and personal exposure measurements; and
- the air pollution mixture, and therefore its potential toxicity, distinctly changed between different microenvironments.

These findings stress that ambient air quality monitoring, as it has conventionally been used in virtually all epidemiological studies, is not suitable to correctly quantify personal exposure or dose; and that, to maximise the impact of policy interventions, more attention must be paid to indoor environments. While mitigation policies often focus on highly polluted outdoor locations such as traffic environments, more recent approaches are starting to acknowledge the importance of indoor environments regarding the air pollution burden of society [139]. Novel exposure analysis approaches, as the one presented here, may help to generate more efficient policies to protect the population from the negative effects of air pollution.

7.3 Limitations and future work

Future developments may lead to more advanced and perhaps even smaller sensing technologies which would help to further characterise health-relevant aspects of personal exposure. Such new sensors could be integrated into improved versions of personal monitoring devices, and possibly be combined with smartphones or smartwatch technologies which are now routinely providing estimates of physiological parameters such as heart rate/variability, $V0_2max$, and even ECG information. Integrating such complex and sophisticated data into health studies is a task for the near future.

Future possibilities may also involve sensors that quantify a larger number of harmful pollutants (such as VOCs) or even real-time feedback to participants to minimise their health risks. Nevertheless, this work has demonstrated the value of research into this direction and defined the general strategy of how miniaturised sensors may be deployed to exploit their full potential.

It is possible, but this is true for any epidemiological study, that, rather than observing the direct health effect of a targeted pollutant, a pollutant in fact serves as a proxy for one or more co-emitted chemical compounds that may impact on health. Research to date has yet to clearly define the differential toxicity of particle compositions, owing to the limited high-quality measurements of pollutant species applied in most epidemiological studies, and the high correlation between multiple pollutants.
By separating regional from local air pollution and classifying exposure by microenvironment, this work has made first steps towards assigning personal exposure to individual emission sources. Integrating such source-segregated exposure information in future epidemiological studies may help to differentiate source-related health effects.

The studies in this work focused on specific subpopulations which inevitably have demographics that do not represent the whole population. However, the exposure and dose estimations of these investigated cohorts changed drastically after applying the novel methodology for reasons that are independent from the characteristics of the cohorts. The importance of personal monitoring rather than ambient monitoring is therefore relevant across multiple subpopulations.

Because it is unfeasible to expand an approach based on personal devices to cohorts that are large enough to represent an entire population, there is an urgent need for a validated personal exposure modelling tool. The methodological framework developed for this work provides a basis of this which can be extended to support and validate a population-scale personal exposure model with detailed time-activity profiles and corresponding measurements at high spatial and temporal resolution.

Epidemiological models linking air quality and heath will need to be adapted to the increasing complexity of the exposure data (high resolution, activity data etc.) in order to exploit the full potential of this new exposure and dose assessment approach.

7.4 Concluding remarks

The findings of this dissertation should lead to a paradigm shift in quantifying air pollution exposure in epidemiological studies and generate important knowledge which might be critical

for the development of efficient strategies to mitigate the detrimental effects of air pollution on the human population.

References

[1] Ali, H., Soe, J. K., and Weller, S. R. (2015). A real-time ambient air quality monitoring wireless sensor network for schools in smart cities. *2015 IEEE 1st International Smart Cities Conference, ISC2 2015*, pages 1–6.

[2] Alphasense Ltd. (2009). Alphasense Application Note 107-06: Intrinsic Safety Information for Approvals. *Retrieved from www.alphasense.com*, pages 1–7.

[3] Alphasense Ltd. (2013). Alphasense Application Note 110: Environmental Changes: Temperature, Pressure, Humidity. *Retrieved from www.alphasense.com*, pages 1–6.

[4] Alphasense Ltd. (2015a). Alphasense Application Note 104: How Electrochemical Gas Sensors Work. *Retrieved from www.alphasense.com*, pages 1–4.

[5] Alphasense Ltd. (2015b). Alphasense User Manual: OPC-N2 Optical Particle Counter. *Retrieved from www.alphasense.com*, pages 1–15.

[6] Alphasense Ltd. (2016). Technical Specification NO2-A4 Nitrogen Dioxide Sensor 4-Electrode. *Retrieved from www.alphasense.com*.

[7] Alphasense Ltd (2017). Technical specification. CO-A4 Carbon Monoxide Sensor 4-Electrode. *Retrieved from www.alphasense.com*.

[8] Alphasense Ltd. (2017). Technical Specification Ox-A4 Oxidising Gas Sensor Ozone + Nitrogen Dioxide 4-Electrode. pages 0–1.

[9] Alphasense Ltd. (2019). Technical Specification NO-A4 Nitric Oxide Sensor. *Retrieved from www.alphasense.com*, pages 10–11.

[10] Andersen, P. C., Williford, C. J., and Birks, J. W. (2010). Miniature personal ozone monitor based on UV absorbance. *Analytical Chemistry*, 82(19):7924–7928.

[11] Avery, C. L., Mills, K. T., Williams, R., McGraw, K. A., Poole, C., Smith, R. L., and Whitsel, E. A. (2010). Estimating error in using ambient PM2.5 concentrations as proxies for personal exposures. *Epidemiology*, 21(2):215–223.

[12] Baron, R. and Saffell, J. (2017). Amperometric Gas Sensors as a Low Cost Emerging Technology Platform for Air Quality Monitoring Applications: A Review. *ACS Sensors*, 2(11):1553–1566.

[13] Berliner Luftguetemessnetz (2018). Stationsdaten: 042 Neukölln | Berliner Luftgüte Messnetz (BLUME) | Luftqualität und Luftgüte in Berlin. *https://luftdaten.berlin.de/station/mc042*.

[14] Berliner Verkehrsbetriebe (2018). station board search.

[15] Biggart, M., Stocker, J., Doherty, R. M., Wild, O., Hollaway, M., Carruthers, D., Li, J., Zhang, Q., Wu, R., Kotthaus, S., Grimmond, S., Squires, F. A., Lee, J., and Shi, Z. (2020). Street-scale air quality modelling for Beijing during a winter 2016 measurement campaign. *Atmospheric Chemistry and Physics*, 20(5):2755–2780.

[16] Bogue, R. (2015). Detecting gases with light: A review of optical gas sensor technologies. *Sensor Review*, 35(2):133–140.

[17] Borrego, C., Costa, A. M., Ginja, J., Amorim, M., Coutinho, M., Karatzas, K., Sioumis, T., Katsifarakis, N., Konstantinidis, K., De Vito, S., Esposito, E., Smith, P., André, N., Gérard, P., Francis, L. A., Castell, N., Schneider, P., Viana, M., Minguillón, M. C., Reimringer, W., Otjes, R. P., von Sicard, O., Pohle, R., Elen, B., Suriano, D., Pfister, V., Prato, M., Dipinto, S., and Penza, M. (2016). Assessment of air quality microsensors versus reference methods: The EuNetAir joint exercise. *Atmospheric Environment*, 147:246–263.

[18] Brauer, M. (2010). How much, how long, what, and where: Air pollution exposure assessment for epidemiologic studies of respiratory disease. *Proceedings of the American Thoracic Society*, 7(2):111–115.

[19] BRE (2013). Main heating systems (BRE report number 286733a). Technical report, Department of Energy and Climate Change.

[20] Brienza, S., Galli, A., Anastasi, G., and Bruschi, P. (2015). A low-cost sensing system for cooperative air quality monitoring in urban areas. *Sensors (Switzerland)*, 15(6):12242–12259.

[21] Brimblecombe, P. (1998). History of Urban Air Pollution. In *Urban Air Pollution — European Aspects*, pages 7–20.

[22] Brook, R. D., Rajagopalan, S., Pope, C. A., Brook, J. R., Bhatnagar, A., Diez-Roux, A. V., Holguin, F., Hong, Y., Luepker, R. V., Mittleman, M. A., Peters, A., Siscovick, D., Smith, S. C., Whitsel, L., and Kaufman, J. D. (2010). Particulate matter air pollution and cardiovascular disease: An update to the scientific statement from the american heart association.

[23] Brunekreef, B. and Holgate, S. T. (2002). Air pollution and health. *Lancet*, 360(9341):1233–1242.

[24] Calenge, C. (2019). Analysis of animal movements in R: the adehabitatLT package.

[25] Caron, A., Redon, N., Thevenet, F., Hanoune, B., and Coddeville, P. (2016). Performances and limitations of electronic gas sensors to investigate an indoor air quality event. *Building and Environment*, 107:19–28.

[26] Castell, N., Dauge, F. R., Schneider, P., Vogt, M., Lerner, U., Fishbain, B., Broday, D., and Bartonova, A. (2017). Can commercial low-cost sensor platforms contribute to air quality monitoring and exposure estimates? *Environment International*, 99:293–302.

[27] Castell, N., Viana, M., Cruz Minguillón, M., Guerreiro, C., Querol, X., Minguillón, M. C., Guerreiro, C., and Querol, X. (2013). Real-world application of new sensor technologies for air quality monitoring. *ETC/ACM Technical Paper*, 16(November):34.

[28] Chatzidiakou, L., Krause, A., Han, Y., Chen, W., Yan, L., Popoola, O. A., Kellaway, M., Wu, Y., Liu, J., Hu, M., Barratt, B., Cai, Y., Chan, Q., Chatzidiakou, L., Chen, S., Chen, W., Chen, X., Elliott, P., Ezzati, M., Fan, Y., Han, X., Hu, M., Jin, A., Jones, R. L., Kelly, F. J., Krause, A., Li, Y., Liang, P., Liu, J., Luo, Y., Qiu, X., Wang, Q., Wang, T., Wang, Y., Wu, Y., Xie, G., Xie, W., Xue, T., Yan, L., Zhang, H., Zhang, J., Zhao, M., Zhu, T., Zhu, Y., Barratt, B., Kelly, F. J., Zhu, T., and Jones, R. L. (2020). Using low-cost sensor technologies and advanced computational methods to improve dose estimations in health panel studies: results of the AIRLESS project. *Journal of Exposure Science and Environmental Epidemiology*.

[29] Chatzidiakou, L., Krause, A., Popoola, O. A. M., Di Antonio, A., Kellaway, M., Han, Y., Squires, F. A., Wang, T., Zhang, H., Wang, Q., Fan, Y., Chen, S., Hu, M., Quint, J. K., Barratt, B., Kelly, F. J., Zhu, T., and Jones, R. L. (2019). Characterising low-cost sensors in highly portable platforms to quantify personal exposure in diverse environments. *Atmospheric Measurement Techniques*, 12:4643–4657.

[30] Choi, S., Kim, N., Cha, H., and Ha, R. (2009). Micro sensor node for air pollutant monitoring: Hardware and software issues. *Sensors*, 9(10):7970–7987.

[31] Cohen, A. J., Brauer, M., Burnett, R., Anderson, H. R., Frostad, J., Estep, K., Balakrishnan, K., Brunekreef, B., Dandona, L., Dandona, R., Feigin, V., Freedman, G., Hubbell, B., Jobling, A., Kan, H., Knibbs, L., Liu, Y., Martin, R., Morawska, L., Pope, C. A., Shin, H., Straif, K., Shaddick, G., Thomas, M., van Dingenen, R., van Donkelaar, A., Vos, T., Murray, C. J., and Forouzanfar, M. H. (2017). Estimates and 25-year trends of the global burden of disease attributable to ambient air pollution: an analysis of data from the Global Burden of Diseases Study 2015. *The Lancet*, 389(10082):1907–1918.

[32] Coley, D. A. and Beisteiner, A. (2002). Carbon Dioxide Levels and Ventilation Rates in Schools. *International Journal of Ventilation*, 1(1):45–52.

[33] Committee on the Medical Effects of Air Pollutants (2018). Associations of long-term average concentrations of nitrogen dioxide with mortality. Technical report, Public Health England.

[34] Committee on the Medical Effects of Air Pollution (COMEAP) (2006). Cardiovascular Disease and Air Pollution. Technical report.

[35] Corradi, M., Pesci, A., Casana, R., Alinovi, R., Goldoni, M., Vettori, M. V., and Cuomo, A. (2003). Nitrate in exhaled breath condensate of patients with different airway diseases. *Nitric oxide : biology and chemistry / official journal of the Nitric Oxide Society*, 8(1):26–30.

[36] Cox, R. M. (2003). The use of passive sampling to monitor forest exposure to O3, NO2 and SO2: A review and some case studies. In *Environmental Pollution*, volume 126, pages 301–311. Elsevier.

[37] Crilley, L. R., Shaw, M., Pound, R., Kramer, L. J., Price, R., Young, S., Lewis, A. C., and Pope, F. D. (2018). Evaluation of a low-cost optical particle counter (Alphasense OPC-N2) for ambient air monitoring. *Atmospheric Measurement Techniques*, 11(2):709–720.

[38] Cross, E. S., Lewis, D. K., Williams, L. R., Magoon, G. R., Kaminsky, M. L., Worsnop, D. R., and Jayne, J. T. (2017). Use of electrochemical sensors for measurement of air pollution : correcting interference response and validating measurements. *Atmospheric Measurement Techniques Discussions*, 2017-138:1–17.

[39] Davalos, A. D., Luben, T. J., Herring, A. H., and Sacks, J. D. (2017). Current approaches used in epidemiologic studies to examine short-term multipollutant air pollution exposures.

[40] Davey, M. W., Stals, E., Panis, B., Keulemans, J., and Swennen, R. L. (2005). High-throughput determination of malondialdehyde in plant tissues. *Analytical Biochemistry*, 347(2):201–207.

[41] De Nazelle, A., Seto, E., Donaire-Gonzalez, D., Mendez, M., Matamala, J., Nieuwenhuijsen, M. J., and Jerrett, M. (2013). Improving estimates of air pollution exposure through ubiquitous sensing technologies. *Environmental Pollution*, 176:92–99.

[42] De Souza-Pinto, N. C., Eide, L., Hogue, B. A., Thybo, T., Stevnsner, T., Seeberg, E., Klungland, A., and Bohr, V. A. (2001). Repair of 8-oxodeoxyguanosine lesions in mitochondrial DNA depends on the oxoguanine DNA glycosylase (OGG1) gene and 8-oxoguanine accumulates in the mitochondrial DNA of OGG1-defective mice. *Cancer Research*, 61(14):5378–5381.

[43] Deanfield, J., Donald, A., Ferri, C., Giannattasio, C., Halcox, J., Halligan, S., Lerman, A., Mancia, G., Oliver, J. J., Pessina, A. C., Rizzoni, D., Rossi, G. P., Salvetti, A., Schiffrin, E. L., Taddei, S., and Webb, D. J. (2005). Endothelial function and dysfunction. Part I: Methodological issues for assessment in the different vascular beds: a statement by the Working Group on Endothelin and Endothelial Factors of the European Society of Hypertension. *J Hypertens*, 23(October):7–17.

[44] Di Antonio, A., Popoola, O. A., Ouyang, B., Saffell, J., and Jones, R. L. (2018). Developing a relative humidity correction for low-cost sensors measuring ambient particulate matter. *Sensors (Switzerland)*, 18(9):2790.

[45] Dinh, T. V., Choi, I. Y., Son, Y. S., and Kim, J. C. (2016). A review on non-dispersive infrared gas sensors: Improvement of sensor detection limit and interference correction.

[46] Dockery, D., Pope 3rd, C., Xu, X., Spengler, J., Ware, J., Fay, M., Ferris Jr, B., and Speizer, F. (1993). An association between air pollution and mortality in six US cities. *The New England journal of medicine*, 329(24):1753.

[47] Doering, F. L., Paprotny, I., and White, R. M. (2012). Mems air-microfluidic sensor for portable monitoring of airborne particulates. *Technical Digest - Solid-State Sensors, Actuators, and Microsystems Workshop*, (c):315–319.

[48] Duan, N. (1982). Models for human exposure to air pollution. *Environment International*, 8(1-6):305–309.

[49] Elen, B., Theunis, J., Ingarra, S., Molino, A., van den Bossche, J., Reggente, M., and Loreto, V. (2012). The EveryAware SensorBox: a tool for community-based air quality monitoring. *Workshop Sensing a Changing World*, (1):1–7.

[50] European Committee for Standardization (1993). Workplace atmospheres — Sizefraction definitions for measurement of airborne particles; BS 6069-3.5:1993. (481):1–15.

[51] Field, A. (2009). *DISCOVERING STATISTICS USING SPSS*.

[52] GBD 2015 Risk Factors Collaborators (2016). Global, regional, and national comparative risk assessment of 79 behavioural, environmental and occupational, and metabolic risks or clusters of risks, 1990-2015: a systematic analysis for the Global Burden of Disease Study 2015. *The Lancet*, 388(10053):1659–1724.

[53] Goldberg, M. S. (2007). On the interpretation of epidemiological studies of ambient air pollution. *Journal of exposure science & environmental epidemiology*, 17:S66–S70.

[54] Goldman, G. T., Mulholland, J. A., Russell, A. G., Gass, K., Strickland, M. J., and Tolbert, P. E. (2012). Characterization of ambient air pollution measurement error in a time-series health study using a geostatistical simulation approach. *Atmospheric Environment*, 57:101–108.

[55] Hamm, N. A., van Lochem, M., Hoek, G., Otjes, R., van der Sterren, S., and Verhoeven, H. (2016). "The Invisible Made Visible": Science and Technology. In *AiREAS: Sustainocracy for a Healthy City: The Invisible made Visible Phase 1*, pages 51–77. Springer.

[56] Han, Y., Chatzidiakou, L., Yan, L., Chen, W., Zhang, H., Krause, A., Xue, T., Chan, Q., Liu, J., Wu, Y., Barratt, B., Jones, R. L., Zhu, T., and Kelly, F. J. (2020a). Difference in ambient-personal exposure to PM2.5 and its inflammatory effect in local residents in urban and peri-urban Beijing, China: Results of the AIRLESS project. *FARADAY Discussions*, in prep.

[57] Han, Y., Chen, W., Chatzidiakou, L., Krause, A., Yan, L., Zhang, H., Chan, Q., Barratt, B., Jones, R. L., Liu, J., Wu, Y., Zhao, M., Zhang, J., Kelly, F. J., and Zhu, T. (2020b). Effects of AIR pollution on cardiopuLmonary disEaSe in urban and peri-urban reSidents in Beijing: protocol for the AIRLESS study. *Atmospheric Chemistry and Physics Discuss.*, (in review).

[58] Hasenfratz, D., Saukh, O., Walser, C., Hueglin, C., Fierz, M., Arn, T., Beutel, J., and Thiele, L. (2015). Deriving high-resolution urban air pollution maps using mobile sensor nodes. In *Pervasive and Mobile Computing*, volume 16, pages 268–285. Elsevier.

[59] Heimann, I., Bright, V. B., McLeod, M. W., Mead, M. I., Popoola, O. A., Stewart, G. B., and Jones, R. L. (2015). Source attribution of air pollution by spatial scale separation using high spatial density networks of low cost air quality sensors. *Atmospheric Environment*, 113:10–19.

[60] Hinds, W. C. (1999). *Aerosol Technology: Properties, Behavior, and Measurement of Airborne Particles, 2nd Edition*. Wiley.

[61] Hu, Y. and Zhao, B. (2020). Relationship between indoor and outdoor NO2: A review.

[62] Ikram, J., Tahir, A., Kazmi, H., Khan, Z., Javed, R., and Masood, U. (2012). View: implementing low cost air quality monitoring solution for urban areas. *Environmental Systems Research*, 1(1):10.

[63] Int Panis, L., de Geus, B., Vandenbulcke, G., Willems, H., Degraeuwe, B., Bleux, N., Mishra, V., Thomas, I., and Meeusen, R. (2010). Exposure to particulate matter in traffic: A comparison of cyclists and car passengers. *Atmospheric Environment*, 44(19):2263–2270.

[64] International Organization for Standardization (1994). Accuracy (trueness and precision) of measurement methods and results - Part 1: General principles and definitions. *BS ISO 5725-1*.

[65] Jerrett, M., Arain, A., Kanaroglou, P., Beckerman, B., Potoglou, D., Sahsuvaroglu, T., Morrison, J., and Giovis, C. (2005). A review and evaluation of intraurban air pollution exposure models. *Journal of Exposure Science & Environmental Epidemiology*, 15(2):185–204.

[66] Jerrett, M., Donaire-Gonzalez, D., Popoola, O., Jones, R., Cohen, R. C., Almanza, E., de Nazelle, A., Mead, I., Carrasco-Turigas, G., Cole-Hunter, T., Triguero-Mas, M., Seto, E., and Nieuwenhuijsen, M. (2017). Validating novel air pollution sensors to improve exposure estimates for epidemiological analyses and citizen science. *Environmental Research*, 158:286–294.

[67] Jiao, W., Hagler, G., Williams, R., Sharpe, R., Brown, R., Garver, D., Judge, R., Caudill, M., Rickard, J., Davis, M., Weinstock, L., Zimmer-Dauphinee, S., and Buckley, K. (2016). Community Air Sensor Network (CAIRSENSE) project: Evaluation of low-cost sensor performance in a suburban environment in the southeastern United States. *Atmospheric Measurement Techniques*, 9(11):5281–5292.

[68] Joint Committee for Guides in Metrology (2008). Evaluation of measurement data — Guide to the expression of uncertainty in measurement. *JCGM 100:2008*.

[69] Jovašević-Stojanović, M., Bartonova, A., Topalović, D., Lazović, I., Pokrić, B., and Ristovski, Z. (2015). On the use of small and cheaper sensors and devices for indicative citizen-based monitoring of respirable particulate matter. *Environmental Pollution*, 206:696–704.

[70] Just, A. C., Wright, R. O., Schwartz, J., Coull, B. A., Baccarelli, A. A., Tellez-Rojo, M. M., Moody, E., Wang, Y., Lyapustin, A., and Kloog, I. (2015). Using High-Resolution Satellite Aerosol Optical Depth to Estimate Daily PM2.5 Geographical Distribution in Mexico City. *Environmental Science and Technology*, 49(14):8576–8584.

[King's College London] King's College London. London Air Quality Network (LAQN). *http://www.londonair.org.uk*.

[72] Klánová, J., Kohoutek, J., Hamplová, L., Urbanová, P., and Holoubek, I. (2006). Passive air sampler as a tool for long-term air pollution monitoring: Part 1. Performance assessment for seasonal and spatial variations. *Environmental Pollution*, 144(2):393–405.

[73] Klepeis, N. E., Nelson, W. C., Ott, W. R., Robinson, J. P., Tsang, A. M., Switzer, P., Behar, J. V., Hern, S. C., and Engelmann, W. H. (2001). The National Human Activity Pattern Survey (NHAPS): a resource for assessing exposure to environmental pollutants. *Journal of Exposure Analysis and Environmental Epidemiology*, 11(3):231–252.

[74] Koehler, K., Good, N., Wilson, A., Mölter, A., Moore, B. F., Carpenter, T., Peel, J. L., and Volckens, J. (2019). The Fort Collins commuter study: Variability in personal exposure to air pollutants by microenvironment. *Indoor Air*, 29(2):231–241.

[75] Kotsev, A., Schade, S., Craglia, M., Gerboles, M., Spinelle, L., and Signorini, M. (2016). Next generation air quality platform: Openness and interoperability for the internet of things. *Sensors (Switzerland)*, 16(3).

[76] Krause, A., Zhao, J., and Birmili, W. (2019). Low-cost sensors and indoor air quality: A test study in three residential homes in Berlin, Germany . *Gefahrstoffe Reinhaltung Luft (Air Quality Control)*, 3(March):87–92.

[77] Krewski, D., Burnett, R. T., Goldberg, M. S., Hoover, B. K., Siemiatycki, J., Jerrett, M., Abrahamowicz, M., and White, W. H. (2003). Overview of the Reanalysis of the Harvard Six Cities Study and American Cancer Society study of particulate air pollution and mortality.

[78] Krupa, S. V. and Legge, A. H. (2000). Passive sampling of ambient, gaseous air pollutants: An assessment from an ecological perspective. *Environmental Pollution*, 107(1):31–45.

[79] Kumar, P., Morawska, L., Martani, C., Biskos, G., Neophytou, M., Di Sabatino, S., Bell, M., Norford, L., and Britter, R. (2015). The rise of low-cost sensing for managing air pollution in cities. *Environment International*, 75:199–205.

[80] Laden, F., Schwartz, J., Speizer, F. E., and Dockery, D. W. (2006). Reduction in fine particulate air pollution and mortality: Extended follow-up of the Harvard Six Cities Study. *American Journal of Respiratory and Critical Care Medicine*, 173(6):667–672.

[81] Lai, H. K., Kendall, M., Ferrier, H., Lindup, I., Alm, S., Haenninen, O., Jantunen, M., Mathys, P., Colvile, R., Ashmore, M. R., Cullinan, P., and Nieuwenhuijsen, M. J. (2004). Personal exposures and microenvironment concentrations of PM 2.5, VOC, NO 2 and CO in Oxford, UK. *Atmospheric Environment*, 38(37):6399–6410.

[82] Lamsal, L. N., Martin, R. V., van Donkelaar, A., Steinbacher, M., Celarier, E. A., Bucsela, E., Dunlea, E. J., and Pinto, J. P. (2010). Ground-level nitrogen dioxide concentrations inferred from the satellite-borne Ozone Monitoring Instrument. *Journal of Geophysical Research*, 115(16):D16308.

[83] Larkin, A. and Hystad, P. (2017). Towards Personal Exposures: How Technology Is Changing Air Pollution and Health Research.

[84] Lewis, A. and Edwards, P. (2016). Validate personal air-pollution sensors. *Nature*, 535(7610):29–31.

[85] Lewis, A. C., Lee, J. D., Edwards, P. M., Shaw, M. D., Evans, M. J., Moller, S. J., Smith, K. R., Buckley, J. W., Ellis, M., Gillot, S. R., and White, A. (2016). Evaluating the performance of low cost chemical sensors for air pollution research. *Faraday Discussions*, 189(0):85–103.

[86] Lewis, A. C., von Schneidemesser, E., Peltier, R. E., Lung, C., Jones, R., Zellweger, C., Karppinen, A., Penza, M., Dye, T., Hüglin, C., Ning, Z., Leigh, R., Hagan, D. H., Laurent, O., and Carmichael, G. (2018). *Low-cost sensors for the measurement of atmospheric composition: overview of topic and future applications*. Number May.

[87] Li, Y., Liu, J., Wang, W., and Zhao, D. (2014). The association between within-visit blood pressure variability and carotid artery atherosclerosis in general population. *PLoS ONE*, 9(5).

[88] Lin, C., Li, Y., Yuan, Z., Lau, A. K., Li, C., and Fung, J. C. (2015). Using satellite remote sensing data to estimate the high-resolution distribution of ground-level PM 2.5. *Remote Sensing of Environment*, 156:117–128.

[London Assembly] London Assembly. Monitoring and predicting air pollution | London city. *www.london.gov.uk/what-we-do/environment/pollution-and-air-quality/monitoring-and-predicting-air-pollution, last accessed 2020-02-26*, pages 1–6.

[90] Lyons, A. J., Turner, W. C., and Getz, W. M. (2013). Home range plus: A space-time characterization of movement over real landscapes. *Movement Ecology*, 1(1):2.

[91] Martins, V., Moreno, T., Minguillón, M. C., Amato, F., de Miguel, E., Capdevila, M., and Querol, X. (2015). Exposure to airborne particulate matter in the subway system. *Science of the Total Environment*, 511:711–722.

[92] Mathers, C. D. and Loncar, D. (2005). Updated projections of global mortality and burden of disease, 2002-2030: data sources, methods and results. *World Health Organization*, (October):1–130.

[93] McKercher, G. R., Salmond, J. A., and Vanos, J. K. (2017). Characteristics and applications of small, portable gaseous air pollution monitors. *Environmental Pollution*, 223:102–110.

[94] Mead, M. I., Popoola, O. A. M., Stewart, G. B., Landshoff, P., Calleja, M., Hayes, M., Baldovi, J. J., McLeod, M. W., Hodgson, T. F., Dicks, J., Lewis, A., Cohen, J., Baron, R., Saffell, J. R., and Jones, R. L. (2013). The use of electrochemical sensors for monitoring urban air quality in low-cost, high-density networks. *Atmospheric Environment*, 70:186–203.

[95] Moltchanov, S., Levy, I., Etzion, Y., Lerner, U., Broday, D. M., and Fishbain, B. (2015). On the feasibility of measuring urban air pollution by wireless distributed sensor networks. *Science of the Total Environment*, 502:537–547.

[96] Monn, C. (2001). Exposure assessment of air pollutants: a review on spatial heterogeneity and indoor/outdoor/personal exposure to suspended particulate matter, nitrogen dioxide and ozone. *Atmospheric Environment*, 35(1):1–32.

[97] Moore, E., Chatzidiakou, L., Kuku, M. O., Jones, R. L., Smeeth, L., Beevers, S., Kelly, F. J., Barratt, B., and Quint, J. K. (2016). Global associations between air pollutants and chronic obstructive pulmonary disease hospitalizations: A systematic review. *Annals of the American Thoracic Society*, 13(10):1814–1827.

[98] Morawska, L., Thai, P. K., Liu, X., Asumadu-Sakyi, A., Ayoko, G., Bartonova, A., Bedini, A., Chai, F., Christensen, B., Dunbabin, M., Gao, J., Hagler, G. S., Jayaratne, R., Kumar, P., Lau, A. K., Louie, P. K., Mazaheri, M., Ning, Z., Motta, N., Mullins, B., Rahman, M. M., Ristovski, Z., Shafiei, M., Tjondronegoro, D., Westerdahl, D., and Williams, R. (2018). Applications of low-cost sensing technologies for air quality monitoring and exposure assessment: How far have they gone?

[99] Morrow, J. D. and Roberts, L. J. (1997). THE ISOPROSTANES: UNIQUE BIOACTIVE PRODUCTS OF LIPID PEROXIDATION. *LipidRes*, 36(1):1–21.

[100] Murray, C. J. and Lopez, A. D. (1996). Global Burden of Disease. *THE HARVARD SCHOOL OF PUBLIC HEALTH*, pages 1–46.

[101] National Research Council (1991). *Human Exposure Assessment for Airborne Pollutants: Advances and Opportunities Committee*.

[102] Nicholson, J. K. (2006). Global systems biology, personalized medicine and molecular epidemiology. *Molecular Systems Biology*, 2:52.

[103] Nieuwenhuijsen, M. J., Donaire-Gonzalez, D., Rivas, I., De Castro, M., Cirach, M., Hoek, G., Seto, E., Jerrett, M., and Sunyer, J. (2015). Variability in and agreement between modeled and personal continuously measured black carbon levels using novel smartphone and sensor technologies. *Environmental Science and Technology*, 49(5):2977–2982.

[104] Novelli, P. C., Steele, L. P., and Tans, P. P. (1992). Mixing ratios of carbon monoxide in the troposphere. *Journal of Geophysical Research*, 97(D18).

[105] Nuvolone, D., Petri, D., and Voller, F. (2018). The effects of ozone on human health. *Environmental Science and Pollution Research*, 25(9):8074–8088.

[106] OpenStreetMap contributors (2017). OpenStreetMap.

[107] Ott, W. R. (1982). Concepts of human exposure to air pollution. *Environment International*, 7(3):179–196.

[108] Özkaynak, H. K., Baxter, L. K., Dionisio, K. L., Burke, J., Özkaynak, H., Baxter, L. K., Dionisio, K. L., and Burke, J. (2013). Air pollution exposure prediction approaches used in air pollution epidemiology studies. *Journal of Exposure Science and Environmental Epidemiology*, 23(6):566–572.

[109] Perrone, R. D., Madias, N. E., and Levey, A. S. (1992). Serum creatinine as an index of renal function: New insights into old concepts.

[110] Piedrahita, R., Xiang, Y., Masson, N., Ortega, J., Collier, A., Jiang, Y., Li, K., Dick, R. P., Lv, Q., Hannigan, M., and Shang, L. (2014). The next generation of low-cost personal air quality sensors for quantitative exposure monitoring. *Atmospheric Measurement Techniques*, 7(10):3325–3336.

[111] Pitz, M., Cyrys, J., Karg, E., Wiedensohler, A., Wichmann, H. E., and Heinrich, J. (2003). Variability of apparent particle density of an urban aerosol. *Environmental Science and Technology*, 37(19):4336–4342.

[112] Poenar, D. P. (2019). Microfluidic and Micromachined/MEMS Devices for Separation, Discrimination and Detection of Airborne Particles for Pollution Monitoring. *Micromachines*, 10(7):483.

[113] Popoola, O. A., Carruthers, D., Lad, C., Bright, V. B., Mead, M. I., Stettler, M. E., Saffell, J. R., Jones, R. L., Mead, M. I., Bright, V. B., Saffell, J. R., and Jones, R. L. (2018). Use of networks of low cost air quality sensors to quantify air quality in urban settings. *Atmospheric Environment*, 194:58–70.

[114] Popoola, O. A. M., Stewart, G. B., Mead, M. I., and Jones, R. L. (2016). Development of a baseline-temperature correction methodology for electrochemical sensors and its implications for long-term stability. *Atmospheric Environment*, 147:330–343.

[115] R Development Core Team, R. (2008). R: A Language and Environment for Statistical Computing.

[116] Rai, A. C., Kumar, P., Pilla, F., Skouloudis, A. N., Di Sabatino, S., Ratti, C., Yasar, A., and Rickerby, D. (2017). End-user perspective of low-cost sensors for outdoor air pollution monitoring. *Science of the Total Environment*, 607-608:691–705.

[117] Rogacev, K. S., Cremers, B., Zawada, A. M., Seiler, S., Binder, N., Ege, P., Große-Dunker, G., Heisel, I., Hornof, F., Jeken, J., Rebling, N. M., Ulrich, C., Scheller, B., Böhm, M., Fliser, D., and Heine, G. H. (2012). CD14++CD16+ monocytes independently predict cardiovascular events: A cohort study of 951 patients referred for elective coronary angiography. *Journal of the American College of Cardiology*, 60(16):1512–1520.

[118] Ross Anderson, H. R., Butland, B. K., van Donkelaar, A., Brauer, M., Strachan, D. P., Clayton, T., van Dingenen, R., Amann, M., Brunekreef, B., Cohen, A., Dentener, F., Lai, C., Lamsa, L. N., and Martin, R. V. (2012). Satellite-based estimates of ambient air pollution and global variations in childhood asthma prevalence. *Environmental Health Perspectives*, 120(9):1333–1339.

[119] Ruckstuhl, A. F., Henne, S., Reimann, S., Steinbacher, M., Vollmer, M. K., O'Doherty, S., Buchmann, B., and Hueglin, C. (2012). Robust extraction of baseline signal of atmospheric trace species using local regression. *Atmospheric Measurement Techniques*, 5(11):2613–2624.

[120] Sandrini, A., Taylor, D. R., Thomas, P. S., and Yates, D. H. (2010). Fractional exhaled nitric oxide in asthma: An update. *Respirology*, 15(1):57–70.

[121] Sarnat, J. A., Schwartz, J., Catalano, P. J., and Suh, H. H. (2001). Gaseous pollutants in particulate matter epidemiology: Confounders or surrogates? *Environmental Health Perspectives*, 109(10):1053–1061.

[122] Sarnat, S. E., Sarnat, J. A., Mulholland, J., Isakov, V., Özkaynak, H., Chang, H. H., Klein, M., and Tolbert, P. E. (2013). Application of alternative spatiotemporal metrics of ambient air pollution exposure in a time-series epidemiological study in Atlanta. *Journal of Exposure Science and Environmental Epidemiology*, 23(6):593–605.

[123] Schneider, P., Castell, N., Lahoz, W. A., Vogt, M., Dauge, F. R., and Bartonova, A. (2017). Mapping urban air quality in near real-time using observations from low-cost sensors and model information. *Environment International*, 106:234–247.

[124] Shaw, P. A., Deffner, V., Keogh, R. H., Tooze, J. A., Dodd, K. W., Küchenhoff, H., Kipnis, V., and Freedman, L. S. (2018). Epidemiologic analyses with error-prone exposures: review of current practice and recommendations. *Annals of Epidemiology*, 28(11):821–828.

[125] Shi, Z., Vu, T., Kotthaus, S., Harrison, R. M., Grimmond, S., Yue, S., Zhu, T., Lee, J., Han, Y., Demuzere, M., Dunmore, R. E., Ren, L., Liu, D., Wang, Y., Wild, O., Allan, J., Joe Acton, W., Barlow, J., Barratt, B., Beddows, D., Bloss, W. J., Calzolai, G., Carruthers,

D., Carslaw, D. C., Chan, Q., Chatzidiakou, L., Chen, Y., Crilley, L., Coe, H., Dai, T., Doherty, R., Duan, F., Fu, P., Ge, B., Ge, M., Guan, D., Hamilton, J. F., He, K., Heal, M., Heard, D., Nicholas Hewitt, C., Hollaway, M., Hu, M., Ji, D., Jiang, X., Jones, R., Kalberer, M., Kelly, F. J., Kramer, L., Langford, B., Lin, C., Lewis, A. C., Li, J., Li, W., Liu, H., Liu, J., Loh, M., Lu, K., Lucarelli, F., Mann, G., McFiggans, G., Miller, M. R., Mills, G., Monk, P., Nemitz, E., O'Connor, F., Ouyang, B., Palmer, P. I., Percival, C., Popoola, O., Reeves, C., Rickard, A. R., Shao, L., Shi, G., Spracklen, D., Stevenson, D., Sun, Y., Sun, Z., Tao, S., Tong, S., Wang, Q., Wang, W., Wang, X., Wang, X., Wang, Z., Wei, L., Whalley, L., Wu, X., Wu, Z., Xie, P., Yang, F., Zhang, Q., Zhang, Y., Zhang, Y., and Zheng, M. (2019). Introduction to the special issue "in-depth study of air pollution sources and processes within Beijing and its surrounding region (APHH-Beijing)". *Atmospheric Chemistry and Physics*, 19(11):7519–7546.

[126] Smith, J. D., Barratt, B. M., Fuller, G. W., Kelly, F. J., Loxham, M., Nicolosi, E., Priestman, M., Tremper, A. H., and Green, D. C. (2020). PM2.5 on the London Underground. *Environment International*, 134.

[127] Sousan, S., Koehler, K., Hallett, L., and Peters, T. M. (2016). Evaluation of the Alphasense optical particle counter (OPC-N2) and the Grimm portable aerosol spectrometer (PAS-1.108). *Aerosol Science and Technology*, 50(12):1352–1365.

[128] Spinelle, L., Aleixandre, M., and Gerboles, M. (2013). Protocol of evaluation and calibration of low-cost gas sensors for the monitoring of air pollution. *JRC Technical reports*, 68.

[129] Stamler, J., Elliott, P., Dennis, B., Dyer, A. R., Kesteloot, H., Liu, K., Ueshima, H., and Zhou, B. F. (2003). INTERMAP: background, aims, design, methods, and descriptive statistics (nondietary). *Journal of human hypertension*, 17(9):591–608.

[130] Steel, R. G. D. and Torrie, J. H. (1960). *Principles and Procedures of Statistics: With Special Reference to the Biological Sciences*. Wiley.

[131] Steinle, S., Reis, S., Sabel, C. E., Semple, S., Twigg, M. M., Braban, C. F., Leeson, S. R., Heal, M. R., Harrison, D., Lin, C., and Wu, H. (2015). Personal exposure monitoring of PM2.5 in indoor and outdoor microenvironments. *Science of the Total Environment*, 508:383–394.

[132] Sun, L., Wong, K. C., Wei, P., Ye, S., Huang, H., Yang, F., Westerdahl, D., Louie, P. K., Luk, C. W., and Ning, Z. (2016). Development and application of a next generation air sensor network for the Hong Kong marathon 2015 air quality monitoring. *Sensors (Switzerland)*, 16(2):211.

[133] The European Parliament and of the council of the European Union (2008). Directive 2008/50/EC of the European Parliament and of the council of 21 May 2008 on ambient air quality and cleaner air for Europe. *Official Journal of the European Union*.

[134] Thermo Fisher Scientific Inc. (2007). Thermo Scientific Model 48i Carbon Monoxide Analyzer.

[135] Thompson, D., Pepys, M. B., and Wood, S. P. (1999). The physiological structure of human C-reactive protein and its complex with phosphocholine. *Structure*, 7(2):169–177.

[136] Thompson, J. E. (2016). Crowd-sourced air quality studies: A review of the literature & portable sensors. *Trends in Environmental Analytical Chemistry*, 11:23–34.

[137] Thurston, G. D., Kipen, H., Annesi-Maesano, I., Balmes, J., Brook, R. D., Cromar, K., De Matteis, S., Forastiere, F., Forsberg, B., Frampton, M. W., Grigg, J., Heederik, D., Kelly, F. J., Kuenzli, N., Laumbach, R., Peters, A., Rajagopalan, S. T., Rich, D., Ritz, B., Samet, J. M., Sandstrom, T., Sigsgaard, T., Sunyer, J., and Brunekreef, B. (2017). A joint ERS/ATS policy statement: What constitutes an adverse health effect of air pollution? An analytical framework.

[138] Torkmahalleh, M. A., Gorjinezhad, S., Keles, M., Unluevcek, H. S., Azgin, C., Cihan, E., Tanis, B., Soy, N., Ozaslan, N., Ozturk, F., and Hopke, P. K. (2017). A controlled study for the characterization of PM2.5 emitted during grilling ground beef meat. *Journal of Aerosol Science*, 103(October 2016):132–140.

[139] UKRI News (2020). £3 million awarded to help tackle air pollution - UK Research and Innovation.

[140] US Environmental Protection Agency (EPA) (1992). *Guidelines for Exposure Assessment*. Number 104.

[141] US Environmental Protection Agency (EPA) (2011). Exposure Factors Handbook: 2011 Edition. *National Center for Environmental Assessment, Washington, DC*, pages 1–1466.

[142] van Donkelaar, A., Martin, R. V., Brauer, M., Kahn, R., Levy, R., Verduzco, C., and Villeneuve, P. J. (2010). Global estimates of ambient fine particulate matter concentrations from satellite-based aerosol optical depth: Development and application. *Environmental Health Perspectives*, 118(6):847–855.

[143] Varga, M., Laposa, A., Kulha, P., Kroutil, J., Husak, M., and Kromka, A. (2015). Quartz crystal microbalance gas sensor with nanocrystalline diamond sensitive layer. *Physica Status Solidi (B) Basic Research*, 252(11):2591–2597.

[144] Wallace, L. (2000). Correlations of personal exposure to particles with outdoor air measurements: A review of recent studies. *Aerosol Science and Technology*, 32(1):15–25.

[145] Walser, A., Sauer, D., Spanu, A., Gasteiger, J., and Weinzierl, B. (2017). On the parametrization of optical particle counter response including instrument-induced broadening of size spectra and a self-consistent evaluation of calibration measurements. *Atmospheric Measurement Techniques*, 10(11):4341–4361.

[146] White, R. M., Black, J., Apte, M. G., and Gundel, L. A. (2008). Development of a Low-Cost Particulate Matter Monitor. Technical report.

[147] WHO (2014). Indoor Air Quality Guidelines: Household Fuel Combustion. *World Health Organization*.

[148] Wilkins, E. T. (1954). Air pollution aspects of the London fog of December 1952. *Quarterly Journal of the Royal Meteorological Society*, 80(344):267–271.

[149] World Health Organisation (2006). *Air quality guidelines for Europe: Global Update 2005*, volume 22.

[150] Xiong, L. and Compton, R. G. (2014). Amperometric gas detection: A review. *International Journal of Electrochemical Science*, 9(12):7152–7181.

[151] Xu, B. and Hao, J. (2017). Air quality inside subway metro indoor environment worldwide: A review.

[152] Yi, W. Y., Leung, K. S., and Leung, Y. (2018). A modular plug-and-play sensor system for urban air pollution monitoring: Design, implementation and evaluation. *Sensors (Switzerland)*, 18(1):7.

[153] Yocom, J. E. (1982). Indoor-outdoor air quality relationships - A Critical Review. *Journal of the Air Pollution Control Association*, 32(5):500–520.

[154] Yu, H., Russell, A., Mulholland, J., and Huang, Z. (2018). Using cell phone location to assess misclassification errors in air pollution exposure estimation. *Environmental Pollution*, 233:261–266.

[155] Zell, H., Quarcoo, D., Scutaru, C., Vitzthum, K., Uibel, S., Schöffel, N., MacHe, S., Groneberg, D. A., and Spallek, M. F. (2010). Air pollution research: Visualization of research activity using density-equalizing mapping and scientometric benchmarking procedures. *Journal of Occupational Medicine and Toxicology*, 5(1):5.

[156] Zhang, J., Hu, J., Zhu, Z. Q., Gong, H., and O'Shea, S. J. (2004). Quartz crystal microbalance coated with sol-gel-derived indium-tin oxide thin films as gas sensor for NO detection. *Colloids and Surfaces A: Physicochemical and Engineering Aspects*, 236(1-3):23–30.

[157] Zhao, J., Weinhold, K., Merkel, M., Kecorius, S., Schmidt, A., Schlecht, S., Tuch, T., Wehner, B., Birmili, W., and Wiedensohler, A. (2018). Concept of high quality simultaneous measurements of the indoor and outdoor aerosol to determine the exposure to fine and ultrafine particles in private homes. *Gefahrstoffe - Reinhaltung der Luft*, 78(3):73–78.

[158] Zielinski, A. T., Kalberer, M., Jones, R. L., Prasad, A., and Seshia, A. A. (2016). Particulate mass sensing with piezoelectric bulk acoustic mode resonators. *2016 IEEE International Frequency Control Symposium, IFCS 2016 - Proceedings*, pages 1–6.

[159] Zou, B., Wilson, J. G., Zhan, F. B., and Zeng, Y. (2009). Air pollution exposure assessment methods utilized in epidemiological studies.

Appendix A

Supplementary materials

A.1 Introduction

A.1.1 Overview of different methods to estimate personal exposure

A.1.1.1 Indirect methods: Stationary measurements and models

Ambient measurements

A traditional approach in epidemiology to estimate a population's exposure to air pollution is using data from static air quality monitoring stations [79]. Equipped with certified reference instruments, these stations provide very accurate and reliable pollutant concentration measurements. The monitoring stations are only located outdoors and, because of their high acquisition and maintenance costs, they are scarcely distributed over large regions (postcode level or more). Consequently, one monitoring station is often used to estimate the exposure of large numbers ($n > 1000$) of individuals.

Satellite measurements

An alternative way to measure air pollution concentrations is using optical instruments attached to satellites. Based on the specific absorption or scattering properties of a pollutant, their surface concentration can be estimated using far-range spectroscopic methods [142, 82]. The spatial resolution of this method is often only in degrees of longitude and latitude (up to > 100 km, e.g. [118]), making the term "high-resolution" in this context referring to resolutions of around 1 km [70, 88].

Satellite air pollution measurements have been used in global epidemiological studies such as Anderson et al. who "did not find evidence of a positive association between ambient

air pollution and asthma prevalence in contrast to reports from within-community studies of individuals exposed to traffic pollution" [118].
The conflicting conclusions between studies based on satellite observations and those based on finer scale exposures indicate that more accurate estimates of personal air pollution exposure are needed to draw reliable associations between air pollution exposure and health outcomes. Air pollution concentrations can vary significantly in space and time because they are affected by various factors such as local emission sources, surface losses or the filtering effects of buildings. Therefore, the correlation between ambient and personal exposure can be very small (R^2=0.09-0.83, median 0.54 [11]) which makes static monitoring stations or satellite observations a poor predictor for personal exposure.

Air quality models
The low spatial resolution of air quality data can be overcome by applying air quality models. They can be based on ambient air pollution observations (from satellites / monitoring stations) or emission inventories (amount of air pollution discharged by different sources over a specified period of time). By taking into account meteorological factors, atmospheric dispersion, air pollution transport dynamics, deposition, local emission sources, industrial activities, atmospheric chemistry, and building ventilation and infiltration, the temporal and spatial resolution of air pollution data can be significantly improved [101]. Air quality models can estimate the air pollution exposures of very large populations, and are useful to predict future pollution scenarios and inform policy makers about the expected outcomes of air pollution mitigation strategies. However, the experimental validation of the model outcomes is challenging, particularly on fine spatial scales.

Microenvironments and time budgets
A microenvironment is a "[volume] of air space with homogeneous pollutant concentration" [48]. If the concentrations of all microenvironments visited by a person were known as well as the amounts of time spent in each location (time budgets), a person's personal exposure could be calculated very accurately. Due to the great number of microenvironments visited in daily life, microenvironmental approaches are usually limited to pollution measurements in the main microenvironments such as home, work/school, and traffic environments (e.g [103, 81, 131]). Instead of directly measuring the pollution concentration in microenvironments, they can also be estimated using air pollution models.
The time budgets (time spent in each location) can be retrieved directly from GPS instruments (e.g. smartphones) or diary entries [41, 154], or they can be estimated based on common

behavioural patterns. Nieuwenhuijsen et al. [103] estimated the personal exposures of school children using a "CalFit" activity tracking software and modelled black carbon concentrations in microenvironments visited by the pupils. The comparison of the estimated results with directly measured personal black carbon exposures showed moderate to good correlations in static indoor environments (home, school; r = 0.59-0.68) and lower correlations during commuting (r = 0.21-0.32).

A.1.1.2 Direct measurements: Personal sampling

Personal samplers are directly attached to an individual which allows them to capture the pollutant concentrations in the immediate environment of the person. Depending on the target pollutant, different sensor types are available:

Light scattering devices

Virtually all portable particulate matter sensors are based on light scattering [98]. The particles pass through a sensor chamber and scatter the light of a laser beam. The detected scattered light contains information about the particle concentration. Volume scattering devices illuminate a number of particles in a defined volume and output, via calibration with test aerosols, a mass concentration of particulate matter. Optical particle counters (OPCs) illuminate individual particles to retrieve information about particulate number and size. The mass concentration is then estimated by assuming a spherical particle shape and a predefined density (for more details see Section 2.1.2). Optical aerosol measurement methods are limited to particle sizes above 300 nm and suffer from RH interference. However, with appropriate data-processing they can achieve great accuracy and reproducibility [44, 29].

Acoustic resonators

Acoustic resonators, such as quartz chrystal microbalances (QCM), detect subtle changes of the resonance frequency of an oscillating body (e.g. a quartz crystal) when exposed to a gas [98]. The adsorption of the gas onto the resonator, or onto a thin film coating it, changes the mass of the resonator and therefore its resonance frequency. Typical analytes are NO [156], NH_3 or CO_2 [143]. These devices are very precise, fast responding and have low production costs. However, they can suffer from significant cross-interference with other gases [136].
Resonating systems can also be used to measure particulate mass concentrations [158]. Compared to optical systems, they can detect particles of all sizes. Their high precision and tiny dimensions ("two orders of magnitude smaller than [currently] commercially available PM sensors" [47]) make them strong candidates for personal sampling. However, these techniques

struggle with signal saturation due to mass loading [146], low particle capture efficiencies and temperature interference. Nevertheless, the technology is greatly progressing at the moment and might gain significant importance in the field of portable PM monitors in the near future [112].

Metal oxide semiconductor (MOS)

Along with electrochemical sensors, MOS sensors are the most commonly used portable gas sensors [116, 93]. When exposed to the target gas, the integrated metal oxide changes its conductivity proportionally to the concentration of the gas. MOS sensors have very low production costs, are simple to use and may detect a large range of gases including O_3, NO_2, CO and NH_3; [93]. However, they suffer from measurement instabilities and drifts and display severe cross-interference with other gases as well as with temperature and RH [116].

Electrochemical (EC) sensors

Electrochemical gas sensors can be amperometric, coulometric and potentiometric. However, amperometric sensors are most suitable for the quantification of atmospheric pollutant gases due to their high sensitivity and good performance under atmospheric conditions. In the following, the term "electrochemical (EC) sensor" will refer to the amperometric type only. Their principle of operation is based on redox reactions of the target pollutant at the sensor electrode surface which cause a measurable electric current that is proportional to the pollutant concentration (more details in Section 2.1.1). Typical analytes are e.g. CO, NO_x, SO_2 and CO. EC sensors need less power and are more reliable and sensitive than MOS sensors, however, they are more expensive and slightly larger [116]. EC sensor measurements may be affected by temperature, RH and pressure fluctuations which can, however, be corrected for by appropriate post-processing [27, 29]. Their cross-interference with other pollutants can be adjusted by selecting appropriate electrode materials and filters, however cross-interference with some gases (e.g. between O_3 and NO_2) still remains [27, 136].

Spectroscopic gas sensors

Spectroscopic measurements are based on light absorption. The intensity I of a laser beam with a certain wavelength λ is attenuated when passing through the absorbing analyte. The light attenuation depends on the path length of the light beam l, the wavelength-specific extinction coefficient ε_λ, and the concentration of the analyte c as described in the Beer-Lambert law (Eq. A.1). The laser wavelength of spectroscopic sensors for atmospheric gases can be in the infrared (IR) or the ultraviolet (UV) spectrum.

The most popular analyte for IR spectroscopic sensors is carbon dioxide CO_2 because of its strong absorption band in the IR (4.3 μm) [16], other analytes include methane CH_4, ammonia NH_3 and formaldehyde CH_2O. Typical analytes for UV absorption include O_3, VOC and NO_2. Spectroscopic sensors can respond very fast to concentration changes [93, 10]. They can suffer from multi-gas interference which can, however, be corrected with filters or correction algorithms [45]. Excellent sensitivities can be achieved by increasing the path length using multipass cells or cavity ring down methods. Overall, spectroscopic gas sensors seem to be unaffected by temperature and RH fluctuations [93] although minor RH interference has been reported [10]. Optical sensors require highly reflective optical equipment which adds significant costs and makes spectroscopic sensors a fairly expensive alternative as portable sensors [136].

$$log_{10}\frac{I_\lambda}{I_{\lambda,0}} = l\,c\,\varepsilon_\lambda \tag{A.1}$$

Photo ionisation detectors

This type of sensors uses high-energy UV light to separate electrons from the gas molecules which are then exposed to an electrical field where they generate a current which is proportional to the rate of ionisation and, hence, related to the gas concentration [27]. All molecules with lower ionisation energies than the photon energy of the UV light (around 10 eV, depending on light source) are ionised which means that they cannot detect specific gases selectively. They can also be affected by interferences with RH and temperature [93, 27]. However, they respond fast to concentration changes and are very sensitive, therefore they can be useful to detect a range of VOCs. Photo ionisation detectors are relatively expensive compared to other portable gas sensors (e.g. EC, MOS or passive samplers) [136].

Passive samplers

Passive samplers or diffusion tubes are based on either chemical absorption or physical adsorption of gaseous pollutant on the sampling material. The concentration is determined by lab analysis of the sampling material after it has been exposed to the pollutant for a defined period of time. Typical pollutants include O_3, SO_2, NO_2 [36] and various VOCs [72]. Passive samplers are easy to use, inexpensive and require no electricity which makes them suitable for large-scale deployments. However, effects of temperature, RH, solar radiation, wind velocity and cross-interference with other gases need to be considered, and the subsequent lab analysis requires additional resources [78]. Furthermore, they can only measure the cumulative exposure, hence a temporal disaggregation is not possible and peak emission events may not be

identified.

Biomarkers

Although not strictly a sensor, biological markers are another direct method to assess personal exposure to environmental pollution. Biomarkers of exposure are "cellular, biochemical, analytical, or molecular measures that are obtained from biological media such as tissues, cells, or fluids and are indicative of exposure to an agent" [141]. They can be residues of the original pollutant, metabolites of the pollutant or the product of an interaction between the pollutant and agents within the organism [140]. Typical analytes are VOCs including e.g. benzene and alkenes. The comparison of biomarker analysis with other direct exposure measurements showed that high correlations between the two assessment techniques can be found [159]. The relationship between the measured biomarker concentration and the ambient exposure information needs to be modelled based on parameters like half-life, kinetics, and metabolic transformation [159]. These parameters might vary from person to person and/or might not be available for large scale studies. Like passive sampling techniques; biomarkers can only give information about the cumulative exposure. Furthermore, the biomarker concentration is the result of all exposure routes including, besides inhalation exposure, also dermal and ingestive exposures. On the other hand, they are an accurate measure of the actual pollutant dose received by the body which is valuable information for determining the health effects of environmental pollutants.

A.2 Design, operation and deployment of the personal air quality monitor

A.2.1 Description of the PAM

A.2.1.1 Operation principle of electrochemical sensors

In this project the concentrations of the air pollutants NO, NO_2, O_3 and CO are measured by amperometric electrochemical sensors. Their principle of operation is based on a three electrode system (Figure A.1): Working electrode (WE), counter electrode (CE) and reference electrode (RE) are put in electrical contact via wetting filters containing an electrolyte liquid (3 - 7 M conc. H_2SO_4) that acts as an ionic conductor [4]. While reference and counter electrode are enclosed in the sensor and not exposed to environmental air, the working electrode is in contact with all gases of the surroundings through a gas permeable membrane. The target gas

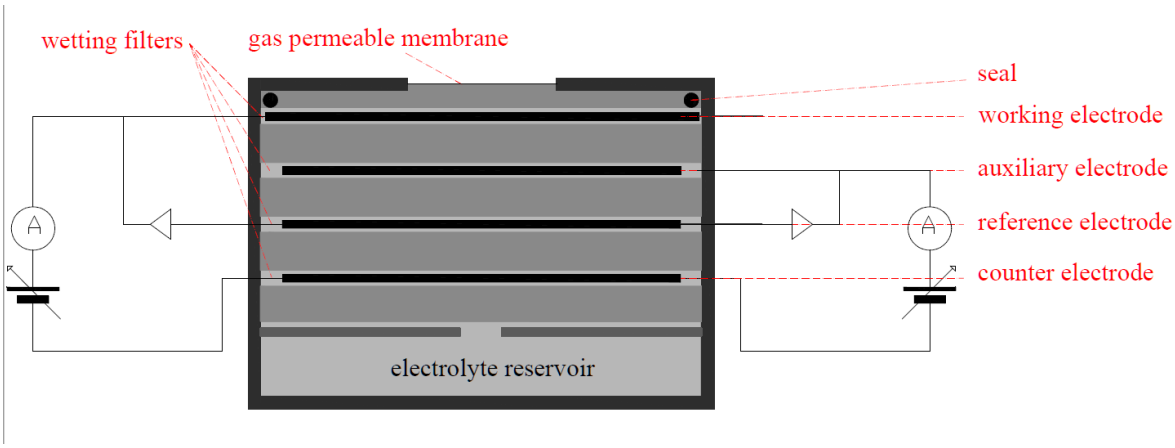

Fig. A.1 Schematic of amperometric four electrode gas sensor. The target gas is oxidised or reduced on the surface of the working electrode which is exposed to ambient air through a gas diffusion barrier. The counter reaction happens at the surface of the counter electrode. The potential of the working electrode is kept constant by the reference electrode. The auxiliary electrode compensates for temperature effects. Graph: Lia Chatzidiakou

reaches the surface of the WE via diffusion and is oxidised (CO, NO) or reduced (NO_2, O_3) at the surface of the WE (see Reaction A.2), causing a change of the electrochemical potential of the electrode. A high surface area and a target gas specific catalyst enhance the reaction rate and the selectivity of each individual sensor.

The change of the electrochemical potential of the WE is balanced out by a complementary reaction at the CE, i.e. if the target gas is oxidised at the WE, oxygen is reduced at the CE to form water, and if the target gas is reduced, the CE oxidises water to O_2 (see Table A.1).

The electrochemical potential of the WE is kept at a constant value by the RE, in order to ensure a constant sensitivity and selectivity while the CE potential is allowed to vary. The electric current measured between the WE and the CE is proportional to the concentration of the target gas. This is converted into voltage by an internal resistor of the sensor so that the raw output signal is given in microvolts.

A fourth electrode, the auxiliary electrode (AE), is built into the sensor to compensate for the temperature dependence of the cell potential. It is identical to the WE with the only difference that it is not exposed to ambient air. Hence, the AE tracks all changes of the cell potential which are not caused by concentration changes of the target gas in the ambient air. Under ideal conditions, the difference between the WE and the AE signal is only dependent on the ambient concentration of the target gas.

$$Ox + ne^- <=> Red \tag{A.2}$$

$$E = E^0 + \frac{RT}{nF} ln\left(\frac{c_{Ox}}{c_{Red}}\right) \tag{A.3}$$

Ox	Oxidant - gas species which is reduced (here: NO_2 or O_3)
Red	Reductant - gas species which is oxidised (here: CO or NO)
E	Electrochemical cell potential
E^0	Standard cell potential
R	Universal gas constant (8.314 J/K mol)
T	Temperature
n	Number of transferred electrons
F	Faraday constant (96485 C/mol)
c_{Ox}, c_{Red}	Concentrations of oxidant and reductant

Table A.1 Electrode and overall reactions of the electrochemical sensors. In each case the first line refers to the reaction at the WE, the second to the reaction occurring at the CE. The cell voltage corresponds to the difference between WE and CE (theoretical Nernst potential), referenced to a standard hydrogen electrode at 25°C [2]

Cell reaction	**Cell voltage**
CO sensor	-1.28 V
$CO + H_2O \rightleftharpoons CO_2 + 2\,H^+ + 2\,e^-$	
$\frac{1}{2}\,O_2 + 2\,H^+ + 2\,e^- \rightleftharpoons H_2O$	
$CO + \frac{1}{2}\,O_2 \rightleftharpoons CO_2$	
NO sensor	-0.27V
$NO + H_2O \rightleftharpoons NO_2 + 2\,H^+ + 2\,e^-$	
$\frac{1}{2}\,O_2 + 2\,H^+ + 2\,e^- \rightleftharpoons H_2O$	
$NO + \frac{1}{2}\,O_2 \rightleftharpoons NO_2$	
NO_2 sensor	-0.16 V
$NO_2 + 2\,H^+ + 2\,e^- \rightleftharpoons NO + H_2O$	
$H_2O \rightleftharpoons \frac{1}{2}\,O_2 + 2\,H^+ + 2\,e^-$	
$NO_2 \rightleftharpoons NO + \frac{1}{2}\,O_2$	
O_3 sensor	0.73 V
$O_3 + 2\,H^+ + 2\,e^- \rightleftharpoons H_2O + O_2$	
$H_2O \rightleftharpoons \frac{1}{2}\,O_2 + 2\,H^+ + 2\,e^-$	
$O_3 \rightleftharpoons O_2 + \frac{1}{2}\,O_2$	

Table A.2 Variable ranges used to clean the data set from erroneous data entries

Variable	**Range**	**Typical value**
Input voltage	0-15 V	12 V
Battery voltage	0-25 V	8.5 V when fully charged
Noise	0-100.000	0.1 (arbitrary units)
Temperature	<100°C	20°C
RH	0 - 100%	60%
Longitude	-180° - 180°	0°
Latitude	-90° - 90°	50°
Acceleration	0.05-10 g	1 g
Speed	0-500 m/s	2 m/s
GPS horizontal dilution of precision	<1000 km	100 m
PM_{10}, $PM_{2.5}$, PM_1	<10 mg/m^3	ambient usually <<1 mg/m^3
EC sensor electrode voltage	1 mV – 10 V	300 mV

A.2.1.2 Allowed variable ranges for raw measurements

Corruption of data rows when writing onto the SD card might lead to erroneous data entries in the raw measurements (e.g. large signal spikes as seen in Figure 2.3). Entries that contain values outside a physically meaningful range (e.g. RH > 100% or Longitude > 180°) were discarded. An overview of the defined data ranges for each variable is given in the following Table.

A.2.1.3 Effects of fast environmental changes on EC sensor performance

The following section (including graphs) has been published in Chatzidiakou et al. (2019) [29]. "To investigate the effect of fast environmental changes on sensor performance, a controlled experiment was set up at a residential house in an urban background area in Cambridge. One PAM was deployed outdoor and a second PAM was deployed indoors. A third PAM was moved rapidly between an indoor and an outdoor location while a detailed time record ("diary") of the transition movements was kept (Figure A.2, top). Commonly encountered residential indoor emission sources such as cooking (e.g. 11:30) and cigarette smoking (e.g. 17:30, PM measurements) were then introduced. The temperature difference between the indoor and the outdoor microenvironment was about 10-15°C (from >20°C indoors to 10-15°C outdoors) resulting in an RH difference of about 20% (30% indoors vs 50% outdoors). While the temperature sensor inside the PAM showed a relatively slow response when moved between indoors and outdoors, a rapid response of the RH sensor was evident (Figure A.2, derivative of

RH). The environmental changes were identified based on the time-derivative of the RH and were clearly distinguished from emission events (cooking, smoking). PM measurements were not affected by the rapid temperature changes; however, short-term transient changes were noticed in the measurements of the EC sensors. Figure A.3 demonstrates that the recovery time of the NO, NO_2 and O_3 sensors was shorter (< 5 min) than that of the CO sensor (15 min)." [29]

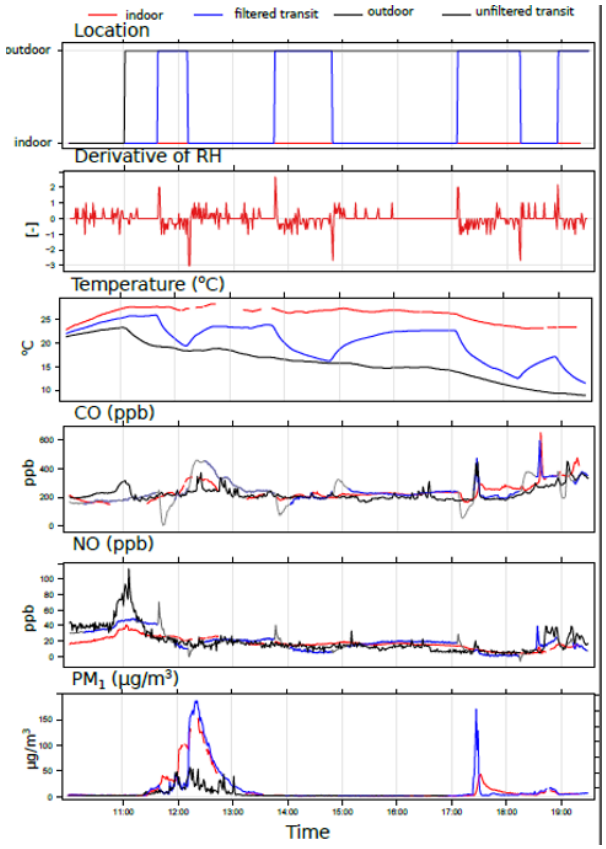

Fig. A.2 "An experiment to characterise sensor responses to rapid environmental changes between different microenvironments. Time-series of one PAM deployed outdoors (black), a second PAM was deployed indoors (red) and a third PAM (grey, original signal) was moved rapidly between the indoor and the outdoor environment in the premises of a residence in an urban background area in Cambridge, UK. The rapid temperature changes resulted in sharp responses of the EC sensors whereas the PM measurements stay unaffected. A selective algorithm based on the on the time-derivative of the RH (dRH) was applied on the data of the moving PAM to flag and remove the false responses (blue line, filtered data) without filtering out short-term pollution events." [29]

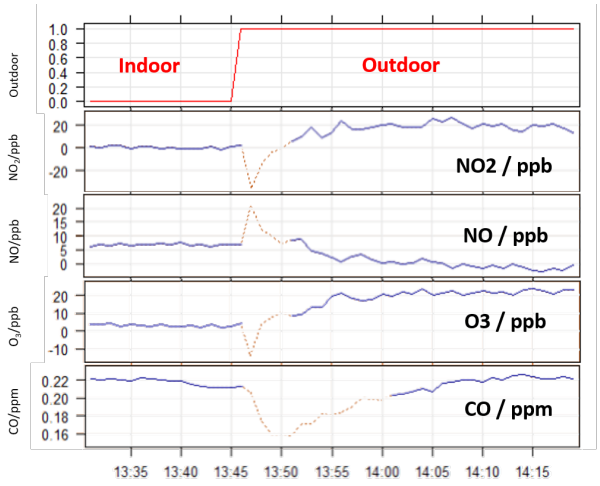

Fig. A.3 "Close-up of one indoor-outdoor transition. The dotted orange line shows the original signal before removing the false temperature response. The blue line shows the remaining measurement after the removal. The stabilisation time after the transition depends on the sensor type with higher times for CO (15 min) and faster recovery times for the rest of the sensors (5 min)." [29]

A.2.2 Measurement campaigns

A.2.2.1 Reliability of London reference measurements during the pilot project

Fig A.4 compares the ambient pollutant concentration measurements from LAQN monitoring station North Kensington [King's College London] and the monitoring roof of the Chemistry department in Cambridge. Generally, the two monitoring stations captured roughly the same trends for all pollutant concentrations. NO_x concentrations are higher and O_3 concentrations lower in London due to higher traffic density.

The CO concentrations in London have a clear offset compared to the Cambridge data which changed (presumably through instrumentation maintenance) around Nov 29^{th}. Because of this artificial offset change the ambient CO measurements from London were discarded and replaced by the Cambridge ambient CO measurements as an approximation for the regional levels.

Around Nov 1^{st} very high CO, NO_x and $PM_{2.5}$ concentrations were recorded at the London monitoring station whereas such a significant increase was not observed in Cambridge. This indicates that the station in London might have captured emissions from local sources in the direct environment. To further investigate, the two stations were compared to the measurements of a PAM that was deployed with a participant in London during that time. Fig A.5 shows the comparison for CO and NO[1]. The baseline of the PAM measurements follows the Cambridge monitoring station much closer than it follows the London station which confirms that the increase of pollution levels on Nov 1^{st} observed at the London reference was caused by a local emission event close to the station. The ambient concentrations of all pollutant species from the London reference were excluded from Oct 31^{st} until Nov 5^{th} 2015 and replaced by the ambient measurements from Cambridge as a closer approximation to the regional air quality.

Table A.3 Range (1^{st} - 99^{th} percentile) and mean concentrations (in brackets) of ambient air pollution concentrations measured at monitoring stations in London (North Kensington) and Cambridge (Chemistry Department).

	London	**Cambridge**
CO	184-1147 (346)	114-428 (217)
NO	0-157 (12)	0-38 (3)
NO_2	3-43 (19)	0-28 (9)
O_3	0-36 (16)	0-40 (21)
$PM_{2.5}$	0-64 (10)	1-33 (9)

[1]CO and NO have no significant indoor sinks (see Section 5.2.1). Hence, the indoor concentrations are expected to be similarly high as outdoors.

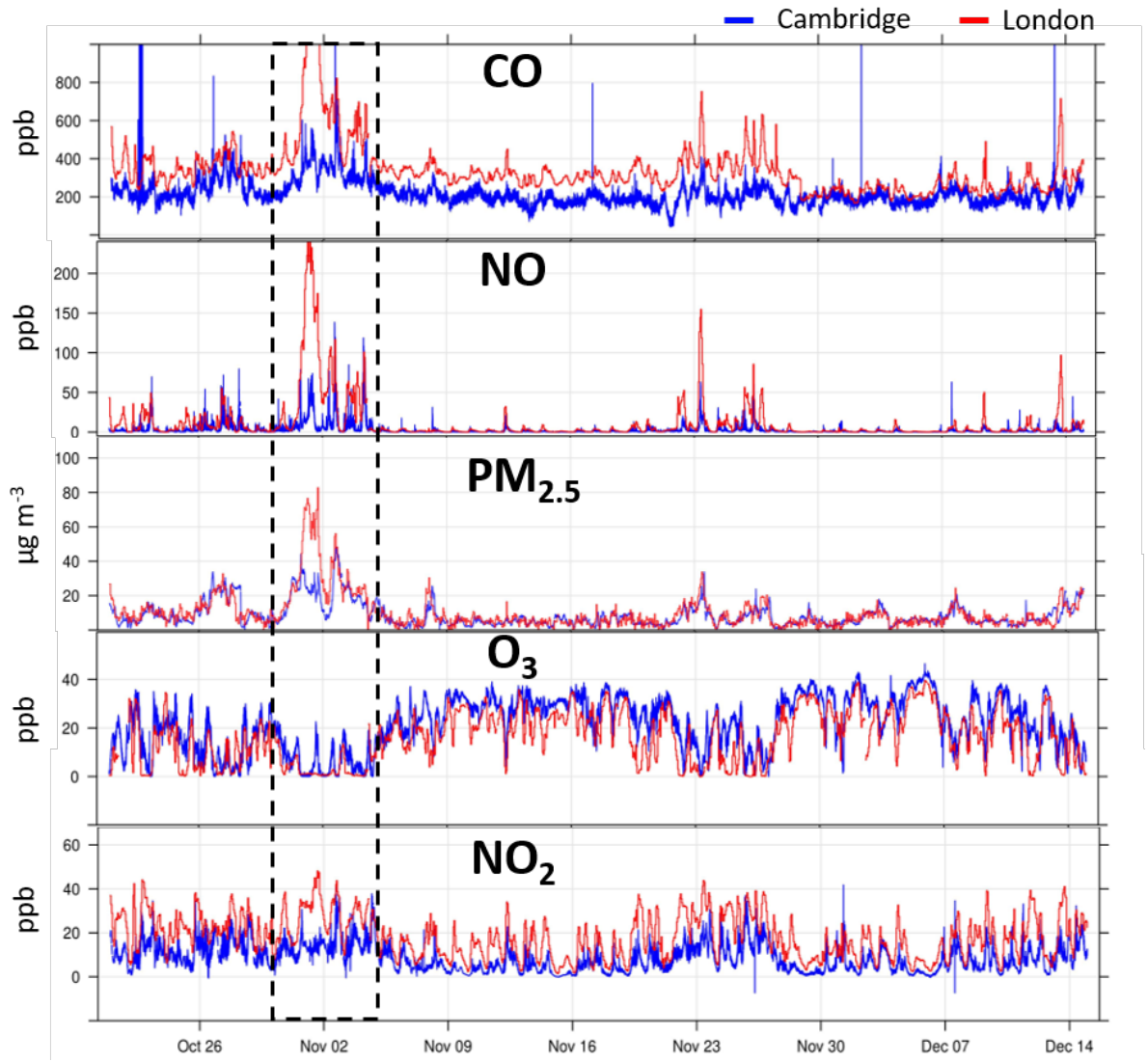

Fig. A.4 Comparison of the ambient measurements from the monitoring stations in London (red) and Cambridge (blue). A quantitative overview is given in Table A.3. The pollution episode highlighted inside the black square is shown in more detail in Figure A.5.

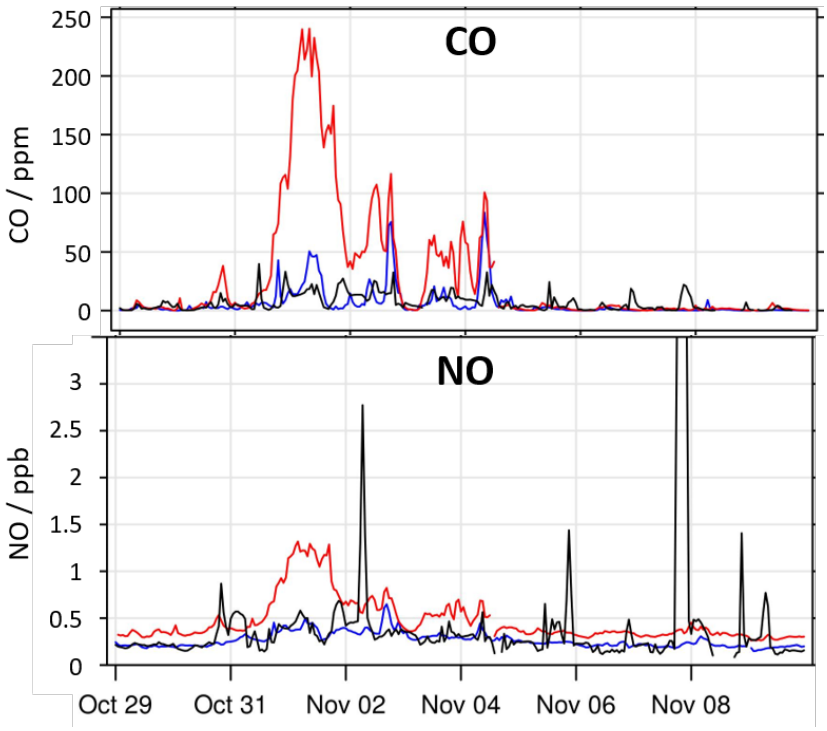

Fig. A.5 Comparison of ambient CO and NO measurements from London (red) and Cambridge (blue) and measurements of PAM 52 (black) which has been deployed in London in the time window marked in Figure A.4.

A.2.2.2 Medical parameters collected in the AIRLESS project

Table A.4 Collected biomarkers during the AIRLESS field campaigns

Health characteristic	**Biomarker**	**Explanation**
Cardiovascular function	Blood serum and plasma	**Monocytes:** type of white blood cells, their count can be predictive of cardiovascular events [117]
		C-reactive protein (CRP): rises rapidly in response to tissue injury, infection and inflammation [135]
Endothelial function	Puls wave velocity / blood pressure	Endothelium: layer of cells inside blood vessels, early indicator for cardiovascular diseases [43]
Oxidative stress	Creatinine	Indicator for renal function [109]
	8-Oxo-2'-deoxyguanosine	Product of DNA oxidation [42]
	Malondialdehyde	Marker of oxidative lipid injury [40]
	8-Isoprostane	Bioactive product of lipid peroxidation [99]
	Metabonomics	Measurement of metabolic responses to environmental stressors [102]
Respiratory	Peak expiratory flow	Measurement of lung function
	Fraction of exhaled NO (FeNO)	Marker for respiratory inflammations [120]
	Exhaled breath condensate	Marker for inflammatory airway diseases [35]

A.2.2.3 Participant movement during the AIRLESS summer campaign

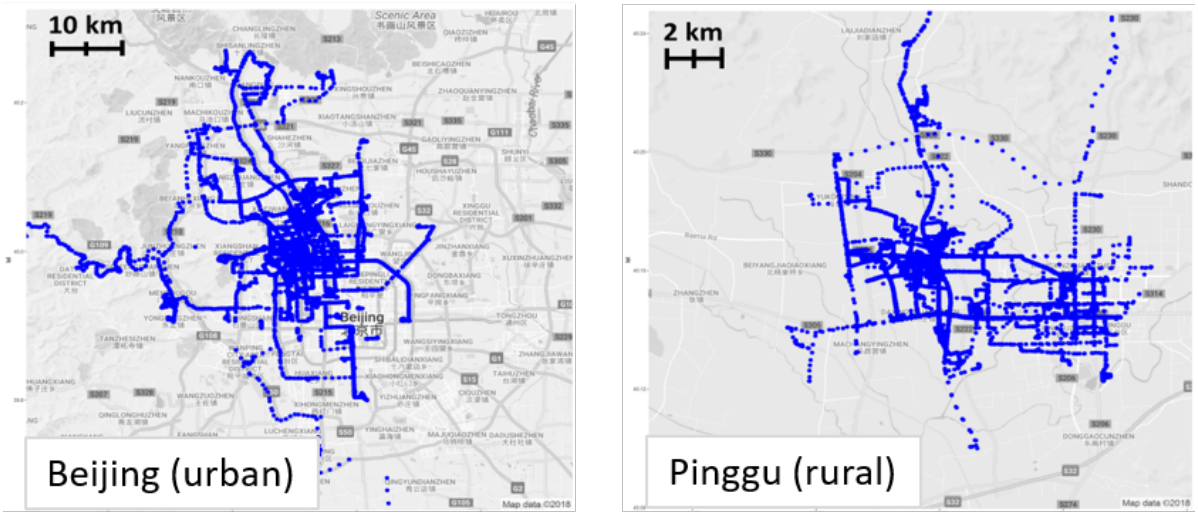

Fig. A.6 Maps indicating the participant movement (blue) of the urban and rural cohort during the summer campaign. The corresponding maps of the winter campaign are presented in Figure 2.13

A.2.2.4 Determination of the exact cooking times of participants in rural Kenyan households

The participants of the case study in rural Kenyan households (Section 2.3.3.2) were asked to fill in a diary form to report which cooking fuels they used for every meal. An example form is given in Figure A.7. Because the participants did not report the exact times of their cooking, they were determined using CO emissions as a proxy.

Figure A.8 illustrates the procedure of determining the exact cooking times. The reported cooking events from the diaries were first roughly placed into time windows (breakfast: 5am - 11 am, lunch: 11 am - 3pm, dinner: 5pm - 12pm, shown in lightblue) and then refined based on measured CO emissions. If the indoor CO concentrations exceeded 1.7 ppm (maximum outdoor concentration measured during the deployment), the data point was flagged as indoor source. The cooking times were defined as the time periods in which the detected indoor sources overlapped with a time window of reported cooking fuel use.

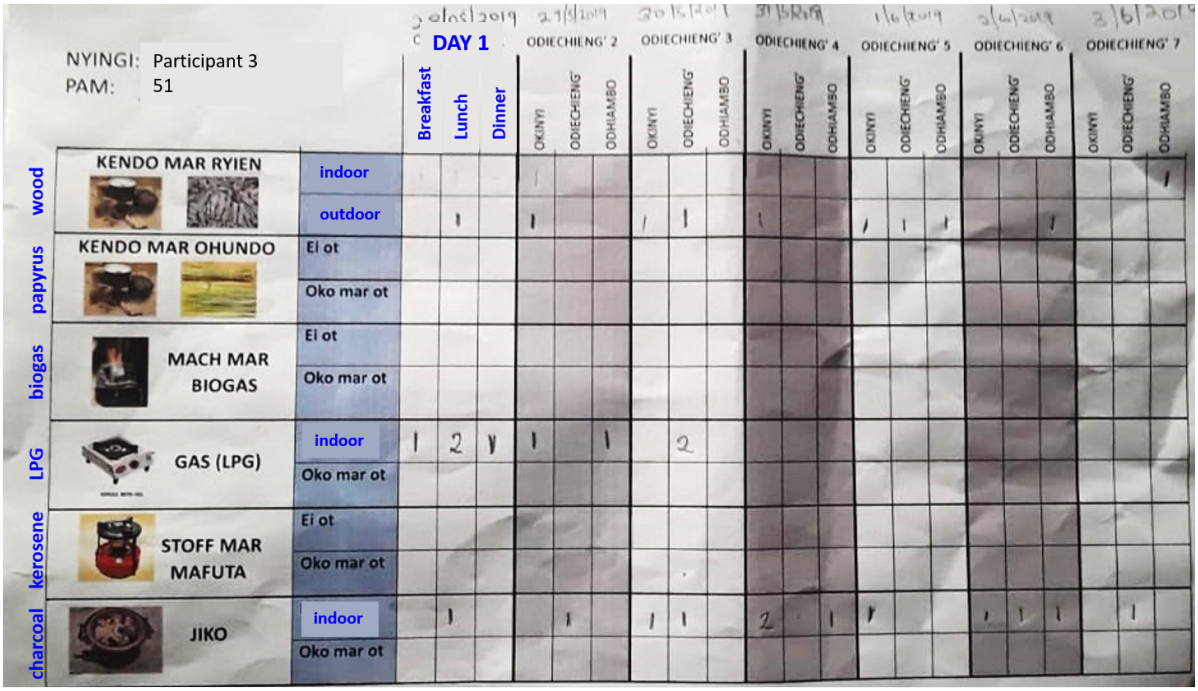

Fig. A.7 Example of a filled in cooking fuel diary of participant 3. The diary forms were given out in the local language (Luo). Translations are given in blue. Participant 3 was from the control group that did not use biogas. They mainly used charcoal for indoor cooking, supplemented with liquid petroleum gas (LPG) and outdoor wood burning.

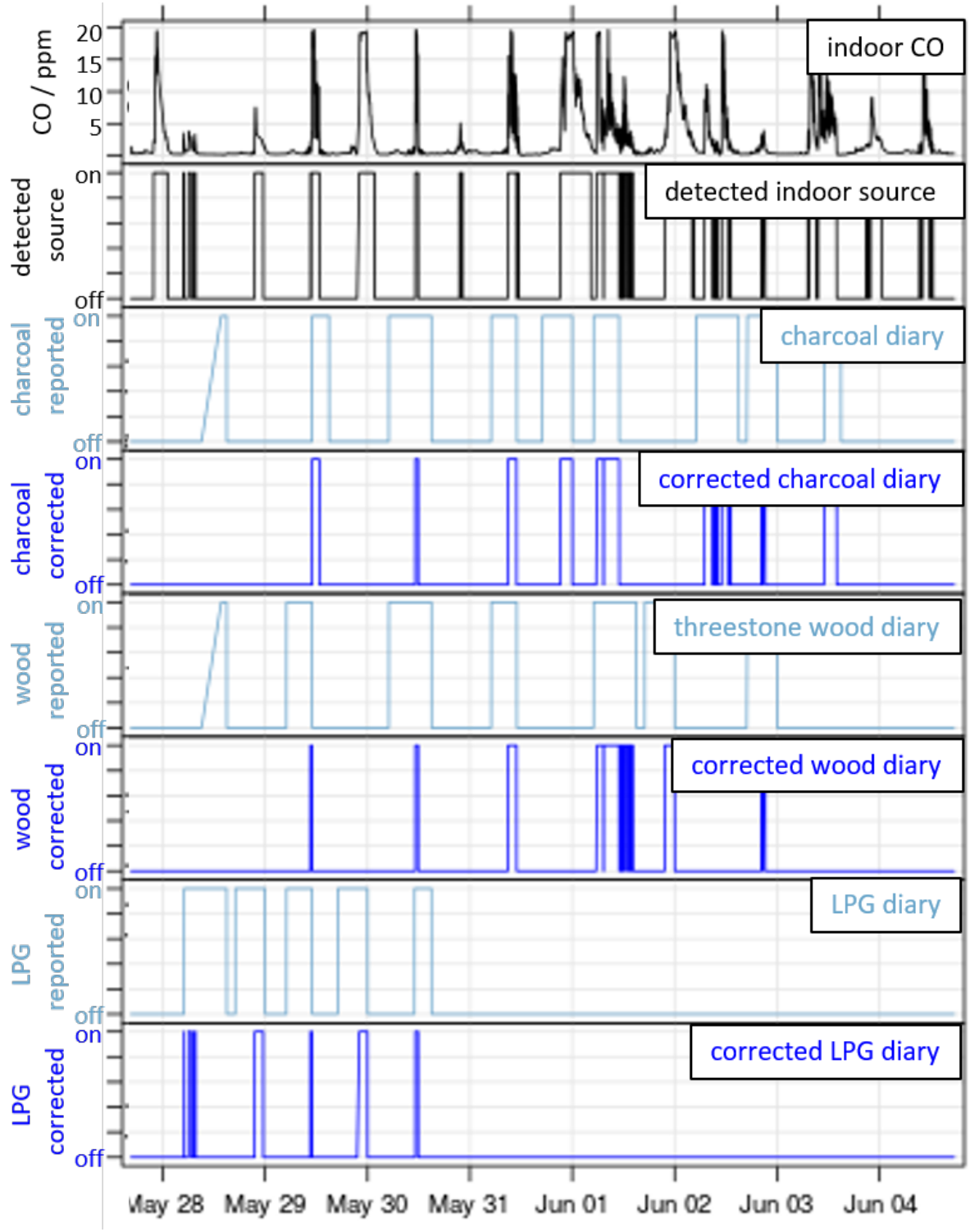

Fig. A.8 Determineation of the exact cooking times. The reported cooking events from the diaries were first roughly placed into time windows (lightblue) and then refined (blue) based on the detected indoor sources from CO observations (black).

A.3 Characterisation of the PAM performance

A.3.1 Temperature ranges measured during the AIRLESS summer campaign

The results of Section 3.2 indicated that the performance of the gas sensors inside the PAM degraded when the sensors were exposed to temperatures above 40°C. Figure A.9 compares the temperature ranges the PAMs were exposed to during field deployment (mainly indoors, green) with the temperatures measured during the summer colocation when the PAMs were placed outdoors for the entire time (red). The figure shows that the sensors were exposed to lower temperatures during the field deployment due to occupants adjusting their thermal environment for comfort.

A.3.2 Sensor reproducibility

"To evaluate the reproducibility of the sensors, the coefficient of determination between the raw PM measurements and working electrode readings of all EC sensor pairs during the four co-locations in the UK and China in both seasons are presented in Table A.5. All EC sensors show excellent correlations across the network with mean $R^2 > 0.80$ with the exception of the NO_2 sensors during the non-heating season in China, possibly affected by the high temperatures that the sensors were exposed to. The coefficient of determination between the OPC-N2 sensors was high across seasons and settings ($R^2 > 0.91$); however, the gradient was lowest in the UK co-location during the heating season." [29]

Table A.5 Summary of reproducibility between sensors in outdoor co-locations in China and the UK that ranged from 7 to 19 days during the heating and non-heating season. Linear fitting equations between sensors generated the coefficient of determination (R^2) and the gradient [m] matrices. The average values of all N sensors for each variable are given, the standard deviations (σ) indicate the variation within the sensor network [29]. The corresponding summary of the linear models with the reference instruments is presented in Table 3.4.

		Heating season		**Non-heating season**	
		China (Dec- Jan)	UK (Oct- Nov)	*China (June)*	UK (April)
	Internal PAM temperature (°C)	10.5 (5.3-18.0)	15.9 (11.0–20.8)	*40.2 (32.7–45.8)*	17.7 (12.2–26.8)
	Internal RH (%)	27 (14-44)	52 (39 -59)	*38 (23 – 55)*	52 (34 – 60)
N sensors		N =59	N=3	*N=59*	N= 3
CO	Maximum mixing ratio (ppb)	6845	357	*916*	276
	R^2 (σ)	1.00 (0.01)	0.98 (0.00)	*0.94 (0.03)*	0.94 (0.00)
NO	Maximum mixing ratio (ppb)	132	19	*5*	6
	R^2 (σ)	0.89 (0.17)	0.80 (0.01)	*0.81 (0.07)*	0.94 (0.005)
NO_2	Maximum mixing ratio (ppb)	98	35	*42*	19
	R^2 (σ)	0.97 (0.04)	0.98 (0.00)	*0.60 (0.12)*	0.89 (0.03)
O_3	Maximum mixing ratio (ppb)	33	30	*109*	44
	R^2 (σ)	0.91 (0.05)	0.80 (0.00)	*0.90 (0.03)*	0.96 (0.01)
$PM_{2.5}$	Maximum conc. (μm^{-3})	432	32	*110*	37
	R^2 (σ)	0.95 (0.17)	0.91 (0.05)	*0.96 (0.01)*	0.98 (0.01)

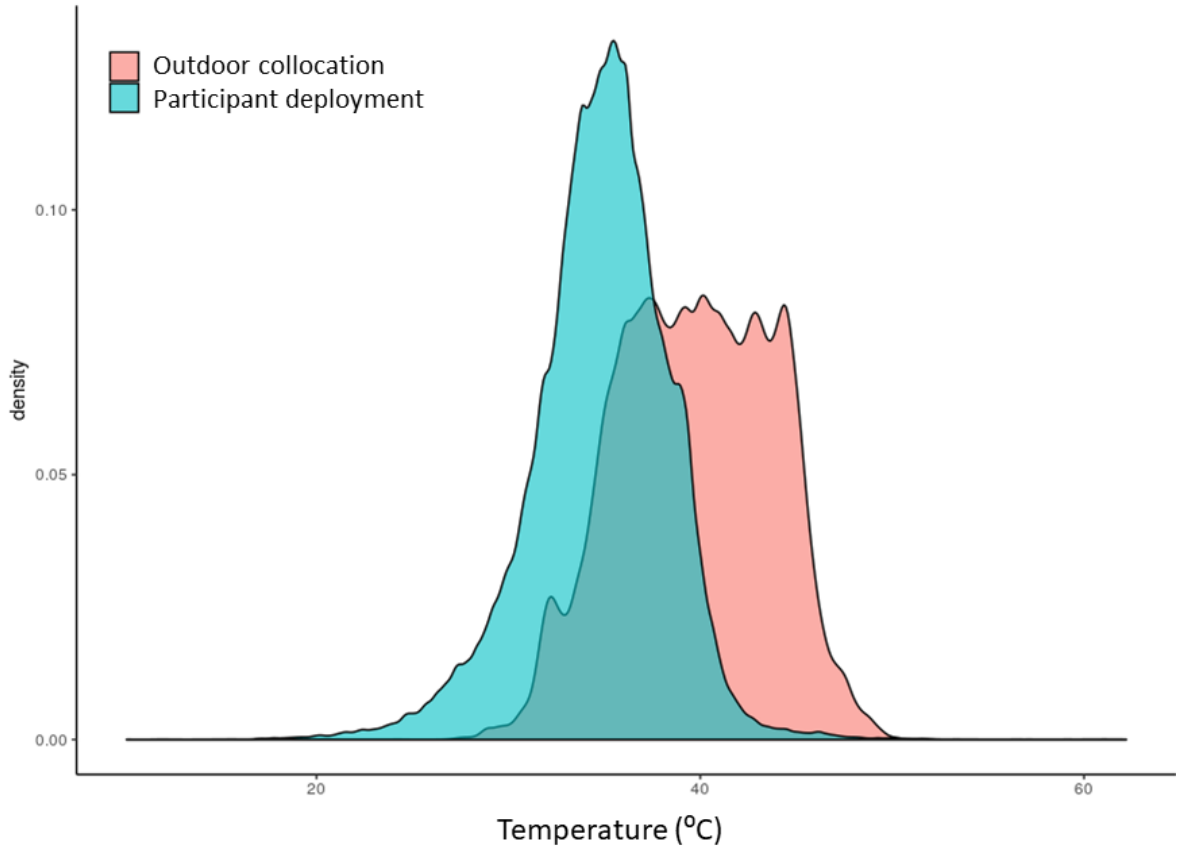

Fig. A.9 Histogram of internal temperatures (on average 7°C higher than ambient temperatures) of 60 PAMs recorded during the co-location period with reference instruments (pink) and during the deployment to participants (cyan) during the non-heating season in China.

A.4 Improving personal exposure estimates: PAM vs monitoring station

A.4.1 Case participant U123

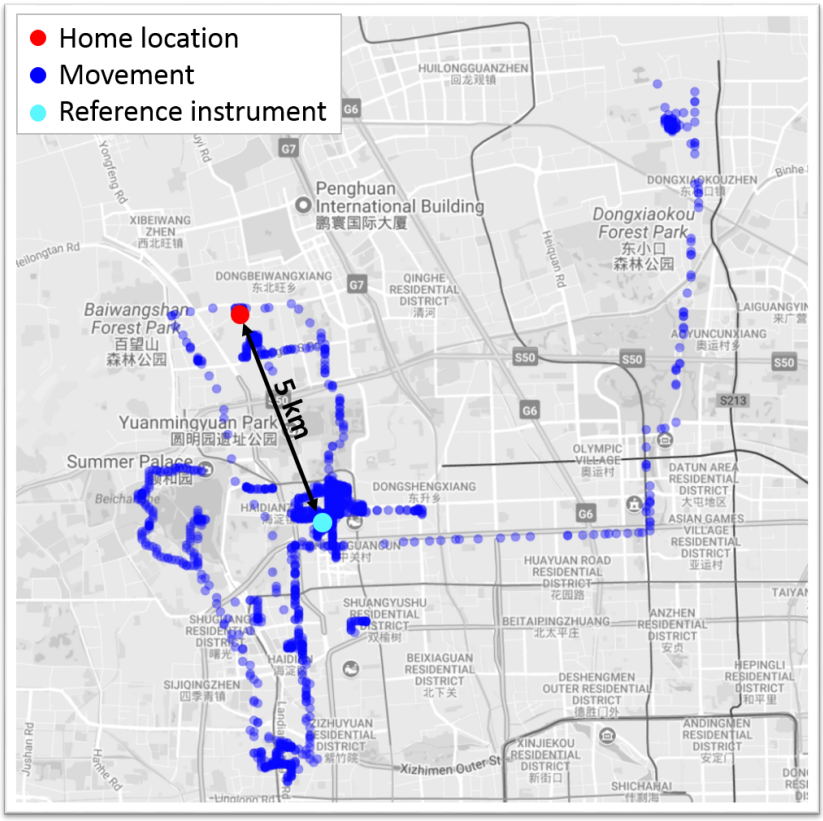

Fig. A.10 Map of the locations visited by participant U123. The red dot refers to the participant's home location, the cyan dot indicates the location of the PKU reference instruments. The distance between home and reference station is approximately 5 km. An air pollution exposure time series of participant U123 can be seen in Figure 4.1

A.5 Source apportionment of personal exposure using networks of mobile sensors

A.5.1 Impact of indoor air pollution sinks on local and regional air pollution

Section 5.3 demonstrated how the total personal exposure to stable pollutants was split into a regional and a local component. This separation is not valid for reactive pollutants ($k_{sink} > 0$, see Figure 5.1) as the regional outdoor levels are reduced by indoor sinks when the air enters the building. The following section will examine how the reactivity of a pollutant affects the ratio between the local and regional component of indoor exposures using the indoor air pollution model introduced in Section 5.1.1.

The analysis will focus on the cumulative exposures (sum of exposure over total time, corre-

sponds to area under the concentration time series).

The regional part of the total indoor pollution $[X_{in}]_{reg}(t)$ originates from regional outdoor pollution $[X_{out}]_{reg}$ penetrating into the building and can be expressed via Equation A.4. The local contribution to the total indoor exposure is generated by indoor sources. Assuming that a source causes a sudden increase of the indoor pollution by $\Delta[X_{in}]_{loc}$ and then ceases exponentially, the local contribution can be expressed through Equation A.5.

$$[X_{in}]_{reg}(t) = [X_{out}]_{reg} \frac{k_{vent}}{\kappa} \tag{A.4}$$

$$[X_{in}]_{local\,peak}(t) = \Delta[X_{in}]_{loc}(t_0)\, e^{-\kappa(t-t_0)} \tag{A.5}$$

$[X_{in}]_{reg}$, $[X_{out}]_{reg}$	regional component of indoor/outdoor air pollution concentration (ppb)
κ	indoor decay rate = k_{vent} + k_{sink} (hour^{-1}; see Section 5.1.1)
k_{vent}	rate coefficient of building ventilation (hour^{-1})
k_{sink}	rate coefficient of indoor pollution sinks (hour^{-1})
$\Delta[X_{in}]_{loc}(t_0)$	increase of indoor pollution caused by indoor emissions at time t_0 (ppb)

By integrating the two equations over time, the local and regional component of the total cumulative exposure can be determined (Equations A.6 and A.7). $[X_{out}]_{reg}$ can hereby be assumed as a constant as the change of the outdoor concentrations is much slower than the loss mechanisms through building ventilation and indoor sinks.

$$\int [X_{in}]_{reg}(t)\, dt = [X_{out}]_{reg} \frac{k_{vent}}{\kappa}\, \Delta t \tag{A.6}$$

$$\int [X_{in}]_{local\,peak}(t)\, dt = \frac{\Delta[X_{in}]_{local\,peak}}{\kappa} \tag{A.7}$$

Equation A.7 describes the cumulative local exposure caused by a single emission event. However, it is likely that the indoor exposure of a person is impacted by multiple (i) emission events of different magnitudes $\Delta_i[X_{in}]_{loc}$. Hence the local component of the indoor exposure changes to Equation A.8:

$$\int [X_{in}]_{local\ total}(t)\, dt = \frac{1}{\kappa} \sum_i \Delta_i [X_{in}]_{local\,peak} \tag{A.8}$$

The ratio between the local and the regional component is calculated via Equation A.9. The ratio depends on the number i and intensities $\Delta_i[X_{in}]_{local\,peak}$ of the local peaks caused by indoor pollution sources (the more frequent the sources and the stronger their emissions, the higher

the contribution of local sources to the overall exposure). Similarly, the ratio depends on the outdoor concentration: the higher the regional outdoor levels, the higher the regional component of indoor exposure. The ratio does, however, not change with κ which contains the indoor reactivity of the pollutant ($\kappa = k_{vent} + k_{sink}$ with $k_{sink} = 0$ for stable pollutants). This means that the ratio between local and regional component is independent from the impact of indoor sinks.

$$\frac{local}{regional} = \frac{\int [X_{in}]_{loc}(t)\,dt}{\int [X_{in}]_{reg}(t)\,dt} = \frac{\sum_i \Delta_i [X_{in}]_{local\,peak}}{[X_{out}]_{reg}\ k_{vent}\ \Delta t} \tag{A.9}$$

A.5.2 Optimum percentile to determine the regional pollution levels from the AIRLESS sensor network

Different percentiles (minimum - 30^{th} percentile) were used to extract the regional outdoor air pollution levels as described in Section 5.1.2 (CO observations, AIRLESS winter campaign, urban sensor network). The extracted backgrounds were linearly fitted to the reference measurements of the urban ambient monitoring station (c.f. Section 5.1.3). The fitting parameters (slope, intercept, adj. R^2, RMSE) are plotted against the selected percentiles in Figure A.11. In line with previous literature, the 10^{th} percentile was identified as optimum.

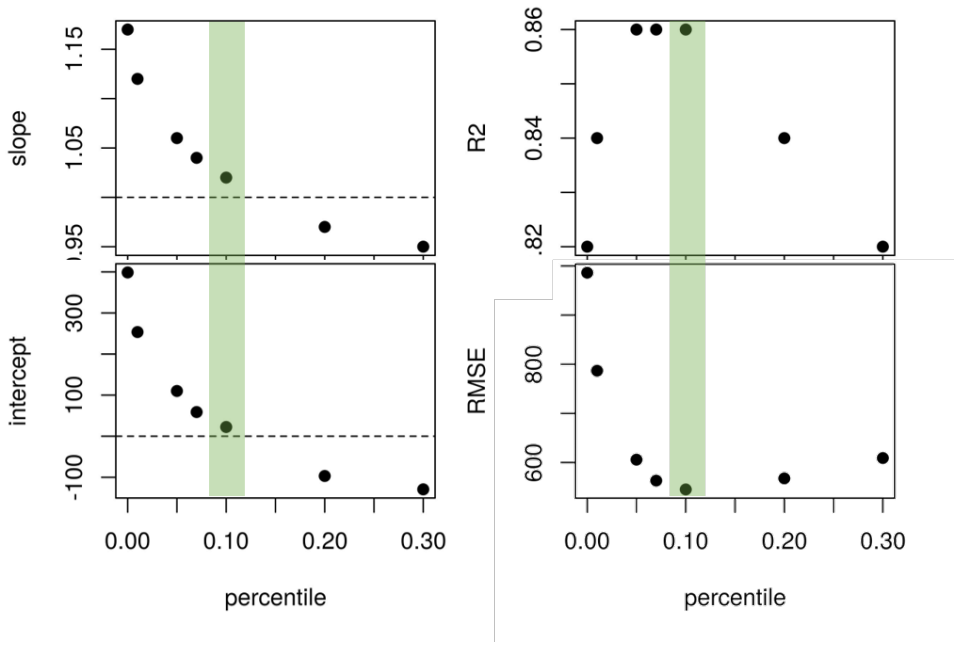

Fig. A.11 Selection of the optimum percentile for background extraction. The 10^{th} percentile (green shaded) was identified as optimum. Dotted line indicates optimum value.

A.5.3 Comparison of the extracted regional pollutant levels from the sensor networks with reference observations

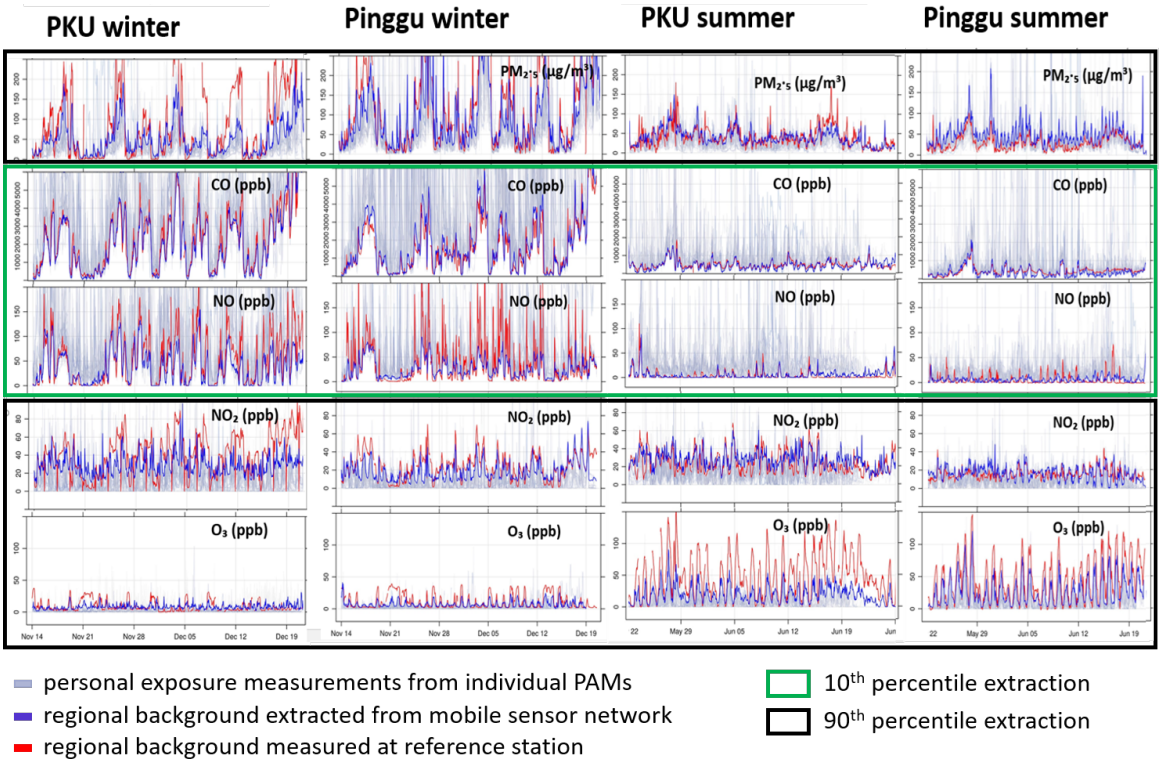

Fig. A.12 Comparison between the regional background concentrations extracted from mobile sensor networks (blue) with reference measurements from monitoring stations (red) for all five pollutants during the AIRLESS winter (left) and summer campaign (right). Individual sensor measurements shown in grey.

Sections 5.1 and 5.2 introduced an approach to determine the regional background concentrations from a network of mobile sensors. Figure A.12 presents the results of this method when applied to the AIRLESS measurements of all pollutant types during the winter and the summer campaigns.

The 90^{th} percentile method generally resulted in underestimations of the outdoor background concentrations because the assumption that one sensor is exposed to outdoor air at any point of time was probably not met. The extracted backgrounds agreed generally better with the reference in summer and in the peri-urban sensor network (Figure A.12), probably due to higher building ventilation in both cases.

The extracted $PM_{2.5}$ concentrations particularly underestimated the outdoor levels in winter, perhaps due to reduced building ventilation to conserve heat, and the use of air purifiers. How-

ever, the features of the outdoor $PM_{2.5}$ trends (e.g. build-up of haze events) were still captured. Similar results were observed for the extracted NO_2 backgrounds.

The 90^{th} percentile method worked excellent to extract the diurnal variations of the outdoor O_3 levels, although the extracted O_3 levels were notably underestimating the outdoor backgrounds, particularly in the urban cohort in summer. The O_3 agreement between the sensor network and reference was very good in peri-urban Pinggu (Figure A.12), again due to higher building ventilation.

Compared to the case of a stable pollutant (CO, Section 5.1.3), the agreement between the extracted backgrounds and the reference was poorer for reactive pollutants. This was due to the limitations mentioned in Section 5.2 (entire network located indoors at certain times; interference with local emission sources). However, the magnitude and general features (e.g. diurnal patterns) were still captured by the network, which can be used for sanity checks of the network performance.

A.5.4 Contribution of local and regional air pollution to the total personal exposure

Table A.6 Quantitative summary of the Figure 5.9. The variation between the participants (SD-standard deviation) is substantially higher for the local components than of the regional components.

	Urban		Peri-urban	
	Regional	**Local**	**Regional**	**Local**
	WINTER			
Mean contribution	1.95 ppm	1.59 ppm	1.67 ppm	3.07 ppm
(% of total exposure)	(55%)	(45%)	(35%)	(65%)
variation (SD)	0.68 ppm	1.56 ppm	0.31 ppm	3.69 ppm
	SUMMER			
Mean contribution	0.44 ppm	0.50 ppm	0.37 ppm	0.53 ppm
(% of total exposure)	(47%)	(53%)	(41%)	(59%)
variation (SD)	0.09 ppm	0.40 ppm	0.09 ppm	0.81 ppm

A.6 Activity-specific personal exposure and dose estimations

A.6.1 Validation of the time-location-activity model

The time-location-activity algorithm was applied to the data of the pilot project. In this project, 38 volunteers from the UK were asked to carry a PAM for 7 days while keeping an activity diary (see Section 2.3.1). The results of the activity model were compared to the entries from the activity diary.

The boxplots in Figure A.13 present the time budgets spent on each activity as reported in the diary logs (left bar) and as predicted by the model (right bar).

The results for the four core locations are shown in the left graph of Figure A.13. The participants spent the majority of their time indoors at home or at work, while travelling and time spent in other static locations accounted only for a small part of their total time budget. The automated model shows an excellent agreement with the activity logs for the location prediction.

The right graph shows the results for the different modes of commuting. The model slightly overpredicts cycling and in-vehicle trips compared with the activity logs. Note, however, that the right graph only covers the time which is labelled as "in-transit" in the left graph and represents only a small fraction of the total time budgets of the participants.

All in all, there was a good agreement between the results of the time-location-activity model and the activity diaries.

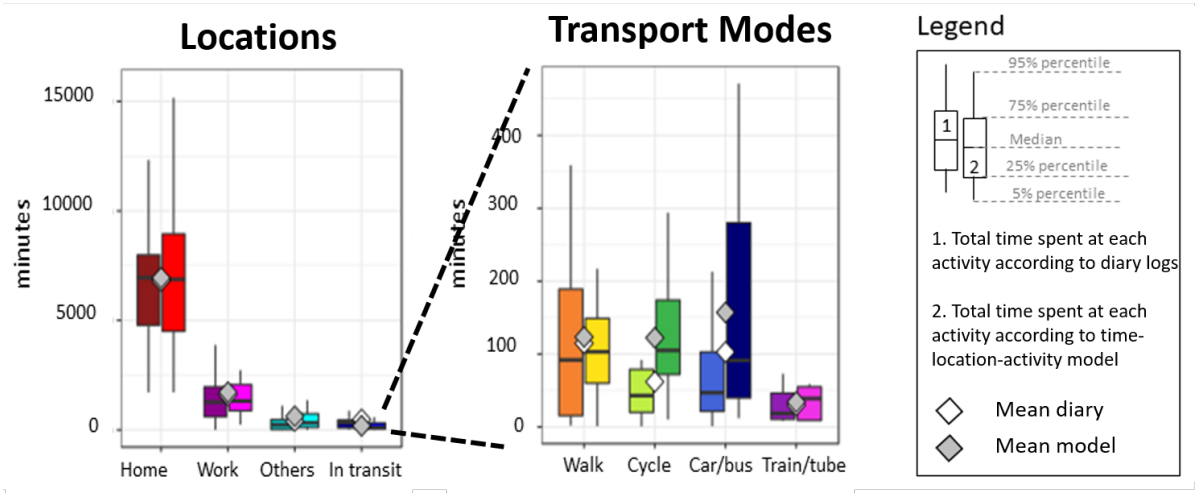

Fig. A.13 Comparison between the results of the time-location-activity model with the activity logs kept by the participants of the pilot project. For each activity, the left boxplot shows the time budget based on diary logs and the right boxplot shows the results of the model. Left: Boxplots showing the time (minutes per week) spent at different locations for 38 participants. Middle: Time budgets of the same cohort for different modes of commuting (i.e. "in transit" category split up). While there is a greater level of discrepancy in the classification of the mode of transport, note that this represents only a small fraction of the total time. Right: Legend of the graph.